UNIVERSITY OF BIRMINGHAM

COMBUSTION PERFORMANCE AND EMISSIONS CHARACTERISTICS OF 2-METHYLTETRAHYDROFURAN AND CYCLOPENTANONE IN A DISI ENGINE

By

Rafiu Kayode Olalere

A thesis submitted to

The University of Birmingham

For the degree of

DOCTOR OF PHILOSOPHY

The University of Birmingham

School of Engineering

November 2023

ABSTRACT

This thesis examines the performance of 2-Methyltetrahydrofuran (MTHF) and Cyclopentanone (CP) fuels to various engine parameters, in particular, engine load, Air fuel ratio (AFR), Spark timing and fuel injection pressure. The effect of the gasoline blends of the two oxygenated fuels were also investigated along with single pulse fuel injections and split injection strategy. 2-Methylfuran (MF), Ethanol and gasoline were used as the based fuel for the study. A spray-guided single-cylinder direct injection spark ignition (DISI) engine was used for the experimentation. Horiba MEXA-7100DEGR Gas Analyser is used to measure gaseous emissions such as hydrocarbon (HC), nitrogen oxide (NOx) and carbon monoxide (CO). Aldehyde emissions and key HCs have been investigated using a Gasmet FTIR. Cambustion DMS 500 is used to measure the particle size distributions. Both MTHF and CP fuels recorded specific fuel consumption advantage over MF and Ethanol and closer to ULG daunting the insinuations that the oxygenated fuels generally lack fuel economy advantages. Due to its higher octane number and faster burning rate, the peak in-cylinder pressure for CP at the high load of 8.5 bar indicated mean effective pressure of about 32.7 % and 34.1 % higher than gasoline and MTHF respectively. The specific fuel consumption and the indicated thermal efficiency for both CP and MTHF was optimised at $1< \lambda < 1.1$. Overall, the optimal fuel injection timing for single pulse width for both CP and MTHF was found to be at 270degbTDCcomb for higher efficiency. However, the optimal timing selected was at the instance of trade off for CO and HC emissions which were both optimised at 240degbTDCcomb. Experiments suggested that split-injection can improve the combustion and emission performance of CP and MTHF but maximum gains were recorded with greater pulse ratios of 2:1 due to improved vaporisation at this pulse ratio. The engine out emission of isNOx is generally higher for CP and MTHF compared to MF, gasoline and Ethanol. However, both CP and MTHF recorded hydrocarbon emissions advantage over MF and ULG. While the higher blends ratio favour the improved engine combustion performance, it comes with unique challenges of

higher NOx emissions and fuel consumption penalty. Ethylene, with recorded components percentage of the HC emissions of 21.9% for MF20, 23.7% for MTF20 and 23.2% for gasoline, consistently remains the highest proportions of HC emissions for the three fuels. Experiments result indicated that the percentage of the unburned furan fuels in the total HC emissions for MF20 and MTHF20 were 1.2 and 1.4 respectively.

ACKNOWLEDGEMENT

First and foremost, Glory be to almighty God, the most gracious, the most beneficent, the most merciful, for making it possible for me to conclude this work despite the arrays of challenges and obstacles.

I would like to register my sincere appreciation and gratitude to Professor Hongming Xu (Primary Supervisor) for his help and invaluable guidance, experience and support that inspired me to the successful completion of my PhD.

This thesis would be impossible without the assistance and guidance of the following individuals, Dr Jose Martin Herreros (Second Supervisor), Dr Chonming Wang and Dr Soheil Zeraati Rezaei your support is greatly appreciated. I like to register my special appreciation to Dr Gengxin and Dr Haoye Liu for their useful comments and feedback for my research work, I also appreciate the technical guidance and the words of encouragement and support from Professor Akbar Ghafourian, Dr Remi Olatunbosun and Dr Raya Al-Dadah during my annual reviews.

I like to offer my appreciation to the laboratory technicians, Peter Thornton, Carl Hingley, Simon Rowan, Jack Garrot, Lee Gauntlett and Lucas Miles Polglase for their support and regular maintenance of the test facilities for successful experimentation. I am sincerely grateful for the cordial relations with all my colleagues at the Future Power Systems department that culminated in the successful completion of this work. In particular, Dr Thomas Lattimore, Dr Changzhao Jiang, Dr Xaio Ma, Dr Dhananjay, Kumar Srivastava, Isaline Lefort, Dr Arumugam Sakunthalai Ramadhas, Dr Mohammadreza Anbari Attar, Dr He Ma and Maria Bogarra Macias.

I like to appreciate the support of Jaguar Land Rover (JLR) for providing the test facility and Shell Global Solutions, UK for supplying the fuels used in this study (gasoline and ethanol). I would also like to thank the TETFund Nigeria and Lagos State University of Science and Technology for providing the funding for the early part of the research study.

Above all my special appreciations goes to my family, Mrs Fatima Olalere, Abdul Malik Olalere, Robiah Olalere, Mariam Olalere, Aisha Olalere and Ibrahim Olalere for their patient and endurance at the time that this work takes me away from them.

Contents

LIST OF FIGURES

LIST OF TABLES

LIST OF ABBREVIATIONS

After Top Dead Center	aTDC
Air- Fuel Ratio	AFR
Air- Fuel Ratio Stochiometric	AFRstoich
Before Top Dead Center	bTDC
Carbon Monoxide	CO
Carbon Dioxide	CO_2
Coefficient of Variation	COV
Crank Angle Degree	CAD
Cyclopentanone	CP
Direct Injection	DI
Direct Injection Spark Ignition	DISI
Department of Energy	DOE
2,5-dimethyl-Furan	DMF
Exhaust Gas Recirculation	EGR
End of Injection	EOI
Ethanol	ETH
Flame ionization detector	FID
Fourier-Transform infrared spectroscopy	FTIR
Gas Chromatograph Mass Spectrometry	GCMS
Hydrocarbon	HC
Higher Heating Value	HHV
Indicated Mean Effective Pressure	IMEP
Intake Valve Closing	IVC
Intake Valve Opening	IVO

Knock Limited Spark Advance	KLSA
Relative Air Fuel Ratio	λ
Lower Heating Value	LHV
Mass Burned Fraction	MFB
Maximum Brake Torque	MBT
Maximum In Cylinder Pressure	Pmax
2-Methylfuran	MF
2- Methyltetrahydrofuran	MTHF
Molecular Beam Mass Spectrometry	MBMS
Motor Octane Number	MON
Nitric Oxide	NO
Nitrogen Oxides	NO_x
Particulate Matter	PM
Part Per Millions	PPM
Port Fuel Injection	PFI
Research Octane Number	RON
Revolution per Minutes	RPM
Rate of Pressure Rise	RPR
Spray- Guided Direct Injection	SGDI

Spark Ignition	SI
Start of Ignition	SOI
Spark Retard	SR
5CAD Spark Retard from MBT or KLSA	SR5
Top Dead Center	TDC
Three Way Catalyst	TWC
Volumetric Air Flow	VAF
Variable Cam Testing	VCT
Volumetric Efficiency	VE
Wide Open Throttle	WOT

LIST OF PUBLICATIONS

1. Olalere, R. K., Zhang, G., Liu, H., Ma, X., & Xu, H. (2025). Experimental study of combustion and emissions characteristics of low blend ratio of 2-methylfuran/2-methyltetrahyrofuran with gasoline in a DISI engine. Fuel, 382, 133799.
2. Olalere, R. K., Zhang, G., & Xu, H. (2024). Experimental Investigation of Gaseous Emissions and Hydrocarbon Speciation for MF and MTHF Gasoline Blends in DISI Engine. International Journal of Automotive Manufacturing and Materials, 6-6.
3. Liu, H., Olalere, R., Wang, C., Ma, X., & Xu, H. (2021). Combustion characteristics and engine performance of 2-methylfuran compared to gasoline and ethanol in a direct injection spark ignition engine. Fuel, 299, 120825.

CHAPTER 1

INTRODUCTION

Two furan fuel candidates, 2,5-dimethyl-Furan (DMF) and 2-methylfuran (MF) have been researched extensively (1-19) as engine fuels by the future power engine research team of the University of Birmingham of which this researcher is a member. The study indicates that both MF and DMF have combustion and emissions characteristics similar to gasoline, which make them easily adoptable to current DISI technologies. The qualitative performance of DMF and MF as engine fuels is the motivation for this researcher to further conduct extensive Engine test on the viability of two other novel biofuels, Cyclopentanone (CP) and 2-metyltetrahydrofuran (MTHF). This chapter gives a general overview of the author's PhD research, which is mainly about combustion and emissions of MTHF and CP in a Direct Injection Spark Ignition (DISI) engine. Background information, overall research objectives, research approaches and the overall thesis outlines are briefly presented in this chapter.

1.1 Background

In the light of growing concerns about the potential irreversible impacts of large-scale hydrocarbon fuel consumption on global climate, there is heightened interest in exploring alternative fuels to replace gasoline (ULG) in engine applications. However, the concentrated energy provided by hydrocarbon has proven hard to replace (20). In 2016, it was internationally agreed that 2°C of global temperature increase is inevitable due to the devastating effect of the hydrocarbon emission on the climate (21). The automotive emissions from the rapidly developing private cars industry has an adverse influence on the energy scenario and environment of the cities (22). According to a report by the International Energy Agency (IEA), in 2019, around 46% of total global oil consumption was attributed to the transportation sector,

which includes road vehicles, aviation, maritime, and rail (23). This sector relies almost exclusively on liquid hydrocarbons as the energy source due to their high volumetric energy density, convenience of use, and easy access to primary resources and relatively low cost. However, combustion of liquid hydrocarbon fuels leads to emission of massive quantities of CO_2 with the associated greenhouse effect and other regulated and unregulated emissions that are injurious to human health. Therefore, it is important to search for alternative and sustainable energy sources for the sector in other to alleviate the environmental concerns with respect to CO_2 emissions, and to improve the air quality from engine emissions pollution and also to confront the current ballooning energy demand on fossil fuels.

Electric vehicles are being proposed by the future engine researchers as a viable alternative to fossil fuel powered vehicles. However, the challenges of battery disposal, battery charging outlets and the required advanced battery technologies are barriers that will potentially takes decades to resolve. On the other hand, Biofuels have attracted the focus of fuels researchers due to the facts that they are renewable (24). The European Union for instance has set a blending of biofuel target of 14 percentage by 2030 (25). Biofuels as a renewable energy source does not always contribute to the challenging incident of rising global temperature and the environmental concerns with respect to the increasing CO_2 emissions that confront the ballooning energy demand. Literature has established four distinct generations of biofuels (26). First generation biofuels are produced from food crops. The second-generation biofuels are produced mainly from ligno-cellulose feed stocks. The third one is produced mainly from algae biomass. Biofuels produced in the fourth-generation categories are usually from genetically engineered microorganism such as fungi, yeast, micro-algae, and cyanobacteria. Bio-ethanol is a typical first-generation biofuels for spark ignition (SI) engines (27, 28) due to the high-octane number (29), and the high oxygen content (30). However, because the first-generation biofuel is made of food crops, it has been blamed for the competing uses of land for food and the impacts of consumption on marginalised people in developing countries (31). The second-generation

biofuels produced from lingo-cellulose feed stocks without competition with food crops have received an increasing amount of attention recently (32). Bio-ethanol can be considered as a second-generation biofuel because it can also be produced from the bio-conversion of ligno-cellulose feedstock (28, 33).

Several authors have reported the limitations of Ethanol as engine fuel. It suffers from several set back, including high water solubility, high costs of productions, high volatility, and low energy density. Engine performance and emissions in cold start are issues due to its high heat of vaporization and low saturated vapour pressure at low temperature. Due to its miscibility with water, the cost of production, transportation, and storage is high (27, 34-37). This is the motivation for the extensive research for a substitute to ethanol as engine fuel. 2-Methyltetrahydrofuran (MTHF) is an organic compound with the molecular formula $CH_3C_4H_7O$. The molecular structure of MTHF contain a methyl group (CH_3) attached to the second carbon (C) of the tetrahydrofuran ring. The tetrahydrofuran ring is a five-member rings containing four carbon atoms and one oxygen atom. It is usually synthesized in limited quantity by catalytic hydrogenation of furfural, a chemical derived from renewable sources (corn cobs, sugar cane bagasse, oat hulls (38)). 2-Methyltetrahydrofuran also found applications as a higher boiling substitute for tetrahydrofuran as a specialty solvent. It also is used in the electrolyte formulation for secondary lithium electrodes and as a component in alternative fuels. It is a valued solvent for low-temperature reactions. 2-Methyltetrahydrofuran forms a glass, which does not crystallize, and is frequently used as a solvent for spectroscopic studies at −196 °C (39).

MTHF is considered for this research because the Department of Energy's Pacific Northwest National Laboratory, United State has developed a new cost-effective multi-step catalytic manufacturing process, to produce 2-methytetrahydrofuran (MTHF) from levulinic acid. This new cost effective production method is expected to greatly increase its use. in addition, the fuel is currently listed among the P- series fuel (which are blends of ethanol, butanol, and MTHF with higher alkanes, and are used to solve the cold start issues of pure ethanol fuels) by the US

department of energy (38). The breakthrough recorded in the production process of MTHF were equally reported by science and nature in 2007 (40-42) and by Yuriy et al. in 2009 (41). MTHF has comparable latent heat of evaporation 375.3kJ/kg similar to gasoline 373 kJ/kg. The volumetric energy density of MTHF (28.97 MJ/l) is much closer to gasoline (31.9 MJ/l). Its initial boiling point (80.3^0C) compares to ethanol (78^0C), makes it more practical as a liquid fuel for transportation (29, 43). Its mass density (854 kg/m^3 at 20°C) is higher than ethanol (790.9 kg/m^3 at 20^0C) and gasoline (744.6 kg/m3 at 20^0C) and the volumetric density and its flash point (-11.1^0C) is lower than MF (22^0C) and ethanol. Most significantly, they can avoid the engine cold-start and combustion stability issues associated to ethanol. The studies on the application of MTHF in SI engines are rather fewer. In 1988, Rudolph et al. found that gasoline with 10% MTHF has power outputs and CO, NOx, and NMHC emissions that most closely resemble pure gasoline in a PFI engine (44). Samuel et al. investigated the emission characteristics of a SI engine fueled with MTHF/gasoline blends with 60% MTHF and found that the blends exhibit much lower CO and HC emissions compared with gasoline (45). In DISI engine studies, both Christensen et al. and Thewes et al. have found that MTHF has worse knock resistance than gasoline (46, 47). A blend of 70% 2-MTHF with 30% di-butylether, was recognized as a fuel with optimum characteristics for diesel combustion (48, 49). Janssen et al. (50) equally identified a blend of 2-MTHF with di-n-butylether as a fuel with optimal characteristics for diesel combustion. In this research study, using the split fuel injection strategy and fuel injection pressures strategy the percentage of NOx emission was reduced by 8% and 3.5% for MTHF CP respectively. Both split injection and fuel injection pressure strategies were used to reduce engine knock tendency in the combustion of MTHF.

Cyclopentanone (CP) is produce by biomass pyrolysis of agricultural waste into furfural, which is then converted to cyclic ketone by aqueous hydrogenation. Cyclopentanone consists of a five-member carbonyl-containing ring. The oxygen atom (O) is attached to the central carbon atom (C) of the Cyclopentanone ring, forming a carbonyl group (C=O). The remaining carbon atoms

in the ring are bonded to hydrogen atoms. Cyclopentanone plays a significant role in the pharmaceutical industry. It is used as a starting material for the synthesis of various drugs, including anticonvulsants, tranquilizers, and analgesics. For instance, cyclopentanone derivatives are used in the production of barbiturates, which are effective in treating seizures and anxiety disorders. The compound's ability to undergo various chemical transformations makes it a valuable intermediate in drug synthesis (51).

While both furan and cyclopentanone contain five-member rings, they differ in their composition and functional groups. Cyclopentanone was considered for this research as engine fuel because of its excellent fuel properties. The fuel is a colourless liquid with low toxicity and has similar specific properties to gasoline and ethanol. It is oxygenated with an oxygen content of 19.05% and it has an H/C ratio of 1.6. Cyclopentanone has a volumetric density of 0.9487 g/cm^3, much higher than that of gasoline and ethanol [40]. Doustdar et al reported that the blend of cyclopentanone in diesel, improved the density and the surface tension of the fuel but reduces the fuel viscosity, lubricity and calorific value. Investigating the combustion behaviour of cyclopentanone in compression ignition engine reported longer ignition delay of the cyclopentanone-diesel blends and increase gaseous emission of CO and THC and less NOx emission compared to the conventional diesel fuel combustion (52). This is the first study where the potential of CP as engine fuel is being exploited and critically investigated. Report of various engine test conducted on CP and MTHF as engine fuels will be documented in chapters 4, 5 and 6 of this thesis write up.

1.2 Objectives and Approaches

This research work is aimed at assessing the feasibility of using MTHF and CP in a DISI engine. The following are the specific objectives of the author's PhD study:

- Effect of engine load, air fuel ratio and fuel injection pressure on the combustion and emissions of MTHF and CP compared to MF, Ethanol and Gasoline in a DISI engine.

- Effect of spark timing, fuel injection timing and the split injection timing on the combustion and emissions of MTHF and CP in a DISI engine.
- Combustion and emissions of MF20, MTHF20 and CP20 compared to MF40, MTHF40 and CP40 in a gasoline fueled DISI engine.

The novelty of this thesis is the detailed combustion and emission analysis of a DISI engine fueled with two novel biofuel candidates, MTHF and CP. The investigation of the total HC emission speciation and the unburnt furan components in the emissions of MF20 and MTHF20 is a new studies that add to the novelty of this work.

1.3 Research Outline

This research study is focused on the combustion characteristics and emissions of 2-methyl-tetrahydrofuran (MTHF) and Cyclopentanone (CP) in a DISI Engine. Engine combustion characteristics evaluated in this report includes heat release rate, Engine in-cylinder temperature and pressure, Combustion phase, Engine operational efficiencies and Specific fuel consumption. Overall, these factors collectively influence the engine performance and emissions behaviour. A Ricardo wave model was used to calculate the cylinder temperatures. The impact of the combustion of the pure and blends fuels on PM emissions were measured and compared with gasoline using DMS500 particle sizers, regulated emissions of CO, NOx and HC were measured and compared to gasoline. Split injections and retarded spark timing were used to regulate the NOx emissions. The knock mitigation effect of MTHF was regulated through retard spark timing and split injection process.

1.4 Thesis Outline

This thesis is made up of seven chapters that is devoted to the study of MTHF and CP combustion in modern DISI engines. A brief overview of each of the followed chapters is presented below.

Chapter 2-Literature Review

Literature relevant to this study are reviewed in this chapter. GDI technology in modern engine system, combustion, and emissions of MTHF and CP and other furan-based fuels in DISI engines, are discussed in detail. Basics review of literature of gasoline and Ethanol and 2-Methylfuran fuels were equally undertaken since the three fuels are used in this study as the benchmark fuels.

Chapter 3- Experimental Setup

This chapter describes details the information about the engine instrumentation set-up for the study. The chapter equally provides key information about data acquisition and recording system along with the description of the single-cylinder research engine and the emission analysers. The procedures for data analysis using relevant software and basic calculations are discussed.

Chapter 4- Combustion of 2-Methyltetrahydrofuran and Cyclopentanone Compared to 2-Metylfuran and Ethanol in a GDI Engine

This chapter examines the sensitivity of 2-metyltetrahydrofuran (MTHF) and Cyclopentanone HJ(CP) to various engine parameters. In particular, engine load, relative AFR, and fuel injection Pressure. 2-Metylfuran, Ethanol and Gasoline were used as the base fuels for this study. The experiment was undertaken at MBT timing and fuels specific MBT/KLSA timing. The increase in oxygen content of each fuel is shown to give rise to improve combustion and emissions performance. The novelty is that MTHF recorded favourable fuel consumption compares to MF and ethanol. and Cyclopentanone displayed improve Peak cylinder pressure and spark advance flexibility compared to Ethanol and MF.

Chapter5- Modern GDI Combustion Modes Using 2-Methyltetrahydrofuran and Cyclopentanone.

Combustion and emissions of 2-Metyltetrahydrofuran and Cyclopentanone was investigated in a DISI engine using the split injection strategies. The effectiveness of split-injection strategies when fueled with Cyclopentanone and 2-Metyltetrahydrofuran are compared to 2-Methylfuran, Ethanol and gasoline. The gains in performance and emissions are examined whilst varying the second injection timing at intermediate and peak load. The spark sensitivity of each fuel were equally investigated in this chapter.

Chapter 6- Combustion of Blends of 2-Methlytetrahydrofuran and Cyclopentanone in gasoline in a GDI Engine.

Combustion and emissions study of volumetric blends of MTHF20 and MTHF40 along with CP20 and CP40 were undertaken in this chapter and the result compared with similar volumetric blends of MF20 and MF40 and neat gasoline. The results of the combustion of MTHF20 and CP20 are compared with that of MTHF40 and CP40. HC speciation for the combustion of MF20 and MTHF20 was evaluated using the Gasmet FTIR. Most significant study in this chapter is the measurement of the unburnt furan species in the combustion of MF20 and MTHF20.

Chapter 7- Summary, Conclusions and Future works.

This chapter provides summaries of the key findings in the research work conducted followed by Conclusions drawn from each section of the thesis and the details recommendations for future work.

CHAPTER 2

LITERATURE REVIEW

This chapter contains a detailed review of relevant pieces of literature on the thesis. The review is scope on GDI technology, productions and applications of furan based fuels and Cyclopentanone, the health and environmental implications of their applications and their combustion and emission characteristics. The background knowledge and the review of literature required by the author to carry out this research study were documented in this chapter. The major area of review includes GDI technology in modern engine systems, combustion, and emissions of furan based fuels and Cyclopentanone in a GDI engine, and discussion of biofuels as alternative engine fuels. Basics review of the literature on gasoline and Ethanol fuels was equally undertaken since the two fuels were used in this study as the benchmark fuels. The chapter concluded by summarising the major factors in the reduction of the regulated and the unregulated gaseous emissions most especially regulations of engine gaseous and particle emissions using biofuels. The author is the first to study the engine combustion and emissions behaviour of neat Cyclopentanone and 2-Methyltetrahydrofuran as engine fuels. The results of several studies on the fuels indicates that Cyclopentanone (CP) shares major semblance in engine performance and emissions characteristics with Bioethanol. While the results of engine combustion on neat 2-Methyltetrahydrofuran (MTHF) show that the fuel shares a high-level correlation with gasoline but with improved emission performance index compared to gasoline.

2.1 GDI Engines

Gasoline direct injection (GDI) engines operate by injecting fuel directly into the combustion chamber and can provide significantly improved fuel efficiency. The gains in fuel efficiency and ability to produce more power are achieved through the higher compression ratios associated

with charge cooling. In addition to precise control over the amount of fuel and injection timings, which are varied according to the load condition (53). The port fuel injection (PFI) system as compared to the carburettor system has some advantages, which include lower exhaust emissions, increase volumetric efficiency, low specific fuel consumption, decreased noise level, and increase drive comfort (54). However, it was established that the port fuel injection system could not meet up with the high expectation for continuous improvement in performance, fuel economy, and the ever-increasing stringent emission legislation (55). The GDI engines give a number of features, which could not be realised with port-injected engines. In conjunction with computerized engine control units (ECU), a gasoline direct injection system can deliver a range of flexible engine timing capabilities (53, 56). The GDI engine has improved accuracy of air/fuel ratio during dynamics, avoids fuel wall film impingement in the manifold, reduces throttling losses of the gas exchange by stratified and homogeneous lean operation. The GDI engine equally has higher thermal efficiency in stratified operation by precisely controlling the injection of fuel into the combustion chamber, and increased compression ratio and lower heat losses. In the GDI engine, there is an improved fuel consumption of about 35% compared to the PFI engine and by extension reduced CO_2 emissions (57). Other merits of the GDI engine are fast heating of the catalyst due to injection during the gas expansion phase, increased performance, and volumetric efficiency due to cooling of air charge, better cold start performance, and better drive comfort (58-60). Researchers have also indicated that GDI is the much sought after engine that combines the Specific power of the gasoline engine with the efficiency of the diesel engine. GDI exhibits the Brake Specific fuel consumption (BSFC) approaching that of a diesel engine with the operating characteristic and specific power output of the SI engine (59). Gasoline direct injection (GDI) is gradually assuming the mass production status. Fuel economy up to 35% is claimed, at urban driving conditions. It also reduces HC emissions at a cold start by using stratified charge combustion (61). Gasoline Direct Injection engines have seen several trends in their manufacturing and development in recent years, driven

primarily by a combination of regulatory requirements and technological advancements.Some of the current trends in the manufacturing of GDI engines includes, downsizing and turbocharging, higher injection pressures, dual injection systems, advanced engine management systems, emission control technologies and hybridization and electrification (62-64)

2.1.1 Mixture Formation and Combustion System in GDI Engine

It is important to recognise the phenomena occurring inside the GDI engine cylinder which ultimately leads to the increase engine efficiency, improve solutions to ecological issues and decrease in fuel consumption. The two most common methods of preparing air-fuel mixture in the gasoline engines is in-cylinder and out-cylinder. While the mixture in the engine with carburettor and port fuel injection is prepared out-cylinder, mixture in the gasoline direct injection engines is prepared in-cylinder (65) These phenomena are illustrated in figure 2.1.

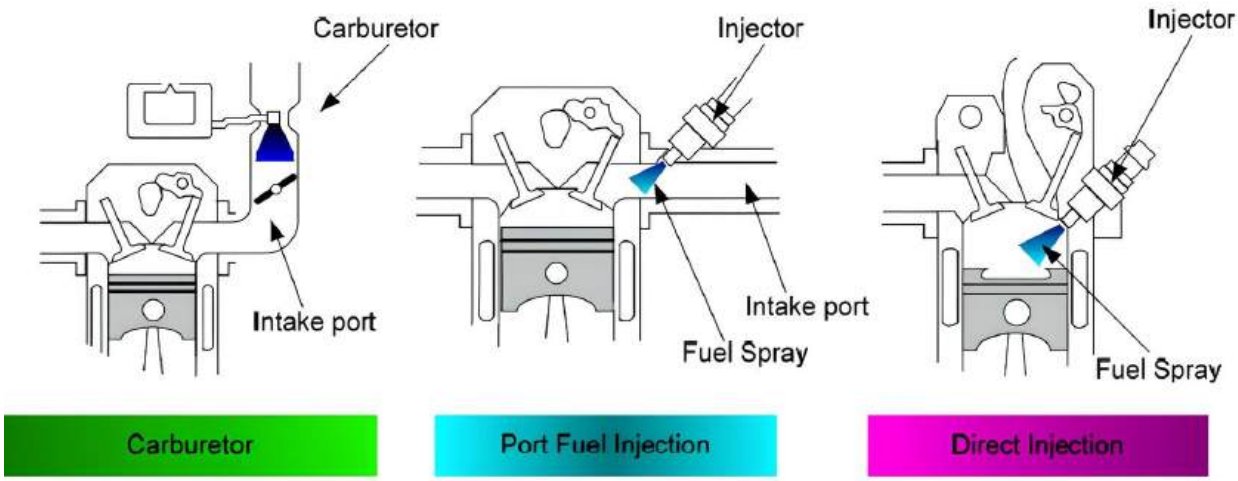

Figure 2.1 The mixture formation systems in the gasoline engines [32].

In the GDI engine, fuel is fed to the injector by a common rail (CR) technology which is able to provide injection pressures well beyond 100bar and fine atomisation, featured with a droplet Sauter mean diameter (SMD) not higher than 20µm. SMD is defined as the diameter of the droplet having the same surface-to-volume ratio as that of the overall spray (66). Only the air flows from the open intake valve are admitted to the cylinder during the induction stroke. The direct injection of fuel into the cylinder makes it possible for the efficient control of the

injection process and may ensure late injection during the compression stroke when the intake valves are closed. The acting of the intake system as a pre-vapourising chamber is an advantage in the PFI engines (58, 67-69). In GDI engines, there is a lack of time for fuel vapourisation, as a result, the fuel is injected into the cylinder at a very high pressure to help the atomisation and vaporization process. The duration for injection timing is little, and advanced injection timing causes piston wetting, and retarded injection timing decreases the sufficient time for fuel-air mixing(69, 70). The liquid film formed in the port area of the intake valve in PFI engines causes delays in fuel vaporization, especially during cold start, it is necessary to increase the fuel amount for the ideal stoichiometric mixture. Increasing HC emissions result from this "over fuelling" during cold start. Alternatively, in a GDI engine, the problems such as increasing HC emissions may be avoided by injecting the fuel directly into the combustion chamber and giving the excess fuel to the engine (56, 71). Additional advantages of (GDI) engines over the PFI engine is the improved cold start performance due to their ability to precisely control fuel metering, resulting in lower mixture enrichment during the cold start. In (GDI) engines the air/fuel mixture can be homogeneous or stratified depending on the working condition of the engine. In the homogeneous air/fuel mixture, AFR is fairly uniform in the combustion chamber volume. The stratified air/fuel mixture ensures an AFR space gradient, richer in the volume near the spark plug and progressively leaner as the distance from the spark plug increases. Both the homogeneous and the stratified charge conditions are attained through the fuel injection timing. The homogeneous charge can be obtained by an early injection, actuated at the beginning of the air induction phase, so as to allow adequate evaporation and mixing of fuel in conjunction with the air motion promoted by the inlet ducts geometries. Generally, such a condition is promoted at high load operation (66). The stratified charge (late injection) actuated during the upward piston stroke of compression with an overall lean mixture for low load and low-speed conditions. Moderate lean charge conditions allow load control without throttling, with a beneficial effect on fuel economy. A remarkable benefit of stratified charge is the rich mixture

near the spark plug gap (this is created by injecting a higher concentration of fuel compared to the rest of the chamber through a careful timing and positioning of the fuel injector ensuring that a denser fuel air mixture is present around the spark plug during the ignition process) which ensure stable ignition and prevents misfiring (61, 66).

2.1.2 Fuel injection strategy and common rail injection system in GDI Engine

Injection strategy is a key factor for engine performance in internal combustion engines. The twin factors of mixture quality and injection timing significantly constitute the fuel-air mixing procedure in the combustion chamber and determine the combustion characteristics of the engine (72). In a direct injection spark ignition engine (DISI), the fuel distribution near the spark plug is greatly influenced by the combustion stability (73). Therefore, the injection strategy in a GDI engine should be carefully determined to ensure a quality fuel-air mixture. Although various injection strategies are currently under investigation for gasoline engines, almost all of these strategies which include split injection and high-pressure injection have already been tried in diesel engines (74). The operating mode of a GDI engine for stable and efficient engine conditions depends on the engine's operating speed and load. The three basic operating modes in a GDI engine are the stratified charge (late injection) with an overall lean mixture for low load and low-speed conditions (61). At partial load conditions, GDI engines operate in stratified charge conditions or in homogeneous mode with a lean mixture and un-throttled (58, 61). In stratified charge conditions, fuel is injected into the cylinder just before the spark plug ignites (late injection). The air/fuel (A/F) ratio distribution in the cylinder is not uniform and the mixture in front of the spark plug is rich, in other places is lean. The cylinder A/F ratio is generally lean and the A/F ratio can access until 40/1 (75). This operation provides significant improvements in fuel economy. Sjoberg and Reuss (76) applied stratified combustion to reduce NO emissions while maintaining high combustion efficiency and stability. GDI engine is operated in homogeneous mode in stoichiometric with slightly reach conditions at high load and speed, this engine gives a better power output (77). The engine can be operated

at a very lean engine condition with an air-fuel ratio exceeding 100 and fully un-throttled operation is possible in this charge mode conditions, but the engine is throttled slightly in this zone and the air-fuel ratio is controlled for the possible introduction of a large quantity of Exhaust Gas Recirculation (EGR) and to supply the vacuum for the brake system. Early injection or homogeneous charge is the fuel injection during the intake stroke to provide a homogeneous mixture (75). Lean combustion is generally considered as a timely solution to the more stringent environmental regulations and global weather concerns in the new era. However, the instability associated with the lean flame significantly keeps the lean combustion technique from being widely accepted as a major combustion technique for general applications (78). A homogeneous mode in stoichiometric conditions is preferred for higher load conditions (78). In the homogeneous mode, the engine is operated under stoichiometric or a slightly rich condition at full load. During operation with a homogenous charge, the adjustment of engine load is done by throttling while during operation with stratified charge, the engine runs with unthrottled conditions, and the engine load is adjusted by fuel/air equivalent ratio (77). The early fuel injection in homogenous operation cools the intake charge as a result of the evaporation of the fuel in the cylinder. There is a consequential improvement in the compression ratios and the volumetric efficiency as a result of the cooling effect and thus higher torque is obtained (79, 80). In the GDI engines, knock is less likely to occur at low and medium loads because only air is compressed during these conditions (81). At full load, early injection of fuel into the cylinder cools the incoming air charge, reducing its temperature and consequently decreasing the tendency for knock to occur. The stratified-charge modes (late injection) and homogeneous (early injection) are shown in figure.2.2. Spray-guided, wall-guided, and air-guided combustion systems are the three modes of combustion in stratified operation, to form an ignitable mixture near a spark plug at the instant ignition (82). The distinction between the different concepts are shown in figure 2.3. This distinction is based on the used method with which the fuel spray is transported near the spark plug (58, 83, 84). The spray-guided technique theoretically has the

highest efficiency. In this technique, systems charge stratification results mainly from the spray dynamics, with very limited contribution from the interaction with the surface of the piston cavity and the bulk air charge motion.

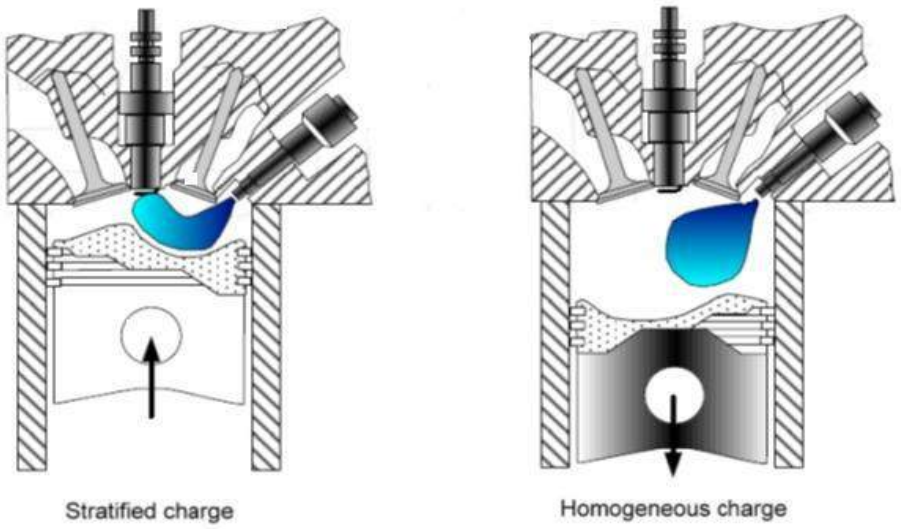

Figure 2.2 Stratified charge and Homogeneous charge mode (56).

The spray-guided combustion process requires advanced injector systems such as piezo injection. The fuel is injected near the spark plug where it also evaporates. Spray-guided combustion systems have the unique benefit of increased stratified operation region, reduced wall wetting, and less sensitivity to cylinder-to-cylinder variation less sensitive to in-cylinder airflow and reduced raw HC emissions. Reported disadvantages are spark plug reliability (fouling) and poor robustness (high sensitivity to variation in ignition and injection timing) (56). In Wall guided systems the stratification process is based mostly on the interaction between the fuel spray and a specially shaped piston surface. When the fuel is injected on the piston surface in a wall Guided combustion system, it does not completely evaporate and, in turn, HC and CO emissions, and fuel consumption increase. To ensure a stable charge stratification a short distance is maintained between the spark gap and the injector tips, as well as a short time interval from injection start and spark ignition, but the related short time available for mixture preparation has negative consequences on soot and HC production. At some cost on stratified

charge stability, the process of mixture preparation can be improved allowing a greater time interval between injection and ignition events and increasing the distance between the injector tip and the spark plug electrode. Wall-guided systems adopt this approach locating the spark plug in the central position while the injector is housed inside position (58, 66).

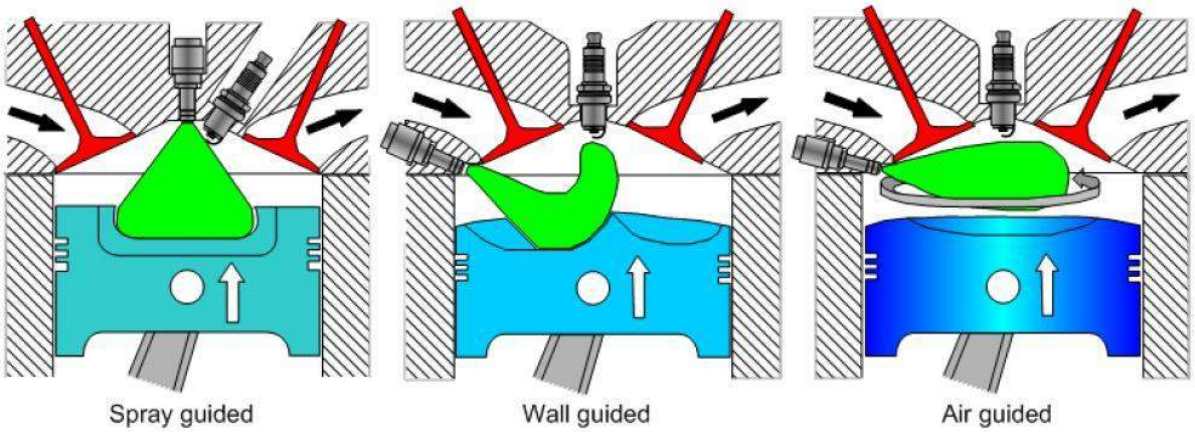

Figure 2.3 Scheme of the different Injection systems in GDI Engine (85).

At the same time, the piston top is specially shaped or is provided with a bowl or cavity facing the injector: the injection event promotes an air flow, directed toward the piston cavity, induction of the spray droplets so as to avoid significant impingement and wetting and guiding them during their evaporation along the cavity surface to reach the spark gap with the AFR conditions suitable for ignition. In air-guided systems, charge stratification is pursued based on the fuel injected into the airflow, which moves the fuel spray near the spark plug. The spark plug and the injector are still in central and side positions, respectively. The airflow is obtained by inlet ports with special shapes and airspeed is controlled with air baffles in the manifold. In this technique, fuel does not wet the piston and cylinder. Most stratified-charge GDI engines use a large-scale air motion (swirl or tumble) as well as a specially shaped piston surface in order to keep the fuel spray compact and to move it to the spark plug (66). In systems with two inlet valves, if allowed by the valve train mechanism, a swirl could be induced by the deactivation of one of them. Since charge stratification depends mainly on on-air motion in the cylinder and not

on spray impingement, there is the advantage of avoiding HC emissions related to fuel wetting of the piston surface.

2.2 Biofuel as alternative fuels

The upsurge in consumption of fossil fuels with the growing economies and the nearing depletion of such fuels has prompted a worldwide probe for their alternatives (145-148). Some of the main reasons for the increasing consumption of Biofuels as alternative fuels are detailed in Table 2.1. Future power engine researchers believe that electric vehicles shall be the ultimate solution to the current challenges of the fossil fuel, however the challenge of battery disposal, charging the battery outlets and the required advanced battery technologies are barriers that will potentially takes decades to resolve (86). On the other hand, Biofuels have emerged as a substitute for fuel oil, especially for oil importing countries. The most important advantage of these fuels is that they are renewable and are being seen as maintainable sources of energy. Some studies have also pointed out that biofuels help minimise environmental emissions (87, 88) Among liquid fuels, there are numerous types of biofuels such as methanol, ethanol, diethyl carbonate (DMC), methyl tertiary butyl ether and alkyl esters of fatty acids, and they can be used either individually as fuels or for blending in petrol as well as in diesel. Historically, bioethanol was utilised industrially in Germany and France as early as 1894 (89). In 1925 Brazil started to use it as a transportation fuel. Its use as fuel was common in Europe and the United States until the early 1900s. However, due to its high production cost, it was ignored especially after the World War II until the oil crisis of the 1970s (90). In the last three decades, the use of bioethanol has gotten more attention as an alternative transportation fuel. Several countries such as Brazil and the USA have long promoted domestic production of biofuels.

There are currently many types of biofuels been used in compression ignition engine as well as in spark ignition engine. These fuels are mostly ethanol, biohydrogen, biodiesel and synthetic fuels. These biofuels are used either individually as fuels or for blending in gasoline and diesel.

Table 2.1 Fossil Fuel Problems and Biofuel Advantage (87, 91-96).

S/N	Challenges of Fossil fuel Consumption	Factors that Promote Biofuels Consumption
1	Burning of fossil fuels and the emissions of Greenhouse gas which exceeded the rate that can be deal with naturally by the planet	The net greenhouse gas emissions by Biofuels is generally low.
2	Photochemical smog Pollutants.	Low Hydrocarbon emissions for most biofuel combustion.
3	Exponential growth of the global energy demand	Biofuels considered as additional source of energy
4	Emissions from the combustion of Fossil fuels causes Carcinogenic, methanogenic and teratogenic effects	Low Hydrocarbon emissions for most biofuel combustion.
5	Acid rain occasion by sulphur constituents	Biofuels comprises of little or no sulphur
6	Rising costs of fossil fuels above the local inflation rates	Biofuels is considered an alternative option for consumers.
7	Fossil fuels are Non-Renewable Energy	Biofuels are renewable.
8	Negative environmental impact	Biofuels have less environmental impact.
9	Macro production of Fossil fuel limits the control on productions to a small number of states and companies (cartels).	Biofuels can be produced on micro scale from many sources providing income to poorer countries that have fewer natural resources.
10	Public loss of faith in nuclear power generation.	Biofuels may be seen as an environmental alternative to nuclear power.
11	Fossil fuels Legislation and taxation.	Biofuels may meet local tax breaks or legislative substitution targets

The oxygenated fuel such as methanol, ethanol, diethyl carbonate (DMC) and methyl tertiary butyl ether, (such as rice bran methyl ester, jatropha methyl ester, karanja methyl ester and peanut methyl ester) have been used as fuel additives. It is also used to raise octane range and to diminish the emissions of carbon monoxide and hydrocarbon in engines.

2.2.1 Biofuels Categorisation and Production

The increasing demand for fossil fuels to keep the modern machinery running is fast depleting the natural reservoir of the global fossil fuel, while simultaneously increasing the global warming and the pollutions to the environment.(97, 98). According to IEA report of 2022, the high-level consumption of the fossil fuels has resulted in the increase CO2 emissions to their highest ever level of 36.3 billion tonnes in 2021 (99). There have been four distinguished generations of Biofuels as indicated in figure 2.4. First generation of biofuel are produced from food crops, the second generations biofuels are produced manly from lignocellulosic feedstocks.

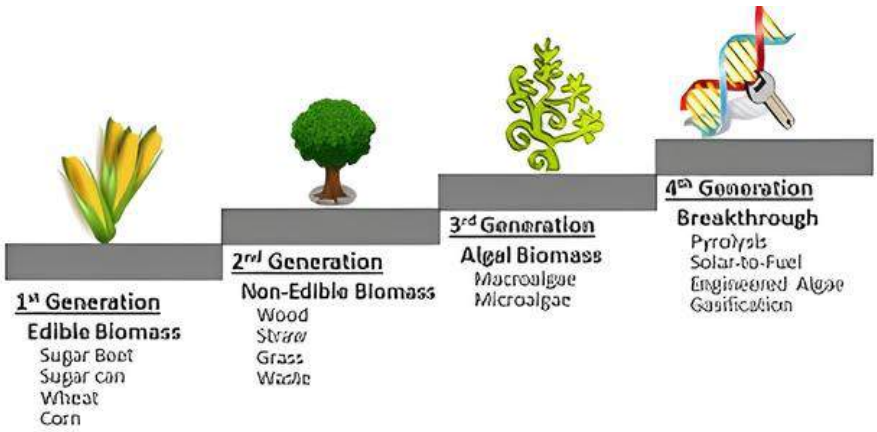

Figure 2.4 Biofuel Generation Classification adapted from Alawan et al 2019 (100).

The third generations of biofuels are produced mainly from algae biomass (101, 102). Biofuels produced in the fourth-generation categories are usually from genetically engineered microorganism such as fungi, yeast, microalgae, and cyanobacteria.

2.2.1.1 First Generation Biofuels

The first generations of biofuels comprise mainly of bio alcohols and biodiesels. Bio alcohols are produced by enzymes and micro-organism via the fermentation of sugars or starches or from cellulose. Bioethanol is a typical first-generation bio alcohol for spark ignition (SI) engine (100, 103) due to the high-octane number (29) and high oxygen content (104). However, because the first -generation biofuels are made of food crops, it has been blamed for the competing uses of land for food in developing countries (36).

Table 2.2 Different biofuel types produced from a variety of feedstocks (105-113).

Feedstock	Biofuel	References
Wheat waste	Biohydrogen	(106)
Sugarcane leaves	Biohydrogen	(107)
Sugarcane leaves	Bioethanol	(108)
Corncobs	Bioethanol	(101)
Rice straw	Biomethane	(110)
Distillery wastewater	Biomethane	(111)
Urban wastewater	Biodiesel	(112)
Sorghum	Biodiesel	(113)

2.2.1.2 Second Generation Biofuels

Second-generation biofuels are considered the more sustainable option since the feed stock is lignocellulosic-based biomass that is abundant, inexpensive, and usually consists of non edible plants (100). The idea behind the second-generation biofuels is to increase the number of biofuels that can be produced without using the biomass sources from Sugar or oil crops. It is

for this reason that lignocellulosic produced bio alcohols are classified as second generation of biofuels (114). There are quite some ways by which this can be achieved one of which is the Gas to Liquid (GTL) process via the Fisher Tropsch process. In this process a biomass such as wood can be gasified and turned into high quality liquid petroleum fuels(113). Gasified biomass can also be used to produce a range of bio alcohols including bioethanol. The second generation of biofuels are produced from lignocellulosic feedstocks without competition with food crops (115, 116). Bio-ethanol is also considered as a second-generation biofuel because it can also be produced from the bio-conversion of ligno-cellulose feedstock (117). However, in the application of engine ethanol suffers from some limitations, such as low energy density, water solubility and cold start difficulty (118, 119). Furan series fuels is considered as another combustion potential example of second-generation biofuels. 2-Methyl furan (MF) and 2-Dimethyl furan has high anti-knocking quality and clean combustion potentials (120). The volume energy density of Methyl tetrahydro furan (MTHF) and MF is higher than ethanol and close to gasoline (120, 121). Both MF and MTHF are almost insoluble in water making it a perfect blend for gasoline fuels.

2.2.1.3 Third Generation Biofuels

The third generations biofuels are known as ‘algae fuel’ or ‘oil algae’ since they are produced from the algae. Algae leads to the production of all types of biofuels such as gasoline, butanol, propanol, and ethanol with high yield approximately10 times higher than the second generations. Figure 2.5 explain the process of the micro-algae-based Biofuel production. Third-generation biofuels from microalgae have significant advantages that includes high growth rates with low cultivation times and high-quality arid land is not required (122). Several studies have explored bioethanol and Table2.3. Pre-treatment of lignocellulosic-based biomass for bioethanol production One of the major demerits of microalgae growth is the requirement for glucose, which is costly and can account for up to total cost of growth media. Mixotrophic cultivation of

microalgae is currently being explored since carbon source can include waste organic material (100).

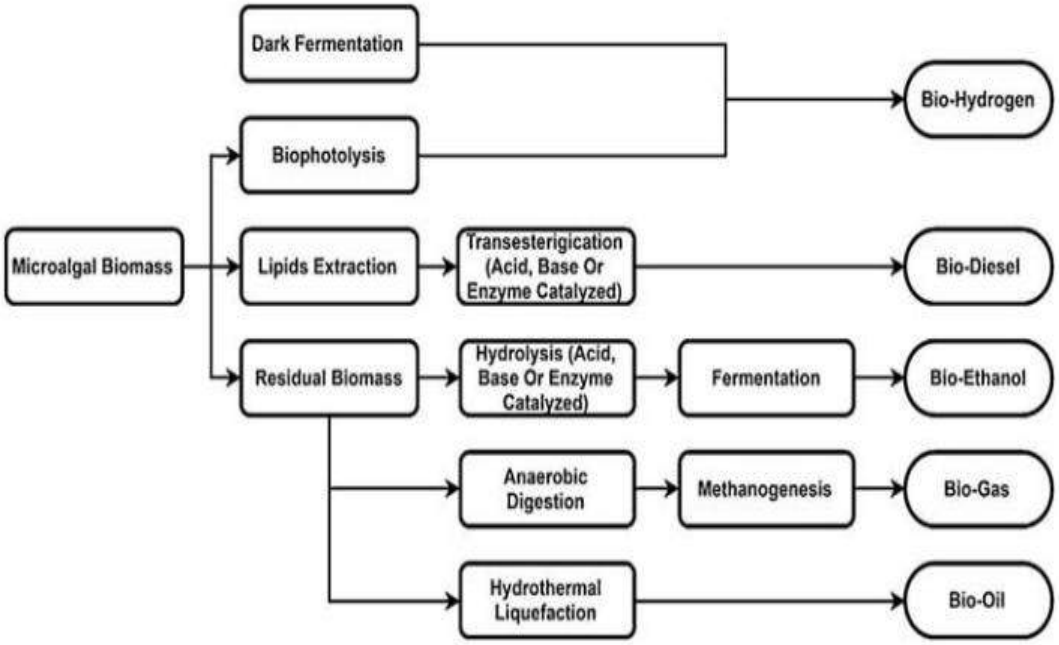

Figure 2.5 Schematic Diagram of Micro-algae-based Biofuel production (100).

2.2.1.4 Fourth Generation Biofuels

Fourth generation Biofuels are usually from genetically engineered microorganisms such as fungi, yeast, microalgae, and cyanobacteria. These modified organisms often have increased carbon entrapment capabilities with overall increases in cultivation, harvesting, and fermentation lipid yield (26). In addition to this, the genetic modification also aims to enhance light penetration by reducing size of the chlorophyll antennae, to reduce photo inhibition by pigment manipulation and to improve photosynthesis efficiency. This cultivation can occur either through a non-contained or contained system with the latter being more efficient albeit incurring high cost. The potential for these genetically modified organisms to be released from these systems is high since they are prone to leakage (123, 124). Owing to this, much of fourth generation biofuels productions processes have been limited to research laboratories because of the associated risks.

2.2.2 Biofuels Policies and Future Needs

Lower cost of Production and advanced technology to boost production should be the twain factors that should dominate the future and global Policies of Biofuels. Required efforts will need to focus on developing highly active and stable catalysts, higher efficiency reactors, continuous operation bioreactors, and minimising the required energy and Green House Gas (GHG) emissions as well as waste (100). Communities will be expected to shift toward green energy through government supports at various levels. The current estimated production price of biofuels/biodiesels does not encourage its adoption over petrol/diesel fuel (125). The absence of clear-cut policies on the part of the government is one of the main reasons for the poor performance of the Biofuel industries. By direct or indirect financial support, the government could create or expand policies to help marketing of Biofuels (87). On the other hand, possible reduction in Biofuel production can be active by tailoring future research from the current algae growth toward focusing more on increasing lipid contents due to its potential to increase the production yield of Biofuels. The third and fourth generations of biofuels are more promising choices because they do not involve in food fuel competitions. Advanced technology for Biofuel production is another valuable parameter that can be used to secure the sustainability of liquid fuel. Improved yield conversion systems and cost effectiveness are key essential tools for widespread commercial production of Biofuels. To achieve this goal, it is essentials to utilise metabolic engineering tools which improve biofuel both quantitatively and qualitatively through the modifications of existing scientific pathways. Extensive research will need to be conducted in the future to identifies more strategies for achieving higher yield more cost-effective production processes. Second and third generation biofuels is seen to have shown better result for greenhouse gas reduction. Overall, the future of liquid biofuel may best be improved by the integration of all the four generations (126).

2.2.3 Bio-ethanol fuels

Bioethanol has been considered as an attractive fuel for internal combustion engines due to its renewable nature which provides both security of supply and reduced net CO2 emissions. According to Dale et al, the attractive properties of Bioethanol include increased octane rating and enthalpy of vaporisation compared to standard gasoline, which allow for the use of increased compression ratios and the possibility of more favourable spark timings, increasing engine efficiency (127-130). Ethanol is the most consumed biofuel in the world and .is the main biofuel used for transportation. Brazil is the second largest bioethanol producer and the greatest exporter. The United States (the greatest producer) and Brazil are responsible for 70% of the world ethanol production(127, 131, 132). The sugar and ethanol industry in Brazil make up 2.3% of the Domestic Gross Product, generating 4.5 million jobs. Additionally, fuel ethanol represents almost 50% of the total fuel volume consumed by cars (and light vehicles) (127). Methanol is likewise one of the most promising engine fuels. It has taken special attention of fuel researcher and developer to use pure methanol and mixture of methanol and gasoline in various percentage ratio in petrol engine and vehicle for number of years. The one of the most common mixture are B85 (85% methanol and 15% gasoline) B10 (10% methanol and 90% gasoline). While methanol traditionally has been derived from fossil fuels (coal, petroleum an natural gases) advancements in technology now enable its production from renewable sources (biomass, wood, landfills and even the ocean), contributing to efforts to reduce greenhouse gas emissions and promote sustainability in the energy and chemical sectors (23). Ethanol can generally be produced from a wide variety of renewable feedstock, which can be roughly classified into those containing considerable amounts of readily fermentable sugars (sugar cane, sugar beets, sweet sorghum), starches and fructose (corn, potatoes, rice, wheat, agave) and cellulosic (Stover, grasses, corn cobs, wood, sugar cane bagasse). Figure 2.6 detailed the gross estimation of ethanol production costs in US dollars/liters from different feedstock and regions.

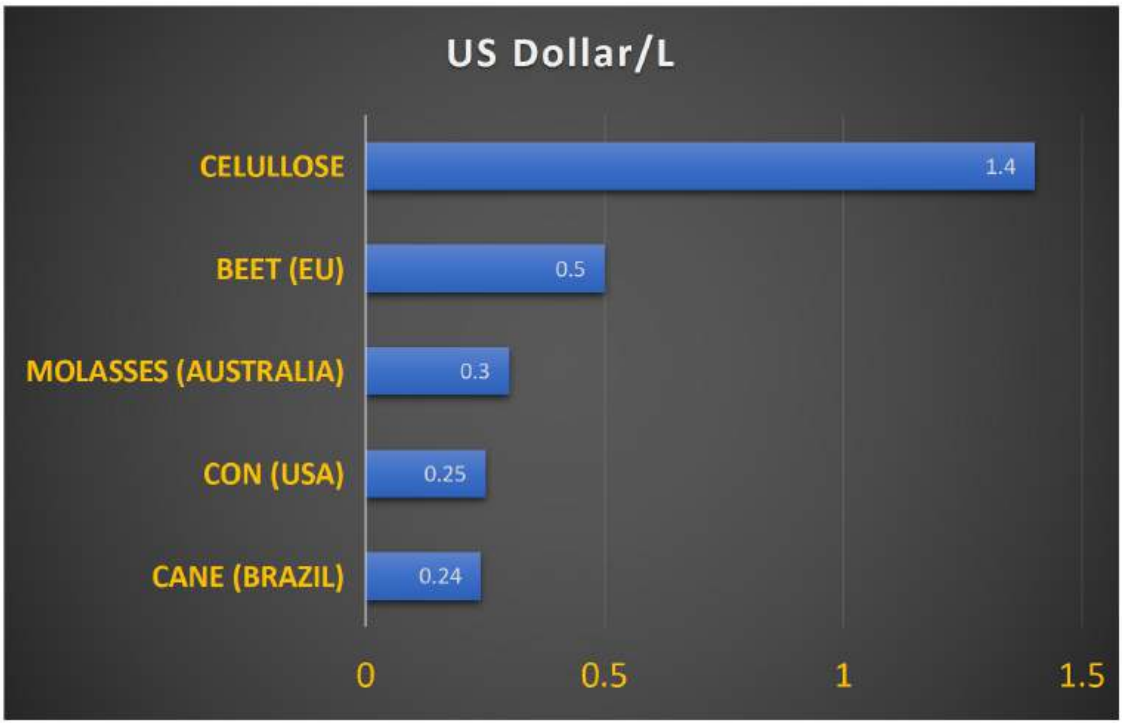

Figure 2.6 Gross estimation of ethanol production costs in US dollars/liters from different feedstock and regions, from several sources available in 2007 (132, 133).

Sugar cane, beet and sweet sorghum provide the simple sugars, as sucrose, glucose and fructose that can be readily fermented by yeasts (134-138). This differs from ethanol production processes based on starchy or lignocellulosic feedstock, where prior hydrolysis of polysaccharides is necessary with increased ethanol production costs (134, 139). A review of literature of engine combustion of Ethanol by Bata et al. (140), Tan at al.(141) and Fikret and Bedri (134) on different blend rates of ethanol–gasoline fuels in engines indicates that the ethanol could reduce the CO and UHC emissions to some degree. Wide flammability and oxygenated characteristic of ethanol is apparently the caused for the reduction of CO emissions. Separate study by Palmer (142) and Thakur et al (119), revealed that a blend of 10% of ethanol in gasoline could reduce the concentration of CO emission up to 30%. According to Devunuri et al. (143) and Ramadhas et. al. (144), the CO emission in ethanol gasoline blends is greatly influenced by the AFR. Using blended ethanol–gasoline fuel instead of neat of gasoline alone, especially under fuel-rich conditions, can lower NOx and CO emissions (132). However,

Manzetti et al. and Chao et al. (145-147), observed in their studies that blended fuels of ethanol–gasoline increases the emissions of formaldehyde, acetaldehyde, and acetone 5.12–13.8 times than those from gasoline. Although using ethanol as engine fuel will lead to the increases emission of the aldehyde, the damage to the environment by the emitted aldehyde in the combustion of ethanol is far less than the damage to the environment from the poly-nuclear aromatics emitted from combustion of gasoline. Therefore, higher percentage of alcohol in blended fuel can make the air quality better in comparison to gasoline(148-150). Annual world fuel ethanol production are detailed in Table 2.3.

Table 2.3 Annual World Fuel Ethanol Production (Mil. Gal.) (131).

Region	2016	2017	2018	2019	2020	2021	% of world Production
United States	15,413	15,936	16091	15778	13,941	15,016	55
Brazil	6,840	6,730	8060	8860	8,100	7,320	27
European Union	1,190	1,250	1300	1350	1,280	1,350	5
China	730	850	810	1010	930	870	3
India	260	250	430	460	540	850	3
Canada	460	460	460	497	429	434	2
Thailand	330	380	390	430	390	360	1
Argentina	240	290	290	290	210	270	1
Rest of World	587	644	709	655	650	820	3
Total	26,050	26,770	28540	29330	26,470	27290	

2.3 Electrofuels and its Production Processes

Electrofuels, also known as e-fuels are synthetic fuels created by harnessing renewable energy to combine hydrogen and carbon dioxide, providing a promising alternative to fossil fuel for reducing greenhouse gas emissions.They are manufactured using captured carbon dioxide or carbon monoxide, together with hydrogen obtained from water splitting (151). The most

common types are the synthetic gasoline, synthetic diesel, synthetic jet fuel, synthetic methane, green ammonia, and e-methanol. The production processes involved are currently energy-intensive and costly, primarily due to the high electricity requirements for electrolysis and the need for efficient carbon capture technologies. The development of more cost-effective and efficient production methods is essential to making e-fuels competitive with conventional fossil fuels (152). The first step in producing e-fuels typically involves the electrolysis of water to generate Green hydrogen (H_2). This process uses renewable electricity (solar or wind or Geo) to split water into hydrogen and oxygen (153). To create e-fuels, CO_2 is captured from the atmosphere or industrial emissions processes. This can be achieved through methods like Direct Air Capture (DAC) or Carbon Capture and Utilization (CCU). The hydrogen produced is then combined with CO2 to synthesize various e-fuels through chemical processes. The sustainability of e-fuels critically depends on how hydrogen is produced, how electricity is generated, and the supply route of the carbon source used in the process. When produced using entirely renewable electricity and sustainable H_2, e-fuels are highly sustainable. Moreover, utilizing CO_2 as a raw material for their synthesis ensures that their combustion does not generate additional green house gas emissions (154-156). Despite these potential benefits, the significant challenges to address on e-fuels are the costs and availability of raw materials necessary for large-scale production, and the localized pollution associated with their combustion (154, 157).

2.3.1 Applications and Merits of Electrofuels

Thousands of automobiles are driven on the streets of the world every day, releasing massive amounts of pollution into the environment. As a result, experts are striving to find a new source of power generation. Long-lasting and environmentally friendly (158, 159). Companies make electric cars as an alternative to engine cars, but the disadvantage of those cars is that they use batteries that have a short working cycle life and are very expensive. As a result, fuel cells were the best choice to be investigated and modified as research, then commercialized worldwide

prediction to meet global needs (160). The electrofuels can be easily stored and transported over long distances without any energy loss. The e-fuels can be used in today's engines and heating systems and thus allow the sustainable use of existing infrastructure in the transport, industry and heating sectors. In aviation industry, the e-fuels are seen as a key solution for decarbonising aviation, where battery technology is currently insufficient for long-haul flights. Synthetic fuels can help reduce the carbon footprint of maritime transport, a sector heavily reliant on heavy fuel oil. While battery-electric vehicles are increasingly popular in automotive industry, synthetic fuels could be used in internal combustion engines, extending the life of existing vehicle fleets while reducing emissions (157). The e-fuels allow the global potential of solar and wind power to be unleashed around the world. When produced using renewable energy and captured CO_2, these fuels can be nearly carbon-neutral, emitting only as much CO_2 during combustion as was captured during their production (161).

2.3.2 Challenges and Current Research and Development in Electrofuels

Battery electric vehicles (BEVs) are in high demand for future transportation systems, but their widespread adoption faces several challenges. These include low specific energy density of batteries, thermal management issues, potential chemical leakages, mechanical failures, short-circuiting risks, and inefficient battery management systems. Fuel cell-based hybrid electric vehicle technology is a promising future solution that can enable pure electric mobility with zero tailpipe emissions (162). Some of the current challenges to the e-fuels energy concepts includes high costs of production of e-fuels due to the high energy input required for electrolysis and CO_2 capture, making them less competitive with fossil fuels. The processes involved in making e-fuels are energy-intensive, leading to lower overall efficiency compared to direct use of electricity, such as in battery-electric vehicles. Ongoing research aims to improve the efficiency of electrolysis and CO_2 capture technologies, reducing the overall energy required and lowering costs. Various pilot projects around the world are demonstrating the feasibility of e-fuels, often focusing on aviation or heavy industry applications.

2.3.3 Future Outlook for the Electrofuels

The removal of fossil fuels from power sectors have proven to be an effective and successful mode of reducing emissions (43). The exploitation of low carbon energy sources such as wind, solar, sustainable biomass, and hydro-power has resulted in technological and economic advancements. However, electricity demands in the future are expected to increase as other sectors, such as industry and transport, shift towards electrification. Although electrification can aid, if low carbon electricity generation prevails, not all transport modes can be transformed, such as heavy transport. Thus, non-fossil based fuels will be necessary if a fully decarbonised transport sector is desired (163). E-fuels offer a promising pathway toward decarbonizing sectors that are challenging to electrify, such as aviation, shipping, and heavy industry. However, they face significant challenges in terms of efficiency and cost. Ongoing innovations in electrolysis, carbon capture, and synthesis processes are crucial for driving down production costs and improving efficiency. While e-fuels are unlikely to fully replace direct electrification in most sectors, they are a vital part of the future energy mix, especially in industries that require high energy density fuels. With increasing regulatory support and technological advancements, e-fuels could play a crucial role in achieving global climate goals by providing a sustainable, carbon-neutral alternative to traditional fossil fuels.

2.4 Furan based fuels

Furan fuels are produced from the hemicellulose fraction of biomass wastes like cornstalks, corncobs and the husks of peanuts and oats and thus do not compete with human food supply chains but convert waste into an energy source (164, 165). These fuels can be generated from the efficient conversion of five-carbon sugars such as xylose and arabinose into furfural and six-carbon sugars such as fructose and glucose into hydroxymethylfurfural (HMF). Furfural and

HMF be further processed to produce furan fuels (41, 166-170). Samples of furan fuels molecules are displayed in figure 2.7.

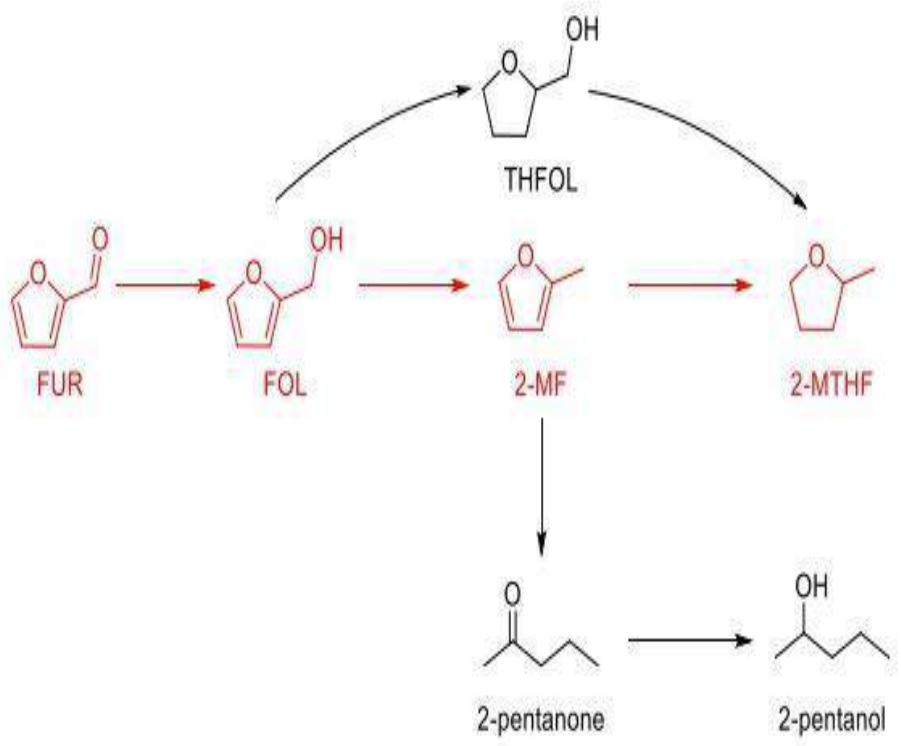

Figure 2.7 Reaction pathways for the conversion of Fur target 2-MF, 2MTHF and other by products (171).

Due to the potential of furan fuels as engine fuels, there have been many different studies of the combustion of furan (169, 172, 173) 2-methyl furan (174-177) and 2,5-dimethyl furan (174, 178-183). Two recent reviews have summarized trends in their combustion (184, 185). Other studies have reported on cyclic ethers including tetrahydrofuran (169, 174, 186-188) and 2-methyl tetrahydrofuran (169, 189-192).

2.4.1 2,5 Dimethylfuran Fuels (DMF)

2,5-dimethylfuran often abbreviated DMF is a heterocyclic compound with the formula $(CH_3)_2C_4H_2O$. The most common way to produce DMF is the hydrodeoxygenation (HDO) of 5-hydroxymethylfurfural (HMF) with H_2 in the presence of metal-based catalyst.

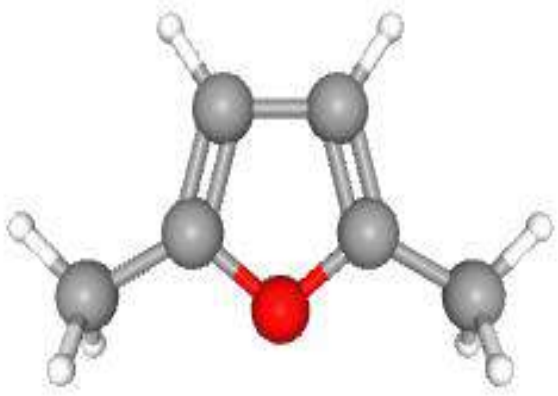

Figure 2.8 3D Conformer Molecular Structure of DMF (193).

A catalytic strategy for the production of 2.5-dimethlyfuran from fructose via intermediate HMF was proposed by Dumesic et al (194). Hoang et al (195) also propose a catalyst-based Synthesis of 2,5-Dimethylfuran from Carbohydrates. In 2019 Yong sun et al developed a multistep high yield route for the production of 2,5-dimethylfuran. In this multistep route, Cu-RU/C catalyst was developed to catalyse the conversion of HMF to DMF, giving 71% yield of DMF from 5wt%HMF at 220^0C UNDER 6.8 atm of H_2 (164) DMF yield of 96% was achieved by Nishirmura et al by carrying out the selective hydrogenation of HMF over the carbon supported palladium-gold (Pd-Au/C) in the presence of hydrochloric acid (196). Saha et al achieved the conversion of HMF to DMF with a high conversion yield of 99% by developing a bimetallic catalyst containing ZN and PD/C components for the conversion (197). Zu et al achieved an excellent conversion yield of DMF of 93.4% from HMF using Ru/Co_3O_4 as catalyst. Figure 2.8 displayed the 3D Conformer Molecular Structure of DMF.

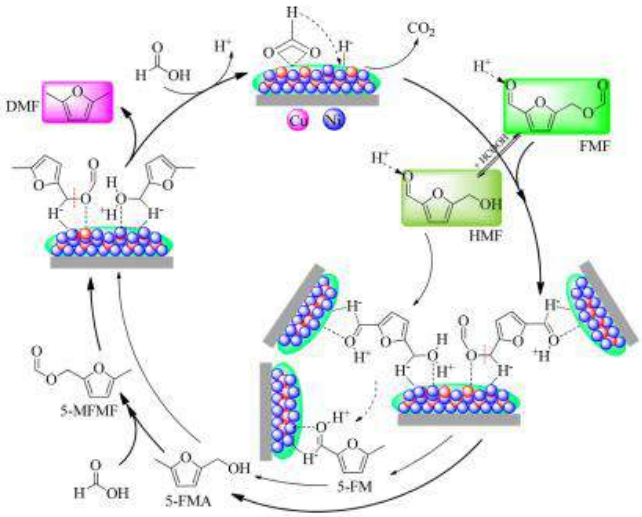

Figure 2.9 Proposed Reaction Pathways for the Conversion of FMF to DMF using Ni-Cu/SBA-15 as catalyst and Formic Acid as Hydrogen donor (164).

These several studies confirmed that noble metals such as PD, An, and Ru, are always good candidates for catalyzing HMF to DMF due to their high catalytic activity and selectivity. DMF has a number of properties that make it attractive as engine fuels (34, 198-200). The energy density is about 40% greater than Ethanol and comparable to gasoline(34, 201). It does not absorb water from the atmosphere because it is insoluble in water. It is chemically stable and require less energy for production compare to ethanol. The stoichiometric air/fuel ratio of dimethylfuran is 10.72 compared to ethanol at 8.95 and gasoline at 14.56. Indicated thermal efficiency of dimethylfuran is similar to that of gasoline (34, 200-203). Figure 2.9 is the Reaction Pathways for the Conversion of FMF to DMF.

2.4.2 2-Methylfuran Fuels (MF)

The production method for Methyl furan (MF) was independently discovered by Dumesic et al in 2007 (194) and Romain et al and Zhao et al in 2007 (42). A highly efficient method of converting fructose to MF were discovered by these fuel researchers as uniquely reported by Nature and Science. (41, 42, 194). The 3D Conformer Molecular Structure of MF is as indicated in figure 2.10.

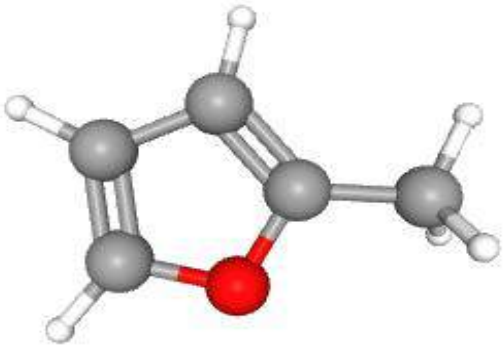

Figure 2.10 3D Conformer Molecular Structure of MF (204).

The selective oxygen removal was accomplished in two steps, the first stage was the removal of the three oxygen atoms through dehydration to produce 5-hydroxymethylfurfural (HMF) and the second stage was the removal of two oxygen atoms through hydrogenolysis to produce MF (205, 206) (34) the reaction sequence are as shown in figure 2.11. MF produce by this method is considered a renewable fuel because Fructose used in the production is abundant and renewable.

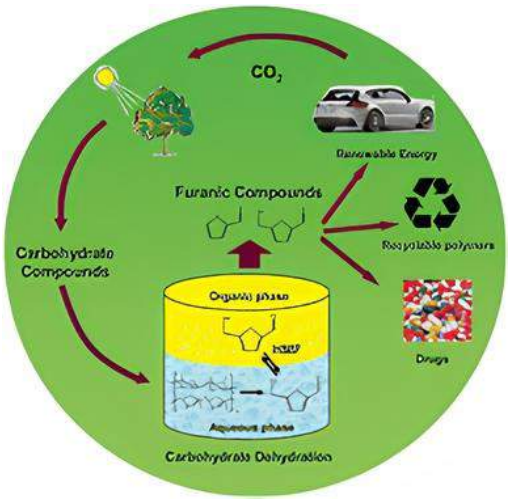

Figure 2.11 Process of Converting Carbohydrate to MF (194).

MF has properties that make it suitable as engine fuel, the initial boiling point of MF (63^0C) is much closer to gasoline (32^0C). Its density (913.2kg/m^3 at 20^0c) is more than that of gasoline at (744.6kg/m^3) and its flash point (22^0C) would overcome the challenge of the cold engine start problem and finally its higher latent heat of vaporisation (358.4KJ/kg) would result in high

engine power out at wide open throttle in a DISI Engine (34, 191, 207-209). The research octane number of MF (103) is higher than gasoline (96.8) (210) making it less susceptible to the engine knock phenomenon.

2.4.3 2-Methyltetrahydrofuran Fuels

2-Methyltetrahydrofuran (MTHF) is an organic compound with the molecular formula $CH_3C_4H_7O$(211). The molecular structure of MTHF contain a methyl group (CH_3) attached to the second carbon (C) of the tetrahydrofuran ring. The tetrahydrofuran ring is a five-membered ring containing four carbon atoms and one oxygen atom. The remaining carbon atoms in the ring are bonded to hydrogen atoms. The oxygen atom is bonded to the second carbon atom, and the second carbon atom is bonded to the methyl group and another hydrogen atom. The 3D Conformer Molecular Structure of MTHF is as shown in figure 2.12. Large scale production of 2-methyltetrahydrofuran (MTHF) is widely reported to occur in good yield from furfural or levulinic acid. Lignocellulosic biomass (corn cob, straw, oat husk, wheat bra and saw dust) mainly consists of cellulose, hemicellulose, and lignin, which can be transformed into a variety of functional platform molecules such as furfural (FUR), levulinic acid and 5-hyfroxymethyfurfural and aromatic molecule(171, 212). Among them, Furfural and levulinic acid were considered to be an important platform chemical in the production of MTHF(213) Furfural can be hydrogenated to produce furfurylalcohol (FOL), tetrahydrofurfuryl alcohol (THFOL) (214) Selective hydrodeoxygenation of furfural produced 2-methylfuran and 2-methyltetrahydrofuran (215, 216). 2-Methyltetrahydrofuran (MTHF), which can be produced from levulinic acid follows the reaction sequence shown in figure 2.11. The first step of the reaction is the conversion of the levulinic acid to α angelica-lactone preceded by the production of γ-valerolactone (GVL) and 1,4-pentanediol (PDO).

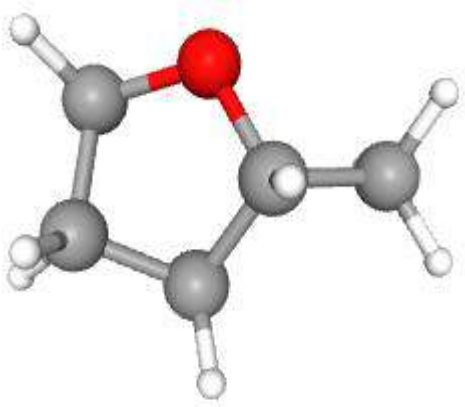

Figure 2.12 3D Conformer Molecular Structure of MTHF (211).

Subsequently, 2-methyltetrahydrofuran (MTHF) was produced from 1,4-pentanediol (PDO) and Levulinic acid was the final stage of production in the reaction network.(197, 217, 218) . This reaction network is as indicated in figure 2.13. 1,4-Dioxane was used with both noble metal (Pd-Re) (217)and non-noble metal (Cu-Ni) (219) catalyst to obtain high yield of MTHF (90%) from levulinic acid.

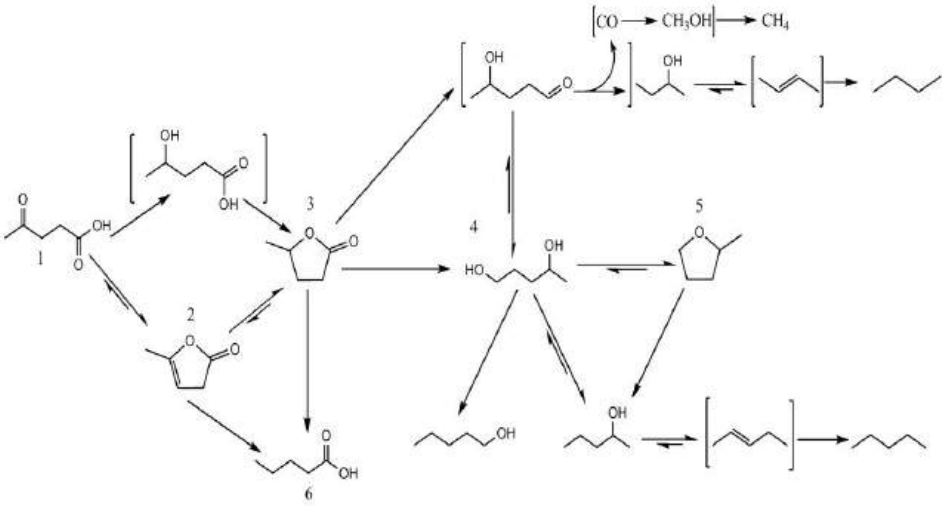

Figure 2.13 Levulinic acid (LA) to 2-methyltetrahydrofuran (MTHF) reaction (220)**.**

2-Methyltetrahydrofuran (MTHF) produced from levulinic acid is part of the oil-free ‘P Series fuels (221) as well as a fuel additive owing to its similarity to gasoline. MTHF is considered as attractive and competitive sustainable product for fuel industry due its low miscibility with

water, excellent stability, high boiling point and easy biodegradability (222, 223) . MTHF is hydrophobic making it more suitable as engine fuel than Ethanol. Despite its low octane number (88.2) compare to gasoline (96.8), MTHF has a higher heating value and a higher density leading to fuel consumption economy similar to ethanol (224). No engine modifications are required for the engine combustion of up to 70% MTHF blends in gasoline whereas only 10 vol % of ethanol in gasoline can be used without engine modifications due to its corrosive tendency (225, 226). MTHF is highly hydrophobic. It has a higher heating value, higher density, low flammability, and lower toxicity compared to bio-ethanol. These characteristics allow the blending of MTHF with gasoline up to about 70% (82).

2.5 Cyclopentanone Fuel

Cyclopentanone is an organic compound with the formula C5H8O. This cyclic ketone is a colourless, volatile liquid. Cyclopentanone can be prepared by the catalytic vapor-phase cyclization of 1,6-hexanediol or adipic esters (227) . Upon treatment with barium hydroxide at elevated temperature the adipic esters undergoes Ketonisation to give cyclopentanone. Its molecule contains 6 non-H bonds, 1 multiple bonds, 1 double bonds, 1 five-membered rings and 1 ketone (alphatic) (228-230). Cyclopentanone consists of a five-membered carbonyl-containing ring. The oxygen atom (O) is attached to the central carbon atom (C) of the cyclopentanone ring, forming a carbonyl group (C=O). The remaining carbon atoms in the ring are bonded to hydrogen atoms. The 3D chemical structure image of Cyclopentanone is shown in figure 2.14. The carbon atoms in the chemical structure of Cyclopentanone are implied to be located at the corners and hydrogen atoms attached to carbon atoms are not indicated. Each carbon atom is considered to be associated with enough hydrogen atoms to provide the carbon atom with four hydrogens. Cyclopentanone is a versatile compound used for the synthesis of fungicides, pharmaceuticals, rubber chemicals, and flavor and fragrance chemicals. Potentionally, it can be used for preparation of polyamides (231). While both furan and cyclopentanone contain five-membered rings, they differ in their composition and functional

groups. Furan contains an oxygen atom within the ring, whereas cyclopentanone contains a carbonyl group (C=O) attached to one of the carbon atoms in the ring.

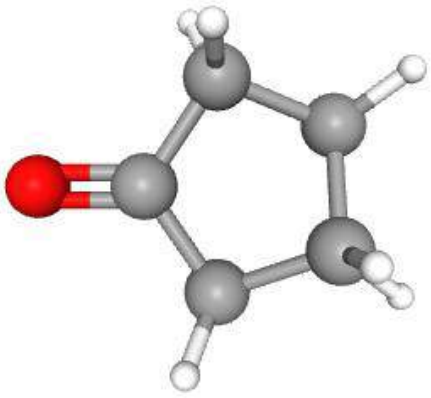

Figure 2.14 3D Conformer Molecular structure of Cyclopentanone (232).

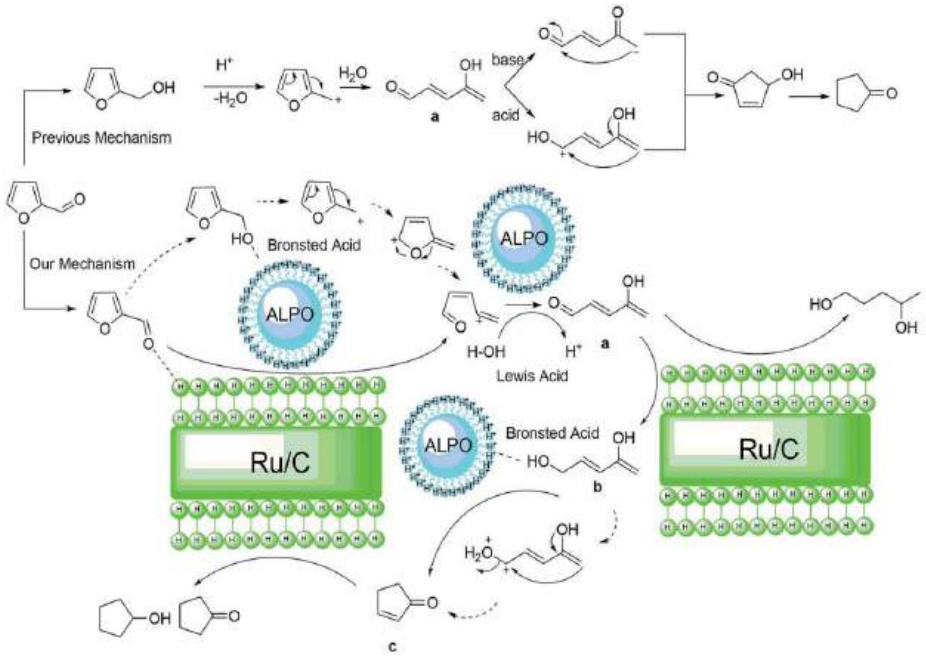

Figure 2.15 Mechanism for the conversion of furfural to Cyclopentanone (CPO) (233).

MF and MTHF are novel products from the hydrogenation product of furfural. Cyclopentanone (CP) another new novel hydrogenation product of furfural. Tao et al 2018 (233) developed a new effective method of high yield production of cyclopentanone from furfural. In this process as indicated in figure 2.15 furfural is firstly hydrogenated to furfuryl alcohol. If furfuryl alcohol undergoes a Piancatelli rearrangement. The product will be 4-hydroxy-2-cyclopentenone, which

will then undergo in depth hydrogenation and dihydroxylation to produce cyclopentanone (CP) and Cyclopentanone (CP) Although the combustion characteristics of many furan fuels have been widely reported, the existing literature on Cyclopentanone only focused on its production technology, there is still scarce literature on the combustion behaviour of CP. Cyclopentanone has some properties that make it contusive as engine fuel. The volumetric density of CP (0.948g/cm^3) is much higher compared to ethanol (789g/cm^3) (234). The heat of vaporisation of Cyclopentanone (433kJ/kg) and is higher than that of gasoline (373kJ/kg) (235). As reported by Heywood, the intake charge temperature is lowered by the higher heat of vapourisation (236). The higher heat of vapourisation of CP provide advantage in lowering the air intake charge temperature resulting in higher power density for CP in internal combustion engine. The stoichiometric air-fuel ratio of cyclopentanone is similar to that of ethanol and lower than that of gasoline and which can lead to higher engine power density. The auto ignition temperature of Cyclopentanone is (718K) much higher than that of gasoline (553K), indicating its excellent potential for resistant to engine knocking in spark ignition engine(235, 237).

2.6 Introduction to Spark Ignition Engine Emissions

Investigative study into the incident of smog in Los Angeles in 1940s lead the USA researcher Haagen-Smith to discover the links between the automotive exhaust emissions and the air pollution (238). Ever since, automotive emissions have been a major issue on government legislation across the globe and the automobile industries have strive assiduously to cope with the government tight policies on emission regulations through elaborate engine research. The exhaust out emissions gases from spark-ignition engine contain oxides of nitrogen (Nitric oxide (NO) and Nitrogen dioxide (NO_2) usually grouped together as NO_X), carbon monoxide (CO) and partially burnt and unburned hydrocarbon (HC). The relative compositions of these gases in the engine out emissions depend on the engine design and operating conditions. Piston blow by gases, and fuel evaporation and release to the atmosphere through bents in the fuel tank and carburettor after engine shut-down, are also sources of unburned hydrocarbons. The formation

of nitric oxide occurred throughout the high-temperature burned gases. NO formation during combustion involves complex chemical reactions between nitrogen and oxygen but the equilibrium is often not reached due to the high temperatures rapid reactions rates in combustion process. The higher the burned gases temperature, the higher is the rate of NO formation. As the burned gases cool down during the expansion stroke the reaction involving NO freeze, and leave NO concentrations far in excess of levels corresponding to equilibrium at exhaust conditions (239). Rich air mixture leads to the formation of Carbon monoxide during the combustion process also at high temperature products, even with lean mixtures, dissociations ensure there are significant CO levels. Later in the expansion stroke, the CO oxidation process also freeze as the burned gas temperature falls. The unburned Hydrocarbon emissions originates from different sources, for example, during the compression and combustion the increasing cylinder pressure forces some of the gas in the cylinder in to the crevices, or narrow volumes connected to the combustion chamber, the volume between the piston rings and cylinder wall are the largest harbinger for the unburnt mixture. Most of the unburnt air-fuel mixture escaped the primary combustion process because the entrance to these crevices is too narrow for the flame propagation to be initiated. This gas which leaves these crevices later in the expansion and exhaust processes, is one source of unburned hydrocarbon emissions. Another possible source is the combustion chamber walls. A quench layer containing unburned or partially burnt air-fuel mixture is left at the wall when the flame is extinguished as it approaches the wall. There are also some sources of unburned hydrocarbon which are believed to be, any engine oil left in a thin film on the cylinder wall, piston and perhaps on the cylinder head. The fuel hydrocarbon components can be absorbed by the oil layers, before and after combustion, making way for a fraction of the fuel to escape the primary combustion process unburned. The spark-ignition engine's exhaust gases contain three major types of pollutants in the following relative amounts: oxides of nitrogen, NOx (mainly NO and small amounts of NO2), 500 to 1000 ppm; carbon monoxide, CO, 1% to 3%; and unburned or

partially burned organic compounds, HC, 500 to 5000 ppm (as C1). In spark ignition engine the three main classification of particulate emission are soot, ash and metallic compounds (240). High injection pressure and clean injector condition are both essential for low particle emissions. Compared to gasoline, the particle emissions from ethanol combustion is less sensitive to the injection system, due to its higher volatility and diffusive combustion which produces less soot (11). One of the more important variables in determining emissions' levels in spark-ignition engines is the fuel-air equivalence ratio, (ϕ = 1/A, where A is termed the relative air-fuel ratio). In general terms, leaner mixtures yield lower emissions until the combustion quality becomes poor and the HC emission rises sharply. Richer mixtures yield low NO emission but steadily rising HC and CO emissions. Understanding the formation mechanism of these components may provide a grounded explanation of this behaviour.

2.7 Regulated and Unregulated Emissions in gasoline Engines

The internal combustion Engine emissions are classified as Regulated (NOx, CO, HC), Particulate emissions, and the unregulated emissions. The regulated emissions, are well documented and restricted by legislation, though, there are variety of other gases that are emitted from internal combustion engines unregulated. One of such is the carbonyl emissions (formaldehyde and acetaldehyde) which is not under emissions restriction by any country except California in USA (241).

2.7.1 Nitrogen Oxides Emissions

Nitrogen Oxides (NOx) emissions are mainly composed of NO molecules and a small amount of NO_2, in a typical ratio of 1 to 100. NO is one of the intermediate products of chemical reactions involving nitrogen and oxygen atoms and molecules, which occur at the high temperature. The formation of Nitric oxide (thermal) is fully explained by the mechanism of the stabilisation of atmospheric nitrogen in oxidizing atmospheres at a high flame temperature

exceeding 1573K or 1300 °C (242-244). Thermal NOx is generally produced during the combustion of both gases and fuel oils (245).

$$O + N_2 \Leftrightarrow NO + N \text{ ----------2.1}$$

$$N + O_2 \Leftrightarrow NO + O \text{----------2.2}$$

$$N + OH \Leftrightarrow NO + H \text{----------2.3}$$

When the combustion is under fuel-lean conditions and there is a rise in temperature, this will lead to an increase of NOx emissions due to increased oxygen radicals forming in the combustion process. However, when the combustion is under fuel-rich condition the oxidation reaction will involve the OH and H radicals (246, 247). High activation energies are required for the dissociation of oxygen molecules and the disengagement of the triple bond of nitrogen. This phenomenon causes the formation of thermal NOx to be largely dependent on the temperature, the degree of air to fuel mixing, the concentration of oxygen and nitrogen in the flame and duration of reaction occurred (248). The environmental problems caused by NOx are now worldwide issues due to the seriousness of ozone reactivity and the amount of formation of smog. NOx combines with water vapor in clouds to produce acid rain which pollutes clean water sources and corrodes metals used in our daily life. Acid rain also harms the growth of organisms in the lake and disturbs the balance of the ecosystem both on land and at sea. Apart from that, acidified soil is the also the result of acid rain and it causes damage to the root system of trees, disabling the nutrient absorption process and disrupting the natural process of photosynthesis (249). When NOx reacts chemically with other atmospheric gaseous compounds such as “Volatile organic compounds” (VOCs) under the sunlight, it will form smog. Smog is forefront to our environmental concerns as it reduces the visibility of surroundings and poses a health hazard to humans which includes irritation of eyes, respiratory and cardiovascular problems such as asthma and headaches(247, 250, 251). There are several factors which affect

the formation of NOx in the engine and they are listed below: The air-fuel ratio: plays a major role in determining the amount of emission of NOx as oxides of nitrogen are formed by the reaction of nitrogen in the fuel with oxygen in the combustion air. When the air to fuel ratio is greater than one which indicates that the combustion is in the lean condition, the fuel mixture has considerably less amount of fuel and excess amount of air. Engines designed for lean burning can achieve higher compression ratios and hence produce better performance. However, it will generate high amount of NOx due to the excess oxygen present in the air (252). Combustion temperature: is also one of the primary factors that influence the formation of NOx. The formation of NOx is directly proportional to the peak combustion temperature, with higher temperatures producing higher NOx emissions from the exhaust (253). The firing and quenching rates also influence the rate of NOx formation where a high firing rate is associated with the higher peak temperatures and thus increases the NOx emission. On the other hand, high rates of thermal quenching result in lower peak temperatures and contribute to the reduction of NOx emission (254). Engine parameters such as load and speed of engine also influence the NOx emissions from the exhaust. When the engine is running under lean conditions, it emits less NOx because lean combustion results in lower temperature which in turn reduces the formation of NOx. However, the nitric oxide (NO) emissions will consequently increase as the engine load increases. The effect of load becomes less significant when the engine is running close to stoichiometric air to fuel ratio. On the other hand, engine speed may increase or decrease the NO emissions as higher engine speed increases the burned gas mass fraction and thus offsets the peak temperature, depending on the exact engine conditions (247).

2.7.2 Carbon monoxide Emissions

Carbon monoxide (CO) is formed mainly under rich-mixture conditions but may be detected in small quantities also under lean conditions. With rich fuel mixtures, there is insufficient oxygen for the complete combustion of the fuel to carbon dioxide (Yuji and Tsuyoshi 1998). When a hydrocarbon fuel burns completely, the oxygen in the air combines with the hydrogen to form

water (H_2O) and with the carbon to form carbon dioxide (CO_2). If the burning is not complete, then some of the carbon atoms only combine with one oxygen atom rather than two, to form carbon monoxide (CO), a highly poisonous gas emissions of CO are therefore influenced primarily by the air-fuel ratio relative to the stoichiometric proportions. Fuel-rich combustion invariably produces CO, and emissions increase nearly linearly with the deviation from stoichiometric engine operation (255). At low engine loads, the air-fuel mixture is typically richer which can lead to incomplete combustion of the fuel, resulting in higher carbon monoxide emissions. As the engine load increases, the air-fuel mixture is adjusted to become leaner resulting in reduced carbon monoxide emissions (256). Various factors can influence carbon monoxide emissions in an engine, includes the engine design, combustion efficiency, fuel quality, and emission control systems. It's worth noting that at high temperature the interplay of various factors, such as air-fuel ratio, turbulence, injection timing, and fuel properties, also impacts CO emissions. Additionally, modern vehicles are equipped with catalytic converters that help reduce carbon monoxide emissions by converting it into carbon dioxide CO_2 a less harmful greenhouse gas. Catalytic converters typically use a combination of metals such as platinum, palladium, and rhodium as catalysts to facilitate the conversion of CO to CO_2. When the exhaust gases containing carbon monoxide pass over the catalytic metal the CO molecules adhere to the surface of the catalytic particles. The oxygen from the exhaust gas interact with the carbon monoxide molecules on the catalyst surface to break the molecule apart, releasing carbon. The release carbon atom then reacts with additional oxygen molecules to form carbon dioxide.

2.7.3 Carbon Dioxide Emissions

The increase in carbon dioxide's (CO_2) content and concentration in the air will increase the earth's surface temperature. As a result, enough ice will melt, leading to an increase in the oceans' level. This phenomenon is known as the "Greenhouse effect". Although, carbon dioxide is a harmless product of the combustion process to the human health, the CO_2 emissions from

the fossil fuels contribute significantly to increase global warming. As indicated in figure 2.16, the domestic transportation contributes 25.7% CO_2 to the within the European Union. The formation of carbon dioxide in spark ignition engine progresses from the complete combustion of all the carbon in the fuels. This requires an adequate supply of oxygen for the combustion process. The presence of sufficient oxygen allows for the oxidation of carbon to CO_2, while hydrogen (H) atoms in the fuel combine with oxygen to form water (H_2O).

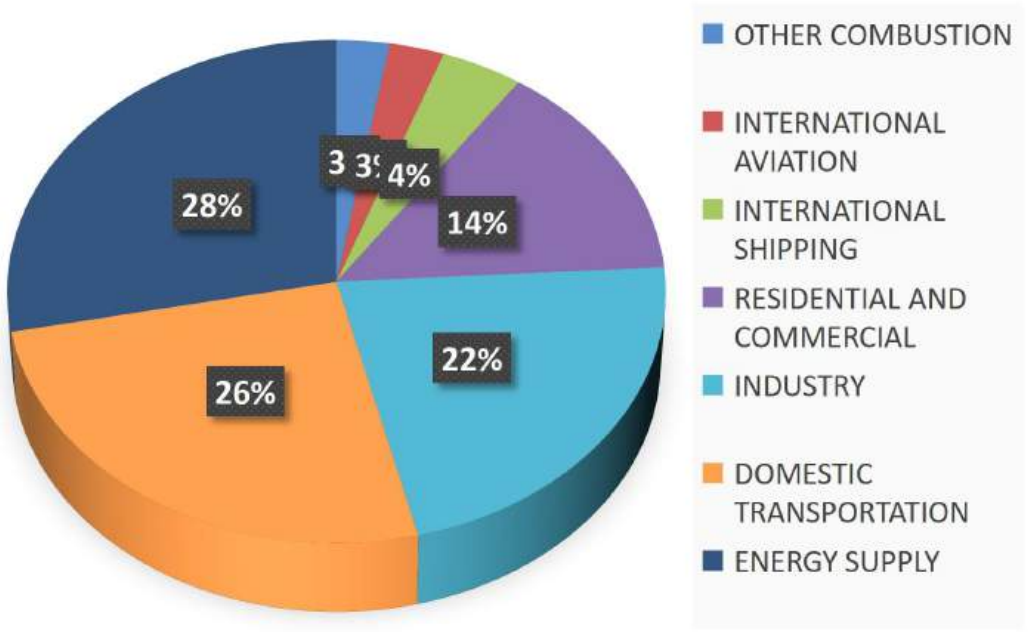

Figure 2.16 Distribution of carbon dioxide by sector in the European Union (257, 258).

In a spark ignition engine, such as a gasoline engine, the carbon dioxide (CO2) emissions generally increase with engine load. It's important to note that the formation of CO2 is an inherent by-product of the combustion process in spark ignition engines. Reducing CO2 emissions from such engines involves optimizing combustion efficiency, improving fuel economy, and adopting alternative fuels or power train technologies that produce lower CO2 emissions. Alternative fuels often come from renewable sources such as biomass. Using fuels

derived from renewable sources avoids the CO_2 emission associated with the combustion of the fossil fuels.

2.7.4 Total Hydrocarbon Emissions

Incomplete combustion leads to unburnt hydrocarbons emissions (HC). The hydrocarbon's emission is closely linked with combustion chamber design, and operating variables such as air-fuel ratio, speed, load, and mode operation mode (259). Moreover, the surface to volume ratio and wall quenching immensely alter and influence the formation of hydrocarbons. Hydrocarbons are released and emitted by exhausts, engine crankcase fumes, and vapor slipping or breaking away from the carburettor. According to the area of the rich mixture, hydrocarbons' value increases when the air-fuel ratio value decreases. When compared, hydrocarbons content by volume is massively lower than carbon monoxide content. Its value is expressed in ppm (parts per million) units, and the following apply 1% of hydrocarbon content by volume = 10000ppm. The existence of local rich mixture pockets at lower temperatures than the combustion chambers' temperature leads to unburnt hydrocarbons' appearance and existence in the exhaust emitted. Furthermore, hydrocarbons also exist as a result of flame quenching near the metallic walls. However, if the oxygen concentration and exhaust temperature are reasonable and applicable for complete oxidation, a massive quantity and portion of this unburnt hydrocarbon may burn during the expansion and exhaust strokes. Otherwise, a significant amount of hydrocarbon will be emitted with the exhaust gas. Rich air-fuel mixtures tend to result in incomplete combustion and higher THC emissions, while lean mixtures can lead to increased unburned hydrocarbons due to inadequate fuel combustion. Efficient combustion ensures that the available hydrocarbons in the fuel are thoroughly burned, minimizing unburned hydrocarbons in the exhaust gases (260). Low engine speeds and light loads, the combustion conditions may not be optimal, leading to incomplete combustion and higher THC emissions. Additionally, cold starts and warm-up periods can result in increased THC emissions until the engine reaches its normal operating temperature. The composition and quality of the fuel used

can affect THC emissions. Different fuel formulations, such as variations in the amount and type of additives or the presence of oxygenates, can influence the combustion characteristics and subsequent hydrocarbon emissions (261).

2.7.5 Particulate Matter Emissions (PM)

Particulate matter (PM) emissions from spark ignition engines primarily comprises of Organic Carbon (OC), Elemental Carbon (EC), Inorganic Compounds and Nitrates, sulphide and silica. These components vary in concentration and composition depending on factors such as the type of fuel used, engine design, operating conditions, and the efficiency of emission control technologies (262). For spark-ignition engines operated with unleaded gasoline the particle matter emissions are further classifies into Ultra-fine particles with diameters less than 100 manometers (PM0.1), particles with aerodynamic diameters less than or equal to 2.5 μm (PM2.5) and particles with aerodynamic diameters less than or equal to 10 micrometers μm (PM10) (263, 264). The particles are formed and grow in the exhaust system due to vapor-phase condensation enhanced by coagulation and, therefore, the exhaust temperature has a significant effect on particulate emission levels. Cold engines emit higher levels of particulate. Unleaded gasoline reduces particulate emissions. Organic particulate (soot emissions) can result from the combustion of excessively rich mixtures or from the combustion of lubrication oil. In mixture-controlled engines in which the lubrication oil is not supplied through the fuel metering system, the exhaust gases contain negligibly small amounts of organic particulate. The Particulate matter emissions in GDI engines can come from either rich pocket in the cylinder, injector dribble/tip wetting, or pool fire on surfaces, depending on the operating mode (homogeneous or stratified, lean or stoichiometric) and fuel used. (atomization, penetration and evaporation) play a critical role in all scenarios (265). The combination of rich regions near fuel films and the potentially high aromatic content in the fuel films may be a key factor in explaining the observed fuel effects on the sooting tendency in GDI engines (Kim et el 2021). Beyond the direct fuel effects, soot formation is a function of fuel atomization and vaporization, which is

often controlled by in-cylinder fluid motion, injection pressure, and injector make and type. Jiao and Reitz modelled soot formation in a GDI engine across a range of operating conditions. The heavier components of gasoline remained on combustion-chamber walls until late in the expansion stroke (266).

2.7.6 Carbonyls

Among the regulated air pollutants belong the Nitrogen Oxides (NOx), Carbon Oxide (CO), total hydrocarbons and Particulate Matter (PM). The unregulated pollutants include Polyaromatic Hydrocarbons (PAH), Carbon Dioxide (CO2), Polyaromatic Hydrocabon are formed during incomplete combustion of organic material through a complex series of chemical reactions involving fragmentations, condensation, and polymerisation of smaller aromatic compounds under high temperature conditions (267). Polyaromatic hydrocarbons (PAHs) can indeed exist in both gaseous and particulate phases. The partitioning between the gas and particle phases depends on factors such as the temperature, atmospheric conditions, and the physical and chemical properties of the PAHs themselves. PAHs are of environmental concern due to their toxicity, persistence, and potential carcinogenicity, and their presence in both phases contributes to their widespread distribution and impact on ecosystems and human health (268, 269). Carbonyl compounds such as aldehydes, where primarily listed are formaldehyde and acetaldehyde (270). Carbonyl emissions refer to the release of carbonyl compounds into the environment. Carbonyl compounds are organic chemicals that contain a carbon-oxygen double bond, also known as a carbonyl group (C=O). These compounds can be emitted from various sources, including both natural and human activities. Carbonyl compounds are emitted from internal combustion engines as products of incomplete combustion of hydrocarbons or oxygenated compounds. They are finally found in the atmosphere, and many authors studied their distribution and reactions in atmosphere of urban and rural areas (271). According to a report by the International Programme on Chemical Safety in 2002, this pollutant has multiple sources, but motor exhaust gas is considered as one of the most important. The fuel composition

can influence the emissions of these pollutants (272). Gasoline contains basically hydrocarbons, but alcohols or methyl tert butyl ether (MTBE) are also added in fuels to decrease exhaust hydrocarbons and carbon monoxide. While MBTE can help reduce CO and HC emissions by enhancing combustion efficiency in gasoline engines, its use is associated with increased emissions of formaldehyde and acetaldehyde (273). However, many carbonyl compounds such as formaldehyde, acetaldehyde and acrolein, have been receiving regulatory attention, due to their consequences as eye irritants, toxic air contaminants, mutagens, and carcinogens (274, 275). Carbonyl emissions have gained attention due to their potential adverse effects on human health and the environment. Formaldehyde, for example, is a known carcinogen and respiratory irritant. Acetaldehyde is also considered a potential carcinogen and may contribute to the formation of ground-level ozone, a major component of smog. These compounds can also contribute to the formation of secondary organic aerosols, which can have implications for air quality and climate (276).

2.8 Emissions Legislations and Policies

Engine emission regulations and policies are measures implemented by governments and regulatory bodies to control and reduce the pollutants emitted from engines, particularly those used in vehicles and industrial machinery. These regulations aim to mitigate the adverse impacts of engine emissions on air quality, human health, and the environment. Different regions and countries have different standards for vehicle emissions. The first automobile emissions standards were enacted in 1963 in the United States, mainly as a response to Los Angeles' smog problems. Three years later Japan enacted their first emissions rules, followed between 1970 and 1972 by Canada, Australia, and several European nations. Policy regulations of Carbon monoxide (CO) and hydrocarbons (HC) were the main concerned of the early standards. Regulations on nitrogen oxide emissions (NO_x) were introduced in the United States, Japan, and Canada in 1973 and 1974, with Sweden following in 1976 and the European Economic Community in 1977. These standards gradually grew more and more stringent but have never

been unified. The Euro standards were first introduced in 1992 and have been progressively tightened over time to encourage the development and adoption of cleaner and more fuel-efficient technologies. The standards primarily focus on limiting emissions of nitrogen oxides (NOx), particulate matter (PM), carbon monoxide (CO), hydrocarbons (HC), and certain greenhouse gases (GHGs), such as carbon dioxide (CO2) all measured in g/km. Each Euro standard sets specific emission limits for different vehicle categories and fuel types. The most recent Euro standard for passenger cars and light commercial vehicles is Euro 6d-TEMP (also known as Euro 6.2), which came into effect on September 1, 2019. This standard introduced more stringent limits for NOx and particulate emissions, including Real Driving Emissions (RDE) tests that measure pollutants during on-road driving conditions. A lot of novel technologies and innovations has been introduced for the regulations of automotive emissions. Most notable was the three-way catalyst (TWC). A significant reduction in emissions can be obtained by removing pollutants from the -exhaust gases by using catalytic converters (this group includes oxidizing catalysts for HC and CO, reducing catalysts for NOx, and three-way catalysts for all three pollutants), thermal reactors for HC and CO, and filters (or traps) for particulate. Other emission control technology or method for the spark ignition engines included alterations and air-fuel ratio adjustments and controlling and adjusting other engine factors such as mixture control under idling or acceleration or deceleration, spark timing, accurate and precise manufacturing of main engine parts such as pistons, rings, cylinder head gasket to minimize crevice volume, cams, valves.

2.9 Health Implications and Physical Hazard Assessment of Spark ignition Engine Emissions

The Occupational Health and Safety Administration (OSHA) has published a Hazard Communication Standard that defines a set of physical and health hazard categories. Petroleum gasoline presents significant health and physical hazard risks, and the key goal is to ensure that

the selected bio-blend stocks for study does not present even greater risks than fossil fuels. The automobiles emissions have both local and global negative influence on the environmental which lead to global warming(255). Globally, gasoline spark-ignition engines are the most known and famous for passenger vehicles. Eventually, there were control methods and techniques developed to reduce exhaust emissions from spark-ignition engines. The most common components of gasoline pose several environmental and human health issues, most commonly respiration, flammability, and toxicity to aquatic life with lasting effects (277) . On human health basis, it has been discovered that exposure to hydrocarbons causes some cancers and tumors. Oxides of nitrogen accompanied by unburned hydrocarbons in sunlight form photochemical oxidants, which have undesirable adverse effects on human health and plants.

2.10 Summary

This literature review ultimately provides the motivation for this research work which is the study of combustion and emission characteristics of Cyclopentanone and 2-Methyltetra-hydrofuran in a modern DISI Engines.

A general review of GDI engine technology was carried out with detail study into GDI technology since the experiments were carried out using a modern GDI engine. The different generations of Biofuels productions (first-fourth) were reviewed, the objective is to provide background information into the development of Biofuels technology. Basic molecular structures and fuel property of three key furan series fuels (MF, DMF and MTHF) were generally discuss and compared to the structure and properties of Cyclopentanone fuels. However, the review of DMF and MF is not high priority for this work, and therefore constitute a small fraction of the review and help as tools for good understanding of MTHF as engine fuels. This review acknowledges the implications of the IC engine emissions to human health and the consequence on the environmental degradation which necessitate the development of IC engines and associated fuels under an imposed emissions regulations. The European Union restrictions

on PM emissions from SI engines are now effective leading to the study and monitoring of individual HCs. The knowledge gap identified in this literature review is the lack of adequate investigations into the combustion and emissions behaviour of Cyclopentanone and Methyltetrahydrofuran in a DISI engine. It was also observed as a knowledge gap lack of investigation into the percentage composition of unburnt furan samples in the combustion of furan based fuel in a DISI engine. This research study is necessitated by the above listed identified knowledge gap. Overall, the review provides the motivation for the research study and provide the background information effective for the design of the research frame work.

CHAPTER 3

EXPERIMENTAL SETUP

This chapter provides a basic description of the single-cylinder spray-guided Medusa thermal engine (DISI) used to carry out the research study. Detailed information about the engine's electronic control systems along with the data acquisition, data processing, and data recording system are equally included in the chapter. The Chapter provides an in-depth analysis of the properties of fuels used for the study as well as the emissions measuring devices used during the experiment. The overhaul of the research engine was undertaken during the tenure of this study, and the old fuel injection pump with complex stages of operations was replaced with a new fuel pump with few simple stage of operations. The airflow rate measuring system was re-calibrated before commencement of the experimentation. Overall this chapter provides an overview of the current test facility. Further detailed descriptions are reported in literature (16, 278-281).

3.1 Engine Experimentation and Instrumentation

This research was conducted in a four-stroke single-cylinder, spray-guided direct injection engine (DISI) as indicated in figure 3.1. The single-cylinder DISI engine used in this investigation is a version of that used in the Jaguar AJ133 (2010) 5.0 litre V8 production engine. The heating and cooling circuit for the engine oil and the coolant are independently heated and pumped during the experiment. To aid the engine combustion stability and to reduce the instance of signal drift, the oil and coolant were heated until their temperatures remain stable. The temperatures for both coolant and lubricant are considered stable at 85 ± 5^{0}C and 90±3°C respectively. All temperatures were measured with a K-type thermocouple. A 100L intake buffer was used to stabilise the intake airflow system. The engine and instrumentation setup shown in Figure 3.1 consists of a direct current (DC) dynamometer, a single-cylinder spray-guided DISI

research engine, and a control, data acquisition, and recording system. A DC dynamometer was coupled to the engine in other to keep the engine speed constant irrespective of the torque output. The engine speed remains constant at 1500rpm (this is the maximum speed beyond which the cycle to cycle fluctuations becomes significant) for all the tests conducted. Kistler 6041A water-cooled pressure transducer was used to measure the in-cylinder pressure.

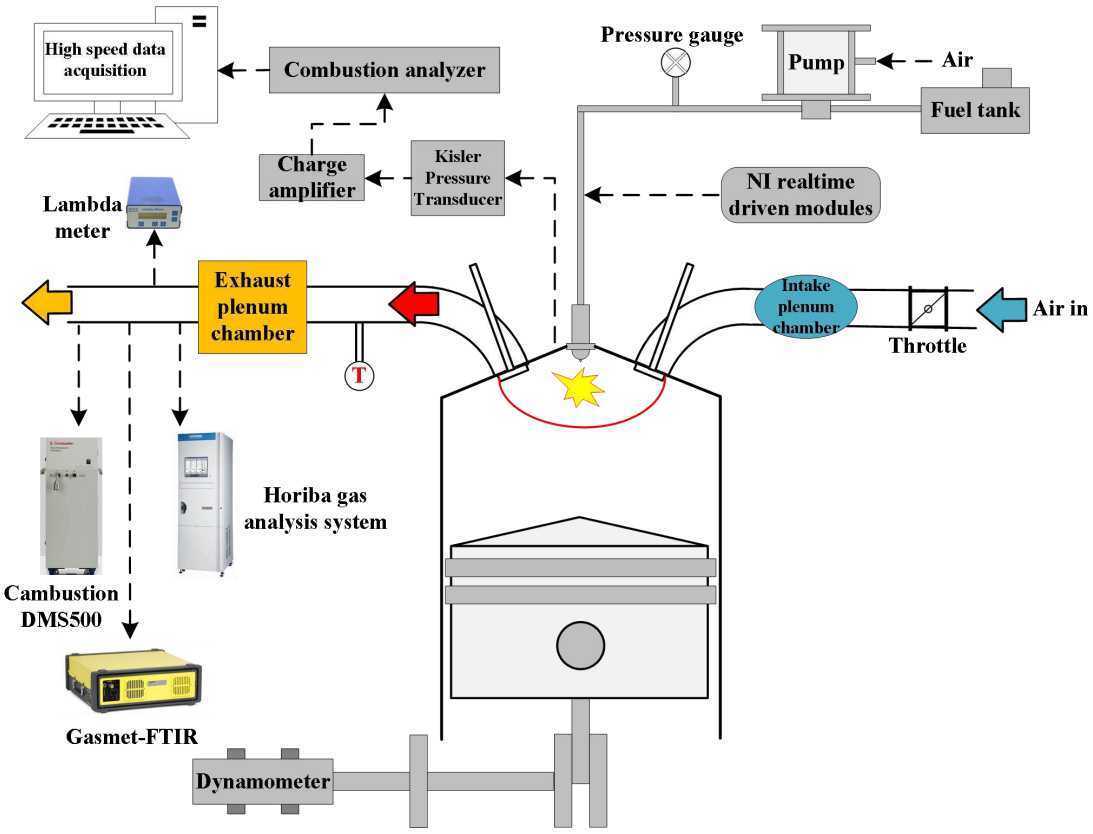

Figure 3.1 Schematic of engine and instrumentation setup.

This water-cooled transducer is securely mounted on the sidewall of the cylinder head. The pressure signal from the pressure transducer is interpreted on the Kistler 5011 charge amplifier. A National Instruments data acquisition card interprets the results by using software developed in-house and written in Lab VIEW programming. The crankshaft encoder signal was used to determine the location of the piston relative to the top dead centre (TDC) and is used by the engine timing control system (ETCS) software to control the timing of the fuel injection, ignition, and variable valve timing. During this experiment, all the control signals are based on

the 1440TTL pulses per cycle clock signals. There is an exhaust plenum attached to the cylinder head. The pressure fluctuations on the exhaust gases are reduced by passing it through the exhaust plum before passing through the Lambda meter to measures the air-fuel ratio. The specific geometric features of the research engine are reported in table3.1 below.

Table 3.1 Medusa DISI Thermal Engine Specification.

Engine Type	4 Stroke,4Valve
Combustion System	Spray guided DISI
Displacement	565.6cc
Bore x Stroke	90mm x 89mm
Compression Ratio	11.5:1
Fuel Type, DI Pressure	MTHF, CP, MF, ETHANOL and ULG. , 15MPa
Engine speed	1500rpm
Injector	Multi-hole Nozzle
Intake valve open	16.5bTDC
Exhaust valve closed	36.7aTDC

Tests were conducted at the direct injection pressure of 15 MPa except where the fuel injection pressure is the understudy. Gaseous emissions were measured using the Horiba mexa 700, the flow sample was collected at about 300cm downstream of the exhaust at the flow rate of about 200L/min. The DMS500 has been widely adopted as particulate measurement equipment for real time measurement of particle size distributions, number and mass. It is a new particle emission measuring device that makes convenient both primary and secondary sample dilution ratios. The standard DMS500 offers measurement from 5 – 1000nm, while a switchable option

offers the ability to select 5nm – 2.5μm measurements. Any instrument measuring below 100nm must take steps to minimize small particle losses. The DMS500 uses a high sample flow (8 litres per minute) and multiple sheath flows inside the charger to significantly reduce losses of small particles. HC emission speciation analysis was undertaking using the Gasmet FTIR technology. The FTIR utilises a gas measurement technology for simultaneous measurements of multiple gases. The ability to detect and measure almost any gas, combined with the robustness and reliability of the technology, makes the FTIR ideal as emissions monitoring devise.

3.2 Single-Cylinder Medusa Thermal Research Engine

Figure 3.2 Single-cylinder engine test facility.

The Single cylinder research engines was limited to comparatively low speed operation due to the inherent out-of-balance characteristics at higher speed. Single-cylinder engine testing allows researchers to specify and control variables that are not as directly controlled in multi-cylinder

engines. Examples include: the ability to specify pressure ratios, controlling the amount of exhaust gas recirculation, controlling the local air-to-fuel ratio within the cylinder and the flexibility of the engine timing operations. The engines are also designed for alternative fuel, wear, optical, crank offset and bore-to-stroke relationship studies. The Medusa thermal engine is fitted with a variable cam timing system, as shown in figure 3.2. The over-square engine configuration has a high compression ratio and swept volume, which maximise efficiency and output power. The Dynamometer manufactured by Maudsley's LTD is attached to the crankshaft to motor the engine. It uses 450-Volt electric power. The speed is manually controlled by a dial in the engine control room, and it can maintain a constant speed or constant engine load with motoring or firing conditions. One of the basic challenges of the modified single-cylinder research engine was its low resistance to knock; its large bore size reduces the resistance to knock. It was recorded by the previous student researchers on the engine that at the maximum brake torque/knock limited spark timing (MBT/KLT) the Engine knocks for ULG 97 occurred at loads of 6.0bar IMEP and above (12). The engine result on the spark timing as recorded by Lattimore et al. is in conformity with the result obtained from the current study in this work. In this research study engine audible knock with 97 RON gasoline fuel was recorded at engine loads between 5.5 and 6.5bar IMEP at MBT/KLT timing.

3.3 Fuel Supply Systems

The engine fuel supply system comprises both a high-pressure (15MPa) direct injection (DI) system and low pressure (3MPa) Port fuel injection system (PFI).

3.3.1 Port Fuel Injection (PFI)

A Port Fuel Injector system (PFI) is installed between the intake manifold and the cylinder head. It runs on a low-pressure supply of 3bar and is used for warming the engine prior to final testing on the Direct Injection system. PFI is a relatively easy system to install and permanent changes are mostly not required. With PFI the air-fuel mixture is prepared in the intake manifold and fed

to the cylinder for combustion. The fuel is pumped from the gasoline fuel tank by an out-of-tank pump and is pumped to the PFI injector through a three-way valve. The water-cooling line avoids excessive heating of the fuel and vapour loss from the system after the fuel exits the PFI injector.

3.3.2 Direct Injection (DI)

The DI fuel system, as shown schematically in Figure 3.3, applies constant pressure to the fuel through the use of a free piston accumulator and a compressed nitrogen bottle supplied by British Oxygen Company (BOC), which is controlled using a high-pressure gas regulator manufactured by the company. The pressure supplied is obtained from a pressure fuel pump. Manufactured by Haskel Milton Roy. The pneumatic pumps automatically reciprocate on a differential piston principle.

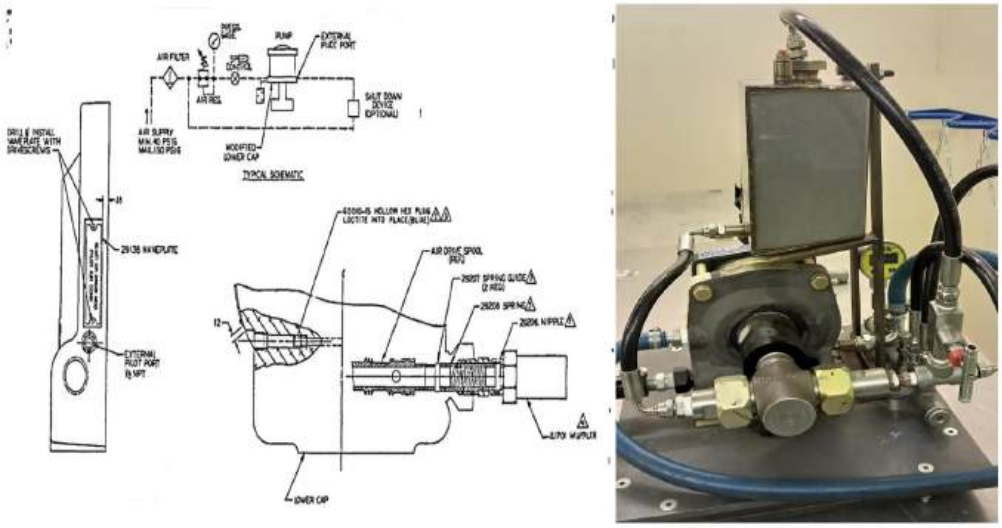

Figure 3.3 Medusa single cylinder Engine DI Pump.

The model coding of Haskell's air-driven liquid pumps indicates the ratio of the air drive piston, and the pump air piston is 4:1. The maximum operating pressure range of the pump is 60MPa. The pump will automatically start to cycle once the pressure is released or if the drive air pressure is increased. This feature makes this type of pump an excellent choice for pressure.

However, only 2L of fuel can be supplied to the accumulator with each charge, necessitating the engine to be stopped at regular intervals in order to refill the system.

The high-pressure DI combustion system consists of a centrally mounted, six-hole injector. The fuel required for the test is pumped from the accumulator cylinder and through to the DI injector using a variety of rigid and flexible tubing and stainless-steel compression fittings. At the end of a test day, the system was then cleaned with gasoline in order to avoid damage to the injector and accumulator seals. In line with the manufacturer specifications the pump was found suitable for pumping gasoline, ethanol, furan series fuels and the blend of ethanol and furan fuels with gasoline at outlet pressures from 50MPa up to 60MPa with an air drive pressure of 6MPa, maximum outlet flow rate of 5kg/hour and Pump displacement of 6.7ml/cycles.

3.4 Engine Cooling System

K thermocouples are used to measure the temperatures at intake, exhaust, engine oil, and the water coolant. A heat exchanger connected to the engine's cooling system was used to control the oil temperature and the engine coolant temperature is controlled by a solenoid valve that regulates the flow of cold water through the heat exchanger. This solenoid valve is driven by the Proportional Integral Derivative (PID). During the course of this study, the test engine was rebuild to reduce the oil and water leakages from the engine. The aluminium top cylinder gasket as indicated in figure 3.4 was replaced with a new copper top cylinder gasket. This top cylinder gasket is located between the engine cylinder head and the engine block. The design and fabrication of the new copper gasket was undertaken by this researcher. The copper gasket was fabricated to accuracy using the CNC Lathe machine. The top cylinder copper gasket design is indicated in Figure 3.4. The purpose of the new copper gasket is to further prevent a loss of compression and to stop engine gases from escaping.

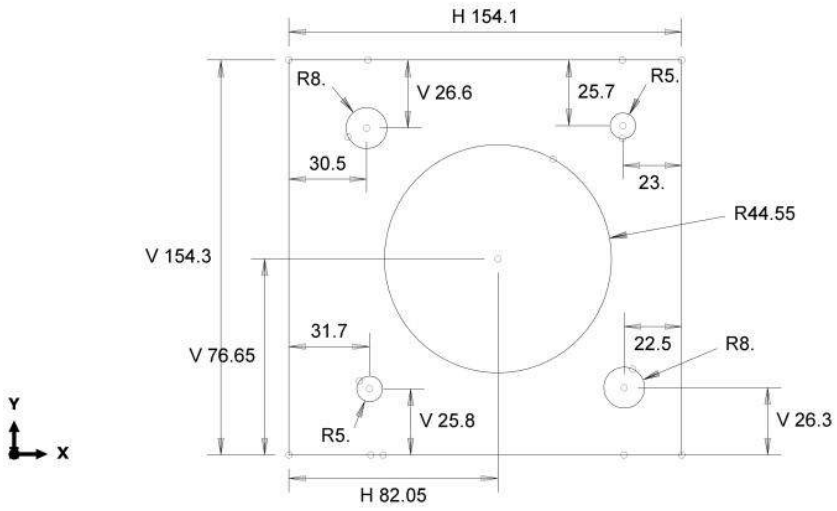

Figure 3. 4 Medusa single cylinder thermal Engine Copper Gasket.

3.5 Engine Combustion System and Injector Configuration

The Medusa thermal engine combustion system consists of a Bosch model six-hole injector of hole diameter 0.30mm that is centrally mounted. The spark plug is mounted beside the injector at an angle of 18degrees to the cylinder axis, as shown in Figure 3.5 below.

Figure 3.5 Layout of the orientation of injector spray plume and combustion systems.

3.6 Engine Timing Control System

The engine timing control system (ETCS) software for the single-cylinder engine is written in a LABVIEW script of National Instruments counter-timer card (model 6602) to control the injection and spark timing parameters. The Internal Combustion Engine group at the University of Oxford developed the original version of the ETCS software but was then modified by

previous researcher at this institution(278, 280, 281) . The software contain a flexible feature that make it easy to adjust in real-time whilst the engine is running, the spark timing and coil charge along with the start of injection timing and injection pulse width. The system is capable of controlling two separate injections per cycle, with each of these two injections having independent pulse widths**.** Engine Load control for spark ignition is achieved through fuel injection regulation using the ETCS software and by the operator adjusting a butterfly throttle valve that is situated in the inlet track. The airflow and fuel injection are regulated until the required engine load is attained. Kistler water cooled pressure transducer type 6041A is used to measure the in-cylinder pressure.

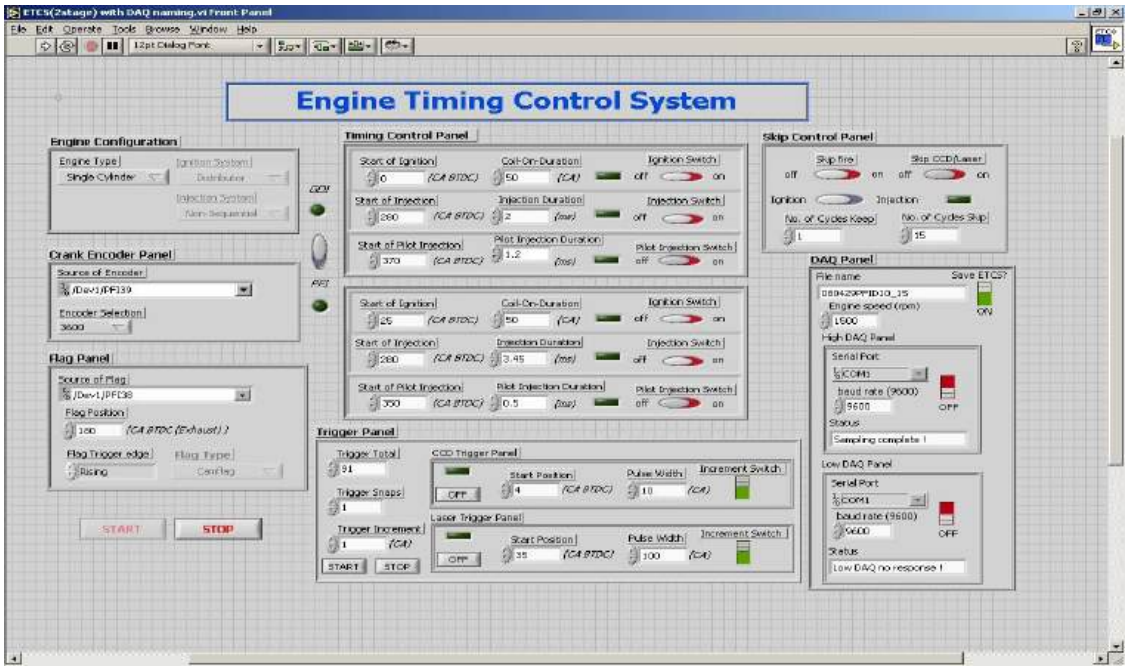

Figure 3.6 Display Panel for Engine Timing Control System.

The Kistler pressure transduce is connected to the data acquisition system via a Kistler 5011 charge amplifier. K ‘thermocouples are used to measure the temperatures at the intake, exhaust, engine oil and engine coolant. A heat exchanger connected to the engine’s cooling system was used to control the oil temperature and the engine coolant temperature is control by a solenoid valve that regulate the flow of cold water through the heat exchanger. This solenoid valve is driving by the Proportional Integral Derivative (PID).

3.6.1 The Timing Control Panel

The timing of the ignition and injection is control in the timing control panel. Both the start timing and the duration of the ignition and or injection can be specified in the corresponding box. ETCS enables split injection operations in which the timing of the pilot injection can be accurately controlled. It should be noted that the start of pilot injection must be earlier than the start of injection in all circumstances. There are two sub panel in the timing control panel. The upper part is for the Direct Injection (DI) and the lower part is for the Port fuel injection (PFI). The ETCS will use the time setting of either PFI or DI timing control depending on the depending on the state of PFI/DI switch. This feature makes it possible to switch seamlessly between DI and PFI with different injection and Ignition timing settings.

3.6.2 The DAQ Communication

The switch in the High DAQ and the Low DAQ panel determines whether the High speed DAQ and the Low speed DAQ are enabled. The file name specifies the common files name that the ETCS programme, High speed DAQ and Low speed DAQ will use when saving data. The engine speed needs to be set to the same as the current engine speed in the experiment. The DAQ communication panel can only be used for single cylinder engine control. Apart from pulse generations using PCI-6602 counter/timer card, the ETCS program can also start the data acquisition during the test via communication with the DAQ PCS. The communication between ETCS PCS and DAQ PCS is realised via RS232 serial points. The ETCS program can notify the DAQ PCS about the sampling rate, files name and also obtain feedback form them about the status of the data acquisition process. The ETCS program can also save the configuration setting of the ETCS front panel into files with specified names. Figure 3.6 shows the logic flow diagram of the communication between ETCS and DAQ PCS.

3.6.3 Ignition Pulse Signals

The ignition TTL pulse is generated by CTR (counter) on the PCI-6602 counter timer card when used in normal ignition mode. CTR1 uses the once/cycle TTL flag pulse as the gate signal and the shaft encoder TTL pulse as the CLK (clock) signal. CTR1 generates a TTL pulse with a specified delay (start timing) and a time basis pulse width (ignition duration) after each time it receives a gate triggering signal. When the Ignition is in skip mode the CRR0 will generate a TTL pulse train known as skip pulse. The skip pulse is at a high state during firing cycles and is at a low state during skip ignition cycles. This pulse train is generated by CRT0 is used as the pause trigger signal for the ignition counter (CTRL1). Thus, the ignition counter can output ignition pulses only during the firing cycle's figure 3.7 show the pulse generation diagram for skip ignition. (No of cycles keep=2, number of cycles skip=1).

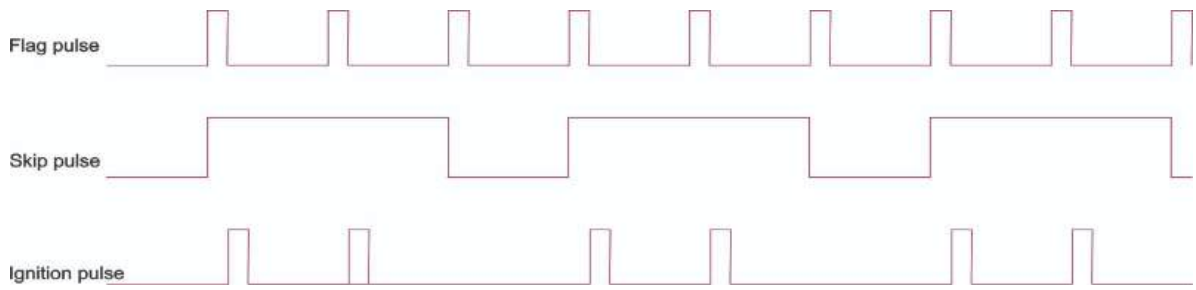

Figure 3.7 The Timing Diagram for a skip ignition.

3.6.4 Injection Pulse Signals

The injection pulse is generated a bit differently compared with the ignition pulse. The reason is that although the start of the injection pulse is crank angle based, the injection duration is time based and the second reason is that there are two injection pulses when split injection is switched on. There are three counters used for injection pulse generations CTR7 is used as the injector trigger counter, CTR6 is for generating main injection pulse and CTR2 is for generating the pilot injection. CTR7 use the shaft encoder signal based on crank angle as the CLK inputs while CTR6 and CTR2 uses the internal clock-based time as the CLK source for the injection duration pulses. Figure 3.8 is the pulse generation diagram for normal split injection.

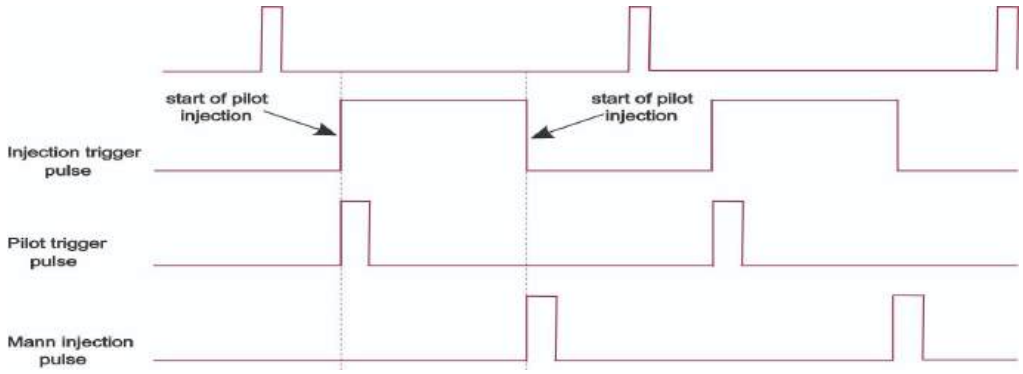

Figure 3.8 Timing diagram for normal split injection.

3.6.5 Crankshaft Encoder Setup

The engine rebuilds that took place during the period of this study witness the crankshaft Nitriding, a process where oxygen is vacuumed out from the surface of the shaft and nitrogen is introduced to penetrates the entire surface. Figure 3.9 is a pictorial view of the Nitrided crankshaft. Overall, nitriding is essential for enhancing increased hardness and wear resistance, corrosion resistance, fatigue Strength Improvement, durability, and reliability of crankshafts in demanding applications.

Figure 3.9 Nitrides Crankshaft for the Single cylinder Medusa thermal engine.

Accurate setting up of the Crankshaft encoder is highly required in order to determine the correct signal for the location of the piston relative to top dead centre (TDC). This encoder

timing signal is used by the ETCS software to control the injection, ignition, and variable valve timings. The timing of this signal is achieved using a stroboscopic light signal. The Engine control software was used to input a spark timing of 0°bTDCcomb (TDC) while observing the stroboscopic response at the flywheel when motoring the engine at low speed. The actual position of the spark is measured by using the stroboscope pick up and the 1/degree markings on the engine flywheel. The light shown on the flywheel indicates the CAD markings; and the reading achieved when the light comes on is recorded and the encoder position is subsequently adjusted until the system is synchronized. The difference in response was determined using the crank angle degree (CAD) markings, which were verified by a previous researcher (Turner, 2010 and Wang 2014). Once this offset is obtained it can be entered into the ETCS software so as to establish an accurate correlation between the control software and the stroboscope.

3.6.6 Valve Train Mechanism

A fixed phase variable cam timing (VCT) system that uses the crankcase oil pressure of about 3.5 bar, was used to control the offset of the camshaft relative to the timing of the camshaft pulley (±25CAD). The VCT system is controlled using the software that measures the pick-up from a hall-effect type sensor, using the LABVIEW script written in using an NI card (6202)., developed by a previous student (Luszcz, 2009), The relative position of the camshaft is determined using the Hall effect type sensor. The hydraulic solenoids mounted in the cylinder head is used to adjust the oil pressure and thus can be used to change the relative camshaft positions. By varying the pulse width to the hydraulic solenoids, the oil pressure changes, and the software then automatically regulates the cam position so that, in stable operation, the timing is maintained to ±0.1CAD. Table 3.2 shows the geometry of the intake and exhaust camshafts and typical of SI engines the camshaft has a high-lift profile.

Table 3.2 Single-cylinder engine camshaft geometry

Valve and Camshaft Geometry- Spark Ignition	
Intake Valve Lift	10mm
Intake Valve Inner Seat Diameter	36mm
Exhaust Valve Lift	9.3mm
Exhaust Valve Inner Seat Diameter	33mm
Intake Valve Duration	250CAD
Exhaust Valve Duration	250CAD

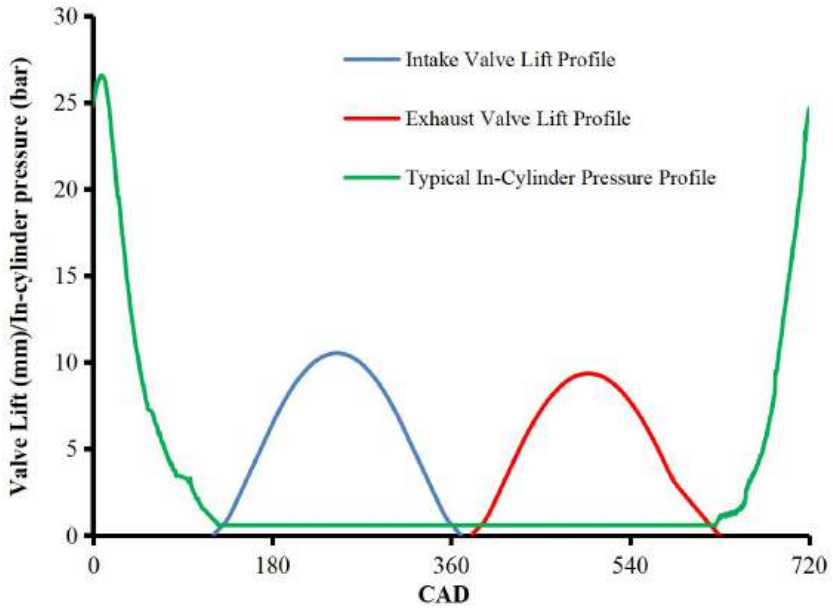

Figure 3.10 Intake and exhaust camshaft profiles (16).

Optimized valve timing conditions were chosen for the intake valve opening (IVO) timing is 16°bTDCintake and the exhaust valve closing (EVC) timing is 36°aTDCintake. This timing was optimised for low load conditions (3.5bar IMEP) as used by the previous research student in the engine group. Figure 3.10 shows the intake and exhaust camshaft profiles for the test engine.

3.7 Variable Cam Timing Setup

After the engine rebuilt, it is necessary to reset the timing of the intake and exhaust cams relative to the crankshaft. This process is carried out by manually rotating the flywheel to

vertically align with the cam lobe of the intake camshafts at 70˚bTDC and exhaust camshafts at 255˚bTDC with the use of timing peg. Exhaust camshaft is the first to be timed and this is achieved by setting it to its vertical position and manually rotating the camshaft until it reaches 255˚bTDC, after which the exhaust camshaft sprocket is fixed to the exhaust camshaft. The flywheel is then rotated clockwise until 70°bTDC, whereby the belt is removed in order to correctly align the intake camshaft. At this timing location, both camshafts are in the reset position.

3.8 Engine Management System for GDI Engine

Engine Management System (EMS) consists of a wide range of electronic and electrical components such as actuators, relays, sensors, and an Engine Control Unit. They work together to provide the Engine Management System with vital data parameters and they provide the car's Engine Control Unit with vital data parameters essential to govern various engine functions effectively. Furthermore, the Engine Management system is incorporated into modern-day engine technologies. These include PFI and GDI systems in Petrol engines and CRDi systems in diesel engines for improved performance (282). Engine sensors are electro-mechanical devices that monitor various engine parameters. An engine uses different types of sensors that include Thermocouples, Resistance Temperature Detectors (RTDs), and Hall Effect sensors. A thermocouple sensor is a temperature-measuring device. It converts temperature into an electric charge. Thermo-couples use two different conductors that contact each other at one or more spots. Thus, it produces voltage. It, in turn, sends the signal in the form of an electric current to the ECU. Thermo-couples are commonly used as temperature sensors. It measures and controls the temperature such as in the case of Engine Coolant Temperature (58). RTDs or Resistance Temperature Detectors also measure the temperature. However, they do so by correlating the resistance of the RTD element with temperature. RTD element is made of pure metals such as platinum, nickel, or copper. An air conditioning evaporator unit uses this type of probe sensor.

The hall-Effect sensor comprises a transducer that varies its output voltage according to the magnetic field. Typically, Hall-Effect sensors detect the speed or velocity. The positioning applications in automobiles use this type of sensor. So, they are used for detecting the Crankshaft speed or its position. the engine sensors provide the Engine Management System with vital data parameters in real-time These engine sensors continuously monitor the engine parameters. They also provide the ECU with changes that occur in the data from time to time. Based on these inputs, the ECU re-calculates the correct air-fuel ratio and ignition timing. It also calculates and supplies the correct amount of fuel to the engine under various load conditions. after calculating the fuel quantity, the ECU sends signals to various relays and actuators. They include the Ignition Circuit, Spark Plugs, Fuel Injectors, Engine Idling Air Control valve, and Exhaust Gas Re-circulation (EGR) valve. Thus, it extracts the best possible engine performance while keeping emissions as low as possible (283). Since all the engine sensors connect to the ECU, in turn, it can also monitor them for a malfunction. The ECU collects signals from faulty engine sensors and stores them in its memory. You can diagnose these faults through two methods. Firstly, by reading the ECU memory with the help of ‘fault codes., or through sophisticated engine diagnostic equipment supplied by the vehicle manufacturers. The Engine Control Unit is a central part of the Engine Management System, which is virtually the 'Brain' of the engine. It plays an important role in collecting, analysing, processing, and executing the data it receives from various sub-systems (284). Furthermore, an ECU comprises a computer that uses a microchip to process the inputs from various engine sensors in real-time. The Electronic Control Unit contains hardware and software. The ECU's printed circuit board (PCB) consists of a micro-controller chip or the CPU (Central Processing Unit). The software is stored on the micro-controller or chips on the PCB. It is possible to re-program the ECU by updating the software or by replacing chips. All the engine sensors send data inputs by way of electrical signals to the ECU. In turn, the ECU controls various actuators, ignition timing, variable valve timing. Based on this data input, the ECU precisely calculates

and delivers the ideal air-fuel mixture It also regulates the idle speed of the engine and limits the top speed of a vehicle. This system is also widely referred to as an Electronic Engine Management System or the EMS (285). Furthermore, it is possible to customize the modern-day ECUs to suit different vehicular applications and varying customer demands. Also, some cars have an individual 'Control Module' for all major systems. A modern car has the following individual Control Modules that control the respective systems. An Engine Control Unit connects to all the individual Electronic Control Modules (ECMs). A modern-day car consists of more than one Control Modules, each exclusive for every major system, which improves performance (286). The manufacturers seldom refer to these systems as car's computers since they are multiple computers instead of a single one. Gasoline Direct Injection (GDI) also known as Petrol Direct Injection/Spark Ignited Direct Injection (SIDI)/Fuel Stratified Injection (FSI) which is the latest Engine fuel injection technology. Additionally, it uses special injectors that spray the petrol at a very high pressure. Unlike the Port fuel injection system (PFI) system, this injector sprays the petrol directly into the combustion chamber just like diesel engines (58). The sophisticated 'Engine Management System' (EMS) precisely controls the mixing of air & fuel. The mixing of air and petrol occurs inside the combustion chamber rather than in the inlet manifold. Thus, this method provides greater control over the combustion process. In addition, it also provides multiple combustion modes which include ultra-lean-burn air-fuel ratios. In modern trends, newer generation engines use GDI in combination with a Turbocharger which improves engine performance (285).

3.9 Instrumentation

The most important aspect of this experimentation is the instrumentation which provides the data to interpret the combustion performance of the engine and the emission characteristics of the fuels. Various ancillary instrumentation are fitted onto the test facility in order to provide the

data that were recorded and analysed in this study. This mostly includes flow rate measurement, temperature, pressure, and engine speed data. Each of these is fully discussed in this section.

3.9.1 Engine Torque and Speed.

The engine speed is kept constant at 1500rpm (±1rpm) by a DC dynamometer, coupled to the engine, and the engine speed remains constant irrespective of the torque output. This is the frequently used speed (1500rpm (±1rpm)) by engine emissions test researchers. The instantaneous torque reading at any particular operating point is provided by the Torque meter placed on the dynamometer. And is useful in finding the MBT spark timings at any point.

3.9.2 Pressure and Temperature Measurements

A Kistler 6041A water-cooled piezoelectric pressure transducer was used to measure the in-cylinder pressure. This water-cooled transducer is securely mounted on the sidewall of the cylinder head. An oil-weight bench machine in the range of 1MPa/1V to 10MPa/10V was used for the calibration of the pressure transducer. The pressure signal from the pressure transducer is interpreted on the Kistler 5011 charge amplifier and they are then sent to the data acquisition system. Although piezoelectric transducers are susceptible to drift and are unsuitable for steady-state measurements, they are effective under transient in-cylinder conditions (278, 287).

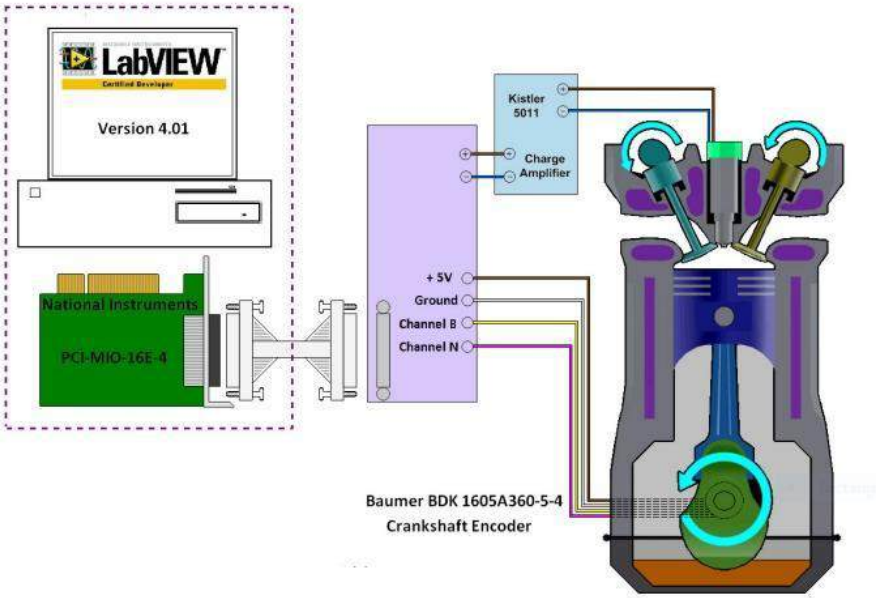

Figure 3.11 In-cylinder pressure data acquisition schematic using Kistler 6041A water-cooled piezoelectric pressure transducer (288).

3.9.3 Heat Release Analysis

The rate at which heat energy is released during the combustion (Heat Release Rate ($dQ/d\theta$)) is calculated in this study using the In-cylinder pressure and the corresponding cylinder volume data based on the equation 3.1 (289) . In the context of a spark ignition (SI) engine, there are several assumptions involves in heat analysis to simplify the complex combustion process in order to make the analysis feasible. These key assumptions are as listed below. It is often assumed that all the fuel reacts with the oxidizer to form the final products without any intermediate or unburned species, meaning all the fuel is burned and converted into products like CO_2, H_2O, and N_2, with no unburned hydrocarbons or partially burned products. The combustion process in SI engines is often modeled as occurring at constant volume (isochoric) within the cylinder. This is known as the Otto cycle assumption and simplifies the thermodynamic calculations. The gases involved in the reaction are often assumed to behave ideally, following the ideal gas law. During the rapid combustion phase, the process is often assumed to be adiabatic, meaning no heat is lost to the surroundings. For simplicity, the mixture

of fuel and oxidizer is assumed to be stoichiometric, meaning it has the exact proportions needed for complete combustion without any excess reactants. It is assumed that the reactants are perfectly mixed, and the reaction occurs uniformly throughout the mixture. Often, the formation of minor species or intermediates during the reaction is neglected to simplify the calculations. A single-zone combustion model is often used, which assumes the entire cylinder content is at the same temperature and pressure. This ignores spatial variations within the cylinder.

$$\frac{dQ}{d\theta} = \frac{\gamma}{\gamma-1} P \frac{dV}{d\theta} + \frac{1}{\gamma-1} V \frac{dP}{d\theta} + \frac{dQ_w}{d\theta} \quad \text{----------(3.1) (290)}$$

Q is the accumulated amount of released heat due to fuel combustion, θ is the corresponding crank angle, γ is the (heat capacity ratio) is the ratio of specific heats and isapproximated depending on the respective parts of the engine cycle. dQ/dθ is the heat release rate with respect to the crank angle θ, $dQ_w/d\theta$ is the rate of heat transfer to the cylinder walls with respect to the crank angle θ. During the combustion process, not all the heat generated by the burning air-fuel mixture is used for doing work. Some of this heat is transferred to the walls of the combustion chamber, including the cylinder head, piston, and cylinder walls. Understanding $dQ_w/d\theta$ is crucial in engine design and analysis, as it helps engineers predict how much energy is effectively converted into useful work and how much is lost, which in turn affects the engine's efficiency and performance. The ratio of the cumulative heat release to the total heat release is the Mass Fraction burned (MFB). This is calculated using equation 3.2 (289).

$$\text{MFB} = \frac{\int_{\theta_s}^{\theta_i} \frac{dQ}{d\theta} d\theta}{\int_{\theta_s}^{\theta_e} \frac{dQ}{d\theta} d\theta} \quad \text{----------(3.2) (289)}$$

The mass fraction burned (MFB) is the accumulated released heat in successive crank angle ranging from the start to the end of the combustion divided by the total heat released in the entire combustion process (17). MFB10, MFB50 and MFB90 are defined as the crank angle

degree (◦CA) when MFB is 10%, 50% and 90%, respectively. Ignition delay is defined as the ◦CA interval between spark timing and MFB10. The combustion duration is defined as the ◦CA interval between MFB10 and MFB90.

3.9.4 Combustion Efficiency

Combustion Efficiency is determined by subtracting the heat content of the exhaust gases (e.g. HCs and CO), expressed as a percentage of the fuels heating value from the total fuel heat potential. The fraction of chemical energy that is burned, compared to that which is supplied, is expressed by the combustion efficiency (54) and equation 3.3 (291) is used for the calculation of combustion efficiency.

$$\eta combution = 1 - \frac{\dot{M}coQLHVco + \dot{M}HCQLHVfuel}{\left[\frac{\dot{m}air}{\dot{m}air+\dot{m}fuel}\right] QLHVfuel} \text{----------(3.3) (291)}$$

$\dot{M}_{CO}$ is the mass fractions of CO, $\dot{M}_{HC}$ is the mass fractions of HC, QLHVco is the lower heating values of carbon monoxide, and QLHV fuel is the lower heating values of the fuel used. The actual calorific value of hydrocarbon is unknown and this is because the hydrocarbons are not speciated. The fuel and the unburned hydrocarbons is assumed to have the same calorific value.

3.9.5 Indicated Specific Fuel Consumption

The use of high-pressure direct injection fuel system for the experiment make it difficult the fuel usage to be measured accurately by the use of a burette or mass balance. The specific fuel consumption on the basis of indicated power (ISFC) is calculated from the inducted gravimetric air flow rate procedure for the measurement of the airflow rate are detailed in section 3.10 below), λ value from an ETAS Lambda Meter (model LA3) and the engine power output.

$$ISFCd = \frac{\dot{m}air * \frac{F}{A} * \lambda}{Power} \text{----------(3.4) (292)}$$

F/A is the stoichiometric fuel air rate, λ is the lambda value and the power represent the engine power output.

3.10 Volumetric Air flow Meter (VAF)

A Romet (model number: G25) VAF meter is a high precision custody transfer grade instrument for airflow rate measurement into the single cylinder thermal engine. The Romet VAF is designed to admit a fixed volume of air for each revolution of the meter. This Air flow meter is expected to register the operating air volume using an eight-digit mechanical counter and via pulses the operating volume can be transferred to an electronic volume corrector (EVC). However, in this experimental study the air flow rate was not measured by this technique. Instead an encoder is coupled to the shaft of air flow meter. National Instruments counter-timer card (model 6202) was used to record and process the TTL signals generated by the encoder. A calibration is required in order to establish the relationship between the volumetric airflow rate in the engine and the frequency of the encoder. This calibration was conducted at different engine volumetric airflow rates and different throttle angles. The orifice plate used to measure the airflow in the engine and the pressure difference created were measured using an inclined u-tube manometer. The recorded data from the study was used to determine the actual flow rate in the engine using the equation developed by Eastop and McConkey, 1993 (293).

$$Q\ (l/min) = C_d A_2 \sqrt{\frac{1}{1-\beta^4}} \sqrt{\frac{2(P_1-P_2}{\rho}} \quad \text{----------(3.5) (293)}$$

β and C_d are dimensionless numbers with respect to the ratio of the orifice plate diameters (d_2/d_1) and (P_2-P_1) is the Pressure difference measured by the U tube manometer.

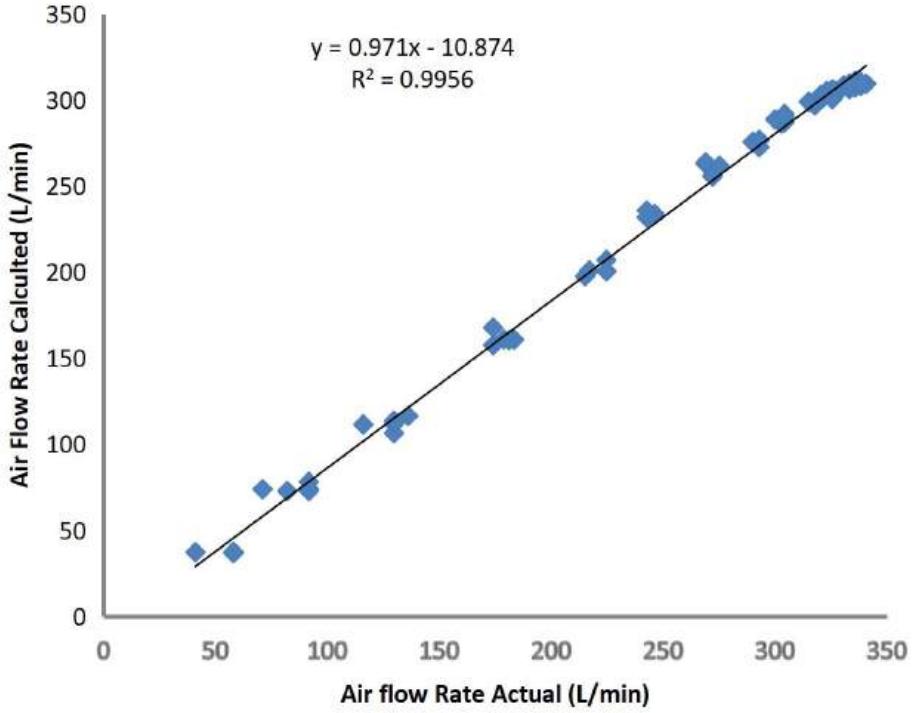

Fig. 3.12: calibration of the Volumetric Air Flow Meter.

The encoder frequency was recorded and the correlation between the two was calculated. The calibration curve for the actual and calculated airflow rates are shown in figure 3.12. The minimum and maximum VAF rates are 200 and 350 l/min respectively. The percentage error between the calculated and actual airflow rates of 1.6% even with R^2 value of 0.9956. The error in the study is mostly due to the U-tube manometer error of limited resolutions as a result of the unsteady flow through the orifice plate and the limited unit pressure difference produced across the orifice plate. To convert the volumetric air flow rate to mass air flow rate in a spark ignition engine, you need to use the density of the air. The relationship between volumetric flow rate and mass flow rate is given by the following formula:

$$\dot{m}=\dot{v}*\rho \text{ ----------3.6 (294)}$$

$\dot{m}$ is the mass flow rate (kg/s), $\dot{V}$ is the volumetric flow rate (m^3/s). and ρ is the air density (kg/m^3).

3.11 Emission Measurement

This experimental study investigates both the legislated and unlegislated European and US emissions referred to as the regulated and unregulated emissions respectively. HC, CO, NOx and PM emissions are measured as the regulated emissions. The Horiba MEXA-7100DEGER analyser is used to measure the gaseous emission while DMS 500 were used to measure the particulate emissions. The unregulated emissions of the unburnt hydrocarbon species are measured using the Gasmet FTIR. These emissions measuring devices are described in the following sub-sections.

3.11.1 Gaseous Emission

In this study Horiba MEXA-7100DEGR tower type exhaust gas analysers are used for the gaseous emission measurements. The Horiba analyser was purged with nitrogen to avoid contamination build-up from a stagnant sampling zone and calibrated using suitable span and zero calibration gases before each test schedule. Also, when not measuring, the analyser was purged. At the start of a test schedule, before any measurements are taken the heated line and pre-filter are maintained at a temperature of 191°C for about 30minutes to burn off the vapour or residuals gases from previous test and to keep HCs from condensation and preventing it from dissolving in water. The exhaust is sampled downstream of the exhaust plenum via a heated line. The analyser modules are calibrated by the use of zero calibration gases and the suitable bottled span. The different exhaust gas components measured and the measurement method used are listed in Table 3.3.

Table 3.3 Exhaust gas components and Measurement Methods.

	HC	CO	CO_2	NO_2
Methods	FID (hot-wet)	NDR (dry)	NDIR (dry)	CLD (dry)
Min (ppm)	0-10	0-100	0-5000	0-10
Max (ppm)	0-5000	0-12%	0-20%	0-1000
Zero gas	N_2/air	N_2	N_2	N_2
Span gas	C_2H_8	CO/N_2	CO/N_2	NO/N_2

The Nitrogen oxide (NO) analysis is undertaking using the chemiluminescence detector. When NO reacts with ozone; photon is emitted. The photon current creates a voltage output which is a function NO concentration in the sample. The ozone in the reaction is created by O2 balanced in N_2. NO_2 is first converted to NO before reacting with ozone and this is used for NO2 measurement. Carbon oxides (CO and CO_2) is analysed using a Non-dispersive infra-red (NDIR) detector. Carbon oxides absorb infrared. The changes in the light intensity when an infra-red beam passes through a sample gas chamber, is used for the analysis of carbon oxides concentration. The concentration of the total HC in the Horiba is measured using flame ionization detector (FID). The process comprises of introducing the sample gas at a high voltage into a hydrogen flame. The hydrocarbon molecules in the high-temperature hydrogen flame environment, is ionized resulting in a current flow between the nozzle and a collector. The total HC in the sample is measured by detecting this ion current and converting it into a voltage output.

3.11.2 FTIR Technology

Fourier transform infrared spectroscopy (FTIR) is a technique used to obtain infrared spectrum based on the amount of absorption or transmittance of IR in a sample. FTIR is frequently used in a wide range of structural analysis and non-destructive measurement applications. The basic

components of FTIR are indicated in figure 3.13. Gasmet FTIR is used for HC emission speciation analysis. It is a powerful gas measurement technology for simultaneous measurements of multiple gases. The ability to detect and measure almost any gas, combined with the robustness and reliability of the technology, makes the FTIR ideal for a wide variety of applications, such as emissions monitoring devise. The devise allows up to 50 compounds to be measured simultaneously. Compounds can be easily added or removed from the analysis application by simple software adjustments that can be performed by the user in the field. In an FTIR analysers, the identity of an unknown compound(s) is determined from the residual spectrum. The Gasmet Technologies' reference library of 300+ compounds is provided to users in the form of continuous application support, this together with the simplicity of altering the analysis settings makes the instrument very flexible and cost effective.

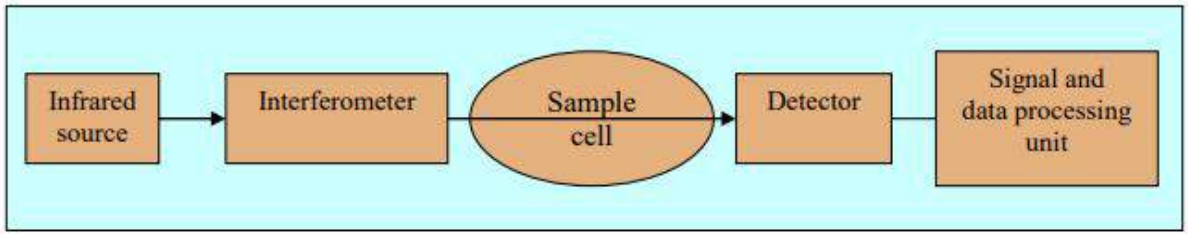

Figure 3.13 The basic components of an FTIR spectrometer.

In normal emissions monitoring application, there are approximately 10-15 compounds (depending upon final instrument configuration) that will be monitored. Typically, these include H_2O, CO_2, SO_2, CO, NO, NO_2, (NOx), N_2O, NH_3, HCl, HF, CH_4, C_2H_4, C_2H_6, C_3H_8, C_6H_{14}, CH_2O. The Gasmet CEMS monitors all of these compounds continuously. The Gasmet CEMS can also measure TOC (Total Organic Carbon); compounds are measured individually and can also be added together by the software to produce a figure for total TOC. That is, the entire spectrum is scanned ten times per second and an average calculated from this is reported for each (user selectable) sampling period. This is a major benefit since it makes unnecessary to have an additional analyser such as FID (Flame Ionization Detector).

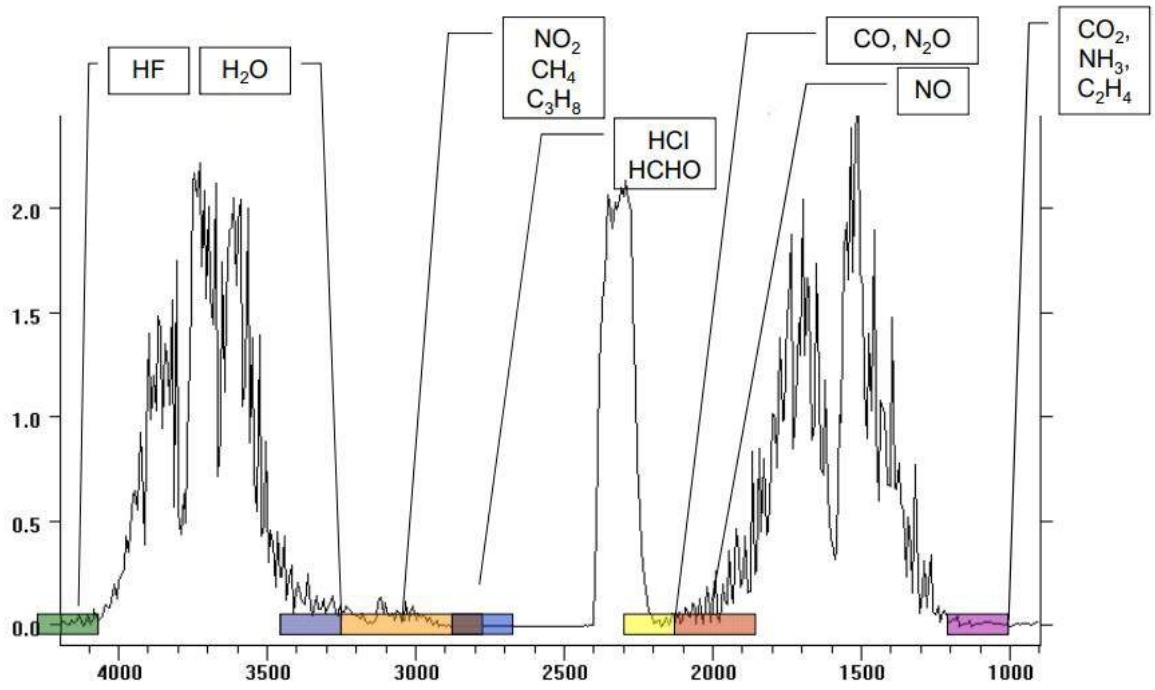

Figure 3.14 Basics HC speciation by FTIR Analysis.

FID analysers require additional maintenance and also need a carrier gas (usually Hydrogen) and Oxygen (zero air) to function. Moreover, an FID does not give any information on the proportions of different hydrocarbons in the sample gas. The Gasmet FT-IR stores the results of the entire spectrum; this is a major benefit since the raw data is available for post processing. Using this feature, we are able to identify compounds that the instrument was not configured to report during the sampling period. In essence, the sample spectra and the analysis results are two separate things with an FTIR – analyser like the Gasmet. Gasmet has the flexibility to post process the data and quantify emission levels of compounds not being reported in real time. Basics HC speciation by FTIR Analysis are display in figure 3.14. The Gasmet uses a hot & wet sample extraction system. The sample is drawn from the stack and passes through heated sample probe, heated lines heated pump to the heated sample cell. Particulate matter is removed from the sample but not moisture. This ensures that we are measuring a representative sample of the flue gas, not a dried or diluted version. Therefore, we can also reliably measure water soluble compounds such as HF, HCl and NH3. Furthermore, this system significantly reduces

maintenance - all that is required is filter cleaning and or changing as needed depending upon the dust burden in the stack.

3.11.3 FTIR Calibration

Each Gasmet analyser is subject to a factory specific calibration, after the manufacturing and final testing have been completed. Each calibration gas is introduced to the instrument in known concentrations in pure nitrogen. Reference spectra are generated in different concentrations to cover the complete measuring range. Gas mixtures are generated and cross interferences tested. The instrument specific calibration ensures the best possible performance. There's no need to do any span calibrations with the Gasmet CEMS since each Gasmet gas analyser has a built-in He-Ne laser. The laser signal is used to measure the exact position of the moving mirrors in the interferometer. The measured interferogram presents the detector signal strength as a function of the mirror position. Now, when we make the FFT (Fast Fourier Transformation) to the measured interferogram, the result is the infrared spectrum. The mirror position scale is transformed to the wavenumber (wavelength) scale, which is thus measured with laser precision. As such, the instrument is continuously calibrated with a He-Ne laser, which provides a stable wavenumber scale. High spectral signal-to-noise ratio and high wavenumber precision are characteristic of the FTIR method. This yields high analytical sensitivity, accuracy and precision. It is necessary to make the zero calibration (background) measurement once a day. The zero calibration compensates for all changes in the signal level or in the instrument. Background spectrum is measured by filling the gas cell with an infrared-inactive gas (for example, dry nitrogen, dry oxygen, or even dry instrument air). No other gases / recalibrations are ever needed; H_2O is the only exception in normal operation. The H_2O calibration must be valid in order to make reliable measurements for other components. We recalibrate H_2O each time an analyzer is serviced, typically during the annual maintenance (that is, once a year). Thus, the Gasmet CEMS does not require span checks per se. However, in some countries the legislation requires span checks to be conducted periodically to prove that the instrument is

responding correctly. Simple span checks can be provided via the valves on the sampling system by simple activation of the span solenoid valve. The background is automatically measured daily on the Gasmet CEMS by purging the sample cell with Nitrogen. This system accounts for any baseline drift and frequency can be programmed by the user (typically 24 hrs or 12 hrs). In addition to the span checks detailed above, a procedure that is commonly known as “Spiking” is also possible through the sample probe. Spiking introduces a calibration gas of known concentration into the sample at the probe, which is mixed with the stack gases so that the entire system can be tested in order to prove the can detect the calibration gas in amongst the actual sample. This can be required to prove that compounds in the sample are not causing interference. With all types of IR – analysers, one source of measurement uncertainty is spectral overlapping i.e. cross interference. In the Calcmet – software cross-interference is automatically taken into account in the analysis settings of each compound. And, should there be a previously unknown compound in the sample, the Calcmet – software gives a warning to the user with an increase in the residual of the compound(s) that are affected by the unknown. The Gasmet CEMS has the MCERTS approval (UK) and TÜV (13. and 17. approvals for continuous emission monitoring. The Gasmet FTIR analyzers also comply with the requirements of US EPA Method 320 - Vapor Phase Organic & Inorganic Emissions by Extractive FTIR. Gasmet Technologies Oy has also ISO 9001 certified Quality Management System.

3.11.4 Particulate Matter Emissions

The PM emissions are measured using DMS500 system. The DMS500 is a combustion particulate emission measuring facility and it classifies particles according to their size by separating them in a parallel differential electrical mobility analyser. PM size distribution basically consists of two modes (295), the nucleation mode and the accumulation mode. The nucleation mode has more influence in number of particles while the accumulation mode is concern with the particle mass distribution due to its higher size. Engine exhaust contains water vapour from the combustion of hydrocarbon fuel. To prevent the condensation of this gas inside

the DMS500 (and consequent damage to mass flow meters and other components) dilution is necessary such that the dew point of the gas being sampled is below the ambient temperature of the instrument. The first dilution stage uses metered compressed air to provide low ratio dilution up to 5:1 during transient engine conditions. This dilution uses dry air to reduce the dew point of the sample gas such that no condensation occurs inside the DMS500. For raw exhaust sampling 1st dilution should normally be 5:1 for gasoline engines. The second stage uses a rotating disc to provide a high dilution ratio which may be varied to maintain good signal to noise ratio while minimising the cleaning requirements of the instrument. The dynamic range indicator on the right of the main interface window shows the current concentration compared with the dynamic range of the electrometers. With high concentration aerosols, the 2nd dilution ratio should be adjusted to keep this indicator predominantly within the green region when sampling combustion particles, or within the green or yellow regions for other aerosols. The main graph displays the measured aerosol spectrum as a red line. The size range displayed is that for which the instrument is calibrated. The Y-axis can be rescaled by clicking on the top or bottom axis labels and overtyping, or it can be reset to the current aerosol concentration by View>Auto-Scale or CTRL-A. A logarithmic y-scale can be selected by View> Logarithmic Y-axis. The spectrum is displayed as size spectral density, dN/dlogdp /cc. This allows easy comparison between spectral measurements from different instruments which may resolve a different number of sizes in a given size range. For engine emissions (the Diesel or GDI .dmd file), whether a peak is classed as nucleation or accumulation is based upon a probability map of peak size (CMD, count median diameter) and width (geometric standard deviation, GSD).

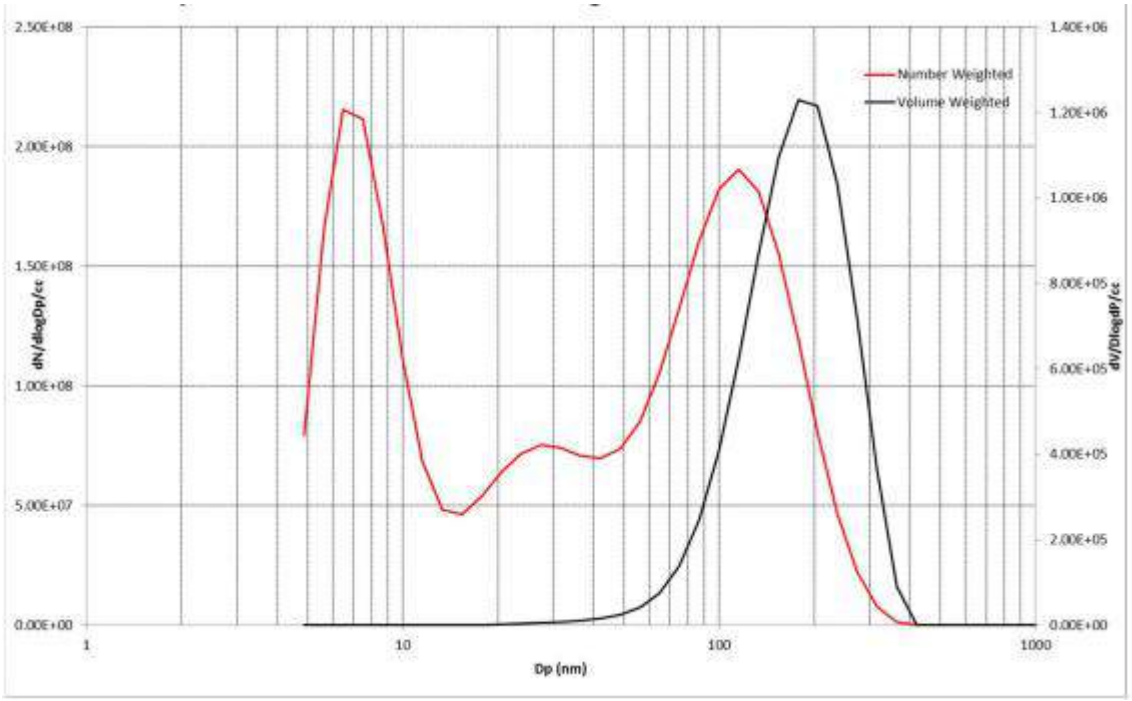

Figure 3.15 Number and Volume Weighted GDI Exhaust Size Distributions.

For each mode, the size (CMD in nm), concentration (in N/cc) and width (GSD) are recorded in the data file. These quantities may be plotted as normal by MS Excel or any other package. Note that the CMD and GSD values are only valid when the concentration for that mode is greater than zero; when plotting these it is often best to test for the concentration being equal to zero and then actively exclude these points from the graph. In determining the average CMD or GSD over a certain time period, it is best to weight the average by concentration for the same reason. The accumulation mode concentration is the quantity to use for Particle Measurement Programme (PMP) type solid particle number comparable measurements. This is because the accumulation mode (for Diesel at least) can be considered to mainly consist of solid particles, and by using this value the nucleation mode (consisting of volatiles) is in effect removed in software. Figure 3.15 display a typical comparison of number and volume weighted in a GDI Exhaust Size spectral sample distributions.

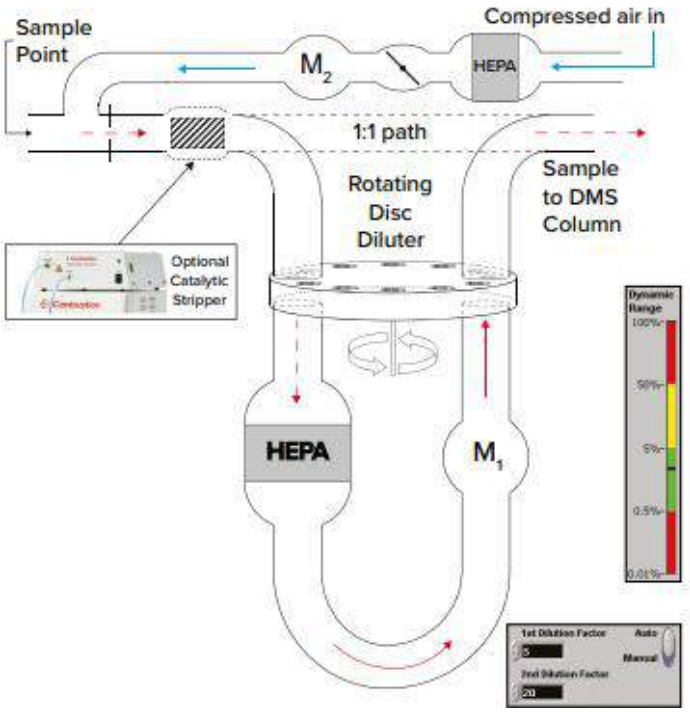

Figure 3.16 DMS500 Sampling & Dilution System (with optional CSA).

When running the Diesel .dmd file, the accumulation mode uses a different calibration to the nucleation mode and discrete spectrum; this gives more accurate results when comparing with PMP number measurements due to differences in the charging of agglomerates to more spherical particles. This produces a three-dimensional animation of the spectrum (or the raw ring currents). The Sampling and dilution System with optional CSA in DMS500 are as indicated in figure 3.16. The spectrum may be animated by dragging the slider, or by double clicking the animation button on the toolbar. The analogue inputs are also plotted below by default, and the graphs may be customised as required using normal MS Excel means. The neat fuels used in this study are Unleaded Gasoline (ULG), Ethanol (ETH), 2-Methylfuran (MF), 2-Methyltetra hydro furan (MTHF) and Cyclopentanone (CP). The properties of the neat fuels discussed in this thesis are shown in Table 3.4. The commercial gasoline and ethanol were supplied by Shell Global Solutions, UK, whereas MF, MTHF and CP were supplied by Fisher Scientific, UK at 99% purity. Two Chinese suppliers were used to complement the supply of 2-Methyltetrahydrofuarn (MTHF) and Cyclopentanone (CP, Shijiazhuang Lida Chemical Co. Ltd.

and Beijing LYS Chemicals Co. Ltd), due the high cost of production in Europe. In all the discussions and figures listed in this paper. The fuels were blended volumetrically. A calibrated laboratory burette were used for the measurement of the blends and the base fuels and vigorously blended together running it to the engine. A fuel properties calibrator table based on the linear transposition of the properties of each of the fuel

Table 3.4 Fuel Properties (16, 34, 140, 190, 200, 207, 234, 235, 296, 297).

Properties	MTHF	MF	CP	ULG	ETHANOL
Molecular formula	$C_5H_{10}O$	C_5H_6O	C_5H_8O	C_2-C_{14}	C_2H_6O
LHV(MJ/Kg)	34.12	31.2	34.8	42.9	26.9
RON	88.2	103	101	96.8	107
MON	71.2	86	89.4	85.7	89
Stoichiometric A/F	11.16	10.05	10.6	14.46	8.95
HV (KJ/Kg)	375.3	358	433	373	840
RVP (Kpa)	13.6	18.5	11.5	32.8,	5.83
Density20^0C(Kg/m3)	854	913.2	948.69	744.6	790.9
H/C ratio	1.96	1.8	1.6	1.795	3
Gravimetric O_2 Content. (%)	18.58	19.49	19.05	2	34.78
Melting Point	-136	-83	-47	-57	-114
Initial boiling point (°C)	80.3	64	130.6	25.4	78.4

components in the blends fuels were used to compute the final property of the blended fuel based on the percentage composition of each of the fuel in the blend. This fuel property model was developed by the Future Engine research team of the University of Birmingham to evaluate the final properties of the blended fuels based on the percentage composition of each fuel in the blend.

3.12 Statistical Analysis of Uncertainties in the Recorded Data

The section provides a guide to the accuracy of the data obtained from this research study. The data collected from this investigation is generally of a very high accuracy level, however, there are data accuracy limitations due to the accuracy of the engine test rig and the emission measuring device accuracy and the accuracy of the data analysis methodology. The accuracy of the engine test rig and emissions measurement systems were obtained from the respective manufacturer instruction manuals. This is in line with the work of previous research students in the engine group (16, 280). In order to ensure the accuracy of the dynamometer speed control a Mentor II Digital DC Drive manufactured by Control Technologies is used. The encoder has a resolution accuracy above 0.01% and the speed-holding accuracy of the drive is 0.1%. The variable cam timing (VCT) accuracy for the steady state positional (valve timing) is typically ± 0.1 CAD, for stable operating conditions. as shown on the system Lab-view control panel. The linearity error of the Kistler 6041A water cooled pressure sensor and the Kistler 5011B charge amplifier are ± 0.5% and $\pm 0.05\%$ of the full scale respectively. At high engine load of 8.5 bar IMEP and engine speed of 1500 RPM, there is often short-term drift and change in IMEP value when compared to the reference sensor. This rift is explained by the manufacturer to be less than ± 0.25 bar for the engine load and less than ± 2% for the speed. The gaseous emissions were measured with a MEXA 7100DEGR, manufactured by Horiba Instruments Limited. In line with the manufacturer manual, the MEXA-7100DEGR has a zero/span drift of no more than ± 1% of the full scale measured over a period of 8 hours. The DMS500 manufactured by the Cambustion Ltd was used for the PM emission measurement. It has a particle count accuracy of $\pm 16\%$. Gasmet FTIR analysers meet the performance requirements laid down in EN 15267-3 (Europe) and PS 15 (U.S.). Linearity deviations are less than 2% of full scale and cross interference effects due to stack emissions gas (H2O up to 40 vol-%) are less than 4% of full scale for certified gases. Measurement accuracy is typically expressed in terms of expanded measurement uncertainty (Uc), a combination of uncertainty sources such as: nonlinearity (lack

of fit), cross-interference, zero and span drift ,temperature, flow rate, pressure, and main voltage. Measurement uncertainty for specific gases (CO, NO, NO_2, SO_2, HCl, HF) has a limit value proportional to emission limit value in the EU Industrial Emissions Directive, and the Gasmet system typically has measurement uncertainties smaller than one half the maximum uncertainty allowed for a certified (EN 15267-3, TÜV, MCERTS) emissions monitoring system. This ensures that Gasmet gas analysers are capable of monitoring not only today's emission limits but also lower limit values that may be introduced in the future. Prior to each test, the engine oil and coolant temperature were allowed to be steady over a period of thirty minutes to ensure steady state operating condition and for improve reliability of data obtained from engine test. The engine tests were repeated thrice for each batch in order to minimise any experimental uncertainty. Whenever possible, the tests were performed over 3 consecutive days, in varying order, in order to minimise the effect of ambient conditions and engine drift, as recommended by leading researchers (297, 298). The repeatability of the data collection was highlighted using the error bars. Sample standard deviation were used for the variability or error bars of parameters tested, this are presented in Equation 3-6.

$$Error\ bar = \pm t_{(\frac{a}{2}*n-1)}(\frac{S}{\sqrt{n}}) \quad \text{----------3.7 (299)}$$

The statistical equation is a sample size and t distribution equation, where n represents sample size; a represents significance level and s represents the sample standard deviation. When the data sample size is less than 30 t distribution equation is used for the sample error bar analysis, if the data sample sizes exceeded 30 Gaussian distribution will be used instead of t distribution. The error bars only address the random errors which occurred in the measurements. The manufacturer manuals provide information on the System errors such as zero errors, and calibration errors.

3.13 Summary

This chapter described the experimental test facilities used in this research study. The spray-guided 4-stroke, DISI single-cylinder thermal engine was used to conduct all the tests. The engine is a variable valve timing (intake and exhaust) system with a compression ratio (11.5:1) and modern gasoline DISI engines. Although the author was fortunate to benefit from the engine setup developed by the previous research students at the University, the facility benefitted from a major engine rebuild and improvements to the engine DI fuel supply system during the tenure of this research work. Firstly, the engine rebuilds witness the Nitriding of the crankshaft, a process where oxygen is vacuumed out and nitrogen is introduced which penetrates the entire surface. The crankshaft Nitriding was done to obtain a high-temperature property of its surface and improve the surface hardness of the shaft as well as to increase its wear resistance and the fatigue life. The top cylinder gasket was redesigned and manufactured in-house using copper alloy material to replace the earlier used one produce on aluminium alloy material. Secondly, the cumbersome DI fuel supply system which normally introduce vapour to the fuel cell during the test operation was replaced with the new highly efficient DI pump manufactured by Haskel Europe Limited. This improved safety in the engine test cell and made fuel refilling easier. Secondly, the creation of separate fuel tank for non-gasoline fuels made it easier to prevent contamination of the gasoline and non-gasoline fuels. This author was fortunate to benefit from the use of the Gasmet FTIR for the measurement of the unregulated emissions. As at the time of the study the FTIR was on lease to the University future engine research group by the GASMET company. Finally, the procedure for minimising error in data collected is briefly discussed.

CHAPTER 4

COMBUSTION AND EMISSION CHARACTERISTICS OF 2-METHYLTETRAHYDROFURAN AND CYCLOPENTANONE

This chapter examines the sensitivity of 2-Methyltetrahydrofuran (MTHF) and Cyclopentanone (CP) to various engine parameters, in particular, engine load, Air fuel ratio (AFR), and fuel injection pressure. 2-Methylfuran (MF), Ethanol and gasoline are used as the based fuel for the study. The effect of varying engine load is examined at the fuel specific MBT/KLSA timing. The increase in oxygen content of each of the oxygenated fuel is shown to give rise to improve combustion and emissions performance. Athough there are documented literatures on the combustion of both gasoline blends of CP and the gasoline blends of MTHF, the novelty of this study is that this is the first study that investigated the combustion characteristics and the emission behaviour of the neat CP and MTHF as engine fuels in spark ignition engine.

4.1 Experimental Procedure

The experiments were performed using a single-cylinder spray-guided DISI engine. The engine specifications are listed in Table4.1. The engine was naturally aspirated with a throttle controlling the intake air flow rate. Constant engine speed (±1 rpm) was maintained for the experiments by the action of a direct current dynamometer coupled to the engine. An in-house software written in Lab-view control the operations of both the High Data Acquisition (HDAQ) and Low Data Acquisition (LDAQ). The engine is runs on the PFI injection system mode for the first 20 minutes to achieve steady state combustion before the experimentation. The engine fuel injection system is switched to GDI mode to replace the PFI injection system when the coolant and oil temperatures stabilises at 358K ±1 and 363K ±1 respectively. Fuel-optimised spark timings, also known as the MBT timings, were used for the tests.

4.2 Effect of Engine Load on combustion and the emissions of MTHF and CP

The combustion characteristics and the emissions of MTHF and CP in a single cylinder direct-injection spark ignition engine (DISI) were investigated at engine loads range of 3.5-8.5bar IMEP. The experiment was conducted at the constant engine speed of 1500rpm and at the stoichiometric engine condition (λ=1). In this work, the MBT timing is defined as the spark timing to produce the maximum IMEP for a fixed throttle position (λ=1). If audible knock occurs, the MBT timing is retarded by 2CAD. At this point, the spark timing is then referred to as the knock-limited spark advance (KLSA) (300). The result of this test was compared to the result of the same test carried out on gasoline ULG 95, MF and Ethanol. The combustion parameters investigated include the cylinder pressure, mass burn fraction, rate of heat release, cylinder temperatures, indicated thermal efficiency, fuel consumption, combustion efficiency, MFB1090 and ignition delay.

Table 4.1 Operating conditions for the Experiment.

Speed rpm	IMEP bar	Injection Pressure	Injection timing cad BTDC	Fuel Type	Spark timing cad BTDC
1500	3.5-8.5	150	280	MTHF, CP, MF, Ethanol and Gasoline	MBT/KLS

4.2.1 Indicated Specific Fuel Consumption and Combustion Efficiency

The indicated specific fuel consumption (ISFCs) for MTHF and CP and the other three fuels at MBT spark timing are shown in figure 4.1a. The experiment was conducted under the MBT/KLT timing as indicated in table 4.1. The effect of gasoline's superior energy density relative to the other fuels is distinctly clear as shown in figure 4.1a, gasoline offers lower ISFCs

across the load range compared to the other four fuels under investigations. MTHF has an improve fuel economy compares to both CP, MF and Ethanol largely because of its higher lower heating values and partly because its high combustion efficiency. As indicated Table 3.4 on page 84, the LHV of MTHF (34.12 MJ/kg) is about 8.5% higher than that of MF (31.2MJ/kg) and about 21.16% higher than that of ethanol (26.9MJ/kg). Despite the lower heating value of CP (34.8MJ/kg) is slightly higher than that of MTHF, the recorded specific fuel consumption of MTHF is lower than that of the CP, this is due to higher combustion efficiency recorded by MTHF compared to CP as indicated in figure 4.1b. Higher combustion efficiency means higher completeness of combustion which results in reduced fuel consumption. Typical combustion efficiencies for SI engines operating under lean conditions, are between 95-98% (54). The 2%-5% incomplete combustion is because of the unreleased chemical energy combusted products like CO, and unburned HCs (278). Ethanol generally exhibits higher combustion efficiency than gasoline and other oxygenated fuels across both low and high loads due to the combine influence of its higher oxygen content, higher flame speed, higher heat of vaporisation, high octane rating and lower combustion temperatures compared to the other four fuel investigated. Ethanol consistently recorded the highest combustion efficiency, closely followed by MF and then MTHF and CP with gasoline recording the lowest combustion efficiency. The observed higher percentage of the combustion efficiency of the four oxygenated fuels compare to gasoline is due to the the higher oxygen content in their molecular structure which promotes complete combustion thereby increasing their combustion efficiency. The oxygen that hinders the fuel consumption performance because it offers no additional energy, paradoxically improves the completeness of combustion (4). Combustion efficiency is equally partly associated with combustion temperature. Higher combustion temperature leads to more complete combustion and HC post-oxidization.

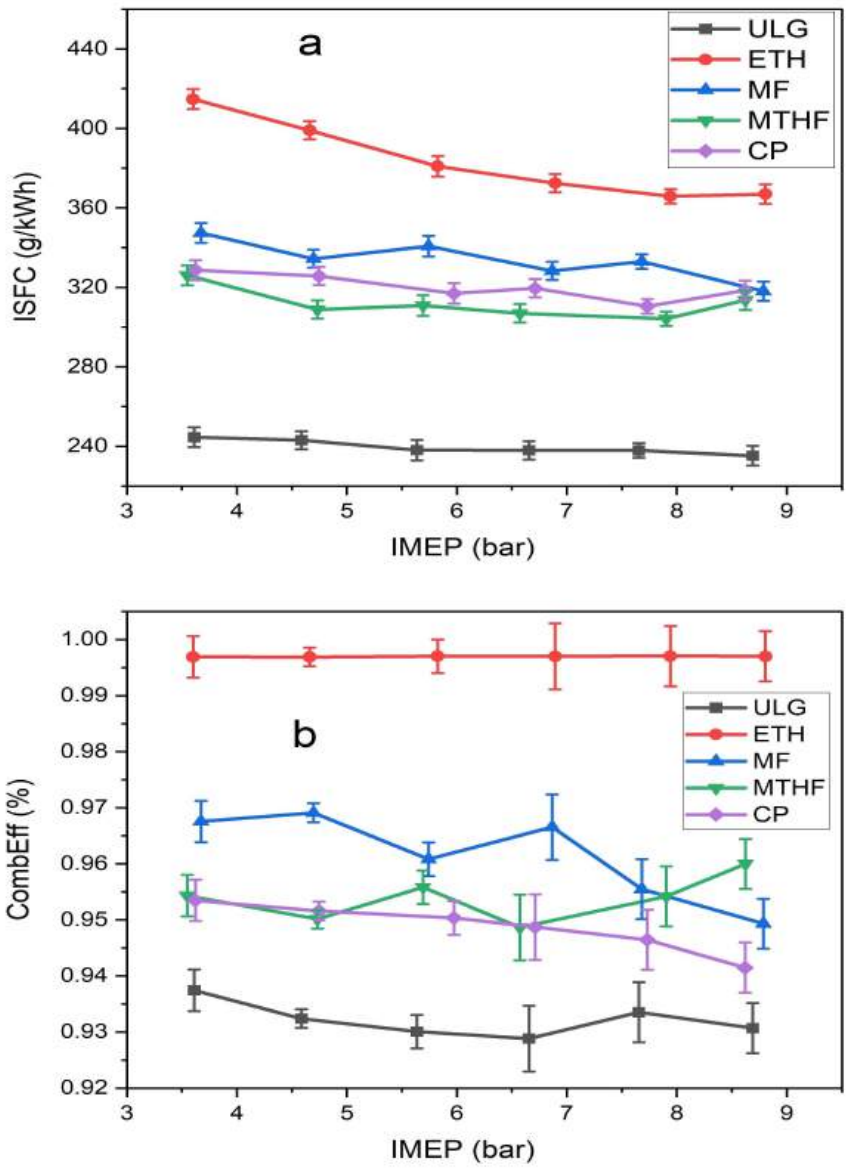

Figure 4.1a) ISFC for the fuels at 3.5-8.5bar IMEP and at MBT/KLT spark timing b) Comb Eff for the fuels at 3.5- 8.5bar IMEP and at MBT/KLT spark timing.

4.2.2 Spark Timing

The fuel optimised (MBT/KLSA) spark timings at the various loads are shown in figure 4.2a. No significant difference was observed on the MBT/KLSA locations for all fuels at the low loads of 3.5bar IMEP. However, as the load increases from 4.5bar IMEP, the MBT/KLSA locations for all the fuels start to differ significantly. CP, MF and Ethanol shows considerable spark advance flexibility especially at the high loads. MTHF displayed similar spark timing pattern to ULG at low and intermediate loads but drop sharply at the high load. The maximum

difference in spark advance between MTHFF and Gasoline is 3CAD at the highest load of 8.5bar IMEP. The spark advance flexibility of Cyclopentanone is superior to MF, MTHF and ULG at the highest load. However, CP display similar spark advance pattern with ethanol. Just like Ethanol the spark advance window of Cyclopentanone did not peak at the maximum load. The most advanced spark timing was observed with CP and ethanol which is about 3CAD, 12CAD, and 15CAD greater than MF, ULG and MTHF respectively at the Peak load. The low octane number of the MTHF. (RON 88) compared to gasoline (RON 96.8) has indicated the effect of Knock will be significant to mitigate against spark advance for MTHF fuel at high loads. Knock-resistant ability of fuels is closely related to their Research octane number (RON) (301) and this decreases with the increase in the fuel carbon chain length and increases with the increase in the fuel carbon chain branches (34, 302). Both MF and MTHF have a methyl group ($-CH_3$) attached to their carbon ring. In MF, the methyl group is attached to one of the carbon atoms in the furan ring, and in MTHF, the methyl group is attached to one of the carbon atoms in the tetrahydrofuran ring. Overall, the research octane number of Ethanol (107) is higher compare to MF (103) which turn is more than the octane number of CP (101) and gasoline (96.8). Ethanol (C_2H_5OH) is an alcohol with a relatively simple molecular structure. It contains oxygen in its molecule, which promotes more complete combustion.

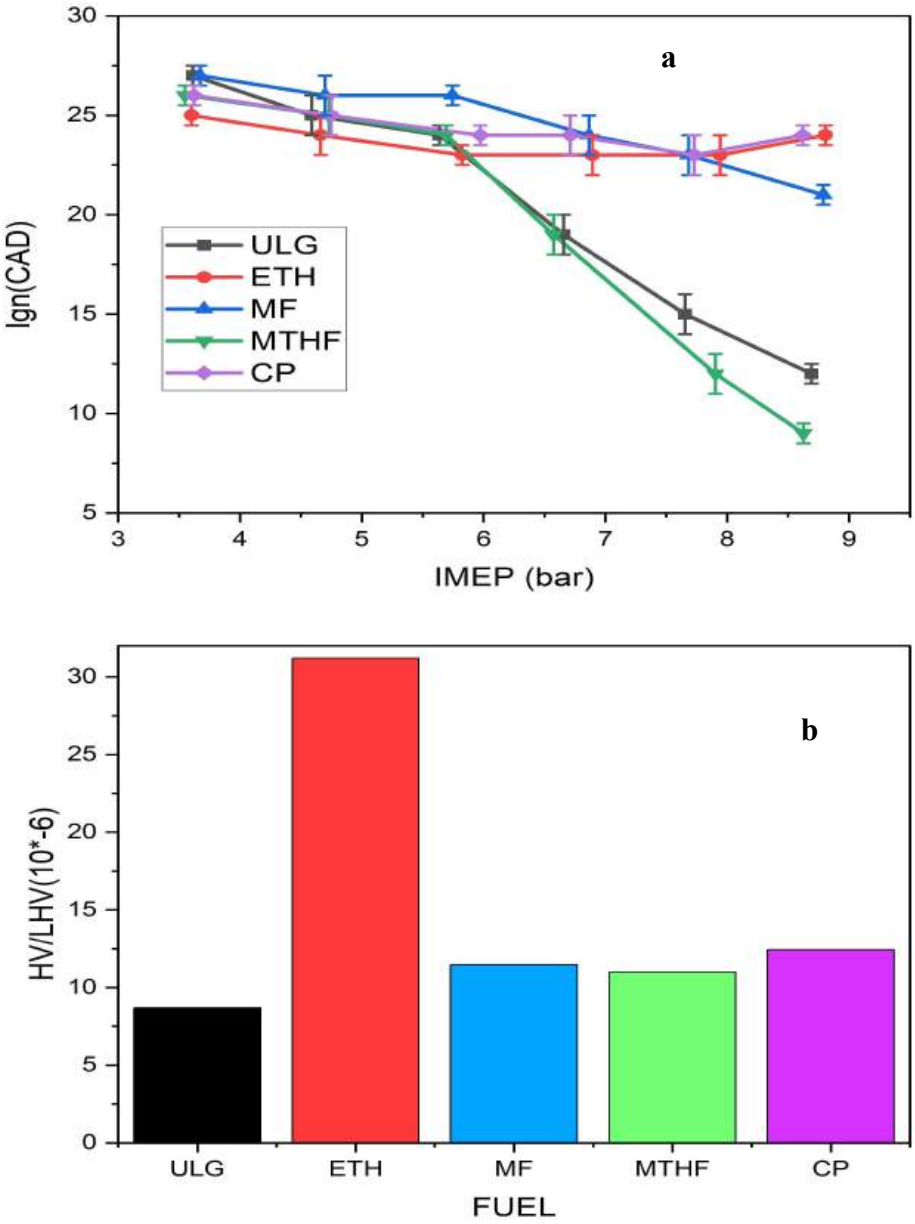

Figure 4.2a) Spark advance for the fuels at the load of 3.5-8.5bar IMEP and b) Ratio of heat of vaporization (HV) and Low Heated Value (LHV) for the fuels.

The higher-octane rating of ethanol is because it has a high resistance to knocking due to its ability to reduce the temperature and pressure at which auto-ignition occurs in the engine. Ethanol (C2H5OH) is an alcohol with a simple structure that burns cleanly and completely. Its oxygen content helps to ensure more complete combustion, reducing the likelihood of knocking. Cyclopentanone (C5H8O) is a ketone with a cyclic structure. While it has some oxygen content, its ring structure can lead to less stable combustion and a higher tendency to knock compared to ethanol. In addition, the simple two-carbon chain of ethanol combusts more predictably than the

five-membered ring of cyclopentanone. The knock suppression ability of fuels can also be explained by another factor which is the history of the fuel combustion temperature which is found to be influenced by the evaporative cooling effect as a result of the direct injection fuel supply.

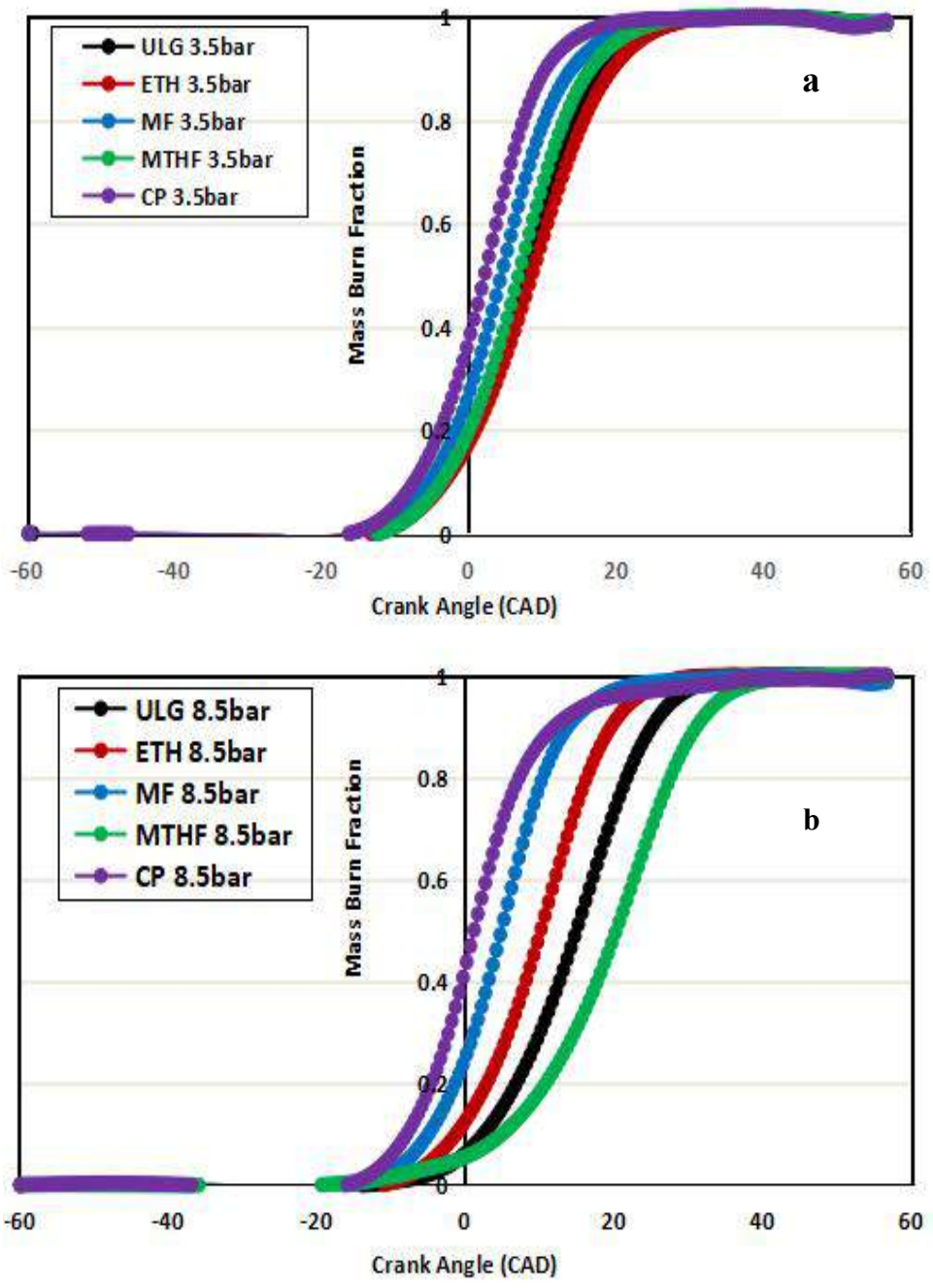

Figure 4.3a) MFB profiles for the fuels at 3.5bar IMEP and b) MFB profiles for the fuels at 8.5bar IMEP.

During the vaporisation process, liquid fuel absorbs heat from ambient air, which lowers the in-cylinder air temperature. The cooling effect between the fuels is evaluated using the ratios of Heat of Vaporisation (HV) and Lower Heating Value (LHV) as shown in figure 4.2b. The HV/LHV represents the amount of heat needed to evaporate the liquid fuel for one unit of fuel energy input. MF has a higher cooling effect compared to gasoline and MTHF. This means that the charge temperature on ignition is lower due to more energy that is absorbed from the vaporisation process. This phenomenon discourages end-gas auto-ignition (303). CP has a HV/LHV ratio higher than that of MF which explain why the spark advance flexibility is higher in CP compared to MF despite the facts that MF has higher octane number compared to CP. The HV/LHV for ethanol is greater than that of the other investigated fuels by 60.5%, 63%, 65.18% and 68.7% for CP, MF, MTHF and ULG respectively.

4.2.3 Combustion Phase and Ignition delay

The Mass Fraction Burned (MFB) profile for MTHF and CP and the other three fuels investigated are as indicated in figure 4.3. All the fuels investigated have similar spark timing at 3.5bar IMEP as indicated in figure 4.3a which explain why there is no clear cut differences in the burning rate of the fuels at 3.5bar IMEP. The trends in figure 4.3b indicates that at 8.5bar IMEP, CP burns faster than the other fuels. Several factors are used to explain the faster burning rate of a fuel which include the fuel volatility, lower heating value and the temperature of combustion. Higher combustion temperatures generally lead to increased MFB, as chemical reactions occur more rapidly at elevated temperatures, the higher combustion temperature of CP compares to the other fuels are as indicated in the later section on figure4.8b. The higher combustion temperature of CP are used to explain the reason for the faster burning rate of the fuel compared to the other four fuels under investigations. At 8.5bar IMEP, the combustion of MTHF is significantly the slowest than other fuels, which is because of retarded spark timing to mitigate the effect of knock at this load. Low combustion rate of MTHF at 8.5bar IMEP is a negative factor for engine efficiency. The combustion duration (defined by 10–90% MFB

interval in CAD) at various loads for each fuel is shown in figure 4.5a. The faster burning rate of oxygenated hydrocarbon has already been reported in many publications (304, 305). In the same trends, CP, MF and ethanol being oxygenated fuels have shorter CD compared to gasoline. The benefit of shorter CD is higher combustion stability and higher cylinder pressure. The trend of shorter CD was reported for MTHF at low and the intermediate loads, however, at high load the combustion duration of MTHF increases sharply by 4CAD compares to MF and 8CAD compares to Ethanol. At high load, the spark timing for MTHF was retarded to mitigate against the effect of knock. The weak cylinder turbulent associated with the retarded spark timing reduces the speed of combustion at this load and this explain the reason for the increases in the combustion duration of MTHF at high load despite been an oxygenated fuel. The ignition delay is divided into physical delay and chemical delay. Physical delay is the time required for atomisation of fuel, air-fuel mixing, and vaporization. Chemical delay includes pre-combustion reactions; it has an effect on premixing of air-fuel vapour and thermodynamic efficiency. The ignition delays for the fuels under investigations, areas indicated in figure 4.5b for the load sweeps (3.5- 8.5bar IMEP). Generally, for the fuel investigated, the ignition delay was observed to be reducing as the load increases. At 3.5bar IMEP, the ignition delay for CP was observed to be shorter than that of the other fuels. At the Peak load of 8.5bar IMEP the ignition delay for MTHF was about 3CAD faster than CP and gasoline and about 4CAD and 6CAD faster than MF and Ethanol respectively. The fuel octane number is a measure of its auto ignition tendency. Fuel with high octane number tends to have longer ignition delay. This explain the longer duration of ignition delay for MF, CP and Ethanol compare to ULG and MTHF at the high load. The ignition delay for MTHF reduces at high load due to the combined effects of increased temperature, pressure, and improved fuel-air mixing, which accelerate the chemical processes that lead to ignition. A longer ignition delay can allow for better mixing of air and fuel, leading to more complete combustion and improved thermal efficiency.

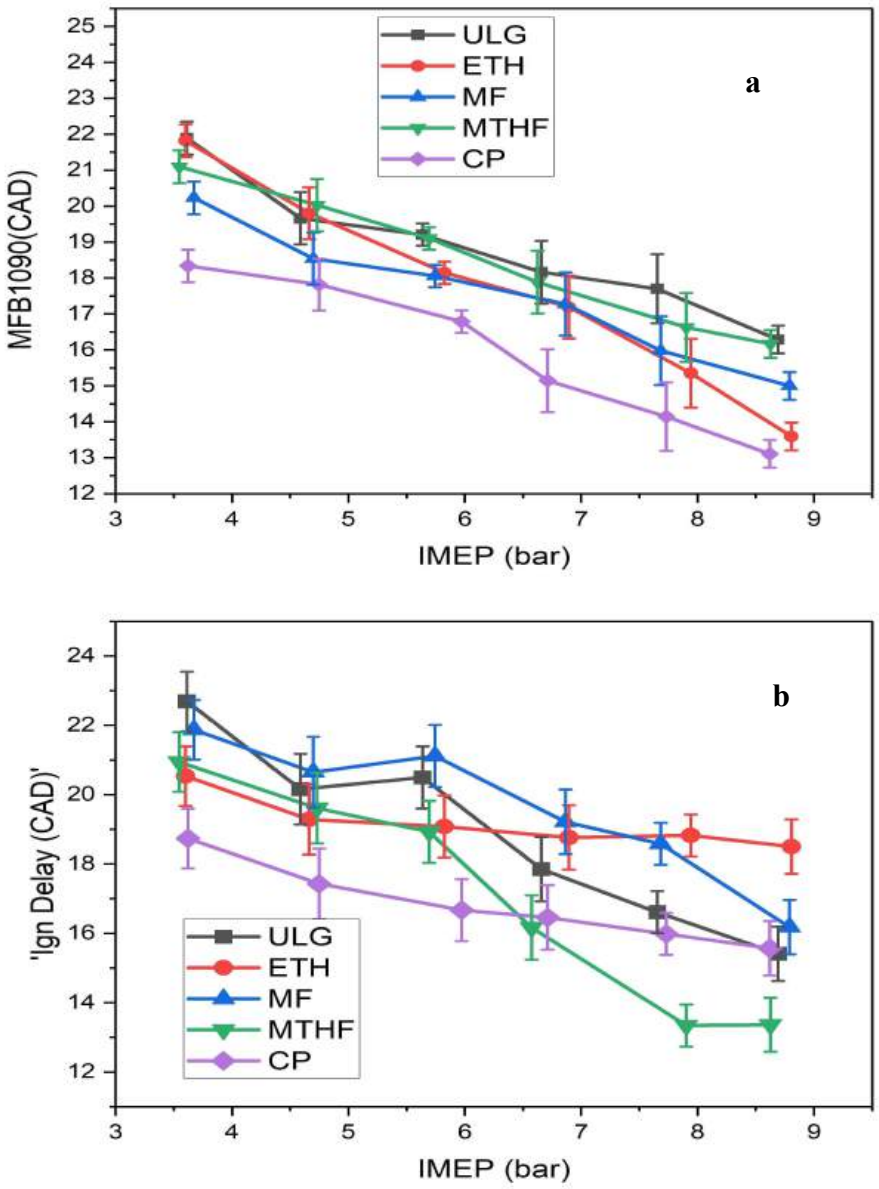

Figure 4.4a) MFB1090 profile for the fuels at the load of 3.5- 8.5bar IMEP and b) Ignition Delay for the fuels at the load of 3.5- 8.5barIMEP.

4.2.4 In-Cylinder Pressure

The in-cylinder pressure for CP, MTHF and the other three fuels at 3.5 and 8.5bar IMEP are as shown in figure 4.6a and b respectively. The pressure profile differences between the fuels investigated are significantly different and sensitive to engine load. At the low loads of 3.5bar IMEP no significant different was observed in the pressure profile for the fuel except that the peak cylinder pressure for CP was significantly higher than the rest of the fuels and the peak pressure for MTHF at this load is comparable to that of MF and Ethanol. The In-cylinder

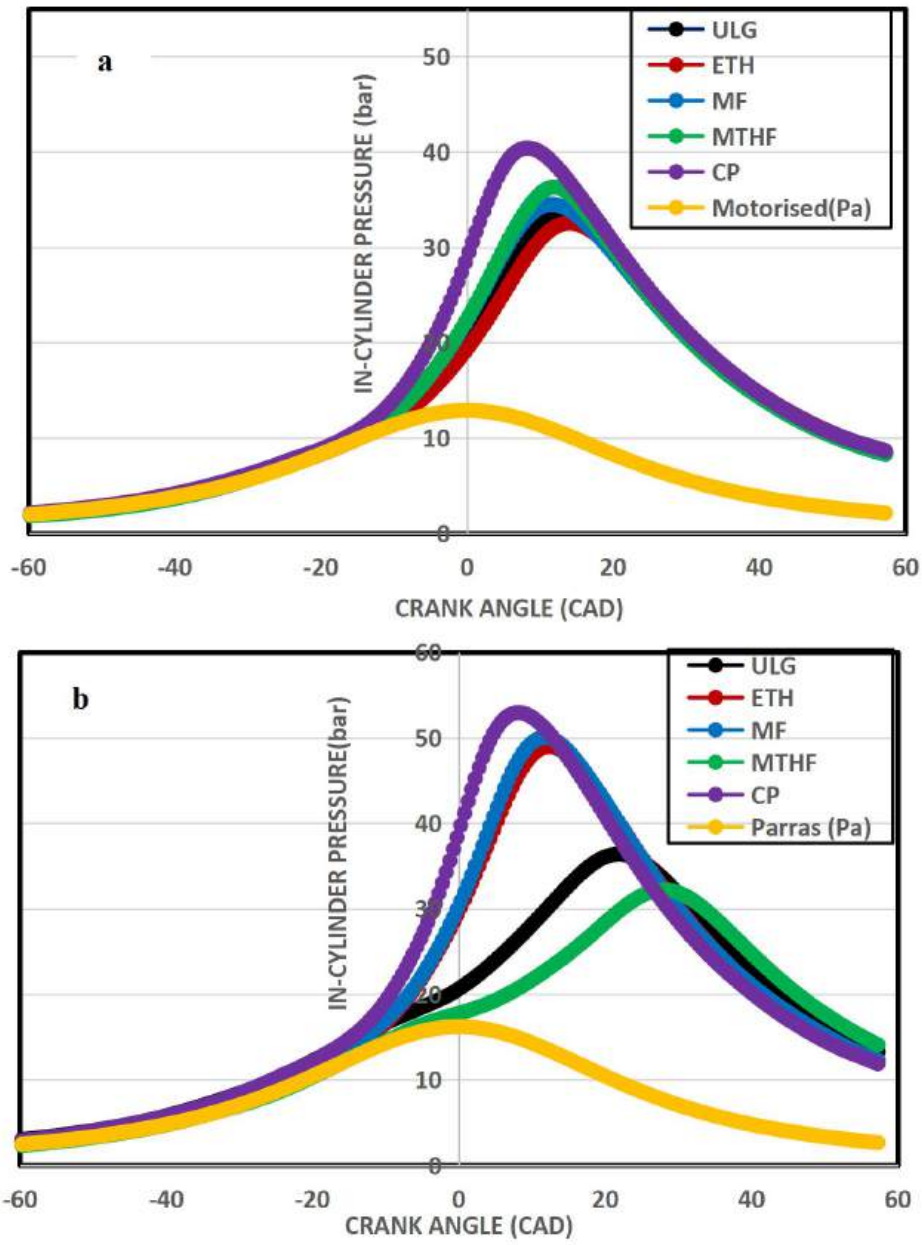

Figure 4.5a) In-cylinder pressure for the fuels at 3.5bar IMEP and

b) In-cylinder pressure for the fuels at 8.5bar IMEP.

pressure traces were captured across 300 engine cycles for all test points. Mean peak in-cylinder pressures are illustrated in figure 4.6.

Pmax for MTHF increases as the load increased from low load of 3.5bar IMEP to 6.0bar IMEP as indicated in the figure but decrease sharply from the load of 7.5bar IMEP to 8.5bar IMEP. This occurred because the spark timings for the engine load of 6.5bar IMEP for MTHF were not knock limited, however from 6.0bar IMEP down to 3.5bar IMEP they were MBT. Pmax for CP

remain consistently the highest across the load ranges for all the fuel investigated. At the peak load of 8.5bar IMEP the Pmax for CP is about 2CAD and 3CAD, 15CAD and 16CAD higher than MF, Ethanol, MTHF and the ULG respectively. Gasoline has a similar trend of Pmax with MTHF, both Gasoline and MTHF peak at the load of 6.5bar IMEP. The combustion duration of both MTHF and ULG is longer compared to that of MF and Ethanol as indicated in Figure 4.-5a. Faster combustion duration leads to higher cylinder pressure.

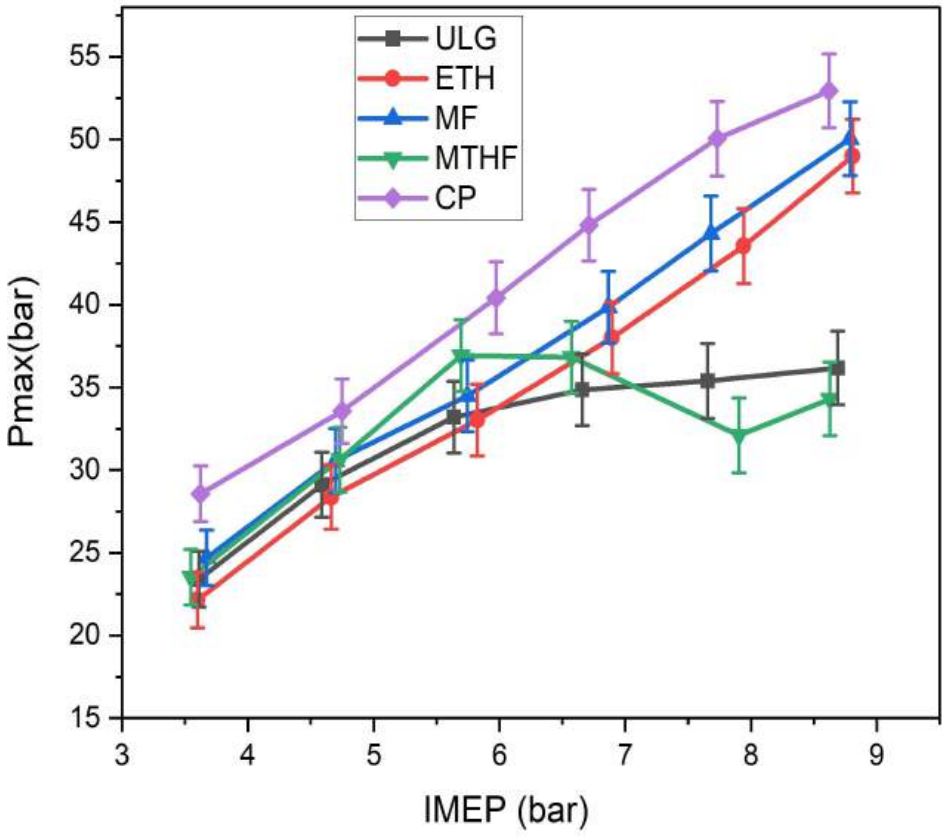

Figure 4.6 Maximum Cylinder Pressure (Pmax) for the fuels at the loads of 3.5- 8.5bar.

High cylinder pressure is desirable to maximize engine efficiency and power output, but it must be carefully managed to avoid engine damage or knocking. High cylinder pressure in spark ignition engines is a result of several factors related to the combustion process, engine design, and operating conditions. These factors interact with each other and contribute to the overall pressure within the engine cylinder. In this study there are two major factors that is consider significant to explain the higher peak pressure for CP, the fuel-optimized MBT/KLSA timing

and faster burning rate. Faster burning rate for CP leads to more heat released around TDC and higher maximum in-cylinder pressure. The timing of the spark plugs ignition plays a crucial role. Advancing the ignition timing can increase cylinder pressure because it ignites the air-fuel mixture earlier in the compression stroke. Although CP and MF and Ethanol have similar fuel-optimised MBT/KLSA timings, the Pmax for CP is consistently higher than MF and Ethanol due to its faster burning rate. A unique benefit of high cylinder pressure is the efficient combustion which leads to lower emissions of nitrogen oxides (NOx) and particulate matter.

4.2.5 In-Cylinder Temperature

The theoretical WAVE model was used to calculate the cylinder pressure for this study. The simulated and the experimental Pmax and the IMEP and agree to within 99.5% at all test conditions. The properties of indolene fuel is used to represent gasoline properties and some indolene properties were used to represent some unknown properties of MTHF and CP. Some of these properties includes the viscosity-temperature behaviour. MFB50 and MFB10-90 are used as input parameters in the SI Wieber combustion function. The purpose is to account for the fraction of unburned gases from the previous cycle that remain in the cylinder. This impacts the initial conditions for the next combustion cycle. Higher residuals can reduce the effective compression ratio and impact the combustion temperature, influencing ignition delay and overall efficiency. The cylinder temperature profile for MTHF and CP and the other three fuels at 3.5bar IMEP and 8.5bar IMEP are shown in Figure 4-8 a and b respectively. CP generates the highest maximum in-cylinder temperature and ethanol the lowest. Though when Ethanol is combusted it releases more energy potentially leading to higher cylinder temperature, however, ethanol has a cooling effect when it evaporates in the combustion chamber and this help to mitigate high cylinder temperature in the engine combustion of ethanol. CP recorded higher cylinder temperatures compares to MF. CP potentially has a higher energy content per unit volume compared to MF, which make CP to release more energy leading to higher energy

cylinder when combusted. The maximum in-cylinder temperature, like peak pressure, is sensitive to spark timing and burning rate.

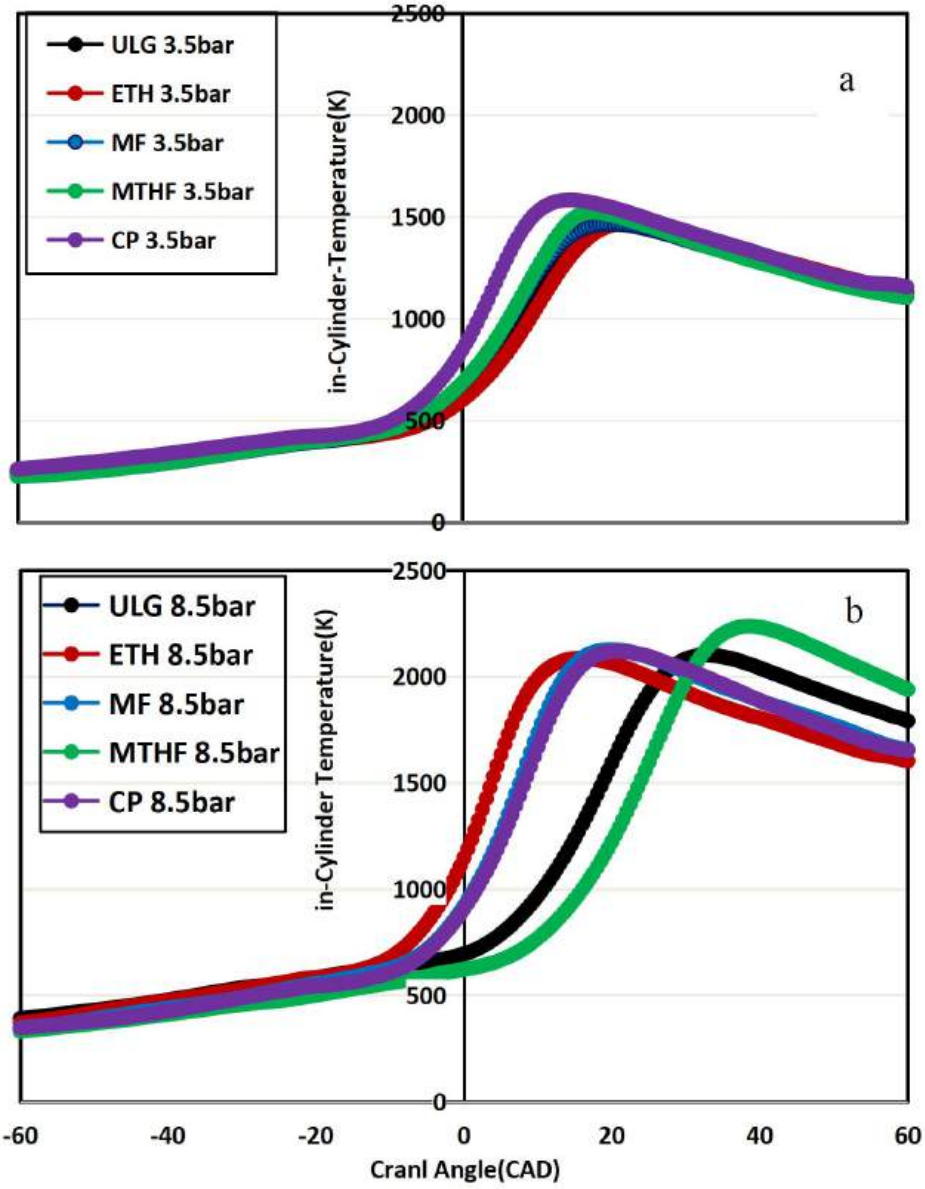

Figure 4.7a) In-Cylinder Temperature profile for the fuels at 3.5bar IMEP and b) at 8.5bar IMEP.

Although MF has similar fuel optimized MBT/KLSA timings with CP, the faster burning rate of CP makes its peak temperature higher than MF. As burning rate increases, maximum in-cylinder temperature increases. Advancing the ignition timing can increase temperatures, while retarding it lower the cylinder temperature. This explains the reason for the lower temperature

of the MTHF at the peak load because of the retarded spark timing. Cylinder temperature influences the flame temperature during combustion. The use of oxygenated fuels can help moderate high flame temperature reducing the production of harmful nitrogen oxides (NOx) emissions, especially at high temperatures.

4.2.6 Indicated Efficiency

Thermal efficiency is sometimes called the fuel conversion efficiency, it is quoted as either brake or indicated. Indicated thermal efficiency. It is derived from measurements taken at the flywheel. The indicated efficiencies at various loads for each fuel are shown in Figure 4-9.

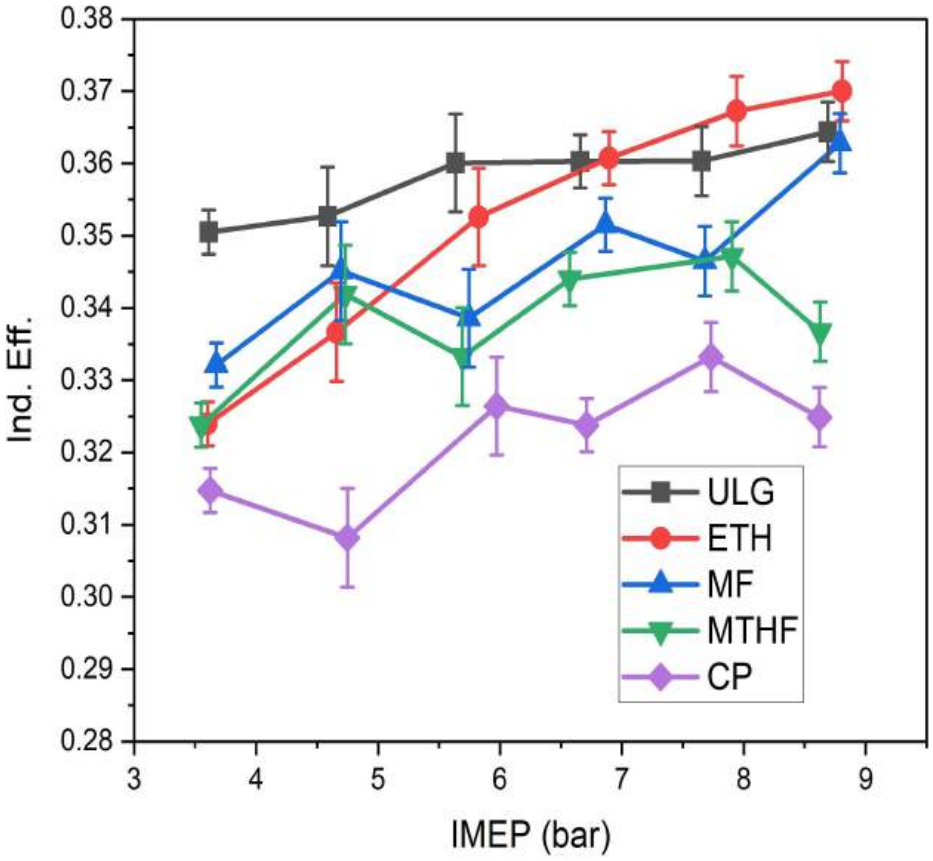

Figure 4.8 Indicated Efficiency for the fuels at load of 3.5- 8.5 bar IMEP.

The thermal efficiency was observed to increase with loads for all the fuels investigated. The thermal efficiency of Ethanol is 1% higher than ULG and 2% higher compares to MF at the peak load. Heat loss is the main source of wasted energy during combustion. High in-cylinder temperature leads to more energy loss to the cylinder wall and exhaust, which partially explains

the lower thermal efficiency of CP and MTHF. Heat of vapourisation of Ethanol (840kJ/kg) is higher compares to CP (433kJ/kg), MF (358kJ/kg), MTHF (375.3kJ/kg) and Gasoline (373kJ/kg). Evaporative cooling reduces heat transfer and increases specific heat ratio, resulting in improved thermal efficiency. This phenomenon explains the reason for the higher thermal efficiency of ethanol compares to the other fuels. ULG recorded thermal efficiency about 3% and 4% higher than MTHF at 3.5bar IMEP and 8.5bar IMEP respectively. Gasoline has a higher indicated efficiency compare to CP and MTHF despite its relatively low heat of vaporisation because of its high energy density which means it contain significant amount of heat energy per unit volume.

4.2.7 Coefficient of Performance of IMEP

Coefficient of variation of IMEP are used to analyses the engine, combustion stability and measure the combustion cyclic variation. The coefficient of combustion for the investigated fuels are as indicated in figure 4.9. The COV of IMEP for Ethanol is consistently lower than other three studied fuels. MF and MTHF display similar trends of COV, Gasoline recorded the highest reading of COV.

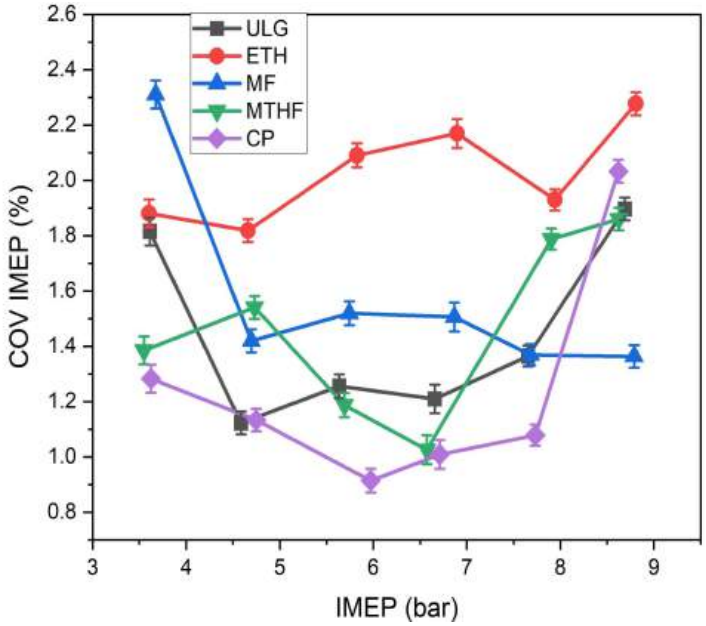

Figure 4.9 COVIMEP for the fuels at load of 3.5- 8.5 bar IMEP.

The coefficient of performance is a measure of the combustion stability and maintaining stable combustion is crucial for engine performance and reliability. For this study the maximum value of acceptable COV is 5% above which the combustion until misfire or combustion instability occurs.

4.2.8 Gaseous Emissions Characteristics of the Fuels

The section generally discusses the result of gaseous emissions for the combustion of the neat fuels of MTH and CP compares to MF, Ethanol and Gasoline. The gaseous emissions discussed are the regulated emission of NOx, HC, and CO. The instantaneous NOx emissions (isNOx) for all the fuels investigated over the load sweep of 3.5-8.5bar IMEP are as indicated in figure 4-10a. The isNOx emission generally increased with load for the fuels. This is because the formation of NOx increases very strongly with combustion temperature. The combustion of fuels with a higher H/C ratio tend to have higher adiabatic flame temperature and consequential higher isNOx emissions. This trend is exhibited in the present data analysis. Between the four oxygenated fuel investigated CP recorded the highest level of isNOx across the entire load range. At the peak load of 8.5bar IMEP, the isNOx emissions for CP is higher by 6%, 13.3%, 20% and 40% for MTHF, MF, ULG and Ethanol respectively. This is explained by the relatively higher adiabatic flame temperature of CP compared to the other fuels. The low emissions of isNOx by ethanol is as a result of its higher combustion efficiency, lower flame temperature and slower combustion rate. The Instantaneous hydrocarbon emissions (isHC) for the fuels are as indicated in figure4-10b. The isHC emissions of the fuel decreases with load due to the increase cylinder pressure at high load which correspondingly lead the cylinder temperature increase. The four oxygenated fuels produce low isHC emissions compare to gasoline, which is partially due to more complete combustion of the oxygenated fuel due to the additional oxygen in their molecules and the efficient combustion lower the unburned hydrocarbon emissions. MTHF uniquely recorded lower isHC emissions of about 62.2%, 75% and 80% compare to MF, CP and ULG respectively. The isHC emissions in this study are uncorrected because the sensitivity of

the FID analyser to oxygenated compounds has not been taken into account. In the context of analyzing exhaust emissions from a spark ignition engine, the Flame Ionization Detector (FID) is commonly used to measure hydrocarbons (HC). However, the FID has a lower sensitivity to oxygenated hydrocarbons (such as alcohols, ethers, aldehydes, and ketones) compared to non-oxygenated hydrocarbons (like alkanes and alkenes). This difference in sensitivity can lead to inaccurate measurements of the total hydrocarbon content in the exhaust gases, especially when the fuel contains oxygenated compounds, such as ethanol or methanol. A common approach to correct for the FID's lower sensitivity to oxygenated compounds is by spliting and analysing the

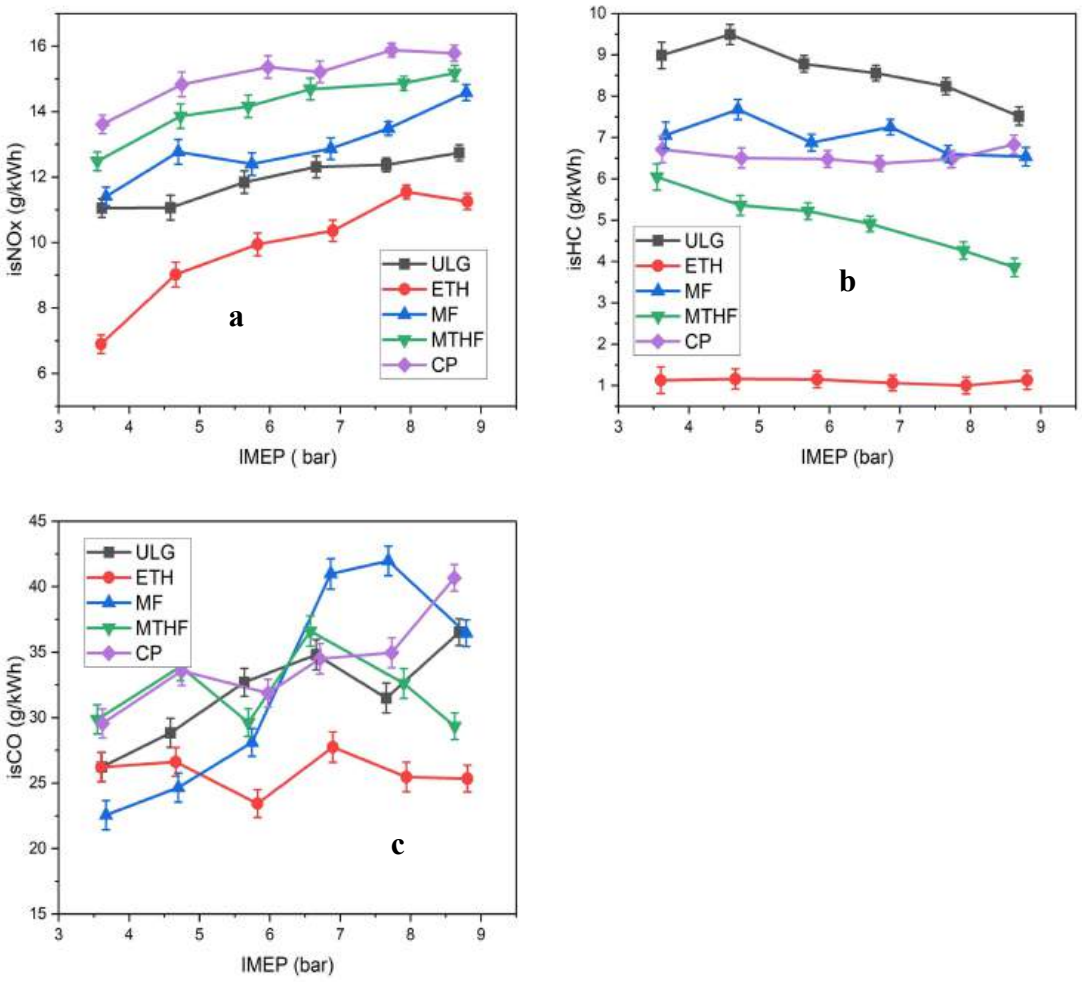

Figure 4.10a) isNOx emissions for the fuels at load of 3.5- 8.5bar IMEP, b) isHC emissions for the fuels at load of 3.5- 8.5bar IMEP and c) isCO emissions for the fuels at load of 3.5- 8.5bar IMEP.

exhaust sample using complementary techniques like Gas Chromatography (GC) coupled with Mass Spectrometry (MS) or other detectors that can differentiate between various hydrocarbons. This allows for specific identification and quantification of oxygenated hydrocarbons, which can then be used to correct the overall hydrocarbon measurement from the FID. Figure 4.10c shows the instantaneous carbon monoxide emissions for the fuels under investigation. The isCO emissions is generally sensitive to mixture homogeneity and air/fuel Stoichiometric. Ethanol consistently produces the lowest isCO emissions as indicated in figure 4-11c. MTHF has recorded lower emissions of isCO by 40% and 60% compare to MF and CP respectively at the maximum load of 8.5bar IMEP. This is partly due to its higher oxygen content and combustion efficiency and relatively higher cooling effect. Gasoline produced less isCO emissions than CP and MF, which is because gasoline is relatively easier to form homogeneous combustible mixture due to its higher volatility property.

4.2.9 PN Spectral Distribution

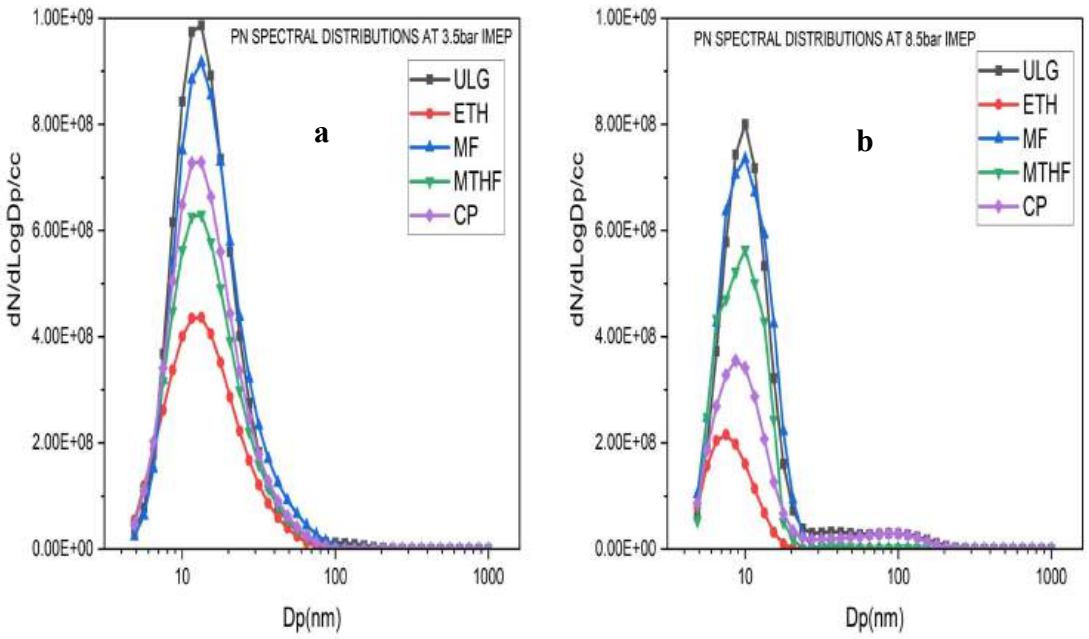

Figure 4.11a) PN spectral distribution for the fuels at 3.5bar IMEP and b) 8.5bar

PM size distribution basically consists of two modes (306), the nucleation mode and the accumulation mode. The nucleation mode has more influence in number of particles while the

accumulation mode is concern with the particle mass distribution due to its higher size. The differential mobility spectrometer DMS500 was used in this experiment for sample measurement. The sample line to the dilution system was maintained at 150^0C to avoid condensation of the particulates. The primary and the secondary dilution ratio were 5:1and 16:1 respectively to ensure good signal to noise level. Samples collection rates were 1HZ at approximately 2minutes. The PM size distributions for the fuel investigated at 3.5bar IMEP are shown in figure 4.11a. At the low load the PN emissions by the ULG is the highest compared to the other oxygenated fuels. The PN emissions by Ethanol is the lowest at this load. The trend of the PN emissions at the peak load of 8.5bar IMEP is indicated in figure4.11b. At this load PN emission by ULG remains the highest but there is a general reduction in the value of the emitted PN by the all the fuels compared to the low load. However, a trases of accumulated mode emissions was observed at this load. Researchers have used diameter range to separate nucleation and accumulation modes. Kittel son suggested: 0–50 nm for nucleation mode and 50–1000nm for accumulation mode (307, 308). Eastwood suggested: 0–100 nm for nucleation mode and 100–900nm for accumulation mode (309).

4.3 Effects of air fuel ratio on the combustion of the fuels

In this work the effect of changing the air fuel ratio on the combustion of MTHF and CP was investigated at high load of 8.5bar IMEP and at the constant engine speed of 1500rpm. At the selected load, the air fuel ratio was varied until a significant drop in performance or stability was seen (COV of IMEP increase >5%). The combustion stability decreases as the mixture becomes leaner, therefore, the lean limit has been selected as the maker to sensitivity instead of the IMEP. At this point, there is high incomplete combustion and the ignition becomes more unreliable and leading to engine misfire. The lean limit is affected by the vapourisation rates and the fuel combustion speed which make the lean limit to be fuels dependent. Once the desired load was found at stoichiometry each of the AFR sweep was then determined using the

injector pulse-width. Firstly, the AFR was enriched (λ<1) until λ=0.8 and then leaned until the lean limit was reached. Engine parameters investigated in this study includes the specific fuel consumption, combustion efficiency, combustion stability (5% COV), the lean limit, and NOx emissions.

Table 4.2 Engine operating conditions for MTHF and CP under different air fuel ratio.

Speed (rpm)	IMEP (bar)	Air fuel Ratio A/F	Injection timing (CAD BTDC)	Fuels	Spark timing (CAD BTDC)
1500	3.5-8.5	0.8,0.9,1,1.1,12 and 1.3	280	MTHF, CP	MBT/KLSA timing

4.3.1 Combustion Stability

The air fuel ratio (AFR) sensitivity is as indicated in figure4-12 At the intermittent load of 5.5bar IMEP the COV for the AFR sweeps for the fuels are as shown in Figure 4-12a, however,

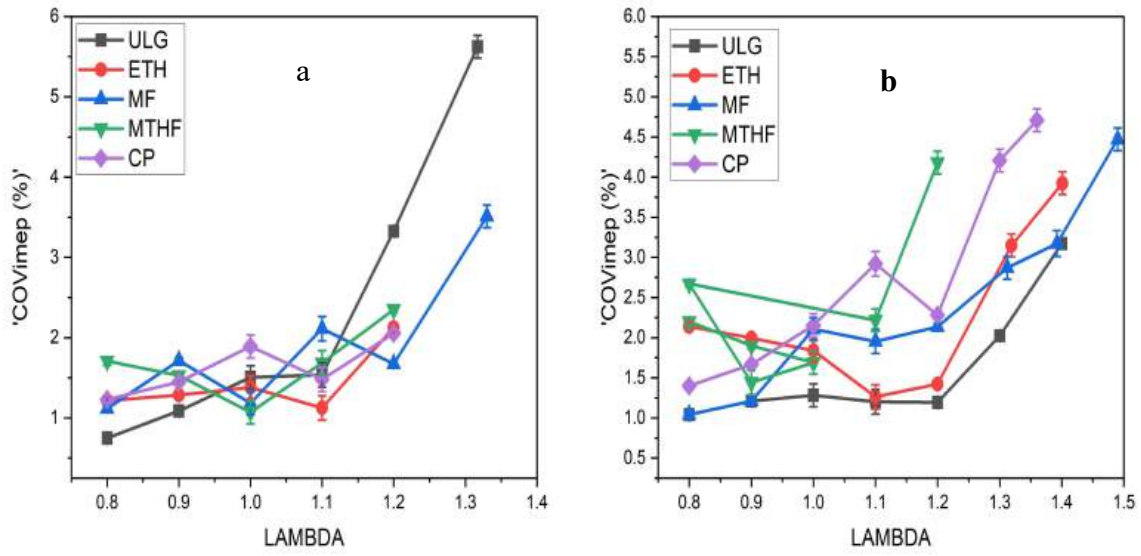

Figure 4.12a) COVIMEP and A/F sweeps for the fuels at 3.5bar IMEP and b) COVIMEP and A/F sweeps for the fuels at 8.5bar IMEP.

the different between the COV of the fuel became more apparent in Figure 4-12b at high load of 8.5bar IMEP. Interpolated or extrapolated was sometimes used to establish the AFR at 5% COV of IMEP in cases when it was not directly achieved on the figure, the gasoline shows higher AFR sensitivities than the bio fuels. This is because oxygenated fuels burn faster than gasoline primarily due to their built-in oxygen content, higher flame speed, lower stoichiometric air-fuel ratio, better mixing, and higher volatility. These factors contribute to more efficient and rapid combustion, making oxygenated fuels quicker to burn than conventional gasoline. MTHF and CP, produces the lowest instabilities. Consequently, the AFR window is much wider. When using MTHF and CP, the COV of IMEP rises quickly above 3% when $\lambda \geq 0.95$.

4.3.2 Fuel Consumption and Engine Efficiency

The Air fuel ratio and fuel consumption of DISI engine are closely related and are critical factors determining the engine performance and emissions.

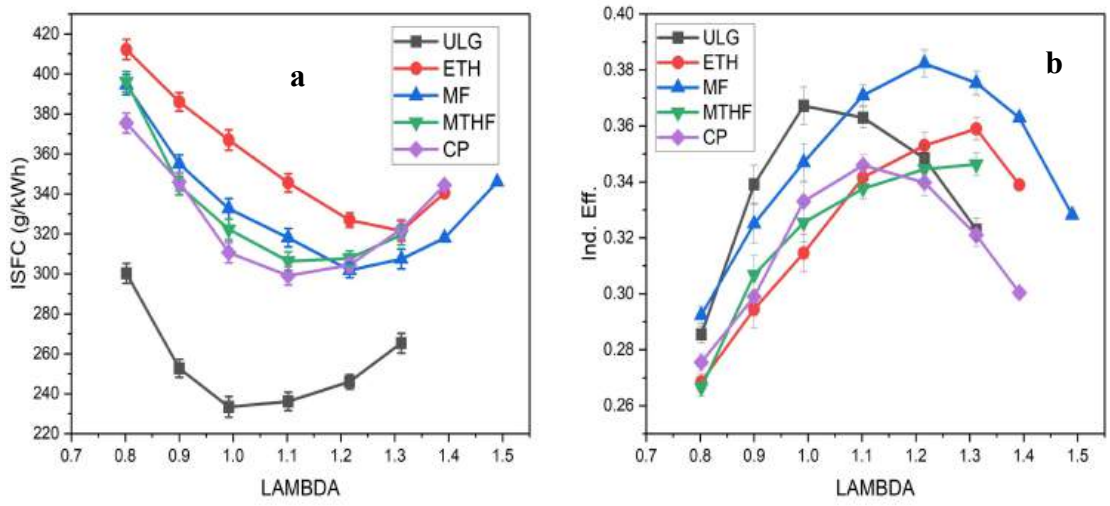

Figure 4.13a) Indicated specific fuel consumption and A/F sweeps at 8.5bar IMEP and b) Indicated efficiency for the fuels and A/F sweeps at 8.5bar IMEP.

When AF is below the stoichiometric the Air fuel mixture is rich and have more fuel than needed. Leading to increase fuel consumption. This trend is depicted in figure4-13a where the fuel consumption for the fuel are highest at (λ=0.8). As expected Ethanol recorded the highest

isFC and gasoline the lowest due to the energy density of the fuels. The isFC for the fuels witnessed a steady decline with the increasing lambda within the fuel lean limit. Figure4-13b shows the effect on indicated efficiency (relative to stoichiometry).

The indicated efficiency at the lean limit is lower than the maximum. For gasoline, the maximum efficiency is at λ≈1.0, whereas at the lean limit (λ≈1.25), the indicated efficiency drops by 1.7%. For MTHF and CP, the maximum indicated efficiency was recorded at λ=1.3 and λ=1.1 respectively. At the lean limit the indicated efficiency of CP has dropped by 13.3% but MTHF was observed to have recorded the maximum indicated efficiency at the lean limit. Both MF and Ethanol recorded the maximum indicated efficiency at λ=1.2 and λ=1.3 respectively. The reason for Ethanol higher indicated efficiency in lean engine condition is because of its the reduced throttle losses which further contributes to improve engine efficiency. High octane rating, high latent heat of vapourisation and higher oxygen contents are some of the other reason responsible for the higher engine efficiency of ethanol in engine lean condition. MTHF has low lean limit due to its low octane number, however, its higher latent heat of vapourisation make it possible to record high engine efficiency in lean engine condition.

4.3.3 Maximum Cylinder Pressure and MFB50

The maximum Cylinder pressure for the fuels at 8.5bar IMEP over the air-fuel ratio sweeps is as

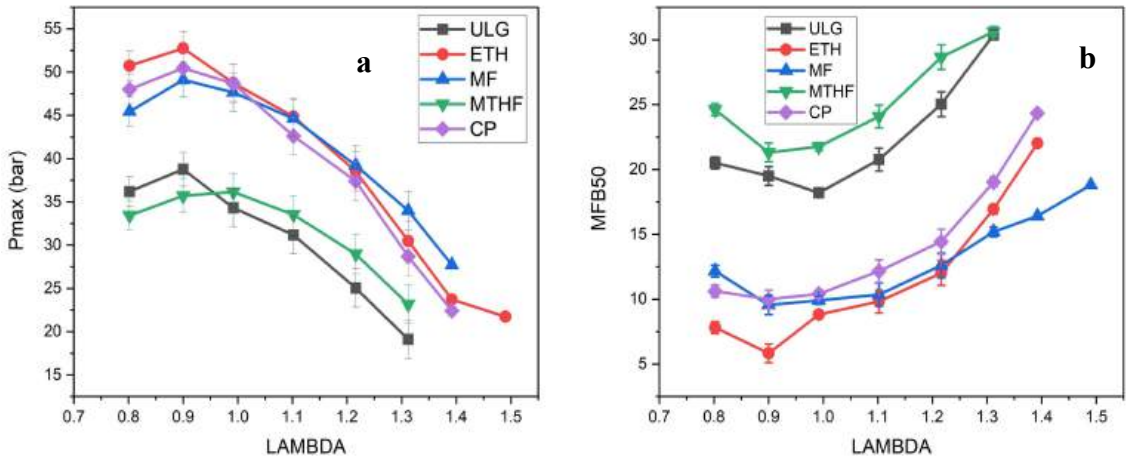

Figure 4.14a) Maximum cylinder pressure Pmax and A/F sweeps for the fuels at 8.5bar IMEP and b) MFB50 and A/F sweeps for the fuels at 8.5bar IMEP.

indicated in figure4-14a. Pmax was observed to drop steadily as the combustion become lean. The maximum Pmax for the fuels was recorded when λ=0.9, thereafter the Pmax reduces steadily up till the lean limit. The different between the Pmax at λ=0.9 and the Pmax at the lean limit is recorded to be 55%, 51.5%, 33.33%, 31,2% and 39.4% for Ethanol, CP,MF, MTHF and the ULG respectively. The reason for the drop of Pmax as the combustion grow lean can be explained by the fact that lean mixtures contains less fuel and therefore generates fewer products per unit volume. With fewer products the pressure generated during the combustion is reduced, which in turn can reduce the cylinder pressures. As recorded in figure 4-14b, the fastest burning rate for all the oxygenated fuels was recorded when λ=0.9, however, fastest burning rate for gasoline was recorded at λ=1. In lean mixture, MFB50 tends to occur at a later crank angle degree, because the excess air makes the combustion to take longer time to complete.

4.3.4 Lean Limit and isNOx Emissions.

The lean limit for each of the fuel under investigations are as indicated in figure4.15a. At the load sweep between 3.5-8.5 bar IMEP, the air fuel ratio was varied until a significant drop in

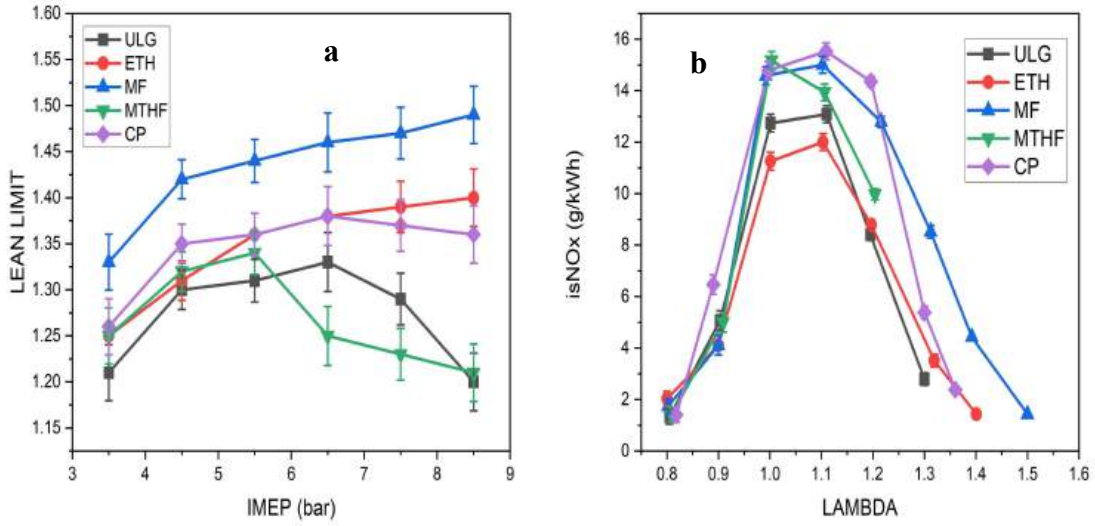

Figure 4.15a) Lean limits at load of 3.5- 8.5bar IMEP and b) isNOx emissions and A/F sweeps for the fuels at 8.5bar IMEP.

performance or stability was seen (COV of IMEP increase >5%). This represent the lean limit for the fuels. Sometime when the limit can not be easily deducted from the figure, interpolation or extrapolation are used to evaluate the lean limit of the fuel as it happens in the case of ethanol. As indicated in figure4.15b MF isNOx emissions is more sensitive to AFR than with the other oxygenated fuels and gasoline Nevertheless, the lowest isNOx emissions are found at leaner AFR and the emissions are much lower at the lean limit than at stoichiometry. The maximum isNOx emission occur at λ=1.2 for all the fuels investigated and at the lean limit the isNOx emission for CP, MF and ethanol has been reduced by almost 80% of the utmost emission value at λ=1.2.

4.4 Effect of Fuel injection Pressure on the combustion of the fuels

The influence of injection pressure on the combustion and the emissions of MTHF and CP were investigated in this section. The load range for the investigation was between 3.5-8bar IMEP at 1bar interval and at the stoichiometric engine condition (λ=1). All the tests for each fuel carried out in this section were done under the fuel-specific optimum spark timings, known as the maximum brake torque (MBT) timings. The fuel injection pressure used for this test are 75bar, 100bar, 150bar and 175bar. The challenge of engine knock in the combustion of MTHF can be address in two ways, either by blending the fuel with an octane booster or by manipulating the in-cylinder parameter to reduce the knock tendency. In similar manner, the need to reduce the high isCO and isNOx emissions from the combustion of CP is intended to be solved through the in-cylinder solution. The author has chosen to work currently on one of the engine fuel injection parameters and the parameter considered for this purpose is the fuel injection pressures. The fuel injection pressure was swept from 75 bar to 175bar for the combustion of both MTHF and CP. The experiments were carried out under stoichiometric engine conditions at constant engine speed of 1500rpm. The operating conditions are listed in Table 4.4 with load sweep of 3.5-8.5bar IMEP. A single stage injection strategy was applied and no EGR was used. For each load,

the maximum brake torque (MBT) spark timing was used, unless knock occurred in advance. In the event of knock, the spark timing was retarded by 2CAD, and was referred as the Knock-Limited Spark Advance (KLSA). The parameter investigated for this study include the cylinder pressure, spark timing sensitivity to the fuel injection pressure, thermal efficiency, fuel consumption, particle emission and the gaseous emissions.

Table 4.3 Engine operating conditions for the combustion of MTHF and CP under different fuel injection pressures.

Speed (rpm)	IMEP (bar)/ LAMBDA	Injection Pressure (bar)	Injection timing (CAD BTDC)	Fuel	Spark timing (CAD BTDC)
1500	3.5-8.5/1	75,100,150 and 175	280	MTHF And CP	MBT/KLSA timing

4.4.1 Effect of Fuel Injection Pressure on Pmax and Spark Timing

The fuel injection pressure sweep was undertaken to investigate the variation of Engine knock with fuel injection pressure in the combustion of the MTHF. The aim is to discover the optimal fuel injection pressure that ensure knock limited spark advance KLSA at high load for the combustion of MTHF and CP. Figure4.16a shows the comparison of peak cylinder pressures at different fuel injection pressures for MTHF similar curve is shown for CP in figure4-16b. it is seen that, the in-cylinder peak pressures increases with the maximum cylinder pressure. This is because, at higher fuel injection pressures, fuel spray break-up and the atomisation of the fuel droplets are enhanced which result in better interaction of air and fuel particles resulting in improved combustion, and in increase of in-cylinder pressures. At the fuel injection pressure of 175bar, Pmax peak at 5.5bar imep for MTHF indicating a more severe incident of the engine

knock compares to the fuel injection pressure of 150bar where the Pmax peak at 6.5bar imep. Higher injection pressures can increase the overall pressure and temperature in the combustion chamber. As the fuel is injected at higher pressures, it evaporates more rapidly, which can raise the local temperature. Higher temperatures can increase the likelihood of auto-ignition of the air-fuel mixture, especially in the regions of the combustion chamber that experience the highest temperatures, contributing to knock. At the fuel injection pressure of 100bar for the MTHF fuel, Pmax peak at 7.5bar imep indicating less cylinder knock that allows maximum brake Torque Timing (MBT).

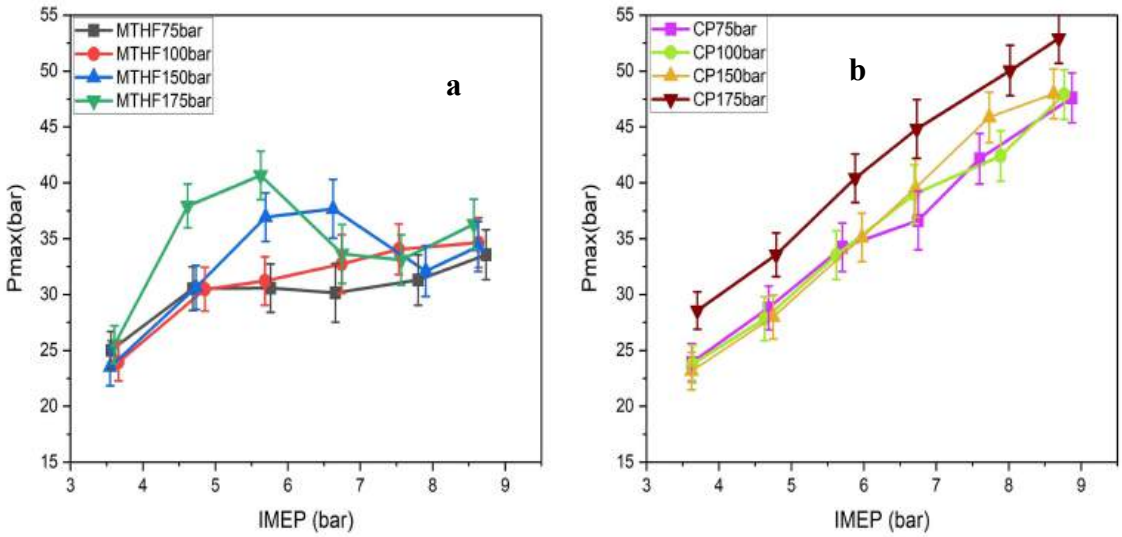

Fig.4.16a) Pmax for MTHF at 75-175bar fuel Injection pressure and b) Pmax for CP at 75-175bar fuel injection pressure.

Though the Pmax at 75bar fuel injection Peak at 8.5bar imep, the cylinder pressure under this fuel injection pressure is too low to be considered appropriate for the combustion of MTHF. From the result of the experiment conducted Fuel injection pressure will be consider suitable for the combustion of MTHF based on the peak cylinder pressure at this injection pressure. However, the cylinder pressure at 75bar and 100bar fuel injection pressure is too low for any suitable engine performance. The most suitable fuel injection pressure is 150bar for the combustion of MTHF because both cylinder pressure and the spark advance is optimised at this

injection pressure. However, other combustion factors and emission behaviour needs to be considered before this major conclusion. The effect of the fuel injection pressure on the combustion of CP follows similar trends as in the Combustion of the MTHF. However, there is higher window of spark advance flexibility in the combustion of CP with fuel injection various as indicated in figure 4-16b. The optimal fuel injection pressure was recorded at 150bar and the Pmax for the fuel injection pressure of 75bar and 100bar is lower than that at 150bar. The Pmax for the high fuel injection pressure of 175bar is actually higher than that of 150bar but is at the expenses of low fuel economy as will be discuss later in this section. The effect of fuel injection pressure on spark timing is shown in figure 4-17.

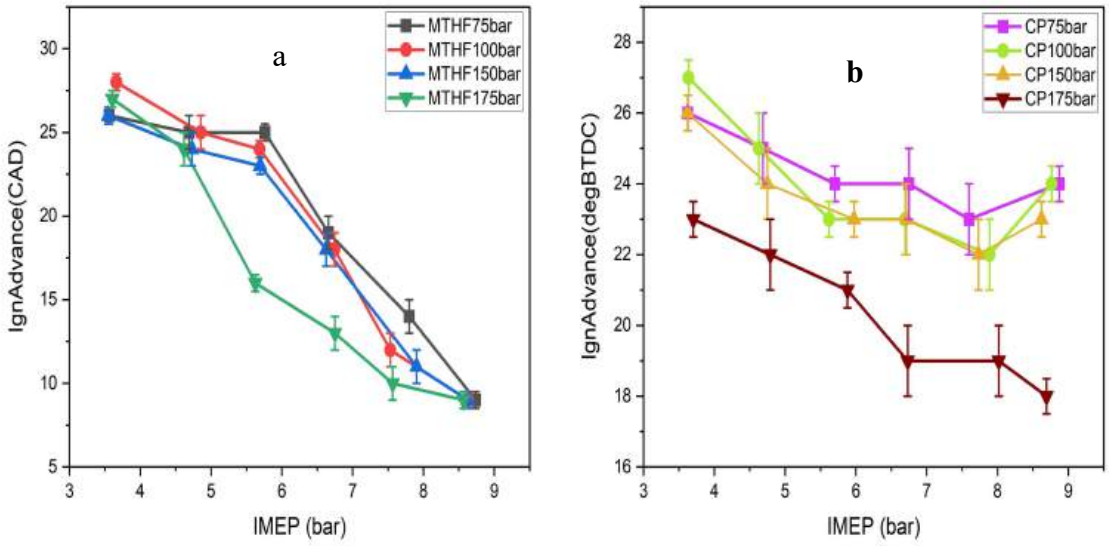

Figure 4.17a) Ignition advance for MTHF at 75-175bar fuel injection pressure and b) Ignition advance for CP at 75-175bar injection pressure.

It became necessary to retard the spark timing as the injection pressures increases because of the attendance increase in cylinder temperature that precede the higher injection pressure which lead to auto ignition at advance timing. The need for advancing the timing of the spark is because fuel does not completely burn the instant the spark fires. The combustion gases take a period of time to expand, and the angular or rotational speed of the engine can lengthen or shorten the time frame. Pre-ignition of the end gas or engine knock occur in fuel with low

octane number at high load, this phenomenon was observed in the combustion of MTHF at high load. This is the reason for retarded spark timing for the combustion of MTHF at high load.

4.4.2 Effect of Fuel Injection Pressure on ISFC and Indicated Efficiency

At the high fuel injection pressures of 175 bar, spark advance is mitigated by the phenomena of engine knock. As indicated in figure 4-17b the optimum fuel injection pressure occurs at 150bar for the combustion of CP. The spark advance ability at the fuel injection pressure of 175bar was inhibited by high cylinder temperature.

An inappropriate injection strategy leads to an abnormal combustion. Among several parameters, many works proved that fuel injection pressure plays a significant role related to combustion quality (33-37). Increasing fuel injection pressure improves the fuel spray pattern and reduces droplet size, leading to better atomization and more efficient mixing of the fuel with air. This results in improved combustion efficiency, enhanced engine performance, and reduced emissions [33]. Figure 4-18a shows the specific fuel consumption for MTHF with the fuel injection sweeps of 75-175bar. The fuel economy increases with the increase in the fuel injection pressures, the optimal fuel economy was recorded at 150bar above this injection pressure. the indicated fuel economy increases as observed in figure 4-18a.

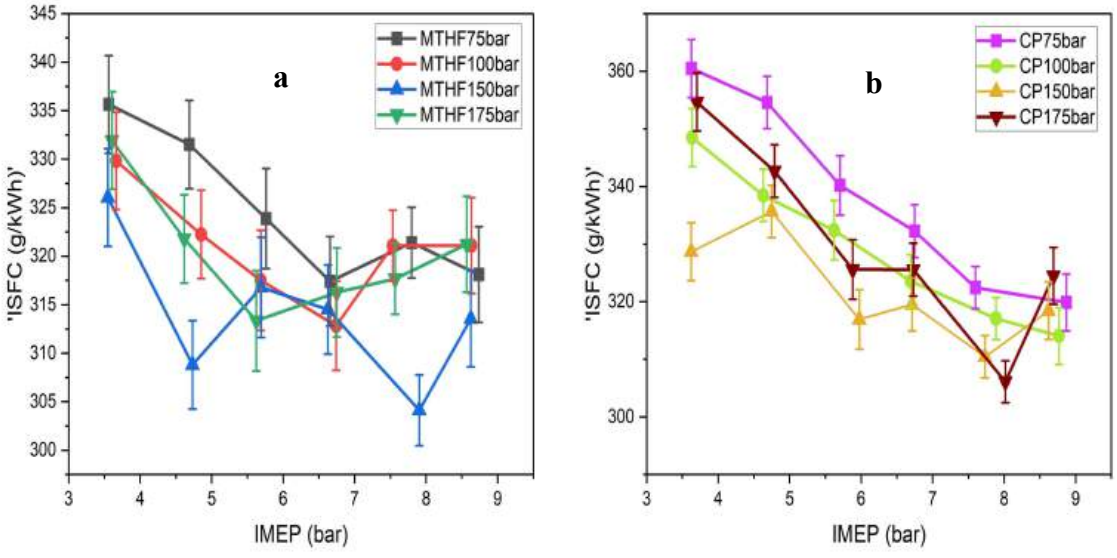

Figure 4.18a) ISFC for MTHF at 75-175bar fuel Injection pressure and b) ISFC for CP at 75-175 bar fuel injection pressure.

For the four-injection pressure investigated except at 175bar the fuel economy increases with load and also as the fuel injection pressure increases. The same trends was observed for the indicated specific fuel consumption of CP over the fuel injection pressure sweep as indicated in figure 4-18b.

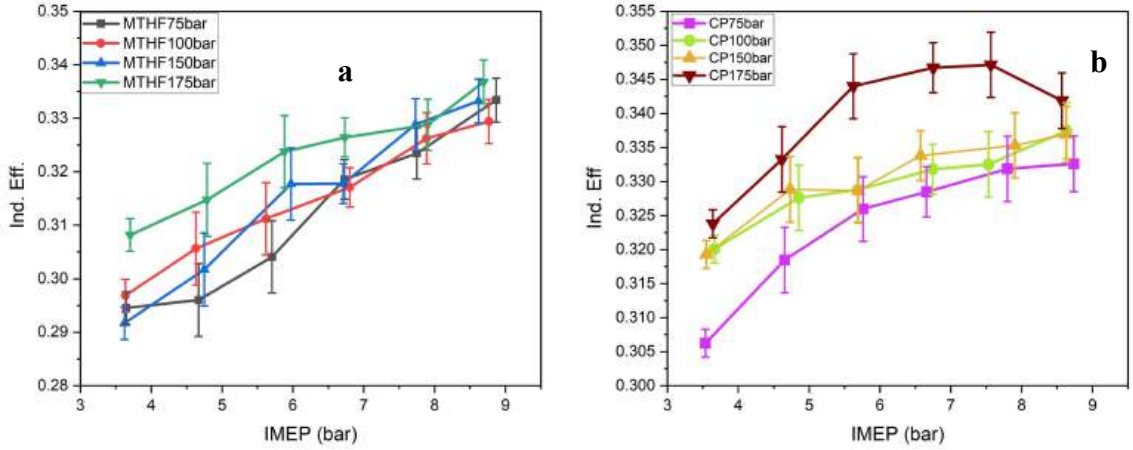

Figure 4.19a) Indicated efficiency for MTHF at fuel injection pressure of 75-175bar and b) Indicated efficiency for CP at fuel injection pressure of 75-175bar.

The optimal fuel economy for the combustion of CP was recorded at fuel injection pressure of 150bar. Higher fuel injection pressure results in better atomisation of the fuel, improve combustion efficiency and fuel economy. However, increasing the fuel injection pressure beyond the optimal level leads to adverse combustion behaviour. The thermal efficiency for the four-injection pressure sweeps are shown in fig.4.19, the thermal indicated efficiency of MTHF increases as the load increase, this is because the cooling heat loss ratio, mechanical loss ratio, and pumping loss ratio decrease at higher load (38). However, at the high load for the fuel injection pressure of 150bar and 175bar the thermal efficiency was observed on the decline. This is because of observed increase in fuel consumption for the fuel injection pressure of 150bar and 175bar at the stated load. One effective way to improve the engine thermal efficiency is to increase the fuel injection pressure. Knock, however, does not allow for high

thermal efficiency, knock depends on the pressure and temperature history of unburned end-gas (38-40).

4.4.3 Effect of Fuel Injection Pressure on Combustion Efficiency

Higher fuel injection pressure can result in better atomisation of the fuel which can result in more complete mixing of the fuel with air and resulted in efficient combustion. Increased fuel injection pressure enhances the atomization, penetration, and mixing of fuel with air, leading to a more uniform and homogeneous fuel-air mixture in the combustion chamber. This homogeneity is critical for achieving efficient and clean combustion in modern engines. However, there is an optimum fuel injection pressure above which point may not yield significant improvement in combustion efficiency. As indicated in figure 4.20a, the optimal fuel injection pressure for the combustion of MTHF is 150bar, Above the optimal fuel injection pressure at 175bar the combustion efficiency has dropped by about 18% at the intermittent load.

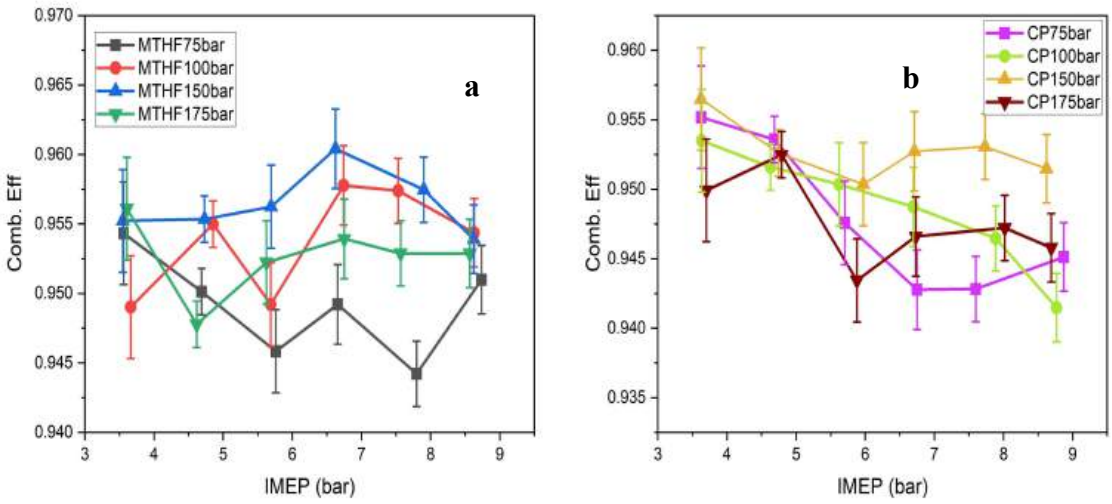

Figure 4.20a) Combustion efficiency for MTHF at 75-175bar fuel injection pressure and b) Combustion efficiency at CP at 75-175bar injection pressure.

Similar trend was observed in the combustion of cyclopentanone as indicated in figure 4.20b, the optimal fuel injection pressure for CP was recorded at 150bar above the recorded value of the combustion efficiency drops significantly.

4.4.4 Effect of Fuel Injection Pressure on Ignition Delay

Ignition delay is the time between the fuel injection and the fuel ignition. This is typically 15-35 degrees before TDC of the power stroke depending on the engine speed. During the period of ignition delay the fuel get mixed with hot compressed air and vaporizes. The period of ignition delay is followed by the spontaneous ignition of the fuel. Delayed ignition allows more fuel to be injected and vaporizes inside the combustion chamber and at high fuel injection period more fuels burn more instantaneously leading to the situation of Engine knock. Figure 4.21 indicates the ignition delay for the combustion of MTHF over the fuel injection pressure sweeps of 75bar to 175bar. It was observed that Ignition delay for the combustion of MTHF reduces with load across the fuel injection sweeps. This is because the increase fuel injection pressure and increase load leads to the corresponding increase in cylinder temperature which necessitate early ignition to prevent auto ignition.

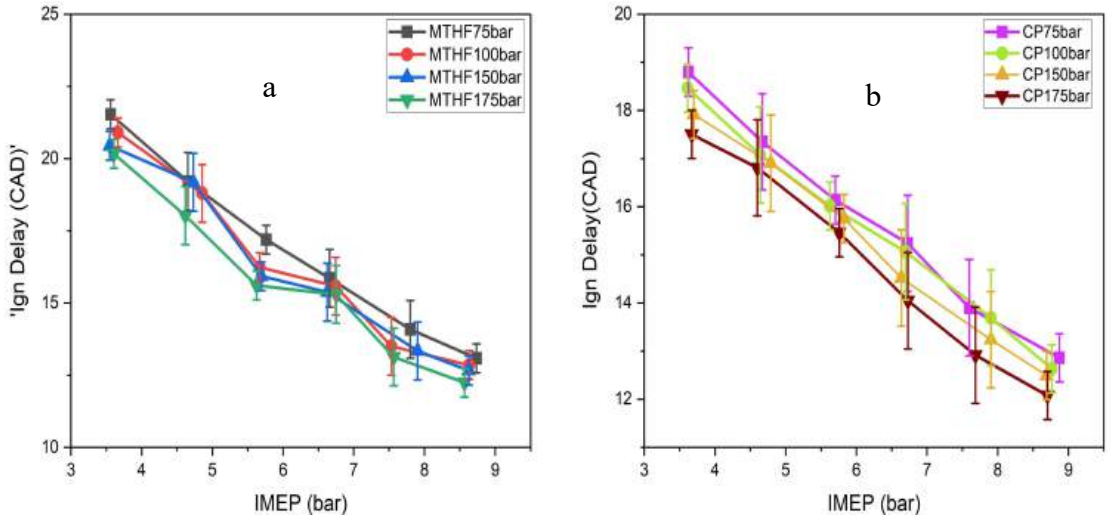

Figure 4.21a) Ignition delay for MTHF at 75-175bar injection pressure and b) Ignition delay for CP at 75-175bar injection pressure.

Combustion duration or the fuel burning time is investigated along with fuel injection sweep in the combustion of MTHF. As indicated in the figure the period for the combustion of MFB1090, which is the crank angle interval between 10% MFB and 90% MFB, reduces with increasing fuel injection pressure. This observation is corroborated in the work of Mittal et.al where it was equally discovered that the results of combustion visualisation in a single cylinder gasoline direct injection engine showed faster flame growth and reduced combustion duration with the increment of fuel injection pressure, and it is observed that the period for MFB1090 decreases with load. Shorter combustion duration leads to increase in peak cylinder pressure. This can be because the faster the combustion, the greater the pressure rise within a shorter span of crankshaft rotation, leading to higher peak pressures before the piston starts to move too far down.

4.4.5 Effect of Fuel Injection Pressure on isNOx and isHC Emissions

Increasing the fuel injection pressure in a direct fuel injection engine can lead to higher temperature and pressures during combustion. This can result in increased cylinder production of nitrogen oxides (NOx) as higher temperatures temperatures are conducive to their formation.

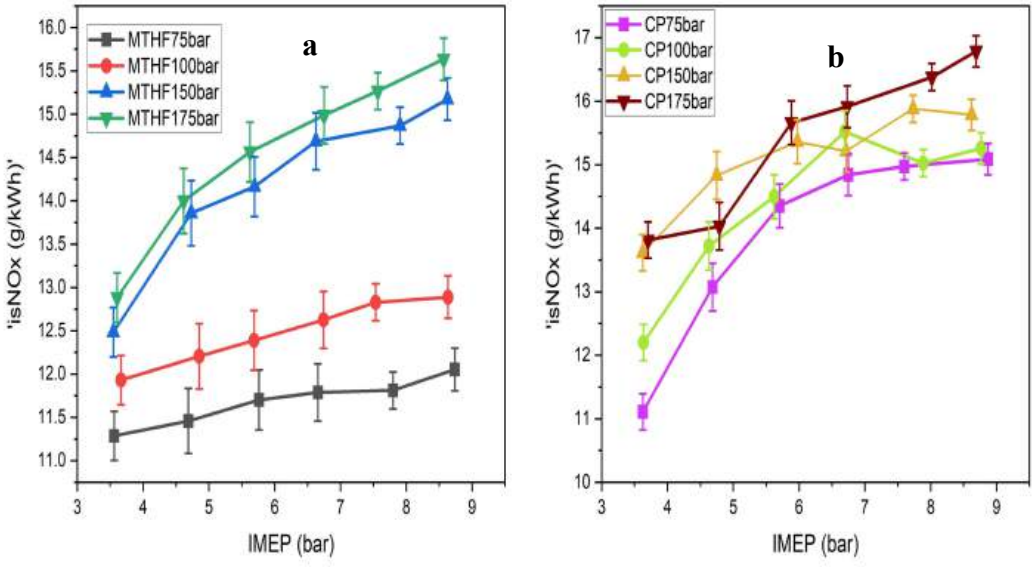

Figure 4.22a) isNOx MTHF at 75-175bar fuel injection pressure and b) isNOx for CP.

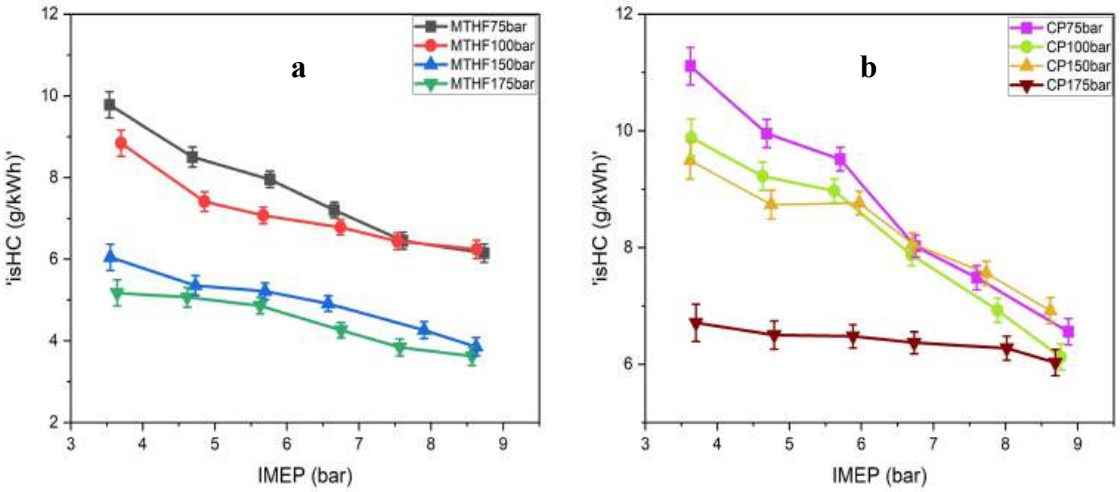

Figure 4.23a) isHC for MTHF at 75-175bar fuel injection pressure and b) isHC for CP from 75-175bar injection pressure.

While higher fuel injection pressure may enhance combustion performance and combustion efficiency, it contributes to increase NOx emissions. As indicated in figure 4-22a the isNOx emission for MTHF increases as the fuel injection pressure increases and as the load increases. At 8.5bar IMEP the isNOx emissions at the fuel injection pressure of 175bar is about 6.4%, 19.3% and 25.8% greater than that of 150bar, 100bar and 75bar respectively. This same trends of the isNOx emissions were observed for CP to increases with the fuel injection pressure as indicated in figure 4-22b. However, at the maximum load of 8.5bar IMEP, the differences between the isNOx emissions for 175bar injection pressure is 6.4%. 15% and 16% for 150bar, 100bar and 75bar respectively. In addition to the high cylinder temperature created by high fuel injection pressure other reason that can explained the higher emission of NOx at higher injection pressure is the increased turbulent created, which promotes availability of oxygen further contributing to higher cylinder temperature and NOx formation. As indicated in figure 4-23, the hydrocarbon emissions for both MTHF and CP reduces significantly as the fuel injection pressure increases and as the load advances. This is because, high fuel injection pressure increases the fuel atomisation enhancing the mixing of fuel with air. This improved atomisation can result in more efficient combustion, reducing unburned hydrocarbon. As indicated in figure

4-23a, the least emission of the isHC for MTHF was recorded at the fuel injection pressure of 175 bar at 8.5bar IMEP. Similar trend of isHC emisssions was recorded for CP in figure 4-23b. However, for CP, at the peak load of 8.5bar IMEP the effect of injection pressure on isHC emissions become low as the differences in values of isHC emissions at this load become insignificant with respect to different injection pressures.

4.5 Summary

This chapter examines the combustion sensitivity of MTHF and CP to various engine parameters and the engine emissions. The result are compared to MF, Ethanol and gasoline. The conclusion of the study are summarised as follows.

MTHF and CP though an oxygenated fuels both recorded specific fuel consumption advantage compares to MF and Ethanol. Due to its higher octane number and faster burning rate, CP shows a better anti knock ability compared to MTHF and gasoline. The Biofuels investigated generally recorded higher combustion efficiency than that of gasoline due to the effect of the additional oxygen content in their molecules which promotes completeness of combustion of the Biofuels. The engine out emission of isNOx is generally higher for CP and MTHF compared to MF, gasoline and Ethanol. However, the HC emissions of CP and MTHF is generally lower than that of MF and ULG but higher than that of Ethanol. In terms of AFR, the limit of lean combustion for MF and CP was greater than Ethanol, ULG and MTHF. The ISFC for the investigated fuels was optimised at $1< \lambda < 1.1$. It was equally observed that the engine efficiency was optimised within this lambda range. The optimal fuel injection pressure (i.e best result of combustion and emission performance) was recorded at 150bar for all the fuels investigated.

CHAPTER 5

MODERN GDI COMBUSTION MODES USING 2-METHYLTETRAHYDROFURAN AND CYCLOPENTANONE.

This section investigates the effect of Spark advance sensitivity, the SOI timing and split injection strategies in a DISI engine fueled with CP and MTHF and the result compared with similar test conducted on ethanol, 2-Methylfuran and gasoline. In this work, the MBT timing is defined as the spark timing that produce the maximum brake torque but, in this case, IMEP is investigated for a fixed throttle position (λ=1). If audible knock occurs, then the knock-limited spark advance timing (KLSA) is adopted. KLSA timing is achieved by retarding the MBT timing by 2CAD. The single-pulse SOI timing sweeps (360-180°bTDCcomb every 30CAD) were conducted at full load to find the highest VE for each fuel. The optimum SOI timing for the fuels were recorded and was then used for the first SOI timing during the split injection combustion. All tests are carried out at constant fuel injection pressure of 150bar and at stoichiometric conditions at the constant engine speed of 1500rpm. This study also investigated the effect of the two-stage injection strategies when using MTHF at full-load. The benefit of injecting fuel into the combustion chamber in multiple stages during the engine intake and compression stroke is to improve combustion efficiency, reduce emissions and optimised the engine performance. and the result enabled greater spark advance and increased torque. This work seeks to investigate if such techniques are transferable to MTHF and CP as Biofuels. The effect of the first injection (2:1) is compared to one which favours an equal split-ratio (1:1) for the investigation of the split injection combustion on MTHF and CP with gasoline as a benchmark fuel and the second SOI timing swept between 240-90°bTDCcomb, in 30CAD intervals. In the two stages fuel injection technique, a small amount of fuel is injected during the early stage of the intake or compression stroke to help cool the air inside the cylinder and create

a stratified air-fuel mixture in the rest of the cylinder (62, 310). This can improve ignition and combustion stability. A larger amount of fuel is injected just before the spark plug ignite during the power stroke to help achieve a more controlled and efficient combustion as the fuel is better atomised and distributed, leading to reduce emissions and improve fuel economy (311).

5.1 Effect of Spark Timing

This study investigates the effect spark advance on IMEP for MTHF, CP, MF, Ethanol and ULG. The spark timing sweep was undertaken at the load of 8.5bar IMEP, because investigations as indicated figure 4.2 in the previous section shows that at this load there is great differences between the combustion of the fuels. In this work, the MBT timing is defined as the spark timing that produce the maximum brake torque but, in this case, IMEP is investigated for a fixed throttle position (λ=1). If audible knock occurs, then the knock-limited spark advance timing (KLSA) is adopted. KLSA timing is achieved by retarding the MBT timing by 2CAD, an arbitrarily safe margin, as is advised (239, 289).

Table 5.1 Operating conditions for the Spark Timing sweep on Test on the fuels

Speed (rpm)	IMEP (bar) & LAMBDA	Injection Pressure (bar)	Injection timing deg. bTDC	Fuels	Spark timing deg. bTDC	Test Procedure
1500	8.5 & 1	150	280	MTHF, CP, MF Ethanol and ULG.	Spark Timing Sweeps	1. Baseline spark timing for ULG. 2. Incremental spark timing advances. 3. Incremental Spark timing retards.

At this point, the spark timing is then referred to as the knock-limited spark advance. One of the key observations in this study was the seeming relationship between the rate of change of IMEP and MBT/KLSA location. It is evident that IMEP decay increases with MBT/KLSA timing spark retard. This rate of decay is otherwise regarded as an indicator of the fuel's spark timing sensitivity (279, 312, 313).

5.1.1 Combustion performance and the Spark Timing.

The spark timing sweep shown in Figure 5-1a at 8.5bar IMEP demonstrates the effect on IMEP using CP, MTHF, MF, ULG and Ethanol. At this load, there is a clear difference between the fuels investigated. MTHF and gasoline, are much more sensitive to spark knock and only retarded timing can be observed. There appears to be a relationship between the MBT/KLSA location and the IMEP sensitivity. The study shows that the rate of IMEP decay (which generally refers to the decrease in IMEP with the increases in spark timing) increases with the more retarded MBT/KLSA timing as indicated in figure 5.1a. Daniel et al in their study of the fuel spark sensitivity identifies this rate of decay as an indicator of the fuel's spark timing sensitivity (279, 313). Figure 5.1b shows the normalised IMEP and spark timing data with the respective MBT/KLSA values as in Figure 5.1a. These sensitivities are clearly indicated in Figure 5.1b, using the term spark retard. The spark retard in this study means the number of retarded CAD from MBT/KLSA. As the term suggests, a negative value is advanced whereas a positive value represents retarded timing. from MBT/KLSA. Ayala et al. had previously used this term to help develop their combustion retard parameter(279, 314). IMEP decay simply refers to how quickly the engine performance decrease as the ignition timing is retarded (315). With CP, MF and ethanol fuels, the rate of decay is symmetrical about MBT and decreases at a lower rate than MTHF and gasoline. This is due to the knock suppression superiority of CP, MF and ethanol compares to MTHF and gasoline. The initial rate of decay also indicates how far the KLSA timing is from MBT. The initial rate of decay using MF and CP is less than with gasoline.

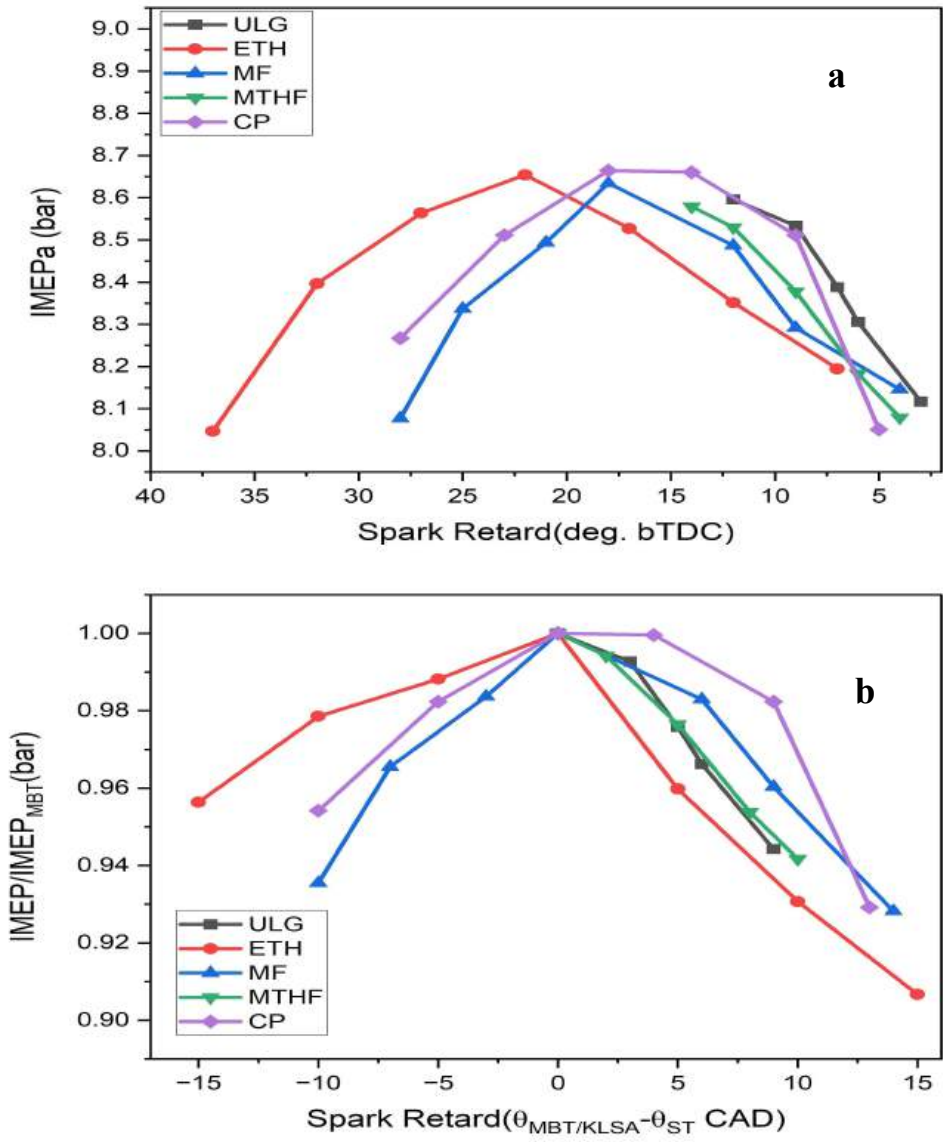

Figure 5.1a) Effect of spark retard on absolute IMEP for the fuels at spark retard and b) effect of spark retard on normalised IMEP for the fuels.

MTHF suggests the KLSA timing for the two fuels (CP and MF) is much closer to its theoretical MBT timing. Within the range of IMEP decay, ethanol is the least sensitive to spark timing variations. This is as indicated in Figure 5-1b at the arbitrary 2.5CAD spark retard location, (SR2.5). There is a loss in IMEP of approximately 1%, 3.5%, 1%. 3.5% and 0.5% from MBT when using Ethanol, MTH, MF, ULG and CP respectively. Evidently, both MTHF and gasoline are the most sensitive to spark timing at this load, due to their low octane number.

5.1.2 Optimum Spark Timing

The MBT/KLSA timings for this study were determined for loads between 3.5bar and 8.5bar IMEP, in 1bar IMEP intervals at fuel injection pressure of 150bar and stochiometric engine condition (ƛ=1) and fixed engine speed of 1500rpm. The spark timing was advanced at each until a significant drop in performance or stability was seen to find the KLSA (IMEP decrease >5% or COV of IMEP increase >3%). Similarly, the spark timing was retarded until a similar drop in performance was seen. To find the required AFRstoich at the anticipated MBT, firstly, the throttle position was fixed and then the fuel injection pulse width was adjusted finely (±1μs). Secondly the spark timing is advance using the previous load as the reference position. The MBT/KLSA timings for each fuel are shown in Figure 4.2 in the previous chapter under the investigation of load and spark timing. There are no significant differences in the fuel MBT timing of the fuels at 3.5bar IMEP, the spark sweeps were relatively flat IMEP around MBT (34°bTDC). However, major variations in the position of the spark timing was observed for each of the fuels as the load increases. The most advanced spark timings are obtained with MF, CP, and Ethanol due to their higher-octane number and faster combustion duration as indicated in the previous chapter. MTHF and gasoline offered resistant to spark advance for the same reasons highlighted above. At the maximum load of 8.5bar IMEP, Ethanol and CP are more advanced by 2.5CAD, 12.5CAD and 15CAD than MF, gasoline, and CP respectively. With MTHF and gasoline fuels the knock margin was enforced as early as 5.5bar IMEP due to their low research octane number, The similarity of gasoline and MTHF despite the lower octane number of the latter suggests that the higher ΔHvap and thus cooling effect of MTHF offsets its lower octane index to have comparable knock suppression.

5.1.3 Spark Timing Sensitivity

It has been observed in the recent times by the fuel researcher that the research octane number that has been used to provide explanations into the sensitivity of spark timing does not considers the effect of charge-cooling with modern DI engine. In addition, the value of research octane

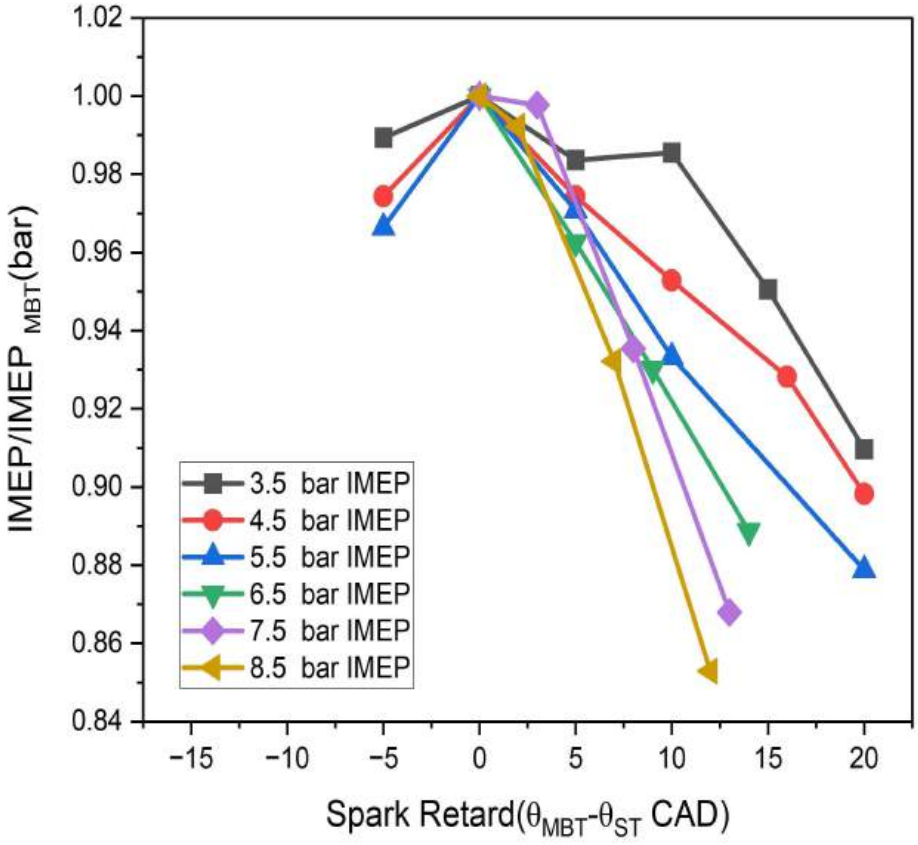

Figure 5.2 Effect of spark retard on IMEP for ULG.

number of fuel beyond the RON values for iso-octane (100RON) are obtained through extrapolation. These have put the CFR tests, developed in the 1930s, under heavy criticism for their relevance to modern engines (316-320). Daniel et al proposed a modern alternative by analysing the spark timing sweeps at various loads at constant speed of 1500rpm to determine the spark sensitivity of each fuel (4, 279, 297). This method is applied in this study to investigate the spark sensitivity of ethanol, MF, MTHF, CP and gasoline. The effect of spark retard on IMEP for gasoline is as indicated in Figure 5.2. The Figure shows that there are clear spark sensitivity observed with loads for gasoline. The IMEP decay increases as the load increases. The decay at SR 5 for instance is <1% at 3.5bar IMEP. However, with each 1bar increment in load, the decay in performance rapidly increases to a maximum of 7.5% at the maximum load of 8.5bar IMEP.

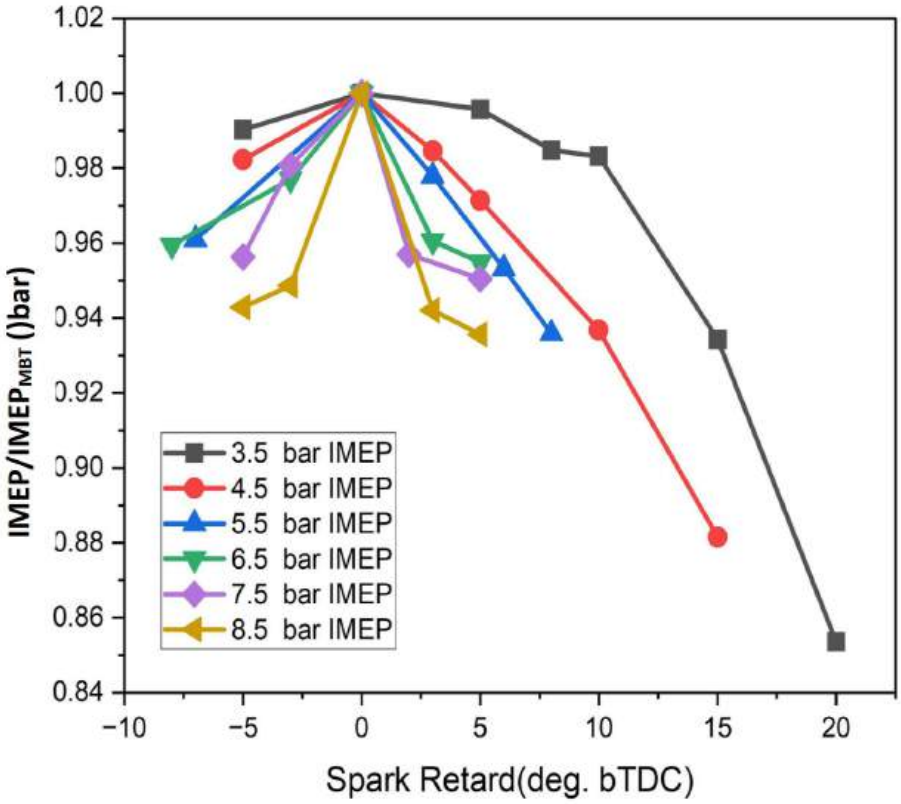

Figure 5.3 Effect of spark retard on IMEP for MTHF.

This increased sensitivity with respect to load is also evident for MTHF in a similar manner to ULG. As indicated in figure 5.3 the decay of IMEP (or spark sensitivity) increases with load. At 3.5bar IMEP, the decay at SR5 for MTHF is about 0.7%, however, at the maximum load of 8.5bar IMEP the decay in performance rapidly increases to 6%. The spark sensitivity of ethanol as indicated Figure 5.4 is symmetric either side of MBT due to its combine advantages of research octane number and heat of vapourisation (Table 3.8). In similar manner to the other fuels, the rate of IMEP decay for Ethanol increases with load. At 3.5bar IMEP, the decay at SR5 for Ethanol is about 0.7%, however, at the maximum load of 8.5bar IMEP the decay in performance rapidly increases to 4.5%. The spark sensitivity for MF and CP as indicated in Figure 5.5 and Figure 5.6 appears to be closer to ethanol than gasoline because the spread between the loads is lower. However, at SR5 the decay for MF and CP are 0.5% and 1%, respectively.

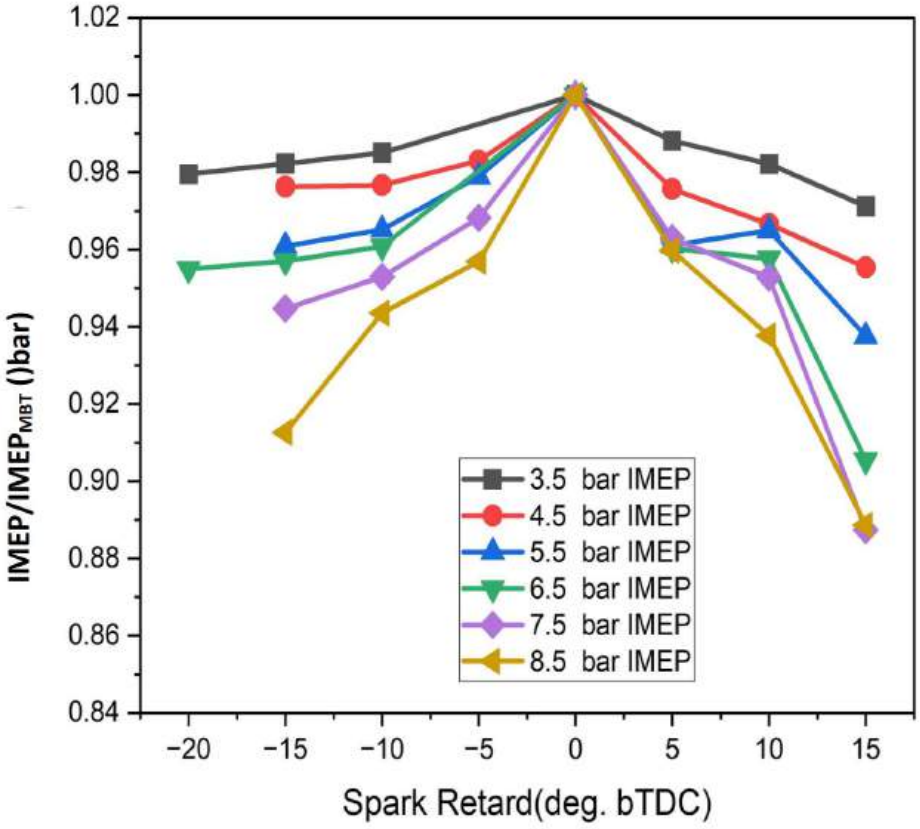

Figure 5.4 Effect of spark retard on IMEP for Ethanol.

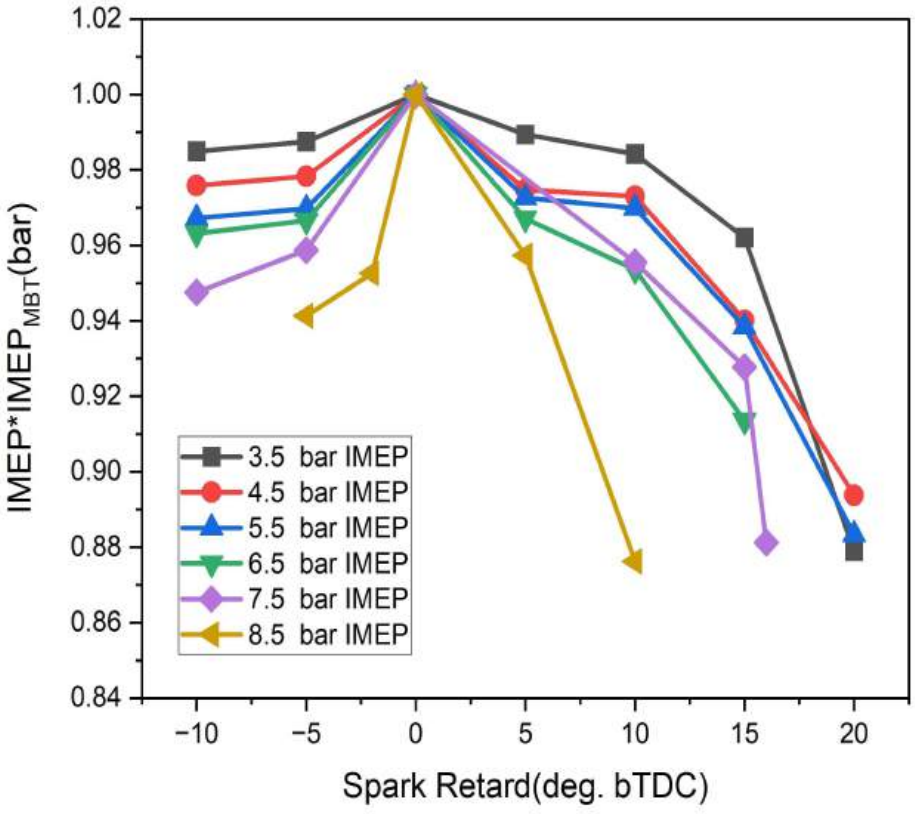

Figure 5.5 Effect of spark retard on IMEP for MF.

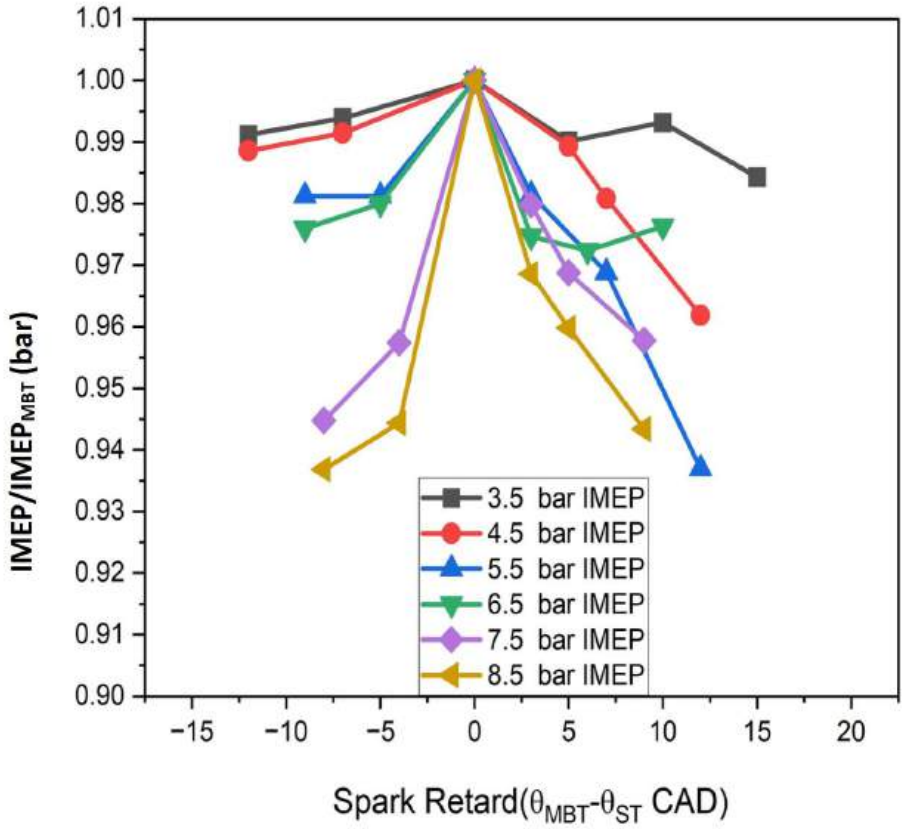

Figure 5.6 Effect of spark retard on IMEP for CP.

This value was observed to increase rapidly with load to 4.8 % and 4.7 % for MF and CP respectively, at the peak load of loads of 8.5bar IMEP. The spark sensitivity of the fuels at the peak load for an arbitrary SR5 can be summarised as ULG (7.5%) > MTHF (6%) > CP (5%) > MF (4.7%) > Ethanol (4.5%). Daniel et al (297) has provided an explanation to the relationship between the fuel spark sensitivity, its octane number and the heat of vaporisation. Typically, fuels researcher employ SR for emissions preservation once the MBT timing is found. This is commonly the spark retard that produces an IMEP of 2% less than that from MBT (236). This helps to quantify the sensitivity and highlights the window of acceptable SR between the fuels. Greater SR gives greater opportunity for emissions optimisation for all fuels (Spark windows). This spark windows generally decreases with load.

5.2 Effect of Single-Pulse Injection Timing at Full Load

To investigate the effect of SOI on engine performance and emissions for the fuels at full load and (λ=1, 1500rpm). The MBT timing was used for each fuel and KLSA timing is used in the case of knock. The test procedure shown in Table 5-1 was followed for each sweep. The baseline points were selected as the single-pulse DI (270°bTDCcomb) based on the SOI tests conducted on gasoline. Thereafter, the SOI timing was swept either side of the single-pulse baseline in 30CAD steps. To examine the entire intake stroke, the fuel injection timing was first retarded towards BDC (180°bTDCcomb) and then advanced to TDC (360°bTDCcomb). The experimental uncertainty was reduced by repeating the test three times to produce an average error bar. During the test, the pulse-width was adjusted finely (±1μs) to maintain stoichiometry, once MBT or KLSA was found.

Table 5. 2 Operating conditions for the SOI timing test on MTHF and CP.

Speed rpm	IMEP bar	Injection Pressure bar	Injection timing CAD BTDC	Fuels	Spark timing Deg bTDC	Test Procedure
1500	8.5	150	180-360	MTHF, CP, MF Ethanol and ULG.	MBT/KLSA timing	Baseline single-pulse DI. Incremental injection timing retard. Incremental injection timing advance.

5.2.1 Effect on Engine Performance and Efficiency

Single-pulse SOI timing sweeps of 360-180°bTDCcomb at 30CAD intervals was conducted on MTHF and CP and the results of the study compared to MF, Ethanol and ULG. The selection of the 30CAD intervals allows the inclusion of TDC, BDC and mid-way through the stroke when the piston speed is close to its greatest, as used by Yang (7, 321). The effect of the fuel injection timing sweeps on the Indicated Mean Effective pressure (IMEP) and the volumetric Efficiency (VE) are discussed in this section. As indicated in figure 5.7, the IMEP reaches 9.3bar and 9.1bar for CP and Ethanol respectively at the fuel injection timing location of 280 degbTDCcomb. which is 9.4%, 7%, 7.1%, 3.5% and 2.3% for CP MF, ethanol, gasoline and MTHF respectively compared to the baseline performance of 8.5bar. Advancing the fuel injection timing allows the fuel to be injected into the combustion chamber earlier during the

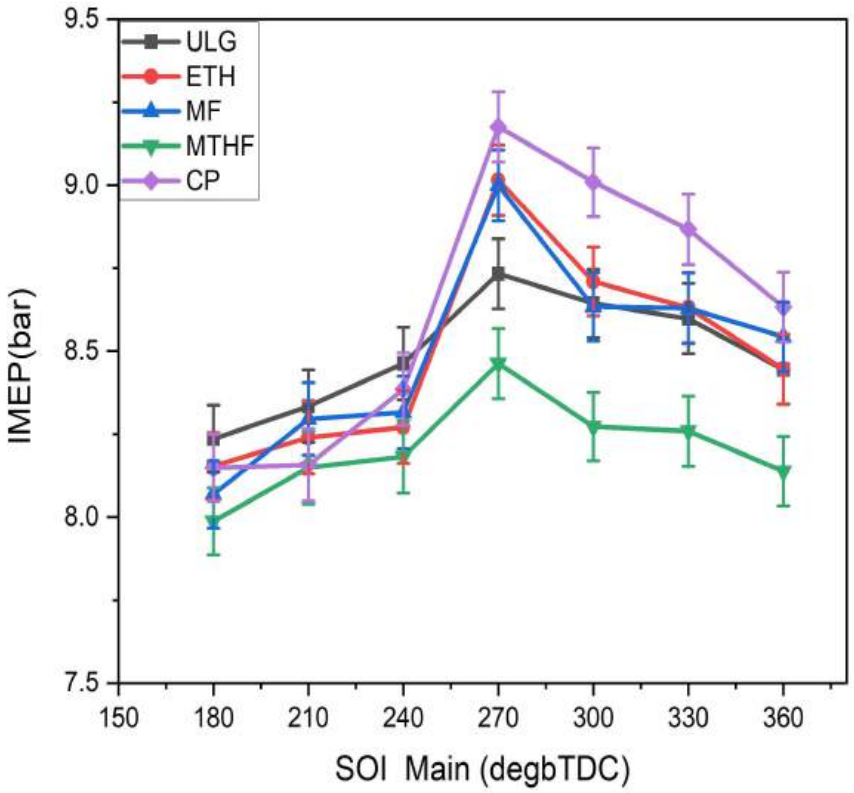

Figure 5.7 The effect of fuel injection timing sweeps (360-180 degbTDCcomb) on IMEP for the investigated fuels.

compression stroke, which minimises fuel impingement on the piston crown. This provides more times for the fuel to mix with air resulting in better fuel-air mixing and improved combustion efficiency leading to higher IMEP (322, 323). The effect of SOI timing on the volumetric Efficiency VE is shown in Figure 5.8. The low VE with early injection strategy (360°bTDCcomb) is more likely to be due to high fuel penetration rate causing piston infringement (324). Early fuel injection timing tends to increase volumetric efficiency by allowing more time for fuel-air mix. On the other hand, late injection timing reduces the VE due to incomplete mixing of fuel-air prior to ignition Two peaks were recorded for the VE of the fuels (210 and 270°bTDCcomb). The optimised VE was recorded 270 °bTDCcomb for all fuels investigated.

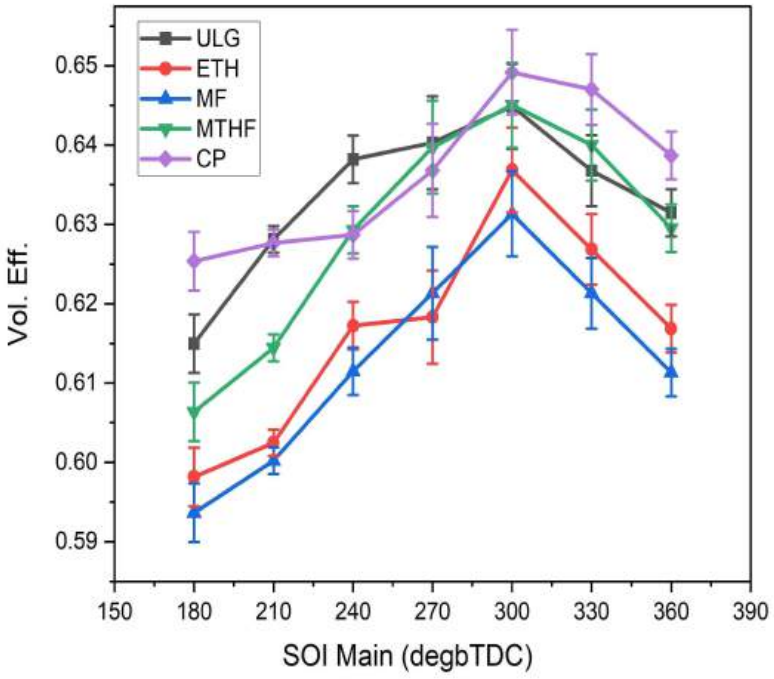

Figure 5. 8 The of fuel injection timing sweeps (360-180 degbTDCcomb) on the volumetric efficiency of the investigated fuels.

5.3 Effect of SOI on ignition timing

When using ethanol, MF and CP no knock occurs and the MBT timing is found. Figure 5.9 shows the effect of fuel injection timing on the spark timing at the maximum load of 8.5bar IMEP. Later SOI timings improve the knock resistance, with no IMEP improvement. Advancing the SOI timings have no negative effect on spark timing with ethanol, MF, and CP. However, with gasoline the spark is retarded. The maintained spark advance when using Ethanol, MF and CP with early SOI timings (due to their higher OI) explains why the IMEP remains high compared to gasoline due to their higher-octane index (302).

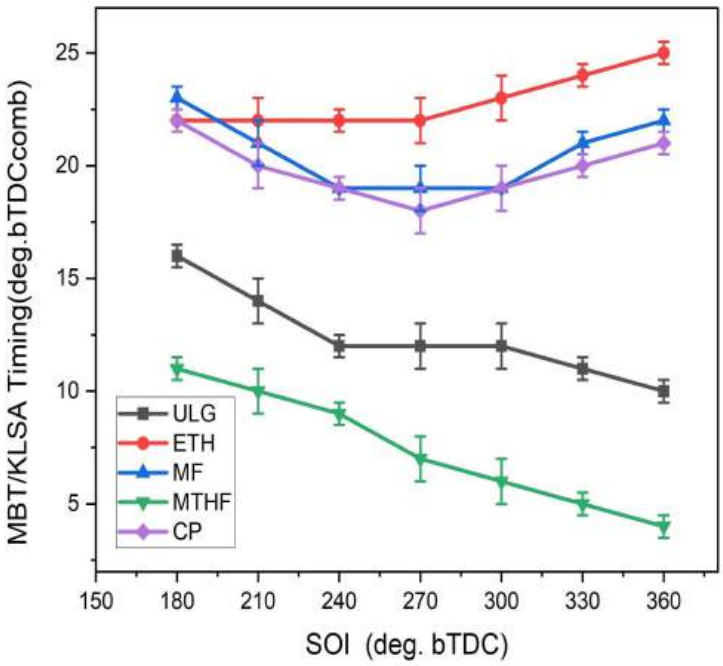

Figure 5.9 Effect of fuel injection timing sweeps (360-180degbTDCcomb) on the MBT/KLSA of the investigated fuels.

5.3.1 Effect of SOI on Pmax and combustion duration

Advanced fuel injection timing increases the temperature and pressure of the cylinder before the piston reaches the top dead center which can result in higher peak cylinder pressure. Figure 5.10 indicates the variation of Pmax with the fuel injection timing. The cylinder peak pressures for

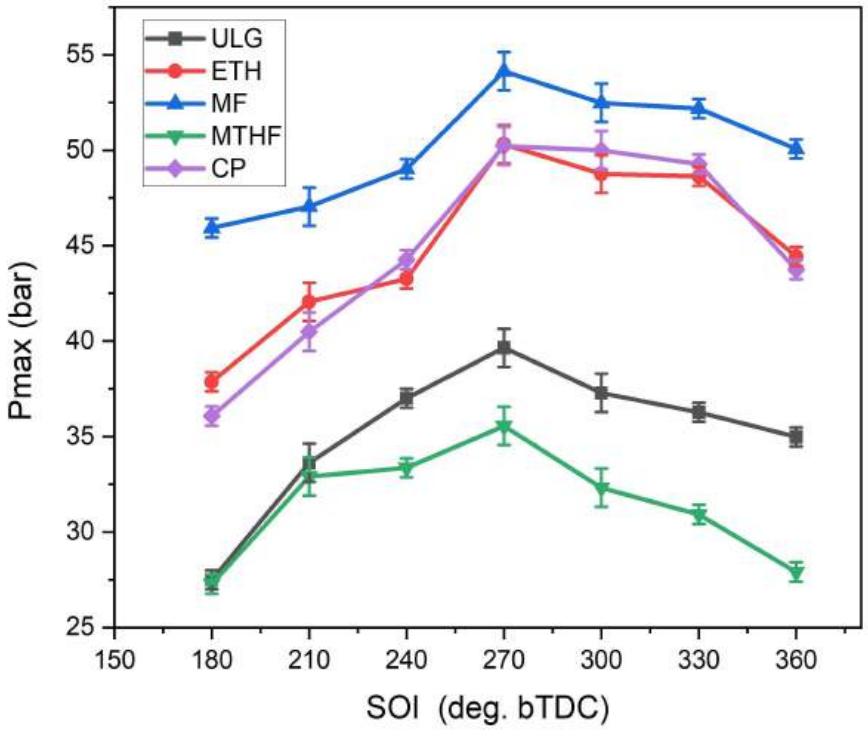

Figure 5.10 Effect of fuel injection timing sweeps (360-180deg.bTDCcomb) on the Peak cylinder Pressure for the investigated fuels.

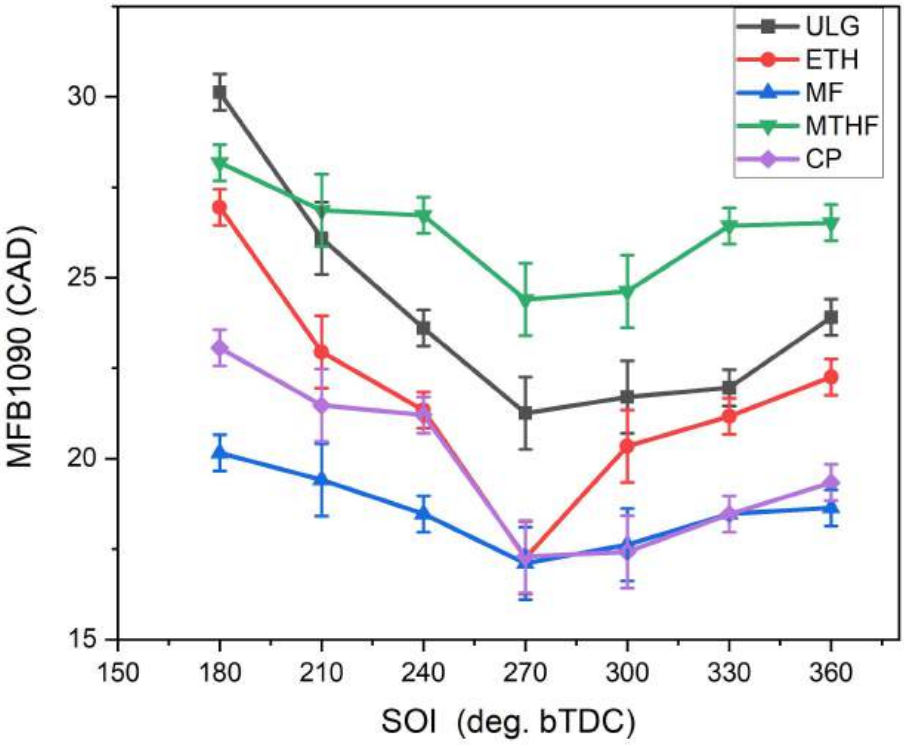

Figure 5.11 The effect of fuel injection timing sweeps (360-180 deg.bTDCcomb) on the Combustion duration (MFB1090) of the investigated fuels.

the fuels occured between SOI of 270 and 240°bTDCcomb. The lowest CAD10-90 exists at SOI of 270 °bTDCcomb as indicated in figure 5.11. Unlike with gasoline, CP and Ethanol, the CAD10-90 when using MF and MTHF is less affected by variations with the fuel injection timing. Advancing the fuel injection timing promote the combustion process in the engine cycle, because the fuel has more time to mix with the air and combust more effectively results in faster combustion duration resulting in higher peak cylinder pressure (302).

5.3.2 Effect of SOI on specific fuel consumption and combustion efficiency.

The effect of SOI timing on the volumetric ISFC and combustion efficiency between the fuels is shown in figure 5.12 and figure 5.13 respectively. As indicated in figure 5-11, the optimum fuel consumptions for all the fuels investigated is obtained at 270°bTDCcomb. As expected ULG has the most economy fuel consumption due to its superior energy density. Early fuel injection

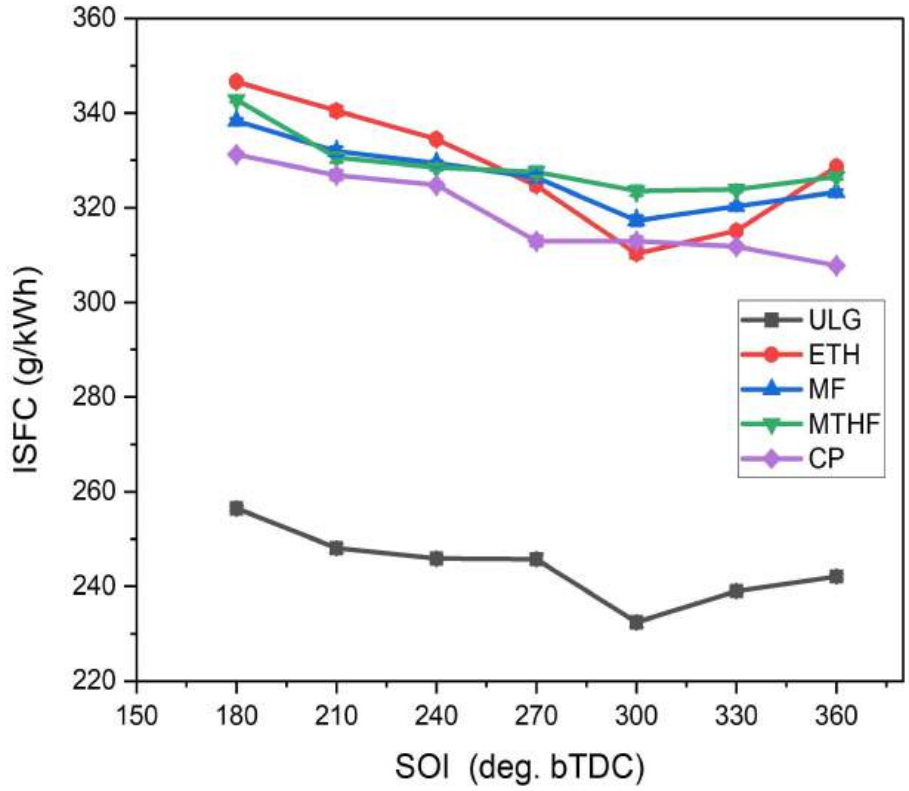

Figure 5.12 Effect of fuel injection timing sweeps (360-180 deg.bTDCcomb) on the ISFC for the investigated fuels.

generally promotes combustion efficiency as it allows more time for fuel air to mix thoroughly before ignition. This can lead to improved fuel consumption. On the other hand late fuel injection result in more fuel consumption. However, there is a trade off with the continuous advancing the fuel injection timing as it can lead to knock if not carefully managed shown in figure 5.12 and figure 5.13 respectively. As indicated in figure 5.12, the optimum fuel consumptions for all the fuels investigated is obtained at 270°bTDCcomb. As expected ULG

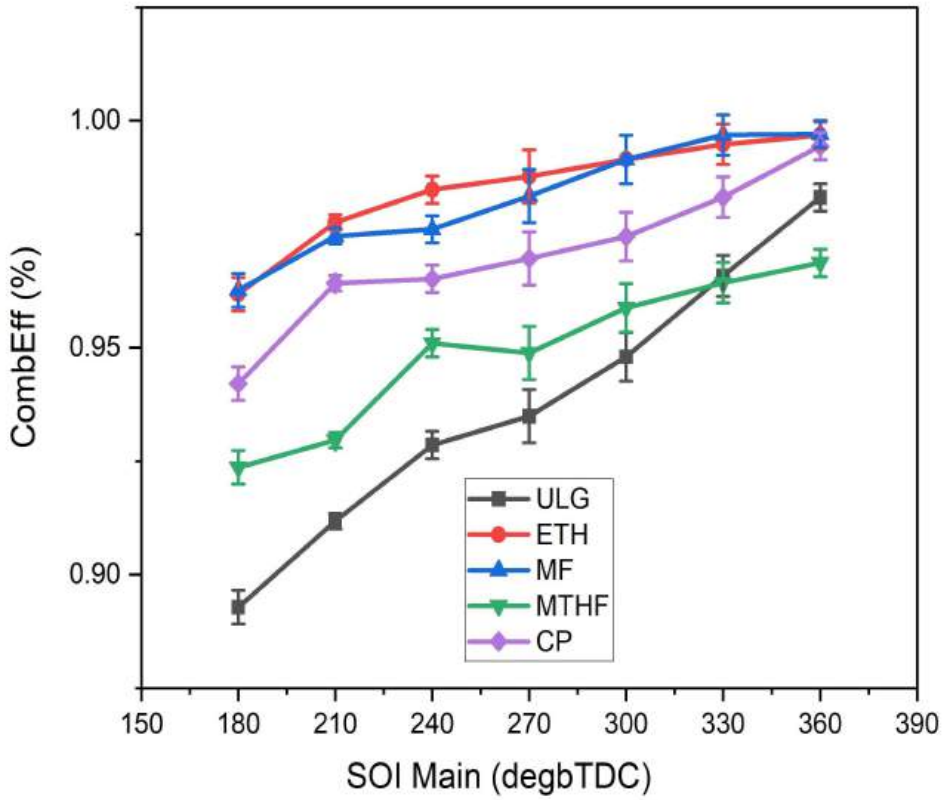

Figure 5.13 The effect of fuel injection timing sweeps (360-180 degbTDCcomb) on the combustion efficiency for the investigated fuels.

has the most economy fuel consumption due to its superior energy density. Early fuel injection generally promotes combustion efficiency as it allows more time for fuel air to mix thoroughly before ignition. This can lead to improved fuel consumption. On the other hand late fuel injection result in more fuel consumption. However, there is a trade off with the continuous advancing the fuel injection timing as it can lead to knock if not carefully managed. This phenomenon is equally reported by Song et al. 2018 (325) on fuel economy, combustion

stability and knock. As indicated in figure 5.13 the fuels combustion efficiency increases progressively with the advanced fuel injection. In all the instances investigated, the optimum for the fuels injection timing are obtained at early SOI of 360°bTDCcomb. This is largely due to the improved mixture preparation, as earlier SOI allows more time for vaporization, helping to combat the low vapour pressure of the oxygenated fuels.

5.3.3 Effect of Fuel Injection Timing on Gaseous Emissions

Instantaneous NOx emissions for the five fuels investigated are as indicated in figure 5.14. Advancing the fuel injection timing was expected to increases the instantaneous NOx emissions because the early injection can lead to higher temperatures leading to increase NOx emissions. However, as indicated in figure 5.14 there is no significant changes in the emitted value of NOx

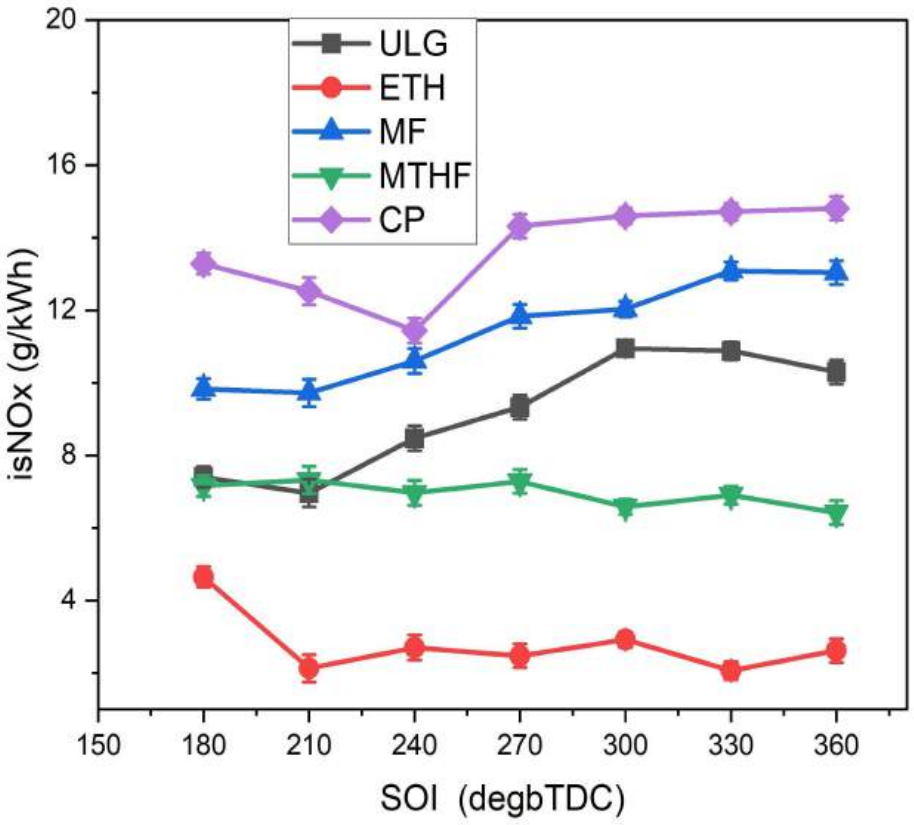

Figure 5.14 The effect of fuel injection timing sweeps (360-180deg.bTDCcomb) on the instantaneous NOx emissions of the investigated fuels.

with the advanced timing. It is significant to state that the highest emissions of NOx for the fuel are obtained at early SOI of 360°bTDCcomb though the margin remains very low with is NOx emissions at the late injections. The maximum differences in CP NOx emissions between the late injection timing of 180°bTDCcomb and early injection timing of 360°bTDCcomb was 1kJ/kghr as indicated in figure 5.14. Similar trends in the variation of isNOx with fuel injection timing were observed for the other fuels. Figure 5.15 shows the trends of the emissions of the instantaneous total hydrocarbon for CP and MTHF compared to MF, Ethanol and ULG across the fuel injection timing sweeps (180 - 360°bTDC) and at the maximum loads of 8.5bar imep.

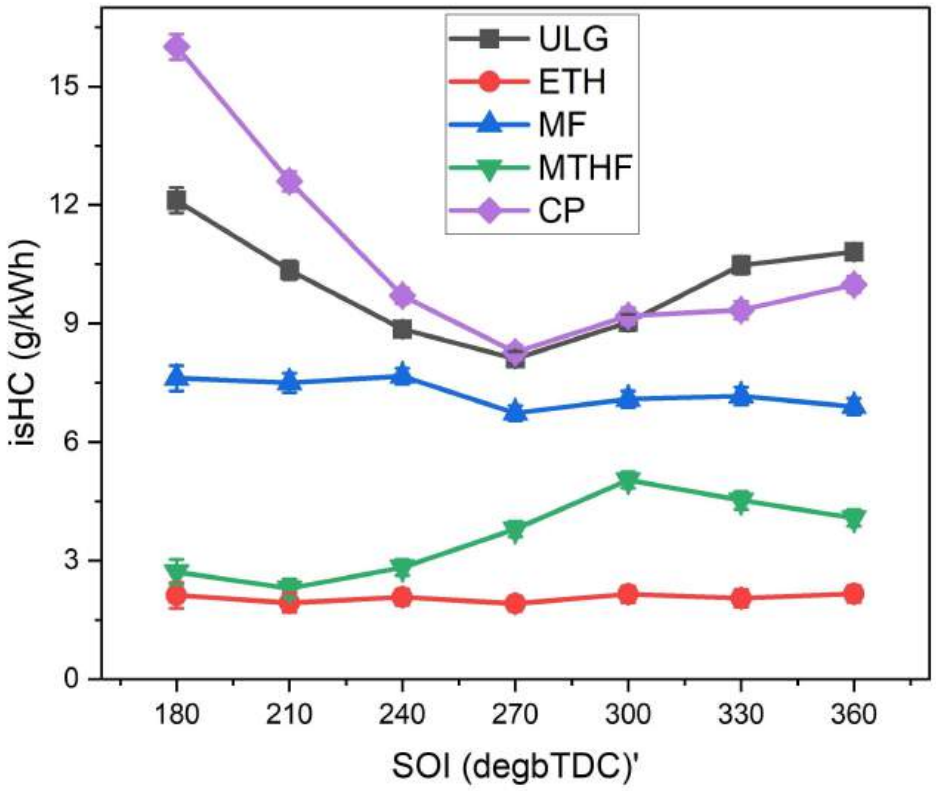

Figure 5.15 The effect of fuel injection timing sweeps (360-180 degbTDCcomb) on the instantaneous HC emissions of the investigated fuels.

The study indicates that the HC emissions decreases as the fuel injection timing advances for all the fuels investigated. At the late fuel injection of 1800bTDCcomb. maximum emissions of the hydrocarbon were observed for the fuels. When fuel is injected earlier in the compression stroke,

it has more time to mix with the incoming air. This can lead to better fuel-air mixing, more uniform combustion, and lower HC emissions. Early injection timing allows the fuel to burn more completely, resulting in reduced unburned hydrocarbons in the exhaust. If fuel injection occurs later in the compression stroke, there may be less time for the fuel to mix adequately with the air before ignition (313, 325). This can lead to incomplete combustion, resulting in higher HC emissions. Late injection can cause unburned or partially burned hydrocarbons to be expelled in the exhaust. As expected, the HC emissions for oxygenated fuels are lower compared to gasoline. The variations of the isCO emissions with the fuels injection timing for MTHF and CP compared to MF, Ethanol and ULG are as indicated in figure 5.16. The isCO emissions for the fuels decrease as the fuel injection timing is advanced. The lowest emission of isCO for the fuels were recorded at very early injection timing of 360^{0}bTDCcomb. The reason

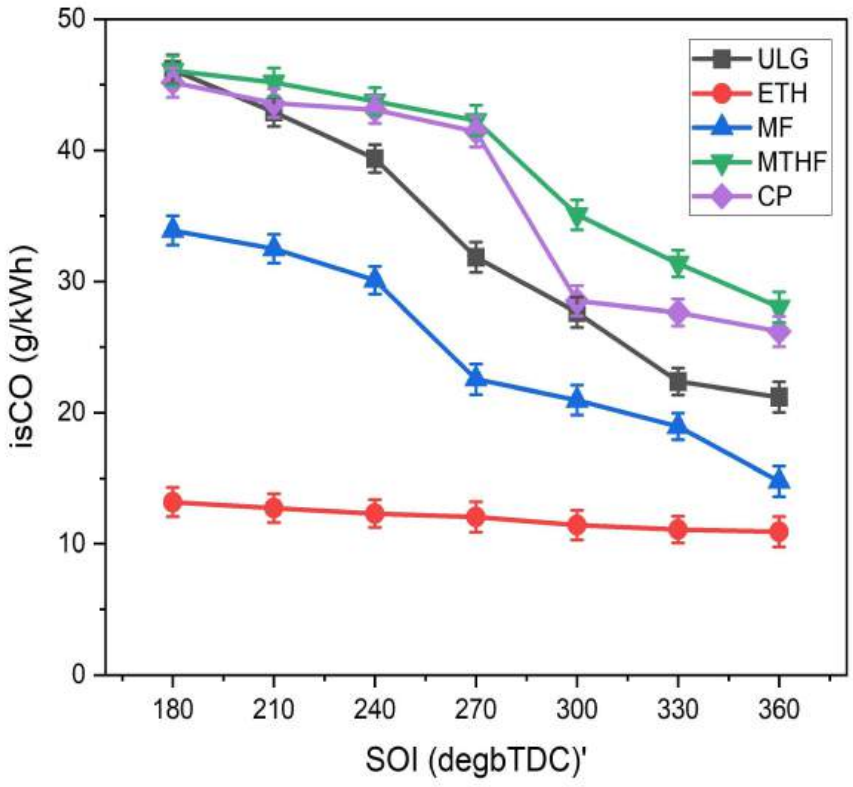

Figure 5. 16 The effect of fuel injection timing sweeps (360-180deg.bTDCcomb) on the instantaneous CO emissions of the investigated fuels.

for this is because injecting fuel earlier allows more time for the fuel-air mixture to homogeneise and ignite evenly. Complete combustion results in fewer incomplete combustions by products like CO. Additionally, early injection timing can help optimize air-fuel mixing, minimising pockets of unburned fuel that could contribute to higher CO emissions. The reason for this is because injecting fuel earlier allows more time for the fuel-air mixture to homogeneise and ignite evenly. Complete combustion results in fewer incomplete combustions byproducts like CO. Additionally, early injection timing can help optimize air-fuel mixing, minimising pockets of unburned fuel that could contribute to higher CO emissions.

5.4 Effect of SOI2 with split ratio on the combustion and emissions of MTHF and CP

The split fuel injection system in a DISI engine is designed to enhance combustion and emission control and to improve the fuel conversion process. This is achieved by dividing the fuel injection into multiple pulses during the intake stroke. This allows for better control over the fuel-air mixtures, promoting more homogeneous combustion and improving the overall engine performance. By splitting the fuel injection, the fuel be efficiently metered with the timing of fuel delivery for different engine operating conditions. This flexibility is expected to enhance the combustion stability, reduce the engine knock tendency and improves the fuel conversion efficiency and in addition minimise the engine out emissions. In addition, the split-injection strategies can be used to increase high-load torque output above that of equivalent single-pulse injections (321). This mode also improves air entrainment, fuel evaporation and vapour diffusion, and reduces the fuel impingement on in-cylinder surfaces (323, 326). The split injection process involve determining the optimum SOI timing with the highest IMEP when using gasoline which is then chosen as the first SOI timing (SOI1).

Table 5. 3 Operating conditions for the split injection test on MTHF and CP.

Speed rpm	IMEP Bar & LAMBDA	Injection Pressure (bar)	Injection timing (SOI2) ^{0}bTDC	Fuels	Spark timing ^{0}bTDC	Test Procedure
1500	8.5 &1	150	240-90	MTHF CP, and ULG.	MBT/KLSA timing	1.Baseline single-pulse DI. 2.Incremental injection timing retard. 3.Incremental injection timing advance.

The second SOI timing (SOI2) was then varied from 240°bTDCcomb (induction stroke) to 90°bTDCcomb (compression stroke) in 30CAD intervals. The majority of SOI2 timings were during the IVO phase, apart from 120 and 90°bTDCcomb (IVC: 126°bTDCcomb). The selected split injection width ratio for this study is 1:1 and 2:1. The tests were performed at constant engine speed of 1500rpm and at the stoichiometric A-F, and the spark timing was advanced to find the respective MBT or KLSA timings. As recommended by Beck et al (298), the tests for both the single-pulse and split-injection timing tests were performed over three consecutive days in order to minimise the effect of engine drift, ambient conditions. Some studies have been carried out in relation to split injection for Gasoline, Ethanol and DMF, however, little is known about split injection strategies for MTHF and CP. This section discusses the effect of split injection on MTHF and CP. The operating conditions for the experiment are as indicated in table 5.3.

5.4.1 Effect of SOI2 with Split Ratio on Engine Performance and Efficiency

Figure 5.17 shows the effect of the split-injection strategies on IMEP. The recorded IMEP with the 2:1 split ratio is consistently higher that of the split ratio 1:1 over the entire SOI2. timing

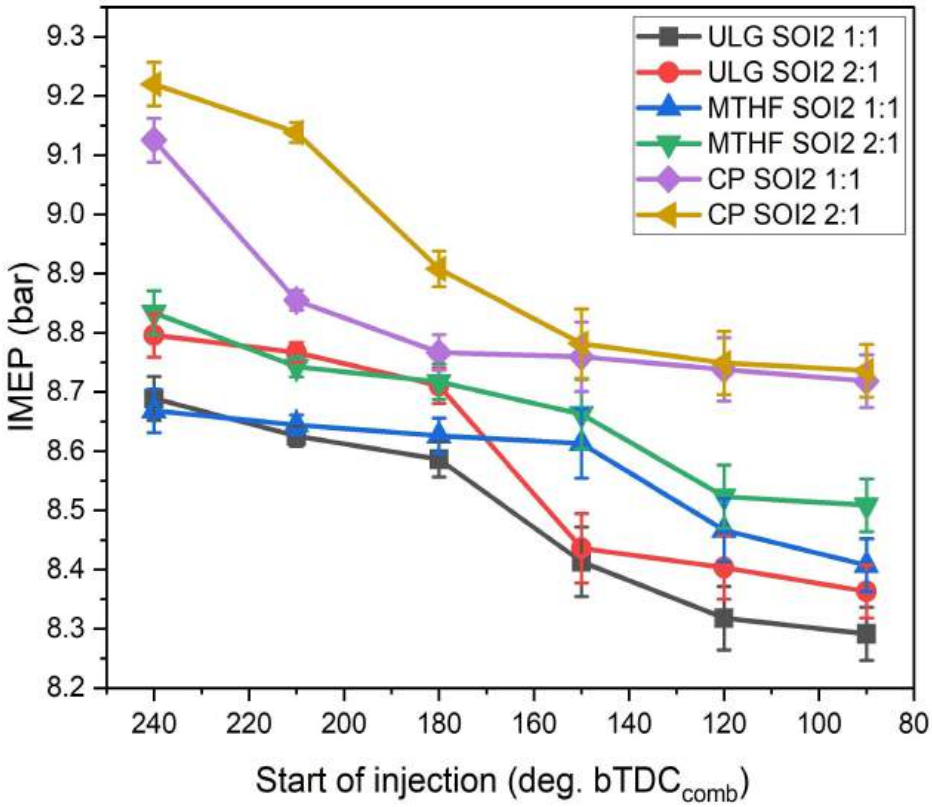

Figure 5.17 Split fuel injection timing sweeps (240-90 degbTDCcomb) on the IMEP of the investigated fuels.

sweep for the three fuels (CP, MTHF and ULG). The reason for the increase in IMEP could be attributed to the reduced fuel impingement with SOI2 which improves fuel droplet evaporation and mixture preparation. This effect is reduced (piston impingement is more likely) as SOI2 enters the compression stroke, especially at 90°bTDCcomb. However, later SOI2 injection is detrimental to performance as observed with the recorded IMEP value at 120°bTDCcomb and 90°bTDCcomb. The recorded performance for the fuels at SOI single pulse width was about 1.2%. 1.4% and 3.5% higher for MTHF, ULG and CP respectively, When compared to the baseline performance for the fuels at late SOI2 split injection. These reductions is explained by the reduced fuel vaporization time because of the lower vapour pressures and high boiling points for the fuels investigated. It is clear from the figure that the ration 2:1 produces higher IMEP compared to using 1:1 pulse width ratio. Serras-Pereira et al. has investigated the effect of the split-injection strategy on piston crown and wall impingement(323). According to the

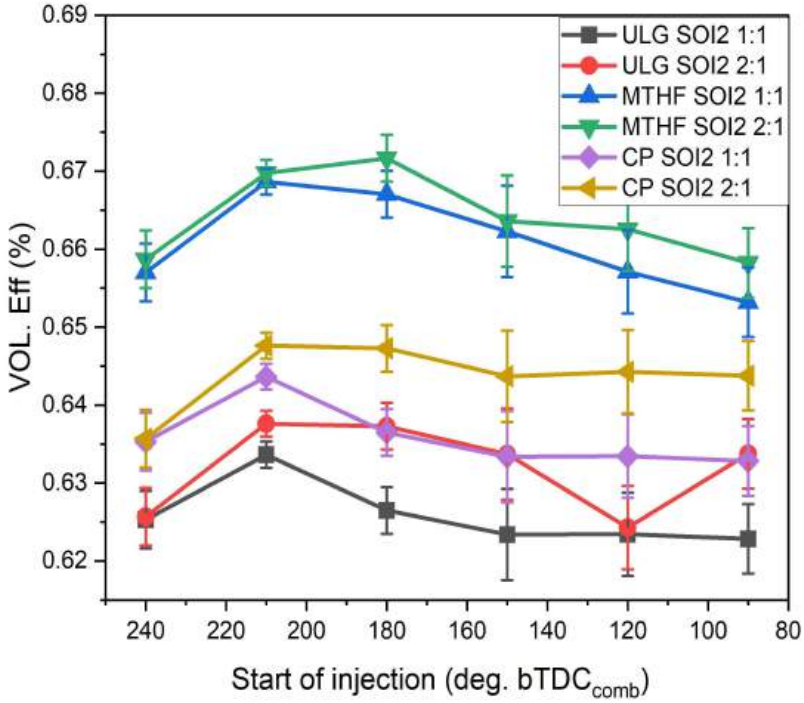

Figure 5.18 Split fuel injection timing sweeps (240-90 deg.bTDCcomb) on the instantaneous volumetric efficiency of the investigated fuels.

studies, in cold engine operation, the effect of split-injection at ambient condition was as effective as raising the engine temperature to 90°C for the single-pulse strategy (323). The Volumetric Efficiency VE for the three fuels under the Split injection condition are as shown in figure5.18. The 1:1 ratio pulse width for the split injection generally produces the higher VE compares to the baseline single pulse SOI but recorded lower value of VE than the 2:1 ratio at all SOI2 injection sweeps for all the fuel investigated. This is due to the charge-cooling effect of the direct injection. The increase in VE with 2:1 over 1:1 is due to more heat transfer with the intake air, whereby the 1:1 ratio is compounded by lower fuel impingement. The maximum VE for ULG and MTHF was recorded at 210 deg. bTDCcomb, whereas for CP the maximum VE was recorded at a later SOI2 of 180 deg. bTDCcomb. Also, when using MTHF and ULG, the VE is less sensitive to variation compared to CP under split injection combustion.

5.4.2 Effect of SOI2 with Split Ratio on Combustion Duration

Split fuel injection helps in effective control of the fuel-air mixture more effectively through reduced cycle to cycle variation in combustion. This reduction in variability contributes to a more consistent combustion duration over the subsequent cycle. As indicated in figure 5.19, SOI2 consistently maintained shorter (10-90) period of combustion compared to the SOI injection pulse width for all the fuel investigated. The fastest combustion duration was achieved at the SOI2 240 degbTDCcomb (induction stroke) for MTHF, CP and ULG.

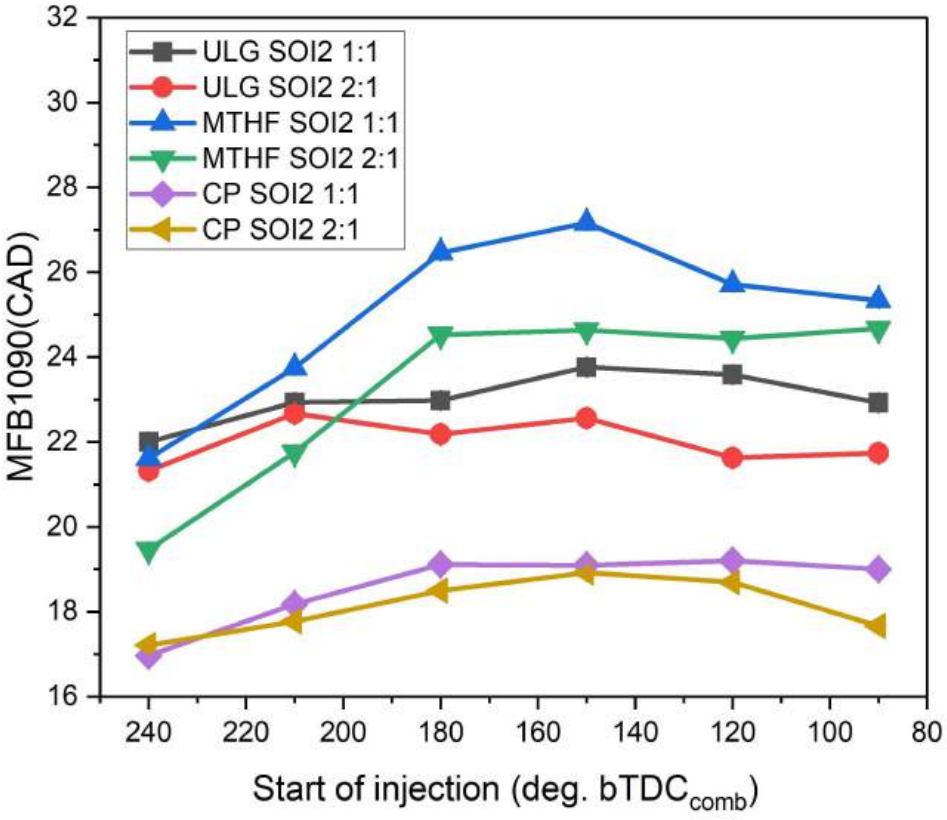

Figure 5.19 Effect of SOI2 timing sweeps (240-90 deg.bTDCcomb) with split ratio on the MFB1090 for MTHF, CP and ULG.

The reason for this is because of improved air-fuel mixing as a result of the much earlier injection which provide more time for the fuel to mix with air promoting a homogeneous pre-mix that combust more rapidly when ignites. Another reason is that advanced the SOI2 timing can enhance the stratified charge formation, where the fuel is concentrated near the spark plug

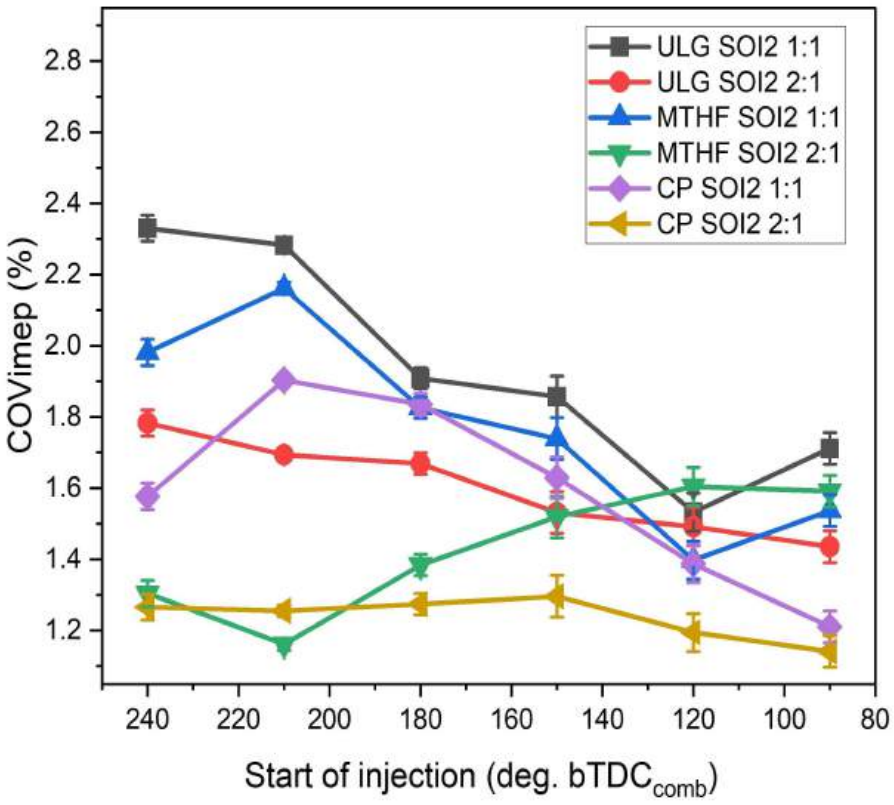

Figure 5.20 Effect of SOI2 timing sweeps (240-90 deg.bTDCcomb) with split ratio for COVimep for MTHF, CP and ULG.

leading to faster and more controlled combustion. This results in a more efficient combustion and subsequently shorter combustion duration. For both MTHF and ULG the combustion duration increases for SOI2 beyond 180degbTDCcomb and the gain of split injection over the single pulse SOI is lost due to the late injection. However, the combustion duration for CP does not display significant variation with late SOI2 injection as indicated in figure 5.20. The split injection has not display much impact on the combustion duration for CP as observed on the two split ratio (1:1 and 2:1) roughly having equal values across the different SOI2 timing indicting the split injection is less effective in improving the combustion duration for CP.

5.4.3 Effect of SOI2 with split ratio on combustion stability, ISFC and efficiency.

Figure 5.20-22 indicates the combustion stability, ISFC and combustion efficiency respectively. As indicated in the figure 5.20, the ratio 2:1 displayed clear benefits in stability compared to the

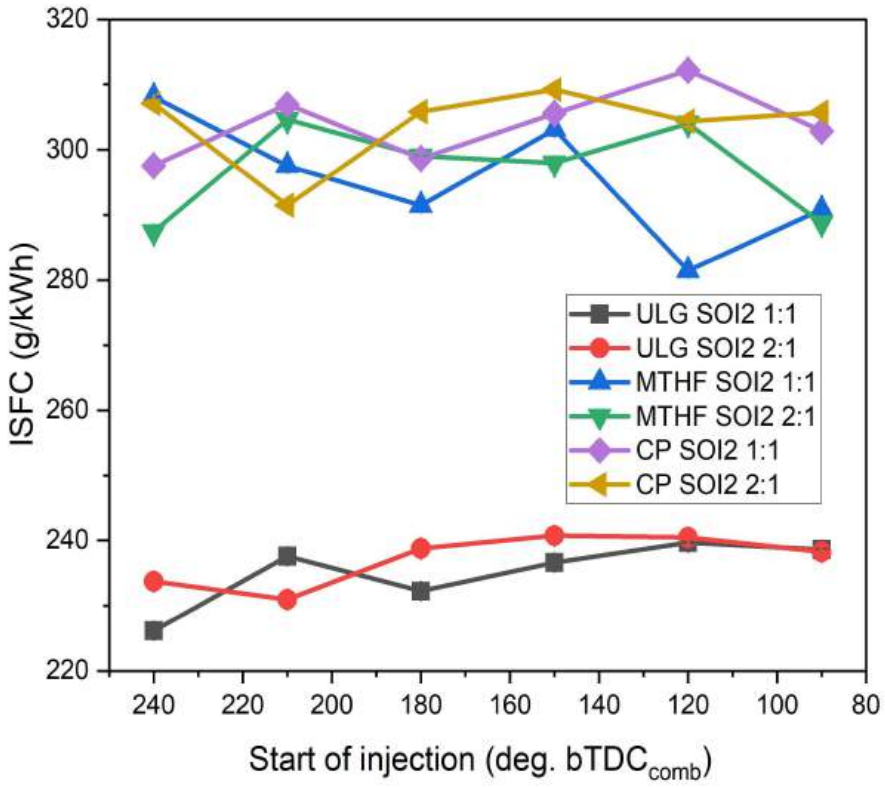

Figure 5.21 Effect of SOI2 timing sweeps (240-90 degbTDCcomb) with split ratio on the ISFC for MTHF, CP and ULG.

ratio 1:1 pulse width ratio. The Indicated Specific Fuel Consumption decreases below the equivalent maximum load single pulse case for both MTHF and ULG. However, for CP, split-injection is less effective at efficient fuel utilisation. As indicated in figure 5.21, apart from 210°bTDCcomb, increasing the SOI2 timings result in an increase in ISFC. The fuel consumption increases with late SOI2. The reason for this is because late injection may result in incomplete combustion due to reduced mixing time and less fuel droplets to vaporize and then diffuse for the completeness of combustion. Additionally, delay combustion can potentially cause higher temperatures and increase heat loss both of which contribute to increase fuel consumption. The highest split fuel consumption was obtained at the late SOI2 of 180°bTDCcomb. As indicated in the figure 5.22 the split ratio 2:1 has less fuel conversion efficiency compared to the split injection ratio 1:1. Split fuel injection can impact the

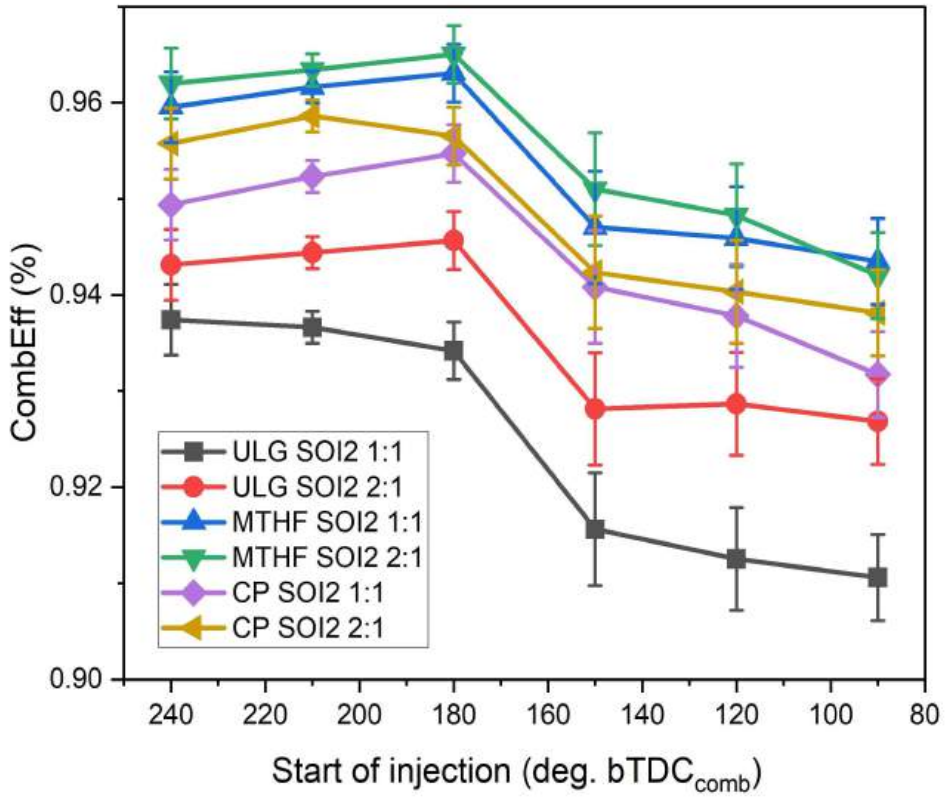

Figure 5.22 Effect of SOI2 timing sweeps with Split Ratio (240-90 degbTDCcomb) on CombEFF. for MTHF, CP and ULG.

combustion efficiency in both positive and negative ways with SOI2 timings at 180°bTDCcomb or later, the combustion efficiency is reduced. Between the two ratios, a lower compromise is seen using 2:1. This is clearer with gasoline as the combustion efficiency at 90°bTDCcomb (SOI2) is 2.3% higher than with 1:1. However the difference is lower with ethanol and DMF at the same SOI2 timing. This suggests that when using the biofuels in split-injection, a greater split-ratio (favouring SOI2), or more injections would help to improve vaporization and avoid piston wetting as such high loads.

5.4.4 Effect of SOI2 with Split Ratio on Gaseous Emissions

The gaseous emissions (NO_x, HC, and CO) are compared between the fuels (MTHF, CP and ULG) at the two split-ratios (1:1 and 2:1) and various SOI_2 timing sweeps (240-90 degbTDCcomb).

5.4.4.1 Nitrous Oxide Emissions (NOx)

The effect of split injection on the isNOx emissions for the investigated fuels is as displayed in figure5.23. The earlier SOI2 timings (240°bTDCcomb and 210°bTDCcomb appears to be the only competitive SOI2 timings as the later SOI2 timings result in dramatic increases in NOx

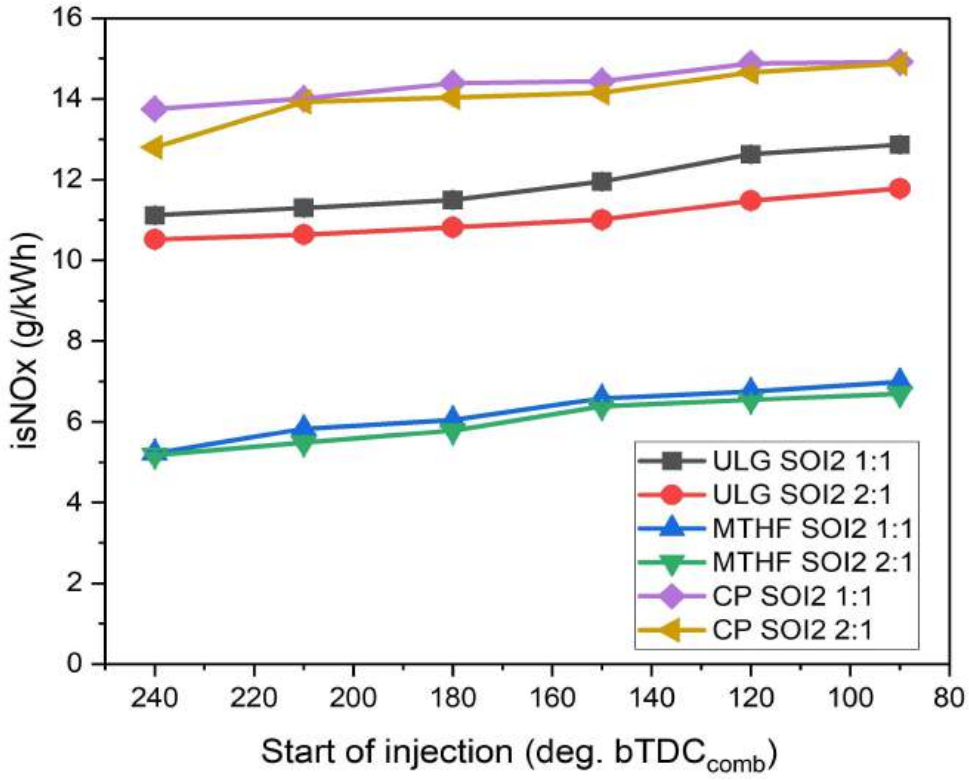

Figure 5.23 Split fuel injection timing sweeps (240-90degbTDCcomb) on the instantaneous NOx emissions for MTHF, CP and ULG

emissions. This is because the charge-cooling effect is reduced at the late SOI2 injection leading to increase in-cylinder temperature (Stone, 1999). Between the split-ratios, the 2:1 pulse width split ratio seems to produce the lowest isNOx emissions compared to the 1:1 ratio for the three fuels (MTHF, CP and ULG). The split injection strategy was observed to give a high payoff for reducing the isNOx emissions from the MTHF. However, little different is observed between the two split ratio and the SOI2 sweeps. For ULG, the largest difference between the two split-injections occurs at an SOI2 timing of 90°bTDCcomb. Little payoff is observed with the isNOx emission for CP under the split injection. The emissions level is high for both split ratios and across the entire SOI2 sweeps.

5.4.4.2 Hydrocarbon Emissions

The isHC are shown in Figure 5.24. The isHC emissions are higher for CP compared to MTHF, and it generally rises with later SOI_2, as seen with $isNO_x$ (Figure 5-22). However, this time the increase is consistently lower with the 2:1 split ratio for all fuels. The isHC emissions are competitive with the single-pulse SOI. Nevertheless, it appears that CP and ULG are more sensitive to later SOI_2 timings as the rise is higher. However, the result with both fuels suggests a payoff with the split injection compared to the single pulse SOI injection For instance, at the least favourable SOI_2 timing (90°$bTDC_{comb}$), the increase in isHC for MTHF from single-pulse.

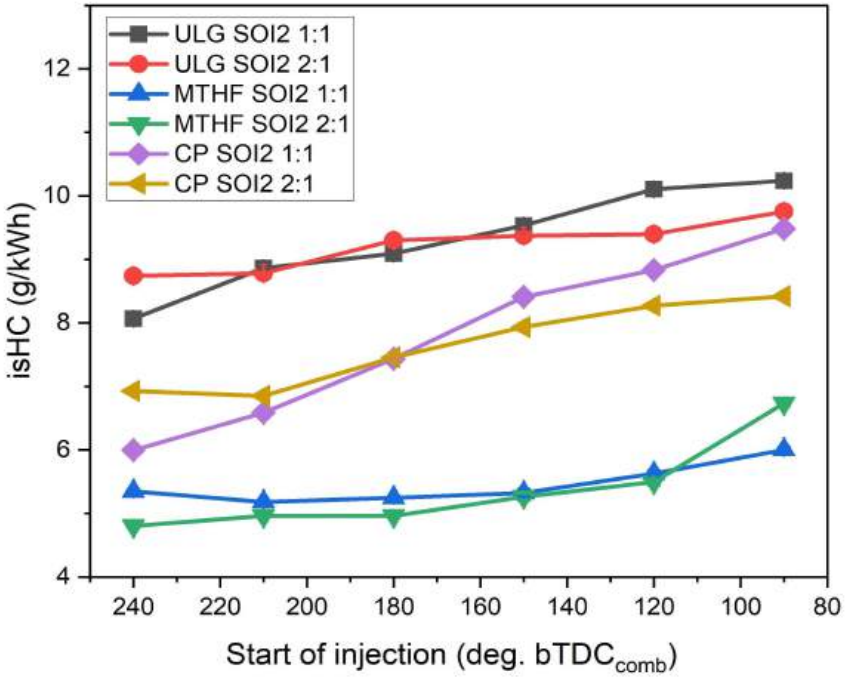

Fig. 5.24 Split fuel injection timing sweeps (240-90 degbTDCcomb) on the instantaneous HC emissions of the investigated fuels.

SOI is > 2g/kWh while with CP> 5g/kWh at the late SOI2 timing using the more favourable 2:1 split-ratio. The reason for this is because of the high fuel vaporisation, which prevents localised pockets of fuel-rich mixtures and promotes complete combustion. The higher oxygen content of the two oxygenated fuels, together with its higher the higher combustion efficiency aids the oxidation of unburned HCs, as indicated in figure5.23 below.

5.4.4.3 Carbon Monoxide Emissions

The isCO emissions are shown in figure 5.25. Once again, SOI2 of 210°bTDCcomb provides the greatest reductions in isCO emissions due to improved vaporization and reduced wetting except on the case of CP where the lowest isCO was recorded at 180°bTDCcomb. The 1:1 split ratio is less beneficial, especially for gasoline, possibly due to higher piston impingement as shown with the later SOI2 timings. Between the two oxygenated fuels, MTHF consistentlyproduces the lowest isCO emissions due to higher combustion efficiencies.

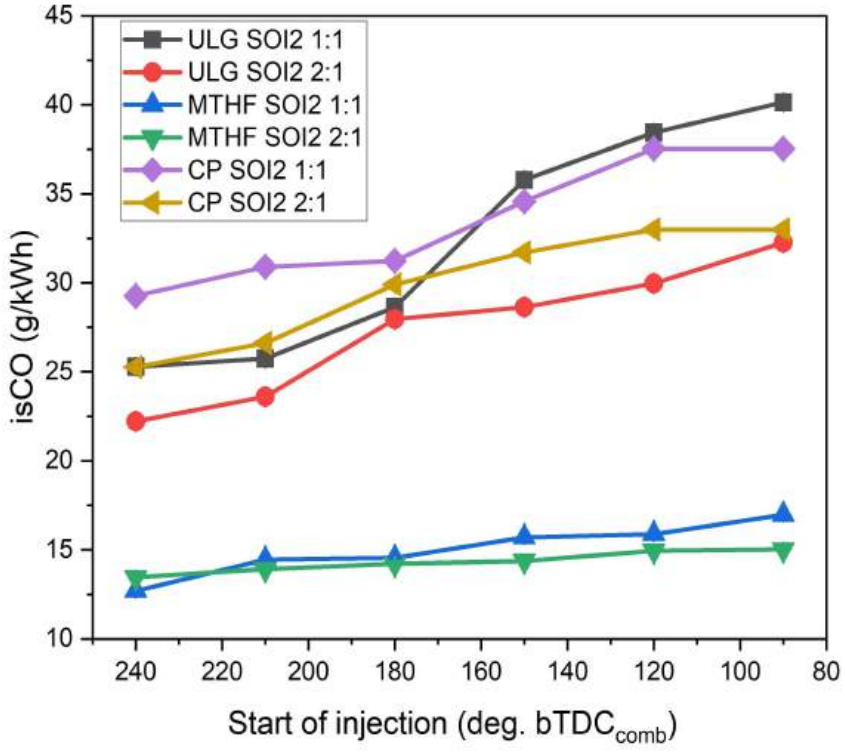

Figure 5.25 Split fuel injection timing sweeps (240-90 degbTDCcomb) on the instantaneous CO emissions of the investigated fuels.

5.5 Summary

This study was carried out to determine the maximum break Torque and Knock Limited Spark Timing for each of the fuels under investigation along with the investigations of the optimal fuel Injection timing using the SOI sweep (360-180 degbTDCcomb). The study was extended to investigate the split-injection technique for improving full-load torque with MTHF and CP. The

Spark sensitivity for the fuels arbitrary SR5 can be summarise as ULG (7.5%)> MTHF(6%) > CP(5%) > MF(4.7%) > ethanol(4.5%). The study shows that the rate of IMEP decay increases with the more retarded MBT/KLSA as indicated in Figure 5.1a. The knock-limited spark advance timing (KLSA) is achieved by retarding the MBT timing by 2CAD as suggested by Heywood, 1988. Overall, the optimal fuel injection timing for single pulse width for the fuel under investigation was found to be 270 degbTDCcomb. This optimal timing was selected after considering some trade off. For instance, the results of both isCO and isHC emissions and combustion efficiency are not optimised at 270 degbTDCcomb, however, key engine performance including the maximum cylinder pressure. Volumetric efficiency, indicated pressure and the specific fuel consumption were optimised at this timing. Experiments suggested that split-injection can improve the combustion and emission performance when using MTHF and Cyclopentanone. However, maximum gains are found. with multiple pulses or greater ratios (2:1) due to improved vaporisation. The result of the split-injection shows higher sensitivity to SOI2 and less sensitivity to biofuels. Compared to the single pulse SOI, there are benefit recorded in relation to engine performance and NOx, HC, and CO emission benefit typical at early SOI2 timings and a 2:1 split ratio when using both MTHF and CP.

CHAPTER 6

COMBUSTION AND EMISSIONS OF GASOLINE BLENDS OF 2-METHLYTETRAHYDROFURAN AND CYCLOPENTANONE IN DISI ENGINE

In this chapter the combustion and emissions of 20% and 40% volumetric blends of gasoline with Cyclopentanone (CP), and 2-methyltetrahydrofuran (MTHF) was investigated and the result of the study compare with neat gasoline and similar blends of 2-Methylfuran (MF).

The selection of 20% and 40% blend ratios of MTHF in gasoline is typically driven by considerations related to improving fuel performance, enhancing combustion efficiency, and reducing emissions. The 20% and 40% blend ratios of cyclopentanone in gasoline are selected to optimize fuel performance, enhance combustion efficiency, reduce emissions, and balance engine compatibility with economic and policy considerations. These specific ratios allow researchers and engineers to explore the potential benefits of cyclopentanone as a fuel additive across different use cases This work was investigated experimentally in a single –cylinder four stroke DISI engine.

6.1 Gasoline blends of MTHF and CP

In this study focused was given to the combustion and emissions characteristics of 2-metyltetrahydrfuran and Cyclopentanone gasoline blend fuel, 20% and 40% volume fraction (MTHF20, MTHF40 CP20 and CP40). This work was investigated experimentally in a single-cylinder four-stroke SI engine at various engine loads (3.5bar-8.5bar imep) and constant engine speed of 1500rpm at stoichiometric combustion conditions. The in-cylinder combustion process as well as engine performance of the blends were compared with gasoline and similar blend of 2-Methylfuran, under gasoline maximum brake torque (MBT) spark timing. The results of

engine tests show that MTHF and CP blends have different combustion properties compares to the neat gasoline and MF blends. The ignition delay is prolonged with the increase of MTHF fraction, which is mainly attributed to its consistently shorter combustion duration and the Pmax was observed to reduce as the blends fraction increases to MTHF40, this is due to reduce resistance to engine knock as the blends fraction increases. CP blends open the window of spark advance flexibly as the percentage of CP increases in the blends. The maximum cylinder pressure Pmax for the blends of CP is much higher than neat gasoline, and the Pmax improvement was observed as the percentage of CP increases in the blends. The experimental conditions and the properties of the blend fuels are detailed in Table 6.1 and Table 6.2 respectively.

Table 6.1 Operating conditions for the combustion of blends of MTHF and CP.

Speed rpm	IMEP bar	Injection Pressure bar	Injection timing& Lambda	Fuels	Spark timing DegbTDC
1500	3.5-8.5	150	280 & 1	MTHF20, MTHF40, CP20 CP40, MF20, MF40, & ULG	MBT/KLSA timing

Table 6.2 Fuel Properties for (ULG, MTHF20, MTHF40, CP20, CP40, MF20 and MF40).

Properties	ULG	MTHF20	MTHF40	CP20	CP40	MF20	MF40
A/F	14.15	13.28	12.71	13.10	12.39	12.98	12.16
H/C	1.922	1.89	1.92	1.81	1.75	1.73	1.59
O/C	0.021	0.063	0.096	0.067	0.101	0.067	0.101
Research Octane Number (RON)	96.8	93.30	98.82	97.64	98.48	98.04	99.28
LHV[MJ/kg]	42.9	40.25	38.60	40.27	38.71	39.48	37.16

For both MTHF and CP, the Emissions of hydrocarbon HC reduces significantly as the blends fraction increases compared with neat gasoline, however the NOx fraction increases with the blends fraction.

6.1.1 Effect of the fuel blends on Combustion Stability

COV IMEP is a measure used to assess the combustion stability or consistency in engine. It is calculated as the percentage of standard deviation of IMEP by the average IMEP. A lower COV of IMEP indicates better combustion stability, which is desirable in engines to ensure smooth and efficient operations. For this study the maximum value of acceptable COV is 5% above which the combustion misfire or combustion instability occurs. As indicated in figure 6.1a the COV IMEP of CP20 and MTHF20 was the least of the fuels investigated across the entire load sweeps. Increasing the volumetric blend ratio for 20% to 40% make the COV IMEP for CP40 and MF40 to drop by 8.3% and 22.2% respectively. However, for MTHF40 the COV IMEP

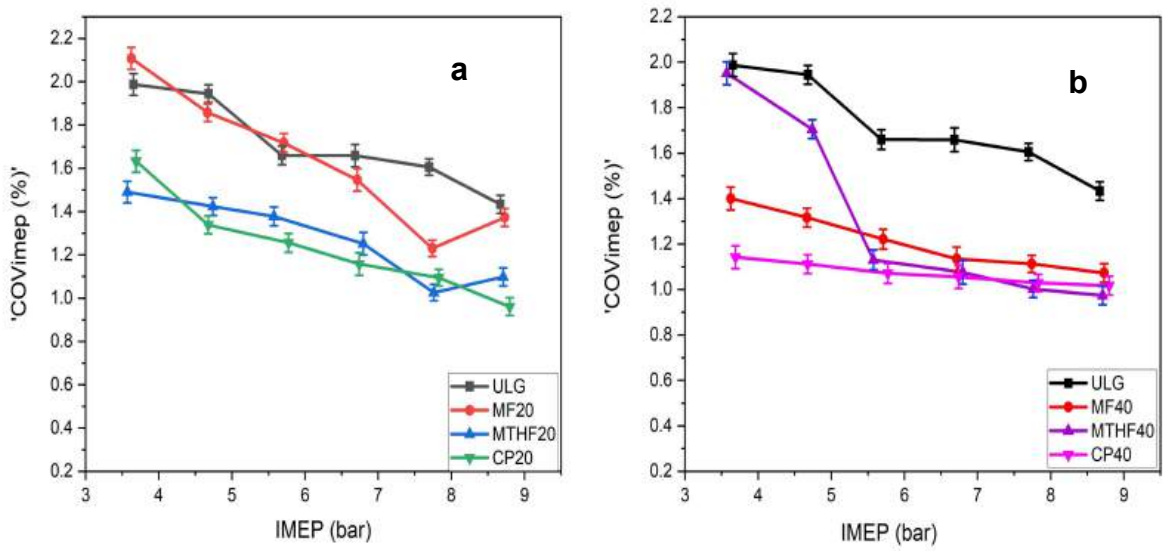

Figure 6.1a) Indicated Efficiency for MTHF20, CP20, MF20 and ULG at 3.5-8.5bar IMEP and b) Indicated Efficiency for MTHF40, CP40, MF40 and ULG at 3.5-8.5bar. IMEP.

increase by 35% at the peak load. Fuel with higher octane number is associated with better knock resistance and consequently improved combustion stability. In addition, fuels flame propagation characteristics equally influences its combustion stability.

6.1.2 Effect of the fuel blends on spark timing and peak cylinder pressure

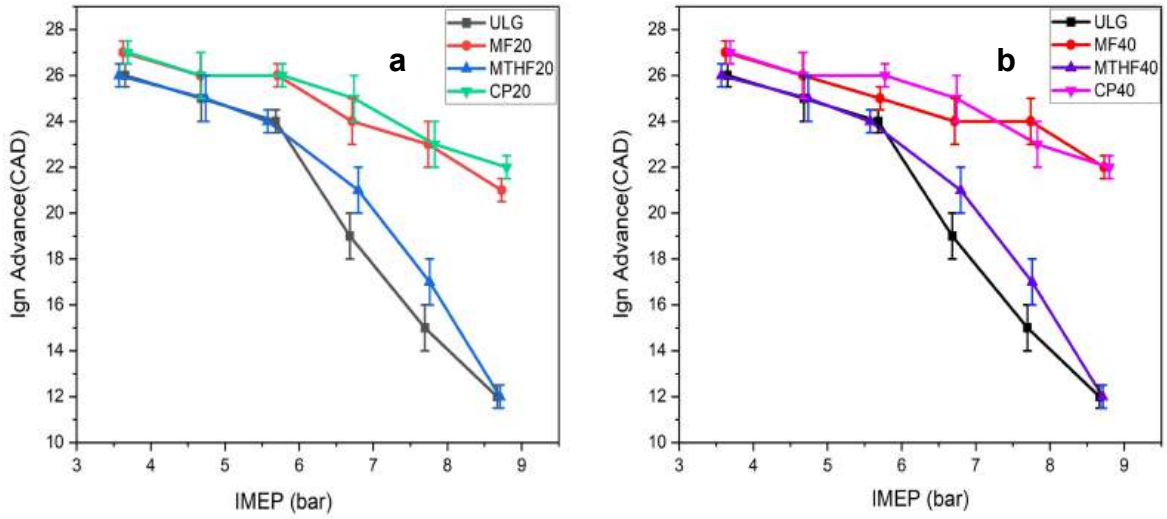

Figure 6.2a) Ignition advance for MTHF20, CP20, MF20 and ULG at 3.5-8.5bar IMEP and b) Ignition advance for MTHF40, CP40, MF40.

The optimised fuel-specific spark timings (MBT/KLSA timings) for the load's sweeps (3.5-8.5bar IMEP) for each of the fuels investigated are shown in figure 6.2. The maximum brake torque (MBT) spark timing was used and in the event of knock, the spark timing was retarded by 2 CAD and was referred to as the Knock-Limited Spark Advance (KLSA). At the low load of 3.5bar IMEP, there are no significant differences in the MBT/KLSA locations for the fuels investigated. However, as the load increases from 4.5 bar IMEP major variations in the MBT/KLSA locations for the fuels were observed. The spark advance trend for MTHF20 is similar to that of ULG between the load of 3.5-5.5bar IMEP as indicated in figure 6.2a. At high load of 6.5-7.5bar IMEP though the spark timing for MTHF20 is significantly retarded. It exceeded the timing for ULG by 2CAD at each of the loads. At the peak load of 8.5bar IMEP both MTHF20 and ULG maintain the same spark timing. Volumetric 20% blends of gasoline

with Cyclopentanone and 2-methylfuran (CP20 and MF20) greatly increases the spark advance window for the blends. The most advanced spark timing was observed with CP20 at the Peak load of 8.5barIMEP. CP20 have spark advance window of 1CAD higher than MF20 but about 12CAD higher than both MTHF20 and the neat gasoline. Increasing the volumetric blend ratio from 20% to 40% shows MF40 has improve spark advance of 1CAD compared to CP40 at the load of 7.5bar IMEP, however both CP40 and MF40 recorded the same spark timing at the maximum load of 8.5bar IMEP. No significant different was observed between the spark timing of MTHF20 and MTHF40. Knock-resistant ability of fuels is closely related to their Research octane number (RON) and this decreases with the increase in the fuel carbon chain length and increases with the increase in the fuel carbon chain branches (34). The octane numbers. of MTHF20 is still less than that of the neat gasoline but it has increased by 6.88% compared to the neat MTHF, The H/C ratio of MTHF20 reduces slightly by 0.11 as indicated in table 6. 2 The combine effect of the increased octane number and reduced H/C ratio leads to reduction in combustion temperature, which mitigate the effect of engine knock and make spark advance achievable for MTHF20. Though the octane number of MTHF40 is less than that of the neat gasoline by 2, it has not significantly impact on the spark advance performance of the fuel. Cyclopentanone is a five-membered ring ketone with the molecular formula C_5H_8O. The octane number of Cyclopentanone is relatively high compared to the base fuel. The two gasoline blends of Cyclopentanone (CP20 and CP40) have Research octane number of 97.64 and 98.48 respectively. This explains the reason for their improved spark advance performance compared to the neat gasoline. As expected, the blends of MF and CP has the highest cylinder pressure at the peak load as indicated in figure 6.3. The recorded Pmax for CP20 at the peak load was 1bar higher than MF20 but 9bar and 7bar greater than that of ULG and MTHF20 respectively. The high value of Pmax for CP20 at the peak load was because it has the shortest combustion duration of the fuels investigated as indicated in figure 5.4. Increasing the volumetric blend ratio from 20% to 40% increases the Pmax for MF40 by 1bar above that of the CP40 at the peak load.

Pmax for MTHF40 equally increases by 3bar compared to that of MTHF20. Both MTHF20 and MTHF40 exhibited high cylinder pressure comparable the two blends of CP and MTHF, but the pressure drops significantly at the higher load because of retarded spark timing for both MTHF20 and MTHF40 at the high loads. Fuel with faster combustion duration and high-octane number will have high peak cylinder pressure. As indicated in figure 6.4, the combustion

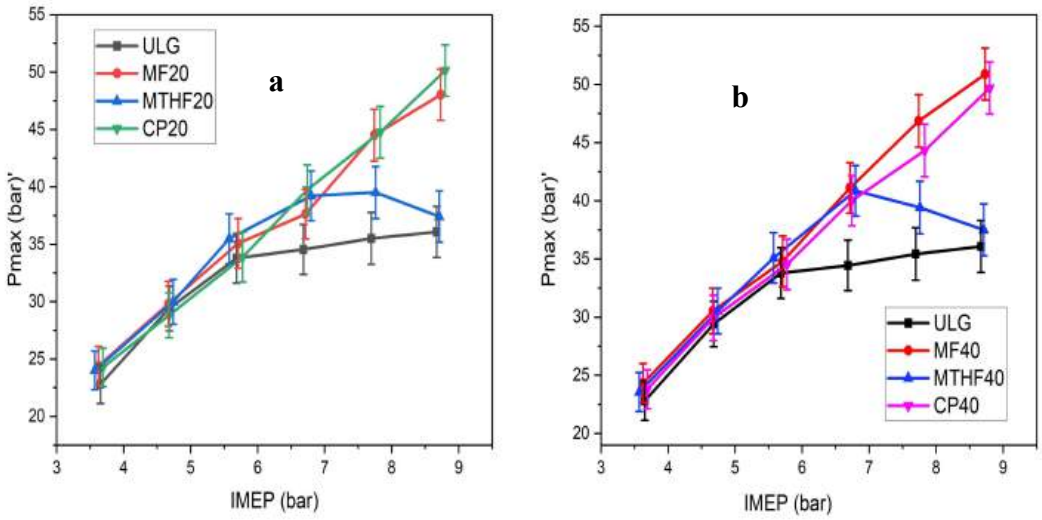

Figure 6.3a) Pmax for MTHF20, CP20, MF20 and ULG at 3.5-8.5bar IMEP. b) Pmax for MTHF40, CP40, MF40 and ULG at 3.5-8.5bar IMEP.

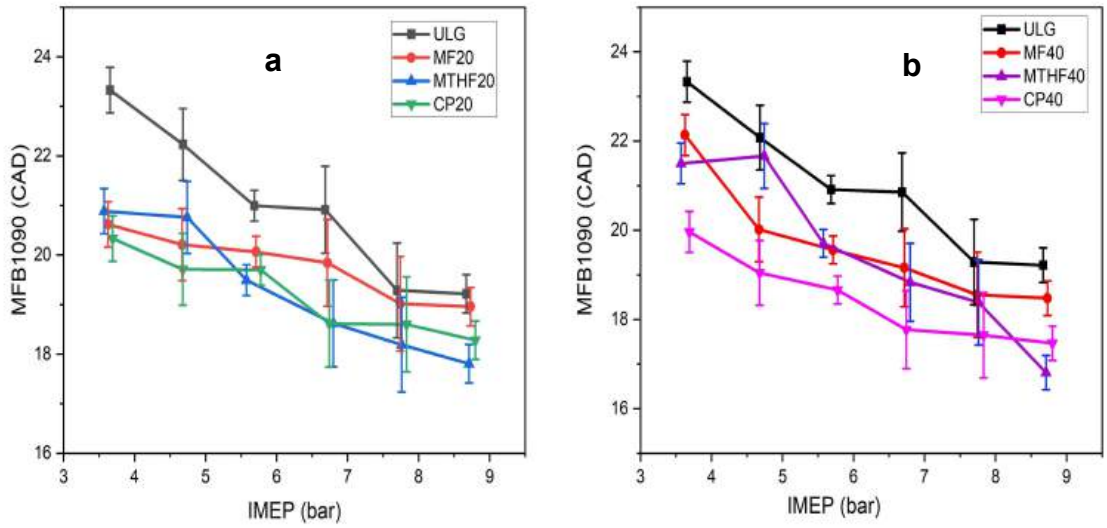

Figure 6. 4a) MFB1090 for MTHF20, CP20,MF20 and ULG at 3.5-8.5bar IMEP and b) MFB1090 for MTHF40, CP40, MF40 and ULG at 3.5-8.5bar IMEP.

duration of CP20 is shorter than MF20, MTHF20 and ULG, if combustion occurs quickly, it generally means that the fuel-air mixture ignites and burns rapidly. This can lead to a sharp rise in pressure because the combustion process releases a large amount of energy in a short time (278) and this explain the reason for the higher peak cylinder pressure of CP20. The resulting octane number of the blends of CP and MF is high compares to the two blends of MTHF and gasoline. This makes possible significant advance in spark timing for CP20 and MF20 at high load. Though MTHF20 and MTHF40 shows the highest peak pressure of the fuels up to the load of 5.5bar IMEP, the knock limited timing mitigated against spark advance for the two blends of MTHF and gasoline at high load leading to low peak cylinder pressure for the fuels. In overall, volumetric increase of the blends from 20% to 40% does not lead to corresponding increase in the cylinder pressure for 40% blends fuels.

6.1.3 Effect of the fuel blends on Combustion Duration and Ignition delay

The combustion duration (CD), (defined by 10–90% MFB interval in CAD) at various loads for each fuel is shown in Fig.6.4. As presented, the fuels have a similar CD at low loads of 3.5 bar imep. The CD for the fuels differs sharply as the load advances and at the peak load of 8.5 bar IMEP, CP20 has the shortest CD by 1 CAD shorter than MF20 and about 2.5CAD and 4.5CAD shorter than MTHF20 and neat gasoline respectively as indicated in figure 6.4. However, the combustion duration of MF20 consistently reduces as the load increases. Figure6.4b indicates the combustion duration of the 40% blend fuels. The combustion duration of CP40, MF40, MTHF40 dropped significant compare to CP20, MF20 and MTHF20. The chemical composition and physical properties such as molecular structure, volatility, octane number, and energy content. are some of the key factors that affects the duration of combustion of fuels. The faster burning rate of the oxygenated fuel was reported by (327). The oxygenated effect of both CP, MF and MTHF will increase the oxygen concentration when blended in gasoline and can promote more complete combustion, leading to shorter combustion duration. During the

ignition delay period, the injected fuel is mixed with the air in the combustion chamber, and it undergoes various chemical and physical processes before it ignites. These In addition, blending of MF and MTHF with gasoline lead to improve spray characteristics, evaporation rate, and air-fuel mixing of the blends in the combustion chamber resulting in shorter combustion duration for the blends. Ignition initiation processes include vaporisation of the fuel, formation of an ignitable air-fuel mixture, and the initiation of the chemical reactions that lead to combustion**.** The ignition delay is divided into physical delay and chemical delay. Physical delay is the time required for atomisation of fuel, air-fuel mixing, and vaporization. Chemical delay has an effect on premixing of air-fuel vapour and thermodynamic efficiency (328). Generally, the ignition delay reduces as the load advances for all the fuel investigated. At 3.5bar IMEP, as indicated in figure 6.5a the ignition delay for CP20 and ULG was observed to be longer than that of MF20 and MTHF20 and the neat gasoline by 1CAD and 2CAD respectively. However, at the Peak load of 8.5bar IMEP, the ignition delay for gasoline and MTHF20 was shorter than that of

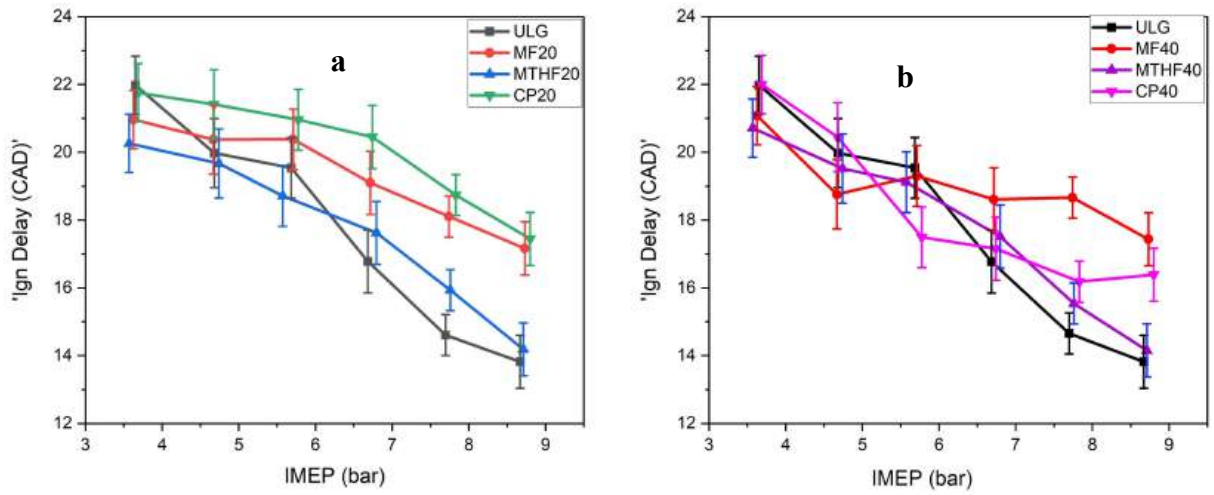

Figure 6.5a) Ignition Delay for MTHF20,CP20,MF20 and ULG at 3.5-8.5bar IMEP and b) Ignition Delay for MTHF40, CP40, MF40 and ULG at 3.5-8.5bar

MF20 and CP20 by 6CAD and 6.5CAD respectively. As indicated in figure 6.5b increasing the volumetric percentage of the blends from 20% to 49% reduces the delay on ignition of CP40 and MF40 by 2CAD and 1CAD respectively compared to the 20% blends. The fuel octane number is a measure of its auto ignition tendency. Fuel with high octane number tends to have longer ignition delay. This explain the higher duration of ignition delay for CP and MF blends compare to ULG and the blends of MTHF.

6.1.4 Effect of the fuel blends on ISFC and the Indicated Efficiency

The Instantaneous specific fuel consumption (iSFC) for the blends and the neat gasoline are as indicated in figure 6.6. The specific iSFC for all the fuels investigated reduces with loads. The inherent properties of fuel play a significant role in iSFC. These properties include the energy content or heating value of the fuel, which is a measure of the amount of energy released per unit of fuel. Fuels with higher H/C ratios, can potentially release more energy during combustion which result in lower iSFC. The indicated specific fuels consumption for the fuel was observed to reduce as the load sweep advance. Gasoline displayed superior fuel consumption economy across the entire load range over the blend fuels. As indicated in figure 6.6a, at the intermittent load of 5.5bar IMEP, the indicated specific fuel consumption of the neat gasoline is about 2% greater than CP20 and about 10.4% greater than both MTHF20 and MF20. Increasing the fuel blends to 40% lead to indicated fuel consumption penalty of about 18,4%, 12.2% and 10% for CP40, MF40 and MTHF40 respectively in comparison to the neat gasoline. This is because of the higher energy density of gasoline compared to the blend fuels. A remarkable observation is the increase in fuel economy as MTHF20 progress to MTHF40. The indicated thermal efficiency recorded for the fuels is as indicated in figure 6.7. The study shows increase in indicated efficiency of the fuels with loads. Higher combustion temperatures generate greater heat loss through the cylinder walls reducing the conversion of fuel energy into useful work and the result is lower indicated efficiency (303). The greater temperature rise during the combustion is determine by the value of the fuel heat of vaporization as indicated in

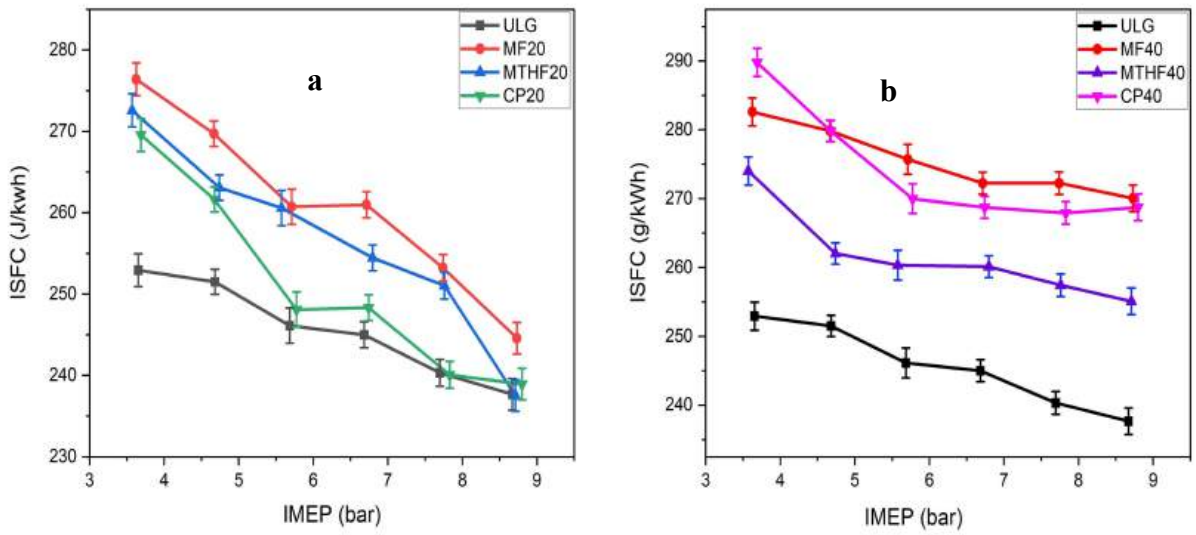

Figure 6.6a) ISFC for MTHF20, CP20, MF20 and ULG at 3.5-8.5bar IMEP and b) ISFC for MTHF40, CP40, MF40 and ULG at 3.5-8.5bar IMEP.

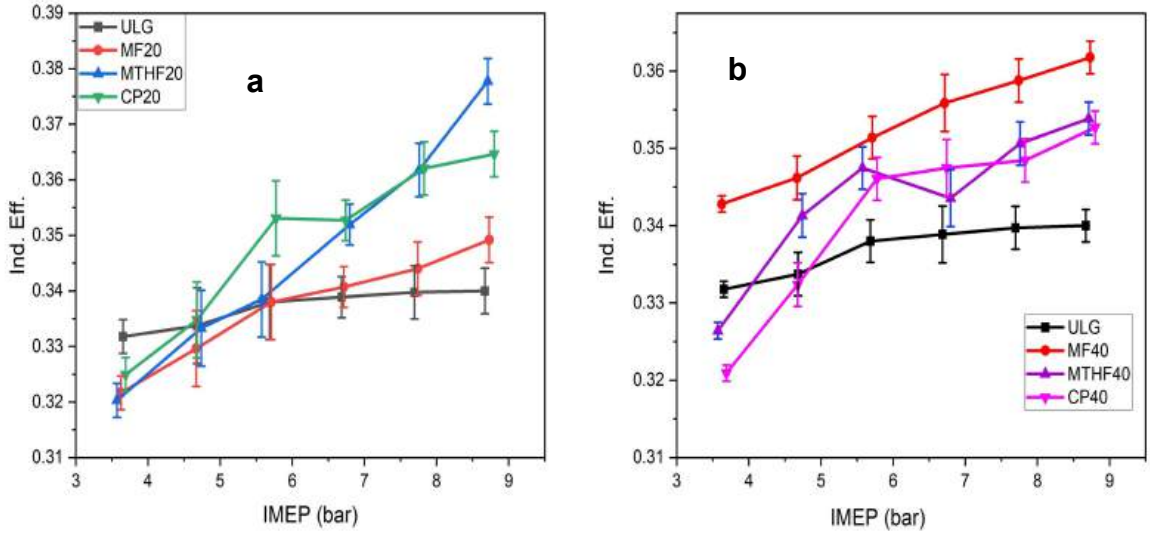

Figure 6.7 a) Indicated Efficiency for MTHF20, CP20, MF20 and ULG at 3.5-8.5bar IMEP and b) for MTHF40, CP40, MF40 and ULG at 3.5-8.5bar.

figure 6.7a, the indicated efficiency of MTHF20 and CP20 is higher compared to MF20 and the neat gasoline across the entire load range. The is due to the higher effect of the evaporative cooling on MTHF20 and CP20 compared to MF20 and the neat gasoline. Increasing the volumetric blend ratio by 20% as indicated in figure 6.7b lead to the increase in the thermal efficiency of MF40 by 2% at the peak load of 8.5bar IMEP. However, the indicated efficiency

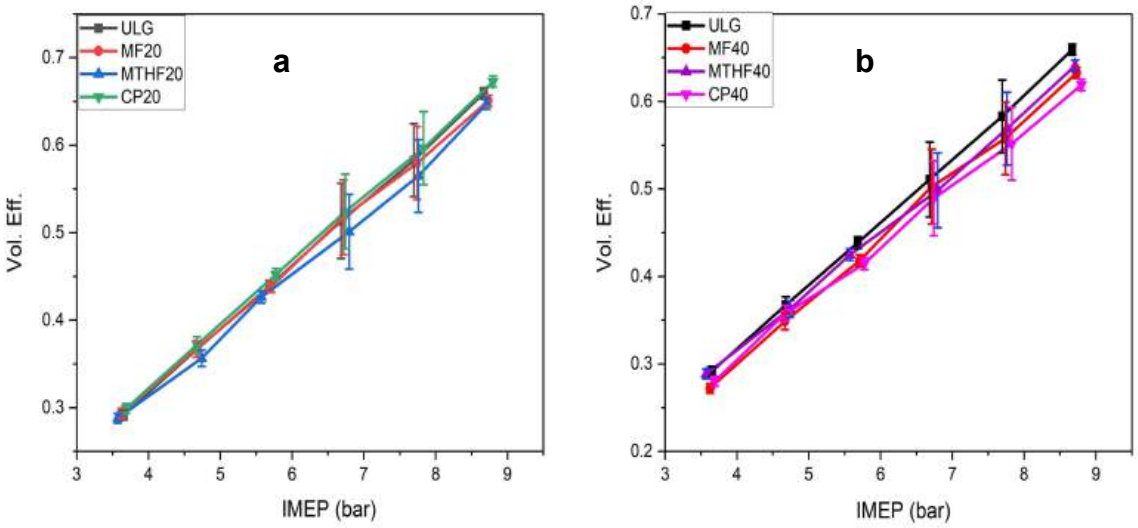

Figure 6.8a) Volumetric efficiency for MTHF20, CP20, MF20 and ULG at 3.5-8.5bar IMEP and b) Volumetric efficiency for MTHF40, CP20, MF40 and ULG

of MTHF40 was observed to have dropped by 4% compared to MTHF20, while CP20 and CP40 maintain the same thermal efficiency at the peak load.

6.1.5 Effect of the fuel blends on Volumetric Efficiency

Different fuels have different combustion characteristics, including the combustion duration and the heat release profiles. These characteristics can influence the pressure and temperature within the cylinder during the intake stroke, which in turn can impact on the Volumetric efficiency (VE). The volumetric efficiency of the fuel was observed to increase as the load sweep advances. As indicated in figure6-8a, no significant different was noticed on the value of the volumetric efficiency of the fuels for the volumetric blend ratio of 20% but VE for MTHF20 was consistently lower than MF20, CP20 and the ULG. across the entire load range. As indicated in figure 6.8b, at 40% volumetric blend ratio, the VE for MTHF40 increases by about 4% compared to MTHF20 at the peak load. The value of VE for CP40 and MF40 drop by margin of 2% and 3% compared to CP20 and MF20 at this peak load.

6.1.6 Effect of the fuel blends on the Gaseous Emissions.

Instantaneous NOx emissions for the fuels investigated was observed to increase with loads. As in figure 6-9a, MTHF20 recorded the lowest emission of isNOx at 8.5bar IMEP. MTHF20 isNOx emissions is less than that of MF20, CP20 and gasoline by 10%, 30% and 40% respectively at the peak load of8,5bar IMEP. This is due to the combine effect of H/C ratio, higher oxygen content and the combustion flame temperature of MTHF20 compares to MF20, CP20 and the neat Gasoline. NOx formation increases with the combustion temperature It has been equally reported that the relative NOx emissions of a fuel can be related to the fuel H/C ratio property. Fuels with higher H/C ratios generally produce lower combustion temperatures because hydrogen combustion releases energy more evenly and with lower peak temperatures compared to carbon combustion. Carbon-rich fuels tend to produce higher peak temperatures, leading to increased NOx formation (34, 303).

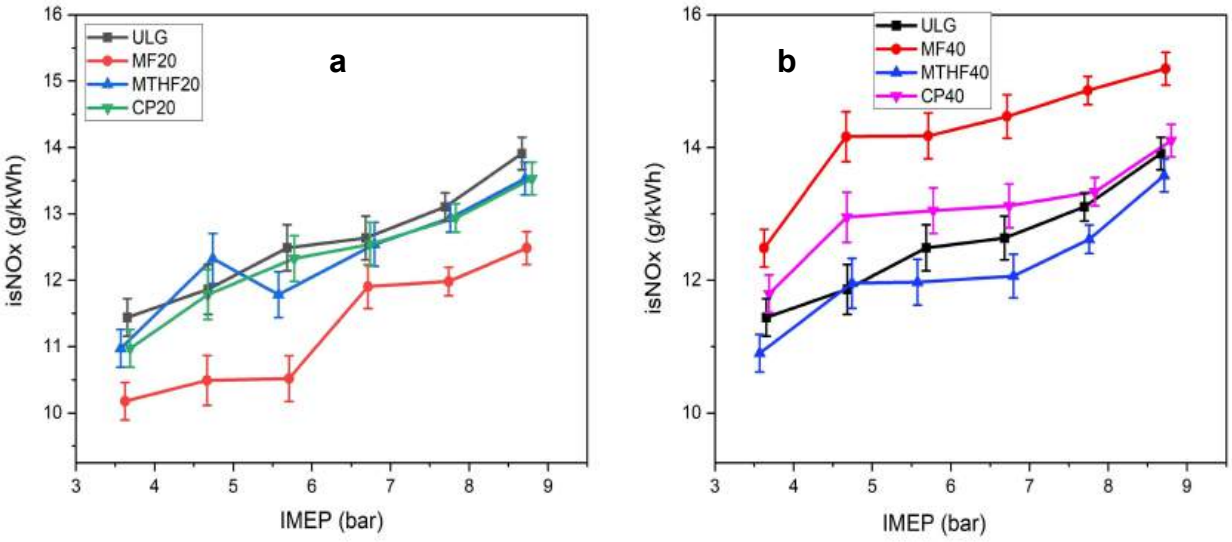

Figure 6.9 a) isNOx emissions for MTHF20, CP20, MF20 and ULG at 3.5-8.5bar IMEP b) isNOx emissions for MTHF40, CP40, MF40 and ULG at 3.5-8.5bar IMEP.

The trends of the NOx emissions in this study conform to the analysis given above. Increasing the volumetric blend ratio by 20% increases the isFC emission of MF40 by 36.3% compared to MF20 at the peak load. In similar manner as indicated in figure 6.8b the isNOx for CP40

increases by 10% compares to CP20. peak load of 8,5bar IMEP. This is due to the combine effect of H/C ratio, higher oxygen content and the combustion flame temperature of MTHF20 compares to MF20, CP20 and the neat gasoline. NOx formation increases with the combustion temperature It has been equally reported that the relative NOx emissions of a fuel can be related to the fuel H/C ratio property (34, 303) The trends of the NOx emissions in this study conform to the analysis given above. Increasing the volumetric blend ratio by 20% increases the isHC emission of MF40 by 36.3% compared to MF20 at the peak load. In similar manner as indicated in figure 6-9b the isNOx for CP40 increases by 10% compares to CP20.

6.2 Effect of Fuel injection Timing on the Combustion of MF20 and MTHF20

Combustion of MF20, MTHF20, and ULG was undertaken in a gasoline-fueled single-cylinder direct-injection spark ignition (DISI) engine at stoichiometric air–fuel ratio (λ=1) and at constant engine speed and fuel injection pressure of 1500rpm and 150 bar respectively. Fuel-specific MBT timing was used to investigate the maximized combustion performance for each fuel at the fuel injection timing sweeps of 180 degbTDC to 280 degbTDC as listed in table 6.3. The purpose of this study was to investigate the percentage of the unburnt furan in the hydrocarbon emissions. The late injection timing of 180-280 degbTDC was selected to ensure the highest possible emissions of the unburnt furan fuels was investigated. The result of the investigation is detailed in section 6.2.1 below.

Table 6.3 Operating conditions for the experiments on HC Speciation.

Speed rpm	IMEP bar	Injection Pressure bar	Injection timing CAD BTDC	Fuel	Spark timing CAD BTDC
1500	5.5bar	150	180- 280	ULG, MF20, MTHF20	MBT/KLSA timing

6.2.1 Effect of fuel injection timing on Pmax and ISFC for MTHF20 and MF20

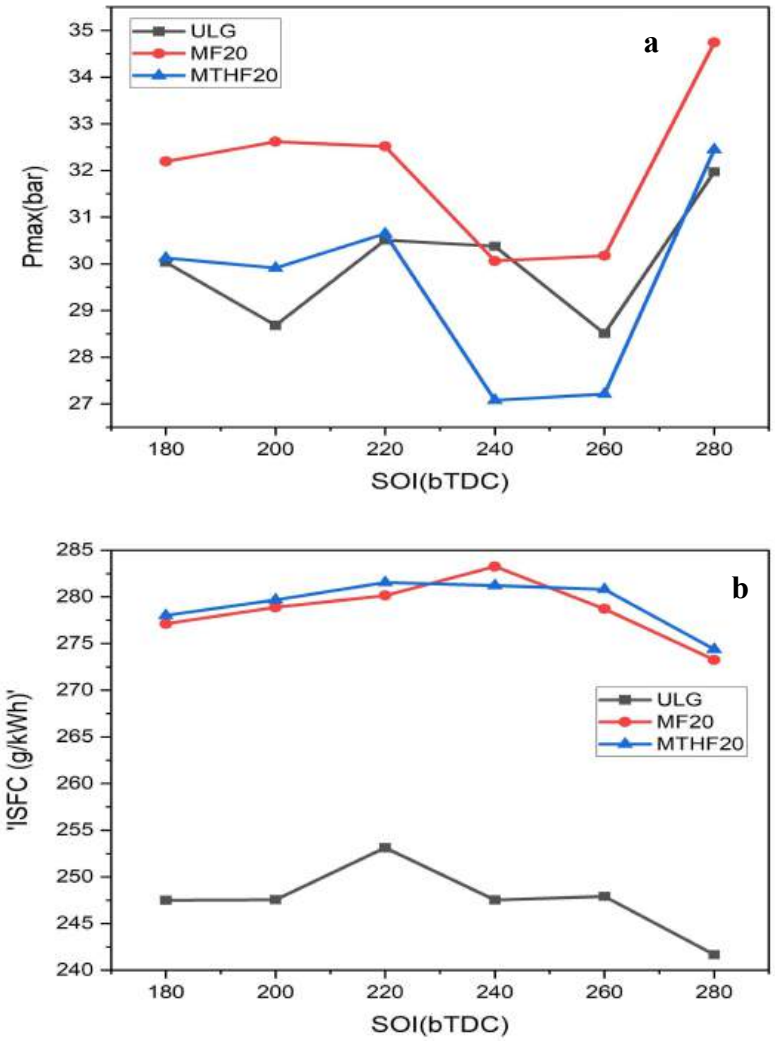

Figure 6.10a) Pmax for MTHF20, MF20 and ULG at fuel injection sweeps 180-280degbTDC and b) ISFC for MTHF20, MF20 and ULG at fuel injection sweeps 180-280bTDC.

Figure 6.10a shows the Peak cylinder pressure at the intermittent loads of 5.5bar imep and at the fuel injection sweeps (180-280CADbTDC) for MTHF20, MF20 and the ULG. The result shows that as the fuel injection timing advances from180 to 280 degbTDC the cylinder pressure peaked twice, at 220CAD and at 280CAD. The peak pressure for MF20 was about 5bar and 2bar higher than gasoline and MTHF20 respectively at 280degbTDC. The timing of fuel injection affects the duration of the combustion process. advancing the fuel injection timing promote the combustion process in the engine cycle. This is because the fuel has more time to mix with the air and combust more effectively. As a result, the combustion duration become

shorter, leading to a higher peak cylinder pressure. The maximum Pmax for the three fuels investigated was obtained at the optimal fuel injection timing of 280degbTDC. The specific fuel consumption curves for the three fuels over the selected fuel injection sweeps (180-280degbTDC) are shown in figure 6.10b. As the fuel injection timing advances towards 280CADbTDC the specific fuel consumption for the three fuels reduces. Advancing the fuel injection timing promotes optimal air-fuel mixture formation in the combustion chamber. This can positively impact on fuel efficiency and reduce fuel consumption. The specific consumption of the ULG is consistently lower than the other two blend fuels across the entire fuel injection timing, this result from the higher energy density of the neat gasoline compared to the blend fuels. In similar trend to the maximum cylinder pressure, the optimum fuel injection timing for the three fuels investigate occurs at 289CADbTDC, the same optimal fuel injection timing that ensures the maximum cylinder pressures for the fuels.

6.2.2 Effect of Fuel Injection Timing on the Ignition Delay and Combustion Durations

Figure 6.11a, shows the ignition delay for the fuel at the late fuel injection of (180 – 280deg bTDC). The ignition delays for the three fuels are least at 28degbTDC and the longest delay in ignition occurred at 260CAD for all the fuels investigated. Managing the ignition delay can help optimize the air-fuel mixture preparation, ensuring better combustion efficiency. Late fuel injection delays the introduction of fuel into the combustion chamber. This can result in a longer time for fuel and air to mix and vaporize before combustion which could lead to leaner air-fuel mixture, where the ratio of air to fuel is higher. Lean mixtures tend to have longer ignition delays compared to stoichiometric or rich mixtures. A shorter ignition delay may not provide sufficient time for proper mixing and vaporization, leading to inefficient combustion and increased emissions. The combustion duration (CD), (defined by 10–90% MFB interval in CAD) at various fuel injection timing for each fuel is shown in figure 6.11b. As presented, both MF20, MTH20 and the ULG recorded the shortest combustion duration at 280CAD. MF20 recorded the

shortest duration of about 1CAD and 2CAD less than MTHF20 and the ULG respectively. The short combustion duration of MF20 was used to explain the high value of Pmax as indicated in figure 6.10a at the same fuel injection timing of 280degbTDC.

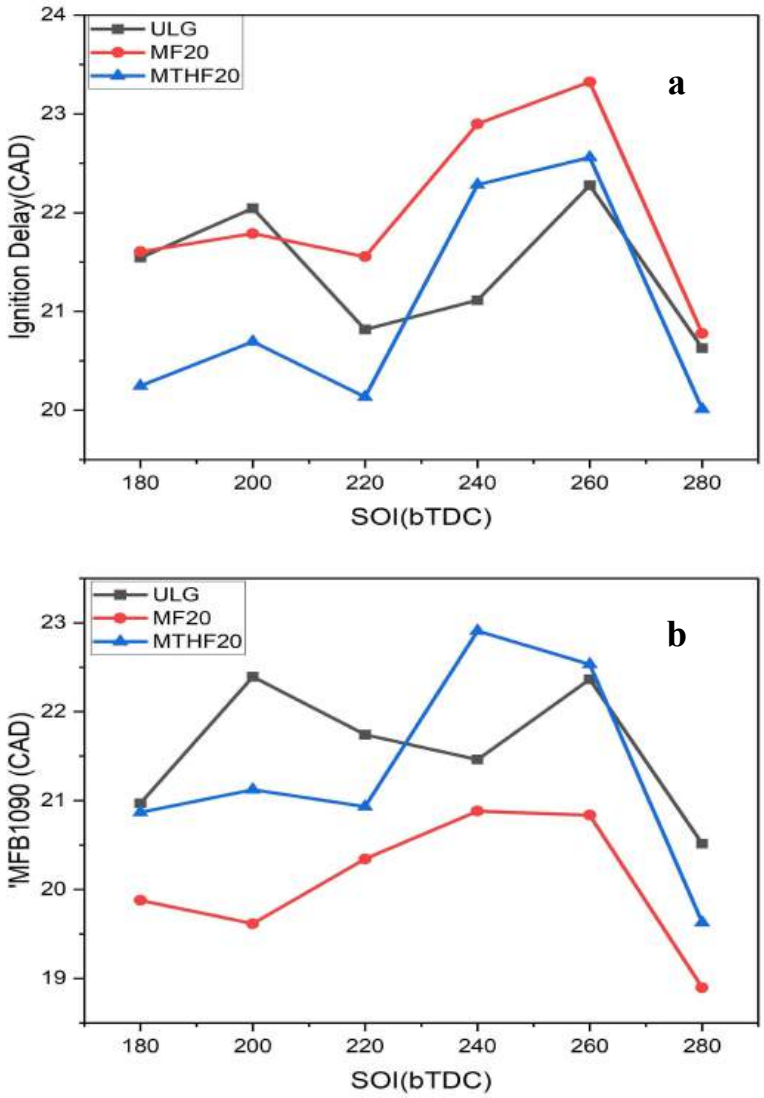

Figure 6.11a) Ignition delay for MTHF20, MF20 and ULG at the fuel injection sweeps and b) MFB1090 for MTHF20, MF20 and ULG at the fuel injection sweeps.

6.3 Effect of fuel injection timing on isNOx emission for MTHF20 and MF20 and ULG

Instantaneous NOx emissions for the three fuels investigated was observed to increase with loads as indicated in figure 6.12a. The maximum differences in NOx emissions between

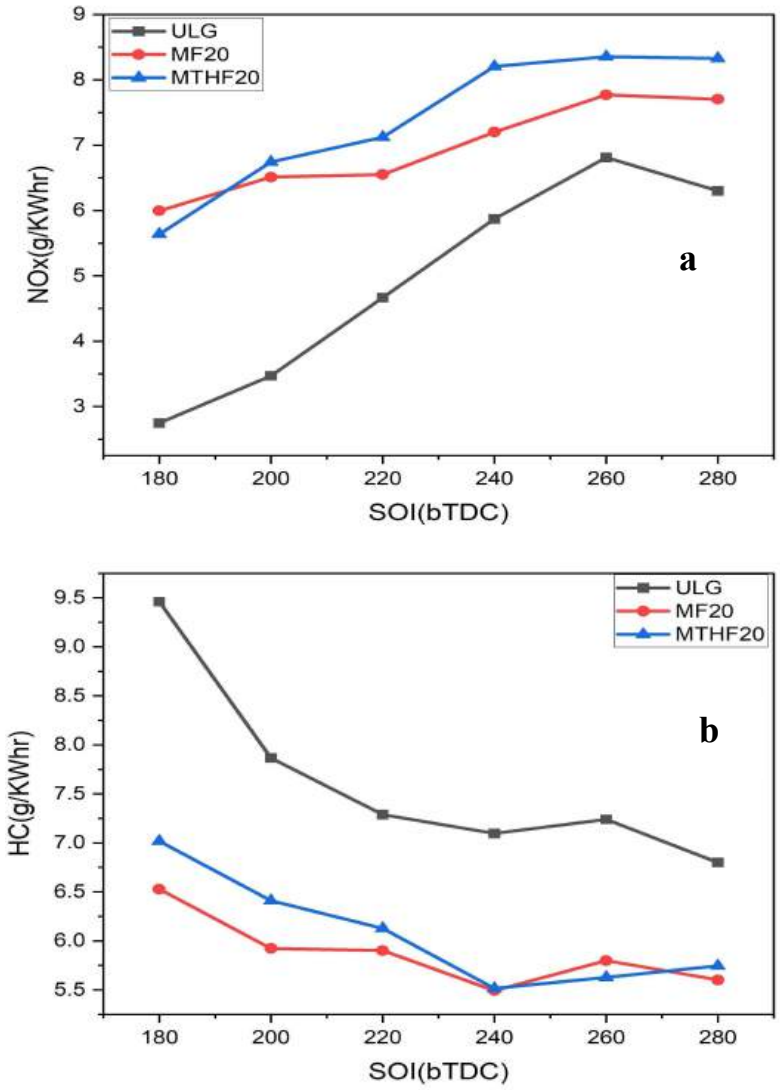

Figure 6.12a) isNOX for MTHF20, MF20 and ULG at selected fuel injection sweeps and b) isHC for MTHF20, MF20 and ULG at seected fuel injection sweeps.

gasoline and the other two fuels is observed at the lower load end of 3.5bar IMEP. MTHF20 and MF20 recorded 12% and 8% increases in NOx emissions respectively, compares to the neat fuel at the highest load of 8.5bar IMEP. This is due to the combine effect of H/C ratio, higher

oxygen content and the combustion flame temperature for the two oxygenated fuel. The blend of MF and MTHF like every other oxygenated fuel have higher oxygen content, which can influence the formation of NOx. The trends of the NOx emissions in this study conform to the analysis given above. Gasoline has the highest instantaneous hydrocarbon (isHC) emissions of the three fuels. The isHC emissions for the fuels reduce with load as indicated in figure 6.12b. At the highest load of 8.5 barimep. isHC emissions of gasoline is about 11% and 33% higher than MTHF20 and MF20 respectively. Oxygenated fuels tend to have lower carbon-to-hydrogen ratios compared to conventional gasoline. This can result in reduced emissions of certain types of hydrocarbons, such as unburned hydrocarbons (UHC), which are commonly associated with incomplete combustion.

6.4 Fuel injection timing and HC speciation for MTHF20, MF20, ULG

Figure 6.12b shows trends of the emissions of the instantaneous total hydrocarbon (isHC)for MF20, MTHF20 and gasoline across the fuel injection timing sweeps (180 – 280degbTDC) and at the intermediate loads of 5.5bar IMEP. The study indicates that the HC emissions decreases as the fuel injection timing advances for the three fuels investigated. At the late fuel injection of 180degbTD maximum emissions of the hydrocarbon were observed for the three fuels. When fuel is injected earlier in the compression stroke, it has more time to mix with the incoming air. This can lead to better fuel-air mixing, more uniform combustion, and lower HC emissions. Early injection timing allows the fuel to burn more completely, resulting in reduced unburned hydrocarbons in the exhaust. If fuel injection occurs later in the compression stroke, there may be less time for the fuel to mix adequately with the air before ignition. This can lead to incomplete combustion, resulting in higher HC emissions. Late injection can cause unburned or partially burned hydrocarbons to be expelled in the exhaust. Retarding the injection timing excessively can lead to knocking or detonation, which is the spontaneous combustion of the air-fuel mixture due to high temperatures and pressures. Knocking can cause an increase in

hydrocarbon emissions as well. HC emissions for oxygenated fuels are lower compare to gasoline.

6.4.1 Investigations of component species in Hydrocarbon Emissions

Figure 6.13a-c shows the percentage of the HC species for the three fuels at the intermediate loads of 5.5bar imep and at the optimum fuel injection timing of 280CADbTDC. FTIR technology by Gasmeth was used to measure the gaseous emissions. The FTIR complies with the requirements of US EPA Method 320-Vapour Phase organic and inorganic emissions by extractive FTIR (329). The FTIR monitors all the species continuously.

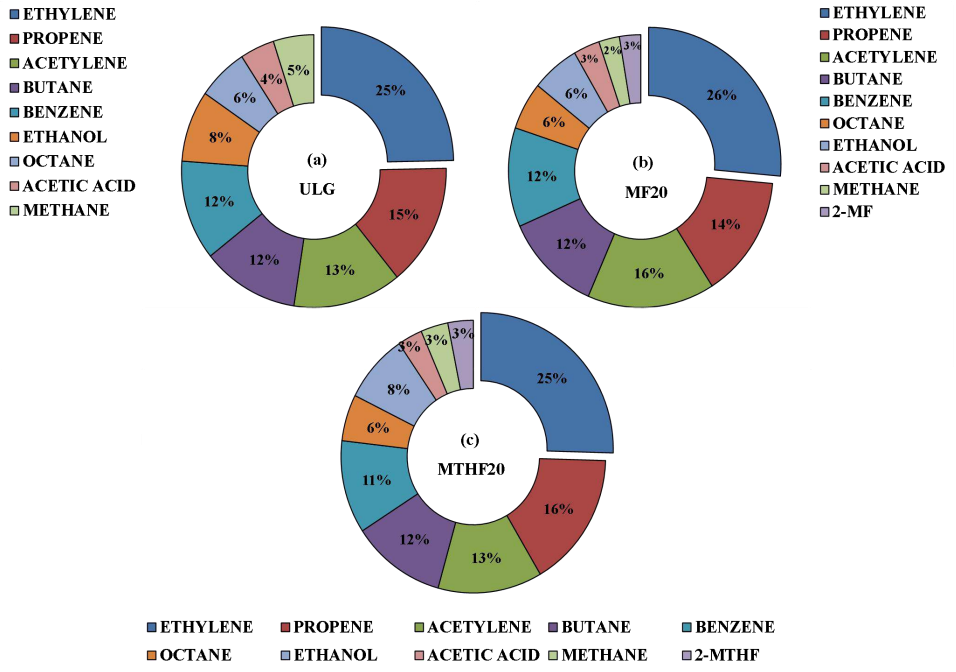

Figure 6.13a) HC components species for MF20, b) HC components species for MTHF20 and c) HC component species for the ULG.

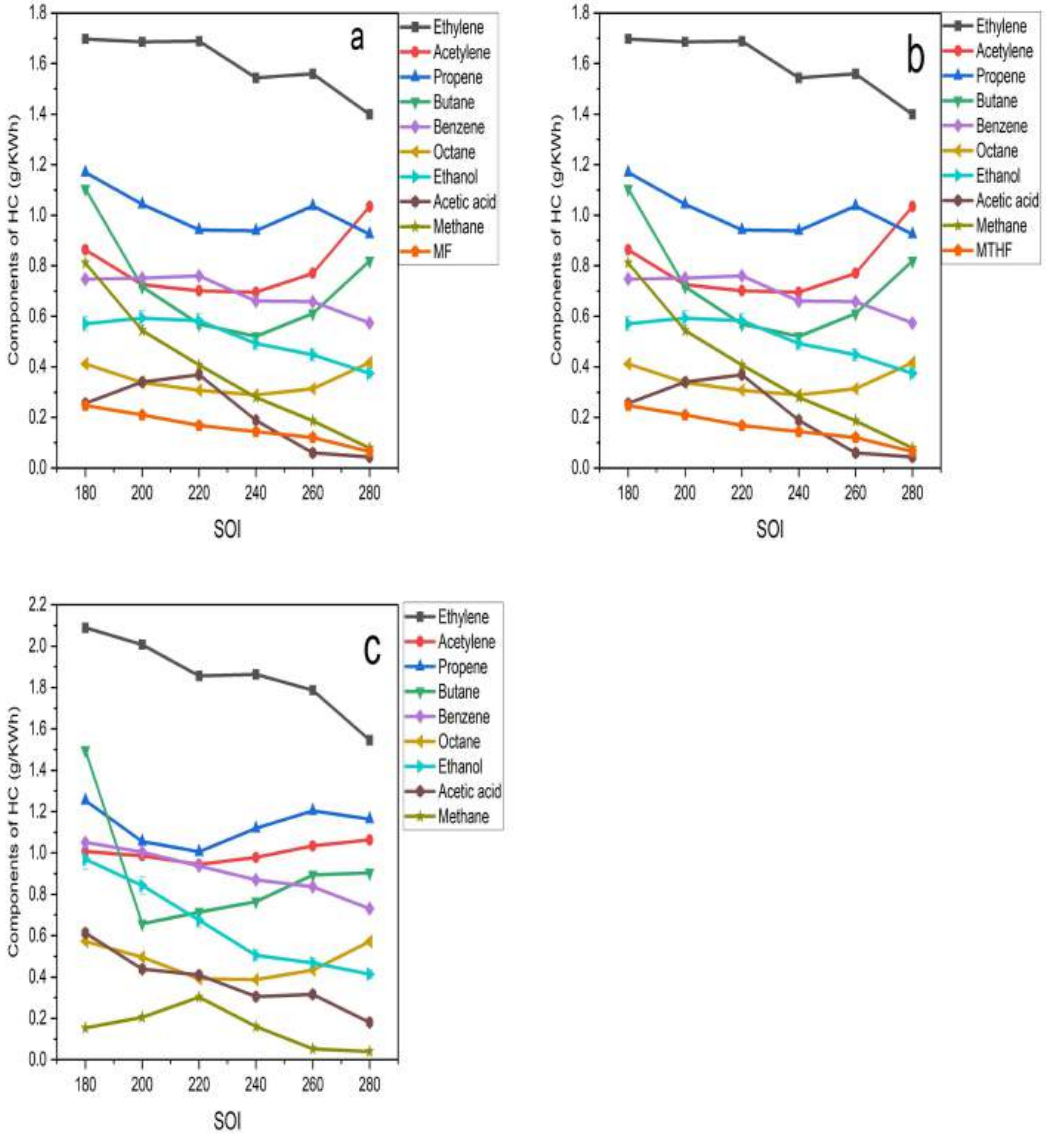

Figure 6. 14a) Variation of HC species with fuel injection timing for MF20, b) Variation of HC species with fuel injection timing for MTHF20 and c) Variation of HC species with fuel injection timing for the ULG.

The entire spectrum is scanned ten times per second and an average calculated from this is reported for each (user-selectable) sampling period. Species are measured individually and can be added together analytically. The unburned furan-based fuel was identified in the FTIR analyser as an unknown species from the residual spectrum. Generally, the HC species proportions of MF20 and MTHF20 are like that of gasoline; however, there are some differences in their percentage compositions. Ethylene, butane, propene, benzene, acetylene,

octane, and ethanol constituted more than 90% of the total HC species for each of the fuels investigated. Gasoline has a higher exhaust proportion of octane, acetic acid, and methane than both MF20 and MTHF20. MF20 blend has higher proportion of acetylene and lower proportion of ethanol than gasoline and MTHF20. As indicated in Figure 6.14 a-c; ethylene with components percentage of 25%, 26% for and 25% for Gasoline, MF20 and MTHF20 respectively, consistently remains the highest components of the isHC. Ethylene is a very stable molecule compared to other hydrocarbons that can be formed during combustion. Its double bond structure (C=C) makes it less reactive than many other potential fragments, allowing it to persist in the exhaust gases (19). Methane is a greenhouse gas, however, its percentage emissions in HC is very low for the three fuels. Ethylene is a greenhouse gas, and excessive emissions contribute to climate change and global warming. It can also react with other air pollutants to form ground-level ozone, which can harm plant life, reduce crop yields, and contribute to smog formation. Exposure to high concentration of ethylene (thousands of parts per million) can cause dizziness, anaesthesia, drowsiness, or other central nervous system effect. Ethylene in the air in an enclosed placed will decrease the amount of oxygen present. Ethylene in the air can indeed affect oxygen levels, but not directly by decreasing the amount of oxygen present. Instead, ethylene is a plant hormone that can accelerate the ripening and aging of fruits, vegetables, and flowers. During the ripening process, these biological materials may increase their respiration rates, consuming more oxygen and releasing more carbon dioxide. This increase in respiration could lead to a decrease in the oxygen concentration in an enclosed space, depending on the amount of ethylene and the volume of produce present. Prolonged exposure to elevated levels of ethylene may lead to more severe respiratory issues and long-term health problems (330, 331). Propene is a volatile organic compound (VOC) and is considered a precursor to ground-level ozone formation, which contributes to the formation of smog. According to the results as indicated in fig.6-16b and c, percentage of the unburn furan in the combustions of MF20 and MTHF20 was observed to be around 3% of the HC. This percentage

of unburn furan could be considered as safe exposure, but further investigation is required in this field. Figure 6-16a-c shows the variation of the Hydrocarbon emissions species with the fuel injection timing. The result indicated that the emissions of all the hydrocarbon species except propene reduces as fuel injection advances toward 280CADbTDC. When the fuel injection timing is advanced, it means that the fuel is injected into the engine's cylinder earlier in the compression stroke. This can cause the fuel-air mixture to ignite too early in the compression stroke. As a result, the combustion process may not be completed fully before the exhaust valve opens.

6.5 Unburnt furan samples and the fuel injection timing

The variations of the percentage of the unburnt furan fuel in the hydrocarbon emissions with fuel injection timing are recorded in figure 6.15. Although both MTHF20 and MF20 have their percentage emission of unburnt furan as 3% of the total hydrocarbon at the optimum injection timing, the unburnt furan emission at the late fuel injection was significantly higher for MTHF20 than that of MF20 by about 80%, these values reduces significantly with the advance in fuel injection timing and at the optimum timing of 280degbTDC the unburnt furan emissions for the two-blend fuel has reduce significantly by 87.5% and 33.3% for MTHF20 and MF20 respectively from the value recorded at 220degbTDC. The danger of unregulated human exposure to furan includes, respiratory distress, increased secretory response, and death (332, 333) and liver and kidneys and to a lesser extent lungs and intestines infections (334). Based on a chronic oral carcinogenicity study in which clear evidence of carcinogenicity was noted in male and female rats and mice. The National Toxicology Program (NTP) classifies furan as “reasonably anticipated to be a human carcinogen” and the International Agency for Research on Cancer (IARC) lists furan as a Group 2B carcinogen (possibly carcinogenic to humans). The U.S. Environmental Protection Agency (EPA) has not classified furan according to its carcinogenicity (334).

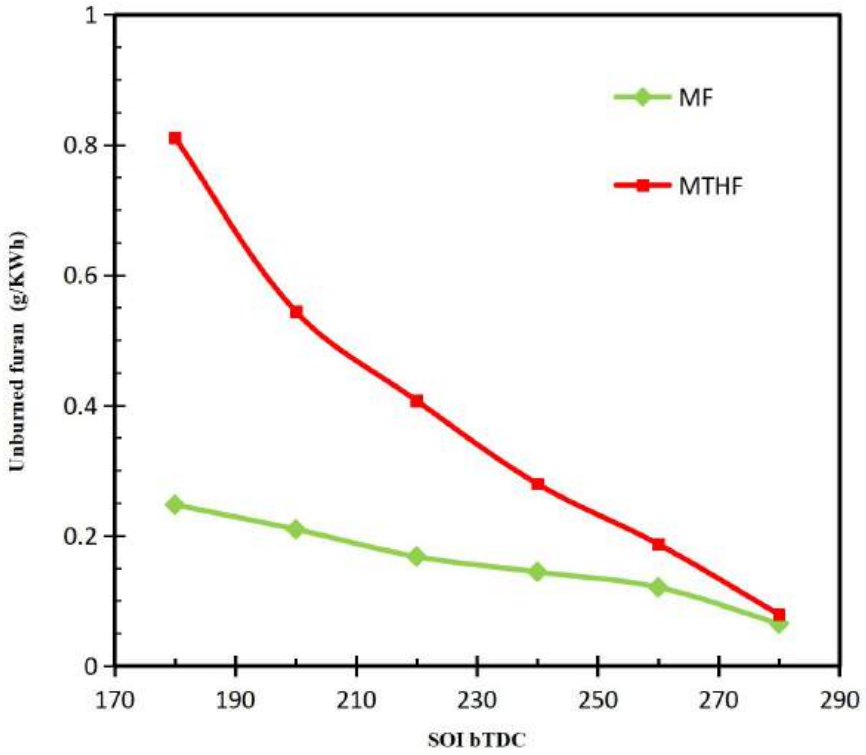

Figure 6.15 Unburn MF20 and MTHF20 over the selected SOI sweep.

6.5.1 Formaldehyde and Acetaldehyde Emissions of MTHF20 and MF20

The formaldehyde emissions of MTHF20, MF20 and gasoline at 5.5bar IMEP are presented in figure 6.16. In Figure6.16a the formaldehyde emissions of the fuels increases as the fuel injection timing advances. early injection. Except at the late injection timing of 180CADbTDC the formaldehyde emission for MTHF20 is higher than that of MF20 for all other investigated injection timing. The acetaldehyde emissions were relatively low compared to the aldehyde emission for the injection timing investigated. As indicated in figure 6-16b, the acetaldehyde emissions for the neat gasoline is generally higher than that of MTHF20 and MF20 across the entire injection timing. The percentage of Gasoline acetaldehyde emissions compare to the blend fuels increases as the fuel injection timing advances. Except at the late injection timing of 180CADbTDC the formaldehyde emission for MTHF20 is higher than that of MF20 for all other investigated injection timing. The acetaldehyde emissions were relatively low compared

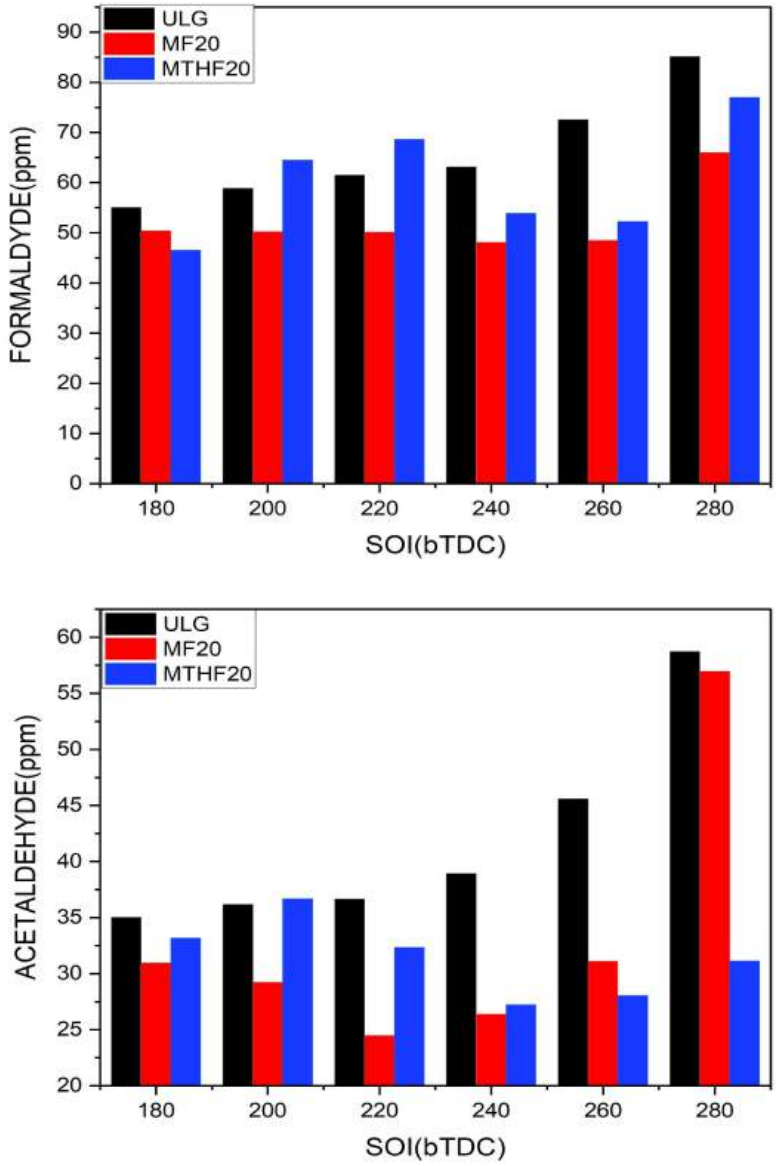

Figure 6. 16 a) Formaldehyde emissions for MTHF20, MF20, and ULG at 5.5bar IMEP and b) Acetaldehyde emissions for MTHF20, MF20, and ULG at 5.5bar IMEP.

to the Aldehyde emission for the injection timing investigated to the Aldehyde. The formaldehyde emissions of MTHF20, MF20 and gasoline at 5.5bar IMEP are presented in figure 6.16. In figure 6.16a, the Formaldehyde emissions of the fuels increases as the fuel injection timing advances. early injection. Except at the late injection timing of 180CADbTDC the formaldehyde emission for MTHF20 is higher than that of MF20 for all other investigated injection timing. The Acetaldehyde emissions were relatively low compared to the Aldehyde emission for the injection timing investigated. As indicated in figure 6.16b, the Acetaldehyde

emissions for the neat gasoline is generally higher than that of MTHF20 and MF20 across the entire injection timing. The percentage of Gasoline Acetaldehyde emissions compare to the blend fuels increases as the fuel injection timing advances. Except at the late injection timing of 180CADbTDC the formaldehyde emission for MTHF20 is higher than that of MF20 for all other investigated injection timing. The Acetaldehyde emissions were relatively low compared to the Aldehyde emission for the injection timing investigated. As indicated in figure 6.16b, the Acetaldehyde emissions for the neat gasoline is generally higher than that of MTHF20 and MF20 across the entire injection timing. The percentage of Gasoline Acetaldehyde emissions compare to the blend fuels increases as the fuel injection timing advances.

6.5.2 Particulate Emissions for Gasoline and the Blend fuels

PM size distribution basically consists of two modes (306), the nucleation mode and the accumulation mode. The nucleation mode has more influence in number of particles while the accumulation mode is concern with the particle mass distribution due to its higher size. The PM size distributions for MTHF20, MF20 and gasoline. at 6.5bar IMEP are shown in figure 6.17 For both MTHF20, MF20 and gasoline. Many researchers have used diameter range to separate nucleation and accumulation modes. Kittelson suggested: 0–50nm for nucleation mode and 50–1000nm for accumulation mode (307, 308). Eastwood suggested: 0–100nm for nucleation mode and 100–900nm for accumulation mode (309).

Table 6. 4 Summary of PM emissions for gasoline, MF20 and MTHF20.

	Nucleation mode			Accumulation mode		
	ULG	MF20	MTHF20	ULG	MF20	MTHF20
Number (#/cm^3)	4.63E+9	3.43E+9	4.22E+9	1.14E+8	2.59E+7	6.31E+7
Mass(μg/cm^3)	0.0085	0.0068	0.0066	0.1229	0.0136	0.0557

In this study, the MATLAB script developed by University of Castilla-La Mancha was used to differentiate the two modes. Fuel properties such as the oxygen contents of the fuels have direct impact on the PM emissions. High oxygenated fuels tend to produce less soot. The soot level can dramatically affect the shape of the particle size distribution. Higher soot emissions increase the chance of gaseous HC adsorption and condensation on its surface forming wet coating, reducing the available hydrocarbons for nucleation. Hydrocarbons are adsorbed or condensed on soot particles, which increase the size and increase the chance for wet soot to collide with each other and form even bigger soot particles. Higher gaseous HC emissions tend to increase the total number of particles and increase the mean diameter for both nucleation and accumulation mode. Generally, an increase in incomplete combustion can lead to higher HC and PM emissions simultaneously, as both are byproducts of unburned or partially burned fuel. However, their exact relationship depends on multiple factors, including the air-fuel ratio, engine technology, fuel type, and operating conditions. From figure 6.17, it is clear that at 5.5 bar IMEP, MF20 has the much lower PM emissions than that of gasoline and MTHF20.

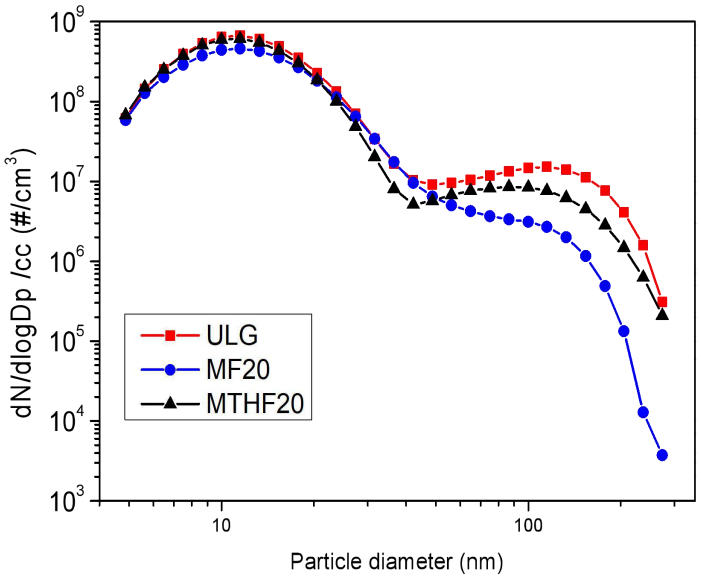

Figure 6. 17 Peak PM emissions for MTHF20, MF20 and gasoline. at intermittent load of 5.5bar imep.

The higher oxygen content in MF20 molecule and lower HC emissions compared with that of gasoline and MTHF20 can be used to explain why MF20 has smaller mean- diameter.

6.6 Summary

This chapter examines the combustion performance and emissions of 20% and 40% volumetric gasoline blends of MTHF and CP in spray guided DISI engine at stoichiometric air/fuel ratio and over the load conditions of 3.5–8.5 bar IMEP. The results are compared to the neat gasoline and similar blends of MF in gasoline. HC emission speciation's and the percentage of unburned furan components of MTHF20 and MF20 were investigated using FTIR technique. The main findings of the studies in this section are briefly summarised in this section as discused below. At the highest load of 8.5bar IMEP, CP20 and CP40 have lower CD10-90 compares to the blends of MTHF and gasoline, however at the low and intermediate load, MTHF20 and MTHF40 was observed to burn faster than gasoline and the blends of CP with gasoline. Due to its higher-octane number and faster burning rate CP20 and CP40 shows a better anti knock ability compared to MTHF20 and MTHF40 and gasoline. At the peak load, the Pmax for CP20 is similar to MF20 but higher than MTH20 and gasoline by 35% and 42% respectively. Similar trends of Pmax were observed in the combustion of the 40% volumetric blend ratio. The fuel consumption penalty increases as the percentage of the blends of CP and MTHF increases from 20% to 40%. By increasing the blend ratio of MTHF from 20% to 40% the fuel consumption increases by about 3% at the peak load, however, increasing from CP20 to CP40 leads to a higher ISFC of about 7.6%. The indicated efficiency for the blends increases with the blend ratio possibly due to greater energy loss and higher cylinder temperature. Ethylene with components percentage of 21.9%, 23.7% and 23.2% for Gasoline, MF20 and MTHF20 respectively, consistently remains the highest components of the total hydrocarbon emissions for the fuels. The percentage of the unburned furan-based fuels to the total hydrocarbon in the emissions of

MF20 and MTHF20 were 1.2 and 1.4% respectively. The 20% blends of MTHF and MF reduces its ignition delay by 10% compared to the neat gasoline at the maximum loads.

CHAPTER 7

SUMMARY, CONCLUSIONS AND FUTURE WORK

The specific aim of this research study was to explore the combustion and emissions characteristics of two biofuels candidates, 2-Methyltetrahydrofuran and Cyclopentanone in modern DISI engines. The characteristics of the two fuels were critically understudied and the summary of the results of the experimental investigations are discussed in the preceding chapters. MTHF was observed to have shared very common similarities with gasoline fuel and in similar manner CP was equally observed to have shared similar trends of engine properties correlation with Ethanol. The trends of correlations make ease of the investigations and allow the relative ease of implementation into current engine technology. However, to maximise performance, the split injection with multiple pulse widths was used for the two fuels (MTHF and CP) for the investigations. The major conclusions from this study are presented in this chapter, and this is closely followed by suggestions for further work.

7.1 Summary and Conclusions

Medusa single cylinder thermal engine with a 4-valve, 4-stroke, close-space concept (spray-guided) DISI research engine with a fixed compression ratio of 11.5:1 were used for this study. The result of this experimental studies are presented in chapters four, five and six in the thesis as summarised below.

Combustion Characteristics and Emissions of 2-Methyltetrahydrofuran and Cyclopentanone

The combustion and emissions sensitivity of MTHF and CP to various engine parameters were examined in this chapter with MF, Ethanol and gasoline as base fuels. MTHF and CP though an oxygenated fuels, both recorded higher specific fuel consumption advantage compares to MF and Ethanol but their specific fuel consumption but much lower than gasoline. The burning rate of CP in CD10-90 is faster compares to MF, MTHF and gasoline

but longer than that of ethanol. However, at the low and intermediate load, the CD10-90 for MTHF was observed to faster than all other investigated fuels between the low and the intermediate load. Due to its faster burning rate and high octane number, CP shows a better anti knock ability compares to MTHF and gasoline. At the peak load, the maximum cylinder presure for CP is 2bar, 3bar, 15bar and 17bar more than Pmax for MF. Ethanol, ULG and MTHF respectively. The limit of lean combustion for MF and CP was greater than Ethanol, ULG and MTHF. The ISFC for the investigate fuels was optimised at $1< \lambda < 1.1$. It was equally observed that the engine efficiency was optimised within this Lambda range. The maximum isNOx emission occur at $\lambda=1.2$ for all the fuels investigated and at the lean limit the isNOx emission for CP, MF and ethanol has been reduced by almost 80% of the utmost emission value at $\lambda=1.2$. The optimal fuel injection pressure was recorded at 150bar for the fuels investigate and the Pmax for the fuel injection pressure of 75bar and 100bar is lower than that at 150bar. The Pmax for the high fuel injection pressure of 175bar is actually higher than that of 150bar but is at the expense of low fuel economy as penalty. The engine out emission of isNOx is generally higher for CP and MTHF compare to MF, gasoline and Ethanol. However, the HC emissions of CP and MTHF is generally lower than that of MF and ULG but higher than that of Ethanol.

Modern GDI Combustion Modes using 2-Methyltetrahydrofuran and Cyclopentanone

The investigated fuels have increasing spark sensitivities with respect to IMEP decay. The order of Spark sensitivity of the fuels are for an arbitrary SR5 can be summarised as ULG (7.5%).> MTHF(6%) > CP(5%) > MF(4.7%) > Ethanol (4.5%). The study shows that the rate of IMEP decay increases with the more retarded MBT/KLSA timing as indicated. Overall, the optimal fuel injection timing for single pulse width for the fuel under investigatiom was found to be 270degbTDCcomb. This optimal timing was selected after considering some trade off between the performance and emission data. The results of the both isCO and isHC emissions and combustion efficiency are optimised at 360degbTDCcomb, however, key engine performance

including the maximum cylinder pressure, Volumetric efficiency, indicated pressure and the specific fuel consumption were too low at this early injection timing. The result of the split-injection shows higher sensitivity to SOI2 and less sensitivity to biofuels. Compare to the single pulse SOI, there are benefit recorded in relation to engine performance and NOx, HC and CO emission benefit typical at early SOI2 timings and a 2:1 split-ratio when using both MTHF and CP.

Combustion and Emissions of Gasoline Blends of 2-Methlytetrahydrofuran, and Cyclopentanone in a DISI Engine

Combustion performance and emissions of 20% and 40% volumetric gasoline blends of MTHF, CP and MF in a single cylinder spray guided DISI engine were investigated in this section. At the peak load of 8.5 bar IMEP, CP20 and CP40 recorded faster burning rate of CD10-90 compares to the blends of MF and MTHF, however at the low and intermediate load, MTHF20 and MTHF40 was observed to burn faster than other fuels. Due to its higher octane number and faster burning rate CP20 and CP40 shows a better anti knock ability compares to MTHF20 and MTHF40 and gasoline. At the peak load, the Pmax for CP20 is similar to MF20 but higher than MTH20 and gasoline by 35% and 42% respectively. Similar trends of Pmax was observed in the combustion of the 40% volumetric blend ratio. The fuel consumption penalty increases as the blends ratio increases from 20% to 40%. The indicated effficiency for the blends increases with the blend ratio possibly due to greater energy loss and higher cylinder temperature. Ethylene with components percentage of 21.9%, 23.7% and 23.2% for Gasoline, MF20 and MTHF20 respectively, consistently remains the highest components of the total hydrocarbon emissions for the fuels. The percentage of the unburned furan-based fuels to the total hydrocarbon in the emissions of MF20 and MTHF20 were 1.2 and 1.4% respectively. The 20% blends of MTHF and MF reduces its ignition delay by 10% compare to the neat gasoline at the maximum loads.

7.2 Future Work

This study has conducted series of combustion and emissions test on CP and MTHF as potential engine Biofuels. However, some additional research is required to better understand the behaviour of the fuels and tackle some of the identified challenges before the two fuels could be finally integrated to the list of viable engine Biofuels.

7.2.1 In depth EGR Analysis

The NOx emissions from MTHF and CP combustion are much higher than with ethanol or MF and gasoline. Therefore, an in-depth analysis of EGR on NOx reduction would be worthwhile for the two fuels. This will provide the opportunity to understand the trade-off between the NOx and PM emissions and the same time provide insight into the effect of EGR on combustion stability when using MTHF and CP.

7.2.2 Combustion of CP in a boosted downsized DISI engine

Combustion of CP in a boosted downsized engine will be an interesting future work. CP will allow the use of high compression ratios or turbocharging due to its high knock resistance. These downsizing' techniques could be conducted along with other viable oxygenated fuels to compare their effect.

7.2.3 Engine Cold Start Combustion

It will equally be an important future study to investigate the combustion of CP and MTHF during cold engine starts. This is important if the use of CP and MTHF is not to be geographically localised like high blends of ethanol and be extended to cold climates

7.2.4 Unregulated and PM Emissions

Another area which requires future in depth study for the fuel under investigations is the understanding of the unregulated emissions for the two fuels. This study did not quantify the light rang hydrocarbon (which contain 1-6 carbon atoms) to mid-range hydrocarbons (which

contain 1-6 carbon atoms) for CP and MTHF should be investigated and the comparison should be made to MF, ethanol and gasoline. Additional Research study could be conducted for PM emissions for CP and MTHF. These studies could include the investigation of the effects of TWC and HC trappers on PM emissions, the study of PM morphology and structure for the two fuels and the impacts of fuel properties such as vapor pressure, molecule structure on PM emissions.

7.2.5 Impact DI injector plugging on CP and MTHF

Injector plugging in GDI engine can be caused by carbon deposit which may adversely affect the injector fuel flow rates, the injector spray quality, and the droplet diameter and penetration distance and the spray angle, Injector plugging can lead to incomplete combustion causing increase in particulate emissions. The impact of MTHF and CP on injector plugging needs to be investigated in detail in future before they are promoted as viable renewable biofuel candidate.

LIST OF REFERENCES

1. Zhong S, Daniel R, Xu H, Zhang J, Turner D, Wyszynski ML, et al. Combustion and emissions of 2, 5-dimethylfuran in a direct-injection spark-ignition engine. Energy & Fuels. 2010;24(5):2891-9.

2. Tian G, Daniel R, Li H, Xu H, Shuai S, Richards P. Laminar burning velocities of 2, 5-dimethylfuran compared with ethanol and gasoline. Energy & Fuels. 2010;24(7):3898-905.

3. Daniel R, Wei L, Xu H, Wang C, Wyszynski ML, Shuai S. Speciation of hydrocarbon and carbonyl emissions of 2, 5-dimethylfuran combustion in a DISI engine. Energy & fuels. 2012;26(11):6661-8.

4. Daniel R, Tian G, Xu H, Wyszynski ML, Wu X, Huang Z. Effect of spark timing and load on a DISI engine fuelled with 2, 5-dimethylfuran. Fuel. 2011;90(2):449-58.

5. Daniel R, Xu H, Wang C, Richardson D, Shuai S. Combustion performance of 2, 5-dimethylfuran blends using dual-injection compared to direct-injection in a SI engine. Applied energy. 2012;98:59-68.

6. Daniel R, Xu H, Wang C, Richardson D, Shuai S. Gaseous and particulate matter emissions of biofuel blends in dual-injection compared to direct-injection and port injection. Applied energy. 2013;105:252-61.

7. Daniel R, Wang C, Xu H, Tian G. Split-injection strategies under full-load using DMF, a new biofuel candidate, compared to ethanol in a GDI engine. SAE Technical Paper; 2012. Report No.: 0148-7191.

8. Wang C, Xu H, Herreros JM, Lattimore T, Shuai S. Fuel effect on particulate matter composition and soot oxidation in a direct-injection spark ignition (DISI) engine. Energy & fuels. 2014;28(3):2003-12.

9. Xu H, Wang C, Ma X, Sarangi AK, Weall A, Krueger-Venus J. Fuel injector deposits in direct-injection spark-ignition engines. Progress in Energy and Combustion Science. 2015;50:63-80.

10. Wang C, Zeraati-Rezaei S, Xiang L, Xu H. Ethanol blends in spark ignition engines: RON, octane-added value, cooling effect, compression ratio, and potential engine efficiency gain. Applied energy. 2017;191:603-19.

11. Wang C, Xu H, Herreros JM, Wang J, Cracknell R. Impact of fuel and injection system on particle emissions from a GDI engine. Applied Energy. 2014;132:178-91.

12. Lattimore T, Wang C, Xu H, Wyszynski ML, Shuai S. Investigation of EGR effect on combustion and PM emissions in a DISI engine. Applied Energy. 2016;161:256-67.

13. Lattimore T, Herreros JM, Xu H, Shuai S. Investigation of compression ratio and fuel effect on combustion and PM emissions in a DISI engine. Fuel. 2016;169:68-78.

14. Xu C, Zhong A, Li X, Wang C, Sahu A, Xu H, et al. Laminar burning characteristics of upgraded biomass pyrolysis fuel derived from rice husk at elevated pressures and temperatures. Fuel. 2017;210:249-61.

15. Wang C, Xu H, Lattimore T. Impacts of low-level 2-methylfuran content in gasoline on DISI engine combustion behavior and emissions. SAE Technical Paper; 2013. Report No.: 0148-7191.

16. Lattimore T. Combustion and emissions of a direct injection gasoline engine using EGR: University of Birmingham; 2016.

17. Liu H, Olalere R, Wang C, Ma X, Xu H. Combustion characteristics and engine performance of 2-methylfuran compared to gasoline and ethanol in a direct injection spark ignition engine. Fuel. 2021;299:120825.

18. Alam MS, Zeraati-Rezaei S, Xu H, Harrison RM. Characterization of gas and particulate phase organic emissions (C9–C37) from a diesel engine and the effect of abatement devices. Environmental science & technology. 2019;53(19):11345-52.

19. Olalere RK, Zhang G, Xu H. Experimental Investigation of Gaseous Emissions and Hydrocarbon Speciation for MF and MTHF Gasoline Blends in DISI Engine. International Journal of Automotive Manufacturing and Materials. 2024:6-.

20. Hosseini SE, Butler B. An overview of development and challenges in hydrogen powered vehicles. International Journal of Green Energy. 2019;17(1):13-37.

21. Álvarez Fernández R, Corbera Caraballo S, Beltrán Cilleruelo F, Lozano JA. Fuel optimization strategy for hydrogen fuel cell range extender vehicles applying genetic algorithms. Renewable and Sustainable Energy Reviews. 2018;81:655-68.

22. Chang X, Ma T, Wu R. Impact of urban development on residents' public transportation travel energy consumption in China: An analysis of hydrogen fuel cell vehicles alternatives. International Journal of Hydrogen Energy. 2019.

23. IEA. Key World Energy Statistics Paris; 2021.

24. Mori D, Hirose K. Recent challenges of hydrogen storage technologies for fuel cell vehicles. International Journal of Hydrogen Energy. 2009;34:4569-74.

25. Bob Flach SLaSB. Biofuels Annual. Global Agricultural Information Network; 2019 7/15/2019. Contract No.: NL9022.

26. Dutta K, Daverey A, Lin J-G. Evolution retrospective for alternative fuels: First to fourth generation. Renewable Energy. 2014;69:114-22.

27. Liu H, Olalere R, Wang C, Ma X, Xu H. Combustion characteristics and engine performance of 2-methylfuran compared to gasoline and ethanol in a direct injection spark ignition engine. Fuel. 2021;299.

28. Koç M, Sekmen Y, Topgül T, Yücesu HS. The effects of ethanol–unleaded gasoline blends on engine performance and exhaust emissions in a spark-ignition engine. Renewable Energy. 2009;34(10):2101-6.

29. Wang C, Janssen A, Prakash A, Cracknell R, Xu H. Splash blended ethanol in a spark ignition engine – Effect of RON, octane sensitivity and charge cooling. Fuel. 2017;196:21-31.

30. Hsieh W-D, Chen R-H, Wu T-L, Lin T-H. Engine performance and pollutant emission of an SI engine using ethanol–gasoline blended fuels. Atmospheric Environment. 2002;36(3):403-10.

31. Cole MB, Augustin MA, Robertson MJ, Manners JM. The science of food security. NPJ Sci Food. 2018;2:14.

32. Sims REH, Mabee W, Saddler JN, Taylor M. An overview of second generation biofuel technologies. Bioresource technology. 2010;101 6:1570-80.

33. Mabee WE GD, Arato C, Berlin A, Bura R, Gilkes N, et al. Update on softwood-to ethanol process development. Appl Biochem Biotechnol 2006:55–70. .

34. Wang C, Xu H, Daniel R, Ghafourian A, Herreros JM, Shuai S, et al. Combustion characteristics and emissions of 2-methylfuran compared to 2,5-dimethylfuran, gasoline and ethanol in a DISI engine. Fuel. 2013;103:200-11.

35. Alexandrino K, Millera Á, Bilbao R, Alzueta MU. 2-methylfuran Oxidation in the Absence and Presence of NO. Flow, Turbulence and Combustion. 2016;96(2):343-62.

36. Tomei J, Helliwell R. Food versus fuel? Going beyond biofuels. Land Use Policy. 2016;56:320-6.

37. Prajapati DKaA. Impact of Biofuel in Internal Combustion Engine. International Journal of Engineering Research & Technology (IJERT). 2016;5(02).

38. International NTR. Summary of data for chemical selection for 2-2-methyltetrahydrofuran (96-47-9). . 1998. Contract No.: CB-50511 (7/00).

39. Aycock DF. Solvent applications of 2-methyltetrahydrofuran in organometallic and biphasic reactions. Organic Process Research & Development. 2007;11(1):156-9.

40. Wei H, Feng D, Shu G, Pan M, Guo Y, Gao D, et al. Experimental investigation on the combustion and emissions characteristics of 2-methylfuran gasoline blend fuel in spark-ignition engine. Applied Energy. 2014;132:317-24.

41. Román-Leshkov Y, Barrett CJ, Liu ZY, Dumesic JA. Production of dimethylfuran for liquid fuels from biomass-derived carbohydrates. Nature. 2007;447(7147):982-5.

42. Zhao H, Holladay JE, Brown H, Zhang ZC. Metal chlorides in ionic liquid solvents convert sugars to 5-hydroxymethylfurfural. Science. 2007;316(5831):1597-600.

43. Olalere RK, Zhang G, Liu H, Ma X, Xu H. Experimental study of combustion and emissions characteristics of low blend ratio of 2-methylfuran/2-methyltetrahyrofuran with gasoline in a DISI engine. Fuel. 2025;382:133799.

44. Rudolph TW, Thomas JJ. NOx, NMHC and CO emissions from biomass derived gasoline extenders. Biomass. 1988;16(1):33-49.

45. Samuel V. Lucas DAL, Mark E. Meyer, J. J. Thomas, Erik E. Gordon. "Exhaust Emissions and Field Trial Results of a New, Oxygenated, Non-Petroleum-Based, Waste-Derived Gasoline Blending Component: 2-Methyltetrahydrofuran,". 1993.

46. Christensen E, Yanowitz J, Ratcliff M, McCormick RL. Renewable Oxygenate Blending Effects on Gasoline Properties. Energy & Fuels. 2011;25(10):4723-33.

47. Thewes M, Muther M, Brassat A, Pischinger S, Sehr A. Analysis of the Effect of Bio-Fuels on the Combustion in a Downsized DI SI Engine. SAE International Journal of Fuels and Lubricants. 2011;5(1):274-88.

48. Tripathi R, Lee C, Fernandes RX, Olivier H, Curran HJ, Sarathy SM, et al. Ignition characteristics of 2-methyltetrahydrofuran: An experimental and kinetic study. Proceedings of the Combustion Institute. 2017;36(1):587-95.

49. Moshammer K, Vranckx S, Chakravarty HK, Parab P, Fernandes RX, Kohse-Höinghaus K. An experimental and kinetic modeling study of 2-methyltetrahydrofuran flames. Combustion and Flame. 2013;160(12):2729-43.

50. Janssen AJ, Kremer FW, Baron JH, Muether M, Pischinger S, Klankermayer J. Tailor-made fuels from biomass for homogeneous low-temperature diesel combustion. Energy & Fuels. 2011;25(10):4734-44.

51. Scognamiglio J, Jones L, Letizia C, Api A. Fragrance material review on cyclopentanone. Food and chemical toxicology. 2012;50:S608-S12.

52. Doustdar O, Wyszynski ML, Tsolakis A, Mahmoudi H. Bio-ketones from lignocellulosic biomass: experimental investigation on fuel properties, combustion and emissions characteristics of cyclopentanone blend with diesel in compression ignition engine. Combustion Engines. 2017;56.

53. Bennett J, Mabille C. 8 - Advanced fuel additives for modern internal combustion engines*. In: Folkson R, Sapsford S, editors. Alternative Fuels and Advanced Vehicle Technologies for Improved Environmental Performance (Second Edition): Woodhead Publishing; 2022. p. 197-229.

54. Heywood JB. Internal combustion engine fundamentals: McGraw-Hill Education; 2018.

55. Ferguson CR, Kirkpatrick AT. Internal combustion engines: applied thermosciences: John Wiley & Sons; 2015.

56. Ozdalya MBÇaB. Gasoline Direct Injection Siano D, editor2010.

57. Stone R. Introduction to Internal Combustion Engines Fourth, editor: SAE International and Macmillan Press; 2012.

58. Mustafa Bahattin Ç, Bulent O. Gasoline Direct Injection. In: Daniela S, editor. Fuel Injection. Rijeka: IntechOpen; 2010. p. Ch. 1.

59. Zhao F, Lai MC, Harrington DL. Automotive spark-ignited direct-injection gasoline engines. Progress in Energy and Combustion Science. 1999;25(5):437-562.

60. Smith JD, Sick V. A Multi-Variable High-Speed Imaging Study of Ignition Instabilities in a Spray-Guided Direct-Injected Spark-Ignition Engine. SAE International; 2006.

61. Queiroz C, Tomanik E. Gasoline Direct Injection Engines - A Bibliographical Review. SAE International; 1997.

62. Duronio F, De Vita A, Montanaro A, Villante C. Gasoline direct injection engines–A review of latest technologies and trends. Part 2. Fuel. 2020;265:116947.

63. Kalwar A, Agarwal AK. Overview, advancements and challenges in gasoline direct injection engine technology. Advanced Combustion Techniques and Engine Technologies for the Automotive Sector. 2020:111-47.

64. Shuai S, Ma X, Li Y, Qi Y, Xu H. Recent progress in automotive gasoline direct injection engine technology. Automotive Innovation. 2018;1:95-113.

65. Bronisław S, Mariusz C. Stratified Charge Combustion in a Spark-Ignition Engine With Direct Injection System. In: Hoon Kiat N, editor. Advances in Internal Combustion Engines and Fuel Technologies. Rijeka: IntechOpen; 2013. p. Ch. 3.

66. Fiengo G, di Gaeta A, Palladino A, Giglio V. Common Rail System for GDI Engines. Modelling, Identification, and Control2013.

67. de Sercey G, Awcock G, Heikal M. Development of a calibrated technique for in situ investigation of air–fuel mixing in engines. The Imaging Science Journal. 2006;54(1):33-45.

68. Li Y, Liu J, Huang W, Wang N. Effect of In-Cylinder Low-Pressure Direct Injection Strategy on the Atomization and Combustion Process of a Small-Scaled Gasoline Wankel Rotary Engine. International Journal of Energy Research. 2023;2023:3716468.

69. Rotondi R, Bella G. Gasoline direct injection spray simulation. International Journal of Thermal Sciences. 2006;45:168–79.

70. Gandhi AH, Weaver CE, Curtis EW, Alger TF, Anderson CL, Abata DL. Spray Characterization in a DISI Engine During Cold Start: (1) Imaging Investigation. SAE International; 2006.

71. Hentschel W. Optical diagnostics for combustion process development of direct-injection gasoline engines. Proceedings of the Combustion Institute. 2000;28(1):1119-35.

72. Song J, Kim T, Jang J, Park S. Effects of the injection strategy on the mixture formation and combustion characteristics in a DISI (direct injection spark ignition) optical engine. Energy. 2015;93:1758-68.

73. Roy MK, Kawahara N, Tomita E, Fujitani T. Jet-guided combustion characteristics and local fuel concentration measurements in a hydrogen direct-injection spark-ignition engine. Proceedings of the Combustion Institute. 2013;34(2):2977-84.

74. Park CW, Oh HC, Kim SD, Kim HS, Lee SY, Bae CS. Evaluation and visualization of stratified ultra-lean combustion characteristics in a spray-guided type gasoline direct-injection engine. International Journal of Automotive Technology. 2014;15(4):525-33.

75. Alger T, Hall M, Matthews RD. Effects of Swirl and Tumble on In-Cylinder Fuel Distribution in a Central Injected DISI Engine. SAE International; 2000.

76. Sjöberg M, Reuss D. NO _x -Reduction by Injection-Timing Retard in a Stratified-Charge DISI Engine using Gasoline and E85. SAE International Journal of Fuels and Lubricants. 2012;5(3):1096-113.

77. Spicher U, Kölmel A, Kubach H, Töpfer G. Combustion in Spark Ignition Engines with Direct Injection. SAE International; 2000.

78. Danaiah P, Ravikumar P, Kumar DV, editors. Lean Combustion Technology for Internal Combustion Engines: a Review2012.

79. Muñoz RH, Han Z, VanDerWege BA, Yi J. Effect of Compression Ratio on Stratified-Charge Direct- Injection Gasoline Combustion. SAE International; 2005.

80. Krishna AS, Mallikarjuna JM, Kumar D. Effect of engine parameters on in-cylinder flows in a two-stroke gasoline direct injection engine. Applied Energy. 2016;176:282-94.

81. Bahattin M, Ozdaly B, Siano D. Gasoline Direct Injection. Fuel Injection: Sciyo; 2010. p. 1-19.

82. Krishna AS, Mallikarjuna J, Kumar D. Effect of engine parameters on in-cylinder flows in a two-stroke gasoline direct injection engine. Applied Energy. 2016;176:282-94.

83. Ortmann R, Arndt S, Raimann J, Grzeszik R, Würfel G. Methods and Analysis of Fuel Injection, Mixture Preparation and Charge Stratification in Different Direct Injected SI Engines. SAE International; 2001.

84. Jüngst N, Kaiser S. Imaging of Fuel-Film Evaporation and Combustion in a Direct-Injection Model Experiment. SAE International; 2019.

85. Çelik MB, Ozdalyan B. Gasoline direct injection. Fuel Injection. 2010:1-17.

86. Sanguesa JA, Torres-Sanz V, Garrido P, Martinez FJ, Marquez-Barja JM. A Review on Electric Vehicles: Technologies and Challenges. Smart Cities. 2021;4(1):372-404.

87. Jeswani HK, Chilvers A, Azapagic A. Environmental sustainability of biofuels: a review. Proc Math Phys Eng Sci. 2020;476(2243):20200351.

88. Chang W-R, Hwang J-J, Wu W. Environmental impact and sustainability study on biofuels for transportation applications. Renewable and Sustainable Energy Reviews. 2017;67:277-88.

89. Rony ZI, Mofijur M, Hasan MM, Ahmed SF, Badruddin IA, Khan TMY. Conversion of algal biomass into renewable fuel: A mini review of chemical and biochemical processes. Frontiers in Energy Research. 2023;11.

90. Packer MA, Harris GCM, Adams SL, editors. Food and Feed Applications of Algae2016.

91. Adler PR, Del Grosso SJ, Parton WJ. Life-cycle assessment of net greenhouse-gas flux for bioenergy cropping systems. Ecol Appl. 2007;17(3):675-91.

92. Lu C, Yu Z, Hennessy DA, Feng H, Tian H, Hui D. Emerging weed resistance increases tillage intensity and greenhouse gas emissions in the US corn–soybean cropping system. Nature Food. 2022;3(4):266-74.

93. Reijnders L, Huijbregts MAJ. Biogenic greenhouse gas emissions linked to the life cycles of biodiesel derived from European rapeseed and Brazilian soybeans. Journal of Cleaner Production. 2008;16(18):1943-8.

94. EC. Directive of the European Parliament and of the Council of the 23rd April 2009 amended July 2021 on the promotion of the use of energy from renewable sources 2021.

95. Rounce P, editor Engine performance and particulate matter speciation for compression ignition engines powered by a range of fossil and biofuels2011.

96. Valera H, Čedík J, Pexa M, Agarwal AK, editors. Regulated and Unregulated Emissions from Methanol Fuelled Engines2021.

97. Nguyen XV, Phan TTH, Cao VL, Nguyen Nhat NT, Nguyen TH, Nguyen XT, et al. Current advances in seagrass research: A review from Viet Nam. Front Plant Sci. 2022;13:991865.

98. Vishwakarma K, Kumar N, Shandilya C, Mohapatra S, Bhayana S, Varma A. Revisiting Plant-Microbe Interactions and Microbial Consortia Application for Enhancing Sustainable Agriculture: A Review. Front Microbiol. 2020;11:560406.

99. IEA. Global Energy Review: CO2 Emissions in 2021, ,. Paris; 2022. Contract No.: License: CC BY 4.0.

100. Alalwan HA, Alminshid AH, Aljaafari HAS. Promising evolution of biofuel generations. Subject review. Renewable Energy Focus. 2019;28:127-39.

101. Sarwer A, Hamed SM, Osman AI, Jamil F, Al-Muhtaseb AaH, Alhajeri NS, et al. Algal biomass valorization for biofuel production and carbon sequestration: a review. Environmental Chemistry Letters. 2022;20(5):2797-851.

102. Vaishnav BaA. THE THIRD-GENERATION BIOFUEL PRODUCTION FROM ALGAE. AGRIALLIS. 2021;3(10).

103. Raj Shah K. The Evolution of Biofuels. Holtsvile, NY 11742 USA; 2021.

104. Zhao Z, Yu X, Huang Y, Shi W, Guo Z, Li Z, et al. Experimental study on combustion and emission of an SI engine with ethanol /gasoline combined injection and EGR. Journal of Cleaner Production. 2022;331:129903.

105. Moodley P. 1 - Sustainable biofuels: opportunities and challenges. In: Ray RC, editor. Sustainable Biofuels: Academic Press; 2021. p. 1-20.

106. Karaosmanoglu Gorgeç F, Karapinar I. Production of biohydrogen from waste wheat in continuously operated UPBR: The effect of influent substrate concentration. International Journal of Hydrogen Energy. 2019;44(32):17323-33.

107. Moodley P, Kana EBG. Optimization of xylose and glucose production from sugarcane leaves (Saccharum officinarum) using hybrid pretreatment techniques and assessment for hydrogen generation at semi-pilot scale. International Journal of Hydrogen Energy. 2015;40(10):3859-67.

108. Moodley P, Gueguim Kana EB. Bioethanol production from sugarcane leaf waste: Effect of various optimized pretreatments and fermentation conditions on process kinetics. Biotechnol Rep (Amst). 2019;22:e00329.

109. Sewsynker-Sukai Y, Gueguim Kana EB. Simultaneous saccharification and bioethanol production from corn cobs: Process optimization and kinetic studies. Bioresour Technol. 2018;262:32-41.

110. Huang W, Yuan H, Li X. Multi-perspective analyses of rice straw modification by Pleurotus ostreatus and effects on biomethane production. Bioresour Technol. 2020;296:122365.

111. Ripoll V, Agabo-García C, Perez M, Solera R. Improvement of biomethane potential of sewage sludge anaerobic co-digestion by addition of “sherry-wine” distillery wastewater. Journal of Cleaner Production. 2020;251.

112. Arora N, Jaiswal KK, Kumar V, Vlaskin MS, Nanda M, Pruthi V, et al. Small-scale phyco-mitigation of raw urban wastewater integrated with biodiesel production and its utilization for aquaculture. Bioresour Technol. 2020;297:122489.

113. Rolz C, de León R, Mendizábal de Montenegro AL. Co-production of ethanol and biodiesel from sweet sorghum juice in two consecutive fermentation steps. Electronic Journal of Biotechnology. 2019;41:13-21.

114. Kowalski Z, Kulczycka J, Verhé R, Desender L, De Clercq G, Makara A, et al. Second-generation biofuel production from the organic fraction of municipal solid waste. Frontiers in Energy Research. 2022;10.

115. Robak K, Balcerek M. Review of Second Generation Bioethanol Production from Residual Biomass. Food Technol Biotechnol. 2018;56(2):174-87.

116. Sims RE, Mabee W, Saddler JN, Taylor M. An overview of second generation biofuel technologies. Bioresour Technol. 2010;101(6):1570-80.

117. Mabee WE, Gregg DJ, Arato C, Berlin A, Bura R, Gilkes N, et al. Updates on Softwood-to-Ethanol Process Development. In: McMillan JD, Adney WS, Mielenz JR, Klasson KT, editors. Twenty-Seventh Symposium on Biotechnology for Fuels and Chemicals. Totowa, NJ: Humana Press; 2006. p. 55-70.

118. Frank D, Neubauer G, Bauer C, Kallo J, Willich C. Exhaust Emission Measurements from a Spark-Ignition Engine Using Fuels with Different Ethanol Content for Aircraft Applications. ACS Omega. 2022;7(34):29923-33.

119. Thakur AK, Kaviti AK, Mehra R, Mer K. Progress in performance analysis of ethanol-gasoline blends on SI engine. Renewable and Sustainable Energy Reviews. 2017;69:324-40.

120. Hoppe F, Burke U, Thewes M, Heufer A, Kremer F, Pischinger S. Tailor-Made Fuels from Biomass: Potentials of 2-butanone and 2-methylfuran in direct injection spark ignition engines. Fuel. 2016;167:106-17.

121. Tuan Hoang A, Viet Pham V. 2-Methylfuran (MF) as a potential biofuel: A thorough review on the production pathway from biomass, combustion progress, and application in engines. Renewable and Sustainable Energy Reviews. 2021;148.

122. Saladini F, Patrizi N, Pulselli FM, Marchettini N, Bastianoni S. Guidelines for emergy evaluation of first, second and third generation biofuels. Renewable and Sustainable Energy Reviews. 2016;66:221-7.

123. Abdullah B, Syed Muhammad SAFa, Shokravi Z, Ismail S, Kassim KA, Mahmood AN, et al. Fourth generation biofuel: A review on risks and mitigation strategies. Renewable and Sustainable Energy Reviews. 2019;107:37-50.

124. Sentanuhady J, Hasan WH, Muflikhun MA, Riccio A. Recent Progress on the Implementation of Renewable Biodiesel Fuel for Automotive and Power Plants: Raw Materials Perspective. Advances in Materials Science and Engineering. 2022;2022:1-19.

125. Committee HoCT. Fuelling the future: motive power and connectivity. 2023.

126. Cavelius P, Engelhart-Straub S, Mehlmer N, Lercher J, Awad D, Bruck T. The potential of biofuels from first to fourth generation. PLoS Biol. 2023;21(3):e3002063.

127. Turner D, Xu H, Cracknell RF, Natarajan V, Chen X. Combustion performance of bio-ethanol at various blend ratios in a gasoline direct injection engine. Fuel. 2011;90(5):1999-2006.

128. Nakata K, Utsumi S, Ota A, Kawatake K, Kawai T, Tsunooka T. The Effect of Ethanol Fuel on a Spark Ignition Engine. SAE International; 2006.

129. Wyszynski LP, Stone CR, Kalghatgi GT. The Volumetric Efficiency of Direct and Port Injection Gasoline Engines with Different Fuels. SAE International; 2002.

130. Wallner T, Miers SA. Combustion Behavior of Gasoline and Gasoline/Ethanol Blends in a Modern Direct-Injection 4-Cylinder Engine. SAE International; 2008.

131. RFA. World Fuel Ethanol Production by Region. Washington DC; 2022.

132. Luiz Carlos B, Thiago Olitta B, Saul Nitsche R. Ethanol Production in Brazil: The Industrial Process and Its Impact on Yeast Fermentation. In: Marco Aurelio dos Santos B, editor. Biofuel Production. Rijeka: IntechOpen; 2011. p. Ch. 5.

133. Bernardes MAdS. Biofuel Production – Recent Developments and Prospects. Rijeka, Croatia: InTech Open Access Publisher; 2011.

134. Yüksel F, Yüksel B. The use of ethanol–gasoline blend as a fuel in an SI engine. Renewable Energy. 2004;29(7):1181-91.

135. Aghaei S, Karimi Alavijeh M, Shafiei M, Karimi K. A comprehensive review on bioethanol production from corn stover: Worldwide potential, environmental importance, and perspectives. Biomass and Bioenergy. 2022;161:106447.

136. Amorim HVd, Basso LC, Lopes ML, editors. Sugar cane juice and molasses, beet molasses and sweet sorghum: composition and usage2009.

137. Eliodorio KP, Cunha G, Lino FSO, Sommer MOA, Gombert AK, Giudici R, et al. Physiology of Saccharomyces cerevisiae during growth on industrial sugar cane molasses can be reproduced in a tailor-made defined synthetic medium. Sci Rep. 2023;13(1):10567.

138. Yuksel B. An investigation of using ethanol as a fuel on the agricultural diesel engine: PhD Thesis, Ataturk University; 1984.

139. Dien BS, Bothast, R.J. A primer for lignocellulose biochemical conversion to fuel ethanol. Nottingham, UK.: Nottingham University Press,; 2009 Last Modified: 08/11/2023.

140. Bata RM, Elrod AC, Rice RW. Emissions From IC Engines Fueled With Alcohol–Gasoline Blends: A Literature Review. Journal of Engineering for Gas Turbines and Power. 1989;111(3):424-31.

141. Huynh TT, Le MD, Duong DN. Effects of butanol–gasoline blends on SI engine performance, fuel consumption, and emission characteristics at partial engine speeds. International Journal of Energy and Environmental Engineering. 2019;10(4):483-92.

142. Palmer FH, editor VEHICLE PERFORMANCE OF GASOLINE CONTAINING OXYGENATES1986.

143. Devunuri S, Porpatham E. Investigations on effects of ethanol blending on performance and combustion characteristics of gasoline fuelled lean burn SI engine. IOP Conference Series: Earth and Environmental Science. 2019;265(1):012019.

144. Ramadhas AS, Singh PK, Sakthivel P, Mathai R, Sehgal AK. Effect of Ethanol-Gasoline Blends on Combustion and Emissions of a Passenger Car Engine at Part Load Operations. SAE International; 2016.

145. Manzetti S, Andersen O. A review of emission products from bioethanol and its blends with gasoline. Background for new guidelines for emission control. Fuel. 2015;140:293-301.

146. Bhatia SC. 26 - Issues relating to biofuels. In: Bhatia SC, editor. Advanced Renewable Energy Systems: Woodhead Publishing India; 2014. p. 688-718.

147. Chao HR, Lin TC, Chao MR, Chang FH, Huang CI, Chen CB. Effect of methanol-containing additive on the emission of carbonyl compounds from a heavy-duty diesel engine. J Hazard Mater. 2000;73(1):39-54.

148. Rice RW, Sanyal AK, Elrod AC, Bata RM. Exhaust Gas Emissions of Butanol, Ethanol, and Methanol-Gasoline Blends. Journal of Engineering for Gas Turbines and Power. 1991;113(3):377-81.

149. Edwin Geo V, Jesu Godwin D, Thiyagarajan S, Saravanan CG, Aloui F. Effect of higher and lower order alcohol blending with gasoline on performance, emission and combustion characteristics of SI engine. Fuel. 2019;256:115806.

150. Energy UDo. Ethanol Benefits and Considerations. 2019.

151. Ababneh H, Hameed B. Electrofuels as emerging new green alternative fuel: A review of recent literature. Energy conversion and management. 2022;254:115213.

152. Segovia-Hernández JG. Advancing E-Fuels Production Through Process Intensification: Overcoming Challenges and Seizing Opportunities for a Sustainable Energy Future-A Critical Review. Chemical Engineering and Processing-Process Intensification. 2024:110107.

153. BRIEFING P. Sustainable synthetic carbon based fuels for transport.

154. Dell'Aversano S, Villante C, Gallucci K, Vanga G, Di Giuliano A. E-fuels: a comprehensive review of the most promising technological alternatives towards an energy transition. Energies. 2024;17(16):3995.

155. Reddy VJ, Hariram N, Maity R, Ghazali MF, Kumarasamy S. Sustainable e-fuels: Green hydrogen, methanol and ammonia for carbon-neutral transportation. World Electric Vehicle Journal. 2023;14(12):349.

156. Bharti S, Chauhan BV, Garg A, Vedrtnam A, Shukla M. Potential of E-Fuels for Decarbonization of Transport Sector. Greener and Scalable E-fuels for Decarbonization of Transport. 2022:9-32.

157. Galimova T, Ram M, Bogdanov D, Fasihi M, Gulagi A, Khalili S, et al. Global trading of renewable electricity-based fuels and chemicals to enhance the energy transition across all sectors towards sustainability. Renewable and Sustainable Energy Reviews. 2023;183:113420.

158. Al-Zaidi MK, Al-Khafaji RQ, Al-Zubaidy DK, Salman MM. A Review: Fuel Cells Types and their Applications. International Journal of Scientific Engineering and Applied Science (IJSEAS). 2021;7(7):375-90.

159. Tseng C-J, Tsai BT, Liu Z-S, Cheng T-C, Chang W-C, Lo S-K. A PEM fuel cell with metal foam as flow distributor. Energy Conversion and Management. 2012;62:14-21.

160. Bvumbe TJ, Bujlo P, Tolj I, Mouton K, Swart G, Pasupathi S, et al. Review on management, mechanisms and modelling of thermal processes in PEMFC. Hydrogen and Fuel Cells. 2016;1(1):1-20.

161. Galimova T, Ram M, Bogdanov D, Fasihi M, Khalili S, Gulagi A, et al. Global demand analysis for carbon dioxide as raw material from key industrial sources and direct air capture to produce renewable electricity-based fuels and chemicals. Journal of Cleaner Production. 2022;373:133920.

162. Singh M, Singla MK, Safaraliev M, Singh K, Odinaev I, Menaem AA. Advancements and challenges of fuel cell integration in electric vehicles: A comprehensive analysis. International Journal of Hydrogen Energy. 2024;88:1386-97.

163. Lester MS, Bramstoft R, Münster M. Analysis on electrofuels in future energy systems: a 2050 case study. Energy. 2020;199:117408.

164. Yong KJ, Wu TY, Lee CBTL, Lee ZJ, Liu Q, Jahim JM, et al. Furfural production from biomass residues: Current technologies, challenges and future prospects. Biomass and Bioenergy. 2022;161:106458.

165. Morgan TJ, Youkhana A, Turn SQ, Ogoshi R, Garcia-Pérez M. Review of Biomass Resources and Conversion Technologies for Alternative Jet Fuel Production in Hawai'i and Tropical Regions. Energy & Fuels. 2019;33(4):2699-762.

166. Binder JB, Raines RT. Simple Chemical Transformation of Lignocellulosic Biomass into Furans for Fuels and Chemicals. Journal of the American Chemical Society. 2009;131(5):1979-85.

167. Thananatthanachon T, Rauchfuss TB. Efficient production of the liquid fuel 2,5-dimethylfuran from fructose using formic acid as a reagent. Angew Chem Int Ed Engl. 2010;49(37):6616-8.

168. Chidambaram M, Bell AT. A two-step approach for the catalytic conversion of glucose to 2,5-dimethylfuran in ionic liquids. Green Chemistry. 2010;12(7):1253-62.

169. Westbrook CK, Curran HJ. Chapter 7 - Detailed kinetics of fossil and renewable fuel combustion. In: Faravelli T, Manenti F, Ranzi E, editors. Computer Aided Chemical Engineering. 45: Elsevier; 2019. p. 363-443.

170. Mittal A, Pilath HM, Johnson DK. Direct Conversion of Biomass Carbohydrates to Platform Chemicals: 5-Hydroxymethylfurfural (HMF) and Furfural. Energy & Fuels. 2020;34(3):3284-93.

171. Peng Y, Xu Z, Yu L, Li X, Yang W. Trimetallic Cu-Ni-Re/Hβ catalyst for the direct conversion of furfural to 2-Methyltetrahydrofuran. Chemical Engineering Journal. 2023;454:139746.

172. Liu R, Zhou X, Zuo T. The pyrolysis mechanism of furan revisited. Chemical Physics Letters. 2000;325(4):457-64.

173. Tran LS, Togbé C, Liu D, Felsmann D, Oßwald P, Glaude PA, et al. Combustion chemistry and flame structure of furan group biofuels using molecular-beam mass spectrometry and gas chromatography - Part II: 2-Methylfuran. Combust Flame. 2014;161(3):766-79.

174. Uygun Y, Ishihara S, Olivier H. A high pressure ignition delay time study of 2-methylfuran and tetrahydrofuran in shock tubes. Combustion and Flame. 2014;161:2519-30.

175. Somers KP, Simmie JM, Metcalfe WK, Curran HJ. The pyrolysis of 2-methylfuran: a quantum chemical, statistical rate theory and kinetic modelling study. Physical Chemistry Chemical Physics. 2014;16(11):5349-67.

176. Wei L, Tang C, Man X, Huang Z. Shock-Tube Experiments and Kinetic Modeling of 2-Methylfuran Ignition at Elevated Pressure. Energy & Fuels. 2013;27(12):7809-16.

177. Weber I, Friese P, Olzmann M. H-Atom-Forming Reaction Pathways in the Pyrolysis of Furan, 2-Methylfuran, and 2,5-Dimethylfuran: A Shock-Tube and Modeling Study. J Phys Chem A. 2018;122(32):6500-8.

178. Djokic M, Carstensen H-H, Van Geem KM, Marin GB. The thermal decomposition of 2,5-dimethylfuran. Proceedings of the Combustion Institute. 2013;34(1):251-8.

179. Yang Q, Liu Z, Hou X, He X, Sjöberg M, Vuilleumier D, et al. Measurements of laminar flame speeds and flame instability analysis of E30-air premixed flames at elevated temperatures and pressures. Fuel. 2020;259:116223.

180. Wu X, Huang Z, Jin C, Wang X, Wei L. Laminar Burning Velocities and Markstein Lengths of 2,5-Dimethylfuran-Air Premixed Flames at Elevated Temperatures. Combustion Science and Technology. 2010;183(3):220-37.

181. Eldeeb MA, Akih-Kumgeh B. Investigation of 2,5-dimethyl furan and iso-octane ignition. Combustion and Flame. 2015;162(6):2454-65.

182. Cheng Z, Xing L, Zeng M, Dong W, Zhang F, Qi F, et al. Experimental and kinetic modeling study of 2,5-dimethylfuran pyrolysis at various pressures. Combustion and Flame. 2014;161(10):2496-511.

183. Liu D, Togbé C, Tran L-S, Felsmann D, Oßwald P, Nau P, et al. Combustion chemistry and flame structure of furan group biofuels using molecular-beam mass spectrometry and gas chromatography – Part I: Furan. Combustion and Flame. 2014;161(3):748-65.

184. Xu N, Gong J, Huang Z. Review on the production methods and fundamental combustion characteristics of furan derivatives. Renewable and Sustainable Energy Reviews. 2016;54:1189-211.

185. Eldeeb M, Akih-Kumgeh B. Recent Trends in the Production, Combustion and Modeling of Furan-Based Fuels. Energies. 2018;11(3).

186. Lifshitz A, Bidani M, Bidani S. Thermal reactions of cyclic ethers at high temperatures. Part 3. Pyrolysis of tetrahydrofuran behind reflected shocks. The Journal of Physical Chemistry. 1986;90(15):3422-9.

187. Dagaut P, McGuinness M, Simmie JM, Cathonnet M. The Ignition and Oxidation of Tetrahydrofuran: Experiments and Kinetic Modeling. Combustion Science and Technology. 1998;135(1-6):3-29.

188. Westbrook CK. Chapter 4 - Sustainable bio-oxygenate fuels. In: Brezinsky K, editor. Combustion Chemistry and the Carbon Neutral Future: Elsevier; 2023. p. 91-115.

189. Simmie JM, Metcalfe WK. Ab initio study of the decomposition of 2,5-dimethylfuran. J Phys Chem A. 2011;115(32):8877-88.

190. Wang J, Wang X, Fan X, Yang K. Shock Tube Experimental and Modeling Study of MTHF Ignition Characteristics at High Temperatures. SAE International; 2015.

191. Eldeeb MA, Akih-Kumgeh B. Recent Trends in the Production, Combustion and Modeling of Furan-Based Fuels. Energies. 2018;11(3):512.

192. Tripathi R, Lee C, Fernandes RX, Olivier H, Curran HJ, Mani Sarathy S, et al. Ignition characteristics of 2-methyltetrahydrofuran: An experimental and kinetic study. Proceedings of the Combustion Institute. 2017;36(1):587-95.

193. Information NCfB. 2,5-Dimethylfuran. 2023.

194. Chheda JADYR-LJN. CATALYTIC PROCESS FOR PRODUCING FURAN DERIVATIVES FROM CARBOHYDRATES IN A BIPHASIC REACTOR. World Intellectual Property,US. 2007.

195. Hoang AT, Pandey A, Huang Z, Luque R, Ng KH, Papadopoulos AM, et al. Catalyst-Based Synthesis of 2,5-Dimethylfuran from Carbohydrates as a Sustainable Biofuel Production Route. ACS Sustainable Chemistry & Engineering. 2022;10(10):3079-115.

196. Nishimura S, Ikeda N, Ebitani K. Selective hydrogenation of biomass-derived 5-hydroxymethylfurfural (HMF) to 2,5-dimethylfuran (DMF) under atmospheric hydrogen pressure over carbon supported PdAu bimetallic catalyst. Catalysis Today. 2014;232:89-98.

197. Saha B, Bohn CM, Abu-Omar MM. Zinc-assisted hydrodeoxygenation of biomass-derived 5-hydroxymethylfurfural to 2,5-dimethylfuran. ChemSusChem. 2014;7(11):3095-101.

198. Zhang P, Su X, Chen H, Geng L, Zhao X. Assessing fuel properties effects of 2,5-dimethylfuran on microscopic and macroscopic characteristics of oxygenated fuel/diesel blends spray. Scientific Reports. 2020;10(1):1427.

199. Christensen E, Fioroni GM, Kim S, Fouts L, Gjersing E, Paton RS, et al. Experimental and theoretical study of oxidative stability of alkylated furans used as gasoline blend components. Fuel. 2018;212:576-85.

200. Daniel R, Xu H, Wang C, Richardson D, Shuai S. Combustion performance of 2,5-dimethylfuran blends using dual-injection compared to direct-injection in a SI engine. Applied Energy. 2012;98:59-68.

201. Shaohua Zhong RD, Hongming Xu,, Jun Zhang, Dale Turner,, Miroslaw L. Wyszynski aPR. Combustion and Emissions of 2,5-Dimethylfuran in a Direct-Injection

Spark-Ignition Engine. Energy fuel. 2010.

202. Liu H, Wang X, Zhang D, Dong F, Liu X, Yang Y, et al. Investigation on Blending Effects of Gasoline Fuel with N-Butanol, DMF, and Ethanol on the Fuel Consumption and Harmful Emissions in a GDI Vehicle. Energies. 2019;12(10).

203. Saurabh Malpani aEJ. 2, 5-Dimethylfuran as A Bio-Fuel. Journal of Environmental Science, Toxicology and Food Technology. 2015;9(5):71-2.

204. Information NCfB. 2-Methylfuran. 2023.

205. Román-Leshko. Biomass-derived furanic compounds for the

production of fuels and chemical intermediate. California Institute of Technology; 2009.

206. Tian Z, Yuan T, Fournet R, Glaude PA, Sirjean B, Battin-Leclerc F, et al. An experimental and kinetic investigation of premixed furan/oxygen/argon flames. Combust Flame. 2011;158(4):756-73.

207. Bhattacharya A. Analysis of laminar premixed flame structure of isooctane/2-methylfuran/air mixtures with a skeletal mechanism. Combustion Theory and Modelling. 2021;25(7):1211-44.

208. Bhattacharya A. A skeletal mechanism for premixed flames of isooctane/2-methylfuran blends2019.

209. Tripathi R, Burke U, Ramalingam AK, Lee C, Davis AC, Cai L, et al. Oxidation of 2-methylfuran and 2-methylfuran/n-heptane blends: An experimental and modeling study. Combustion and Flame. 2018;196:54-70.

210. Ma X, Jiang C, Xu H, Ding H, Shuai S. Laminar burning characteristics of 2-methylfuran and isooctane blend fuels. Fuel. 2014;116:281-91.

211. Information NCfB. 2-Methyltetrahydrofuran.; 2023.

212. Dumesic JA, Roman-Leshkov Y, Chheda JN. Catalytic process for producing furan derivatives from carbohydrates in a biphasic reactor. Google Patents; 2015.

213. Chen S, Wojcieszak R, Dumeignil F, Marceau E, Royer Sb. How catalysts and experimental conditions determine the selective hydroconversion of furfural and 5-hydroxymethylfurfural. Chemical reviews. 2018;118(22):11023-117.

214. Bhogeswararao S, Srinivas D. Catalytic conversion of furfural to industrial chemicals over supported Pt and Pd catalysts. Journal of Catalysis. 2015;327:65-77.

215. Zhou K, Chen J, Cheng Y, Chen Z, Kang S, Cai Z, et al. Enhanced catalytic transfer hydrogenation of biomass-based furfural into 2-methylfuran over multifunctional Cu–Re bimetallic catalysts. ACS Sustainable Chemistry & Engineering. 2020;8(44):16624-36.

216. Islam MK, Wang H, Rehman S, Dong C, Hsu H-Y, Lin CSK, et al. Sustainability metrics of pretreatment processes in a waste derived lignocellulosic biomass biorefinery. Bioresource Technology. 2020;298:122558.

217. Upare PP, Jeong M-G, Hwang YK, Kim DH, Kim YD, Hwang DW, et al. Nickel-promoted copper–silica nanocomposite catalysts for hydrogenation of levulinic acid to lactones using formic acid as a hydrogen feeder. Applied Catalysis A: General. 2015;491:127-35.

218. Al-Shaal MG, Wright WR, Palkovits R. Exploring the ruthenium catalysed synthesis of γ-valerolactone in alcohols and utilisation of mild solvent-free reaction conditions. Green Chemistry. 2012;14(5):1260-3.

219. Elliott DC, Frye JG. Hydrogenated 5-carbon compound and method of making. Google Patents; 1999.

220. Al-Shaal MG, Hausoul PJ, Palkovits R. Efficient, solvent-free hydrogenation of α-angelica lactone catalysed by Ru/C at atmospheric pressure and room temperature. Chemical Communications. 2014;50(71):10206-9.

221. Obregón I, Gandarias I, Al-Shaal MG, Mevissen C, Arias PL, Palkovits R. The role of the hydrogen source on the selective production of γ-valerolactone and 2-methyltetrahydrofuran from levulinic acid. ChemSusChem. 2016;9(17):2488-95.

222. Adeleye AT, Louis H, Akakuru OU, Joseph I, Enudi OC, Michael DP. A Review on the conversion of levulinic acid and its esters to various useful chemicals. Aims Energy. 2019;7(2):165-85.

223. Soszka E, Jędrzejczyk M, Keller N, Ruppert AM. High yield production of 2-methyltetrahydrofuran biofuel with reusable Ni-Co catalysts. Fuel. 2023;332:126118.

224. Yanowitz J, Christensen E, McCormick RL. Utilization of renewable oxygenates as gasoline blending components. 2011.

225. Serrano-Ruiz J. Energy Environ. Sci. 2011, 4, 83–99; b) EI Gürbüz, DM Alonso, JQ Bond, JA Dumesic. ChemSusChem. 2011;4:357-61.

226. Serrano-Ruiz JC, Dumesic JA. Catalytic routes for the conversion of biomass into liquid hydrocarbon transportation fuels. Energy & Environmental Science. 2011;4(1):83-99.

227. Akashi T, Sato S, Takahashi R, Sodesawa T, Inui K. Catalytic vapor-phase cyclization of 1, 6-hexanediol into cyclopentanone. Catalysis Communications. 2003;4(8):411-6.

228. Hronec M, Fulajtarová K. Selective transformation of furfural to cyclopentanone. Catalysis Communications. 2012;24:100-4.

229. Zhou M, Li J, Wang K, Xia H, Xu J, Jiang J. Selective conversion of furfural to cyclopentanone over CNT-supported Cu based catalysts: Model reaction for upgrading of bio-oil. Fuel. 2017;202:1-11.

230. Zhang Y, Fan G, Yang L, Li F. Efficient conversion of furfural into cyclopentanone over high performing and stable Cu/ZrO2 catalysts. Applied Catalysis A: General. 2018;561:117-26.

231. Takahashi T, Ueno K, Kai T. Vapor phase Beckmann rearrangement of cyclopentanone oxime over high silica HZSM-5 zeolites. Microporous Materials. 1993;1(5):323-7.

232. Information NCfB. Cyclopentanone. 2023.

233. Shen T, Hu R, Zhu C, Li M, Zhuang W, Tang C, et al. Production of cyclopentanone from furfural over Ru/C with Al 11.6 PO 23.7 and application in the synthesis of diesel range alkanes. RSC advances. 2018;8(66):37993-8001.

234. Chen H, Su X, He J, Zhang P, Xu H, Zhou C. Investigation on combustion characteristics of cyclopentanol/diesel fuel blends in an optical engine. Renewable Energy. 2021;167:811-29.

235. Bao X, Jiang Y, Xu H, Wang C, Lattimore T, Tang L. Laminar flame characteristics of cyclopentanone at elevated temperatures. Applied energy. 2017;195:671-80.

236. Heywood J. 1988, Internal Combustion Engine Fundamentals, McGraw-Hill, New York.

237. Tong Q, Chen H, He J, Su X, Wei Z, Sun F, et al. Experimental studies of combustion and emission characteristics of diesel engine fueled with diesel/cyclopentanone blend. Energy Reports. 2021;7:6756-68.

238. Hoekman SK, Welstand JS. Vehicle emissions and air quality: The early years (1940s–1950s). Atmosphere. 2021;12(10):1354.

239. Heywood J. 1988, Internal Combustion Engines Fundamentals, McGraw-Hill.

240. Güney B, Aladağ A. Microstructural characterization of particulate matter from gasoline-fuelled vehicle emissions. Journal of Engineering Research and Reports. 2020;16(1):29-39.

241. Goldwine G, Sher E, Sher D. Comparison of Regulated and Unregulated Emissions and Fuel Economy of SI Engines with Three Fuels. SAE International Journal of Fuels and Lubricants. 2019;12(3):189-210.

242. Ozgen S, Cernuschi S, Caserini S. An overview of nitrogen oxides emissions from biomass combustion for domestic heat production. Renewable and Sustainable Energy Reviews. 2021;135:110113.

243. Schwerdt C. Modelling NOx-formation in combustion processes. MSc Theses. 2006.

244. Linse D. Modeling and Simulation of Knock and Nitric Oxide Emissions in Turbocharged Direct Injection Spark Ignition Engines: Cuvillier Verlag; 2013.

245. Obayes O, Aldhaidhawi M, Najee M. Emission Formation Comparison of Spark Ignition Engines Using Different Fuels. Kerbala Journal for Engineering Science. 2022;2(2):145-56.

246. Shrestha KP, Seidel L, Zeuch T, Mauss F. Detailed kinetic mechanism for the oxidation of ammonia including the formation and reduction of nitrogen oxides. Energy & fuels. 2018;32(10):10202-17.

247. Chaichan MT, Abass QA. Study of NOx emissions of SI engine fueled with different kinds of hydrocarbon fuels and hydrogen. Al-Khwarizmi Engineering Journal. 2010;6(2):11-20.

248. Cox L. Nitrogen oxides (NOx) why and how they are controlled: Diane Publishing; 1999.

249. Odell PR. Why carbon fuels will dominate the 21st century's global energy economy: Multi-Science Publishing Company Brentwood; 2004.

250. Ladommatos N, Abdelhalim S, Zhao H. Control of oxides of nitrogen from diesel engines using diluents while minimising the impact on particulate pollutants. Applied Thermal Engineering. 1998;18(11):963-80.

251. Buruiana DL, Sachelarie A, Butnaru C, Ghisman V. Important Contributions to Reducing Nitrogen Oxide Emissions from Internal Combustion Engines. International Journal of Environmental Research and Public Health. 2021;18(17):9075.

252. Ouellette P, Douville B, Hill P, Ursu B, editors. NOx reduction in a directly injected natural gas engine. Proceedings of the 1998 Fall Technical Conference of the ASME, IC Engines Division, ICE; 1998.

253. Michaels H, Fulper C, Kolowich B. Nitrous oxide emission factors for mobile sources. EMISSION INVENTORY: LIVING IN A GLOBAL ENVIRONMENT- VOLUME 2. 1998:831-42.

254. Soltic P, Hausberger S, editors. On-Road Emission Measurements and emission modeling results for a tractor-semi trailer in Trans-Alpine operation. 13th International Scientific Symposium Transport and Air Pollution Boulder, Colorado, USA; 2004.

255. Abouemara K, Fikry S. Emission Control Technologies in Spark Ignition Engines. Journal of Student Research. 2020;9(1).

256. Awad OI, Mamat R, Ibrahim TK, Hammid AT, Yusri I, Hamidi MA, et al. Overview of the oxygenated fuels in spark ignition engine: Environmental and performance. Renewable and Sustainable Energy Reviews. 2018;91:394-408.

257. Leitão NC, Balogh JM. The impact of intra-industry trade on carbon dioxide emissions: The case of the European Union. Agricultural Economics. 2020;66(5):203-14.

258. Galán-Martín Á, Vázquez D, Cobo S, Mac Dowell N, Caballero JA, Guillén-Gosálbez G. Delaying carbon dioxide removal in the European Union puts climate targets at risk. Nature Communications. 2021;12(1):6490.

259. Lakshminarayanan P, Aghav YV, Lakshminarayanan P, Aghav YV. Hydrocarbon Emissions from Spark Ignition Engines. Modelling Diesel Combustion. 2010:147-66.

260. Leach F, Kalghatgi G, Stone R, Miles P. The scope for improving the efficiency and environmental impact of internal combustion engines. Transportation Engineering. 2020;1:100005.

261. Wen M, Yin Z, Zheng Z, Liu H, Zhang C, Cui Y, et al. Effects of Different Gasoline Additives on Fuel Consumption and Emissions in a Vehicle Equipped With the GDI Engine. Frontiers in Mechanical Engineering. 2022;8:924505.

262. Sher E. Handbook of air pollution from internal combustion engines: pollutant formation and control: Academic Press; 1998.

263. Zaharia C. Particulate matter (settled particles, coarse PM10, fine PM2. 5 or PM1, ultrafine particles) in urban atmosphere: characteristics, quality control and health effects.

264. Leach FCP. Particulate emissions from gasoline direct injection engines: University of Oxford; 2014.

265. Singh E, Kim N, Vuilleumier D, Skeen S, Cenker E, Sjöberg M, et al. Particulate Matter Emissions in Gasoline Direct-Injection Spark-Ignition Engines: Sources, Fuel Dependency, and Quantities. Fuel. 2023;338:127198.

266. Jiao Q, Reitz RD. The effect of operating parameters on soot emissions in GDI engines. SAE International Journal of Engines. 2015;8(3):1322-33.

267. Reizer E, Viskolcz B, Fiser B. Formation and growth mechanisms of polycyclic aromatic hydrocarbons: A mini-review. Chemosphere. 2022;291:132793.

268. Jäger C, Huisken F, Mutschke H, Jansa IL, Henning T. Formation of polycyclic aromatic hydrocarbons and carbonaceous solids in gas-phase condensation experiments. The Astrophysical Journal. 2009;696(1):706.

269. Chimjarn S, Delhomme O, Millet M. Temporal distribution and gas/particle partitioning of polycyclic aromatic hydrocarbons (PAHs) in the atmosphere of Strasbourg, France. Atmosphere. 2021;12(3):337.

270. Gaffney JS, Marley NA. The impacts of combustion emissions on air quality and climate–From coal to biofuels and beyond. Atmospheric Environment. 2009;43(1):23-36.

271. Zervas E, Montagne X, Lahaye J. Emission of alcohols and carbonyl compounds from a spark ignition engine. Influence of fuel and air/fuel equivalence ratio. Environmental science & technology. 2002;36(11):2414-21.

272. Hasan AO, Abu-Jrai A, Ala'a H, Tsolakis A, Xu H. Formaldehyde, acetaldehyde and other aldehyde emissions from HCCI/SI gasoline engine equipped with prototype catalyst. Fuel. 2016;175:249-56.

273. Organization WH. Trichlorfon: World Health Organization; 1992.

274. Fan C, Song C, Lv G, Wang G, Zhou H, Jing X. Evaluation of carbonyl compound emissions from a non-road machinery diesel engine fueled with a methanol/diesel blend. Applied Thermal Engineering. 2018;129:1382-91.

275. Baraj E, Víden I. Assessment of Carbonyl Compounds in Exhaust Gases from Spark and Compression Ignition Engines in Prague. 2019.

276. Diodiu R, Bucur E, Galaon T, Pascu LF. Indoor air exposure to aldehydes and ketones in rooms with new and old furniture of a new office building. 2015.

277. McCormick RL, Fioroni G, Fouts L, Christensen E, Yanowitz J, Polikarpov E, et al. Selection criteria and screening of potential biomass-derived streams as fuel blendstocks for advanced spark-ignition engines. SAE International Journal of Fuels and Lubricants. 2017;10(2):442-60.

278. Wang C. Combustion and emissions of a direct injection gasoline engine using biofuels: University of Birmingham; 2014.

279. Daniel RL. Combustion and emissions performance of oxygenated fuels in a modern spark ignition engine: University of Birmingham; 2012.

280. Turner DM. The combustion and emissions performance of fuel blends in modern combustion systems: University of Birmingham; 2010.

281. Luszcz P. Combustion diagnostics in Homogeneous Charge Compression Ignition optical and thermal single cylinder engines: University of Birmingham; 2009.

282. Team C. Energy management systems. Requirements with guidance for use. 2018. Contract No.: 50001:2018.

283. Ashok B, Denis Ashok S, Ramesh Kumar C. A review on control system architecture of a SI engine management system. Annual Reviews in Control. 2016;41:94-118.

284. Valle RM, Barros JEM, Baeta JGC, Pujatti FJP. Mapping procedure applied to general engine management system for spark plug engines. SAE Technical Paper; 2004. Report No.: 0148-7191.

285. Pereira BCF, Pereira BS, Teixeira ELS, Laganá AAM, Cipparrone FAM, Santos MMD. Design, Implementation and Testing of a Spark-Ignition Engine Management System. Journal of Control, Automation and Electrical Systems. 2023;34(3):554-65.

286. Mohammed S, Mohamed M, Abdalmawla T. Design and Simulation of Engine Management System. The 7th International Conference on Engineering & MIS 2021; Almaty, Kazakhstan: Association for Computing Machinery; 2021. p. Article 29.

287. Xu S, Wang Z, Prucka R, Filipi Z, Prucka M, Dourra H, editors. Physical model for real-time simultaneous estimation of intake mass and cylinder pressure in an si engine. Internal Combustion Engine Division Fall Technical Conference; 2016: American Society of Mechanical Engineers.

288. Rounce PL. Engine performance and particulate matter speciation for compression ignition engines powered by a range of fossil and biofuels: University of Birmingham; 2011.

289. Stone R. Introduction to internal combustion engines: Springer; 1999.

290. Mauro S, Şener R, Gül M, Lanzafame R, Messina M, Brusca S. Internal combustion engine heat release calculation using single-zone and CFD 3D numerical models. International Journal of Energy and Environmental Engineering. 2018;9:215-26.

291. Christensen M, Johansson B, Hultqvist A. The effect of piston topland geometry on emissions of unburned hydrocarbons from a homogeneous charge compression ignition (HCCI) engine. SAE Technical Paper; 2001. Report No.: 0148-7191.

292. Vornicu V, Ulian T, Rakosi E, Manolache G, Talif S, editors. Prediction of spark ignition engine fuel consumption for different functional conditions using a theoretical model. IOP Conference Series: Materials Science and Engineering; 2019: IOP Publishing.

293. Eastop TD, Mc Conkey A. Applied thermodynamics for engineering technologies. 1986.

294. Vojtíšek M, Kotek M. Estimation of engine intake air mass flow using a generic speed-density Method. J Middle Eur Constr Des Cars. 2014;12(1):7-15.

295. Eastwood P. Particulate emissions from vehicles: John Wiley & Sons; 2008.

296. Alrayyes T. The Effect of Ethanol-Gasoline Blends on SI Engine Energy Balance and Heat Transfer Characteristics: University of Nottingham 2010.

297. Daniel R, Tian G, Xu H, Shuai S. Ignition timing sensitivities of oxygenated biofuels compared to gasoline in a direct-injection SI engine. Fuel. 2012;99:72-82.

298. Beck C, Stevenson P, Ziman P. The impact of gasoline octane on fuel economy in modern vehicles. SAE Technical Paper; 2006. Report No.: 0148-7191.

299. Nuamah K, Bundy A, editors. Calculating error bars on inferences from web data. Intelligent Systems and Applications: Proceedings of the 2018 Intelligent Systems Conference (IntelliSys) Volume 2; 2019: Springer.

300. Hoth A, Kolodziej CP. Effects of knock intensity measurement technique and fuel chemical composition on the research octane number (RON) of FACE gasolines: Part 2–Effects of spark timing. Fuel. 2023;342:127694.

301. Poursadegh F, Brear M, Hayward B, Yang Y. Autoignition, knock, detonation and the octane rating of hydrogen. Fuel. 2023;332:126201.

302. Westbrook CK, Mehl M, Pitz WJ, Sjöberg M. Chemical kinetics of octane sensitivity in a spark-ignition engine. Combustion and Flame. 2017;175:2-15.

303. Daniel R, Tian G, Xu H, Wyszynski ML, Wu X, Huang Z. Effect of spark timing and load on a DISI engine fuelled with 2,5-dimethylfuran. Fuel. 2011;90(2):449-58.

304. Wang C, Xu H, Daniel R, Ghafourian A, Herreros JM, Shuai S, et al. Combustion characteristics and emissions of 2-methylfuran compared to 2, 5-dimethylfuran, gasoline and ethanol in a DISI engine. Fuel. 2013;103:200-11.

305. Yang B, Sun W, Moshammer K, Hansen N. Review of the influence of oxygenated additives on the combustion chemistry of hydrocarbons. Energy & Fuels. 2021;35(17):13550-68.

306. P E. Particulate emissions from vehicles: John Wiley & Sons, Ltd; 2008.

307. Ursem B. Climate Shifts and the Role of Nano Structured Particles in the Atmosphere. Atmospheric and Climate Sciences. 2016;06(01):51-76.

308. Kittelson DB. Engines and nanoparticles. Journal of Aerosol Science. 1998;29(5-6):575-88.

309. Armas O, Gomez A, Mata C. Methodology for measurement of diesel particle size distributions from a city bus working in real traffic conditions. Measurement Science and Technology. 2011;22(10).

310. Bozza F, De Bellis V, Teodosio L. Potentials of cooled EGR and water injection for knock resistance and fuel consumption improvements of gasoline engines. Applied Energy. 2016;169:112-25.

311. Golzari R, Li Y, Zhao H. Impact of port fuel injection and in-cylinder fuel injection strategies on gasoline engine emissions and fuel economy. SAE Technical Paper; 2016. Report No.: 0148-7191.

312. Kammermann T, Merotto L, Bleiner D, Soltic P. Spark-induced breakdown spectroscopy for fuel-air equivalence ratio measurements at internal combustion engine-relevant conditions. Spectrochimica Acta Part B: Atomic Spectroscopy. 2019;155:79-89.

313. Duan Q, Kou H, Li T, Yin X, Zeng K, Wang L. Effects of injection and spark timings on combustion, performance and emissions (regulated and unregulated) characteristics in a direct injection methanol engine. Fuel Processing Technology. 2023;247:107758.

314. Ayala FA, Gerty MD, Heywood JB. Effects of combustion phasing, relative air-fuel ratio, compression ratio, and load on SI engine efficiency. SAE Transactions. 2006:177-95.

315. Maurya RK, Maurya RK. Engine Performance Analysis. Reciprocating Engine Combustion Diagnostics: In-Cylinder Pressure Measurement and Analysis. 2019:223-80.

316. Kalghatgi GT. Fuel anti-knock quality-Part I. Engine studies. SAE Transactions. 2001:1993-2004.

317. Kalghatgi GT. Fuel anti-knock quality-Part II. Vehicle Studies-how relevant is Motor Octane Number (MON) in modern engines? SAE Transactions. 2001:2005-15.

318. Mittal V, Heywood J. The relevance of fuel RON and MON to knock onset in modern SI engines. SAE Technical Paper 2008-01-2414. 2008.

319. Mittal V, Heywood JB. The shift in relevance of fuel RON and MON to knock onset in modern SI engines over the last 70 years. SAE International Journal of Engines. 2010;2(2):1-10.

320. Hauber J, Huber K, Nell R. New GKI-Gasoline Knock Index for Rating of Fuel's Knock Resistance on an Upgraded CFR Test Engine. SAE Technical Paper; 2018. Report No.: 0148-7191.

321. Yang J, Anderson RW. Fuel injection strategies to increase full-load torque output of a direct-injection SI engine. SAE transactions. 1998:498-505.

322. Yin C, Zhang Z, Sun Y, Sun T, Zhang R. Effect of the piston top contour on the tumble flow and combustion features of a GDI engine with a CMCV: a CFD study. Engineering Applications of Computational Fluid Mechanics. 2016;10(1):311-29.

323. Serras-Pereira J, Aleiferis P, Richardson D, Wallace S. Mixture preparation and combustion variability in a spray-guided DISI engine. SAE Transactions. 2007:1332-56.

324. Fry M, King J, White C. A comparison of gasoline direct injection systems and discussion of development techniques. SAE Technical Paper; 1999. Report No.: 0148-7191.

325. Song K, Wang X, Xie H. Trade-off on fuel economy, knock, and combustion stability for a stratified flame-ignited gasoline engine. Applied Energy. 2018;220:437-46.

326. Li T, Nishida K, Zhang Y, Onoe T, Hiroyau H. Enhancement of stratified charge for DISI engines through split injection (Effect and its mechanism). JSME International Journal Series B Fluids and Thermal Engineering. 2005;48(4):687-94.

327. Cairns A, Stansfield P, Fraser N, Blaxill H, Gold M, Rogerson J, et al. A study of gasoline-alcohol blended fuels in an advanced turbocharged DISI engine. SAE International Journal of Fuels and Lubricants. 2009;2(1):41-57.

328. Alagu K, Venu H, Jayaraman J, Raju VD, Subramani L, Appavu P, et al. Novel water hyacinth biodiesel as a potential alternative fuel for existing unmodified diesel engine: Performance, combustion and emission characteristics. Energy. 2019;179:295-305.

329. Gasmet. FTIR Gas Analyzer Instruction and operating manual.DX4040. Helsinki, Finland.; 2013. Contract No.: Pulttitie 8A, F-I 00880.

330. Sheet SD. Ethylene. 5005 LBJ Freeway,Dallas: Occidental Chemical Corporation; 2017 16-Jan-2017. Contract No.: M49062 - ANSI - EN.

331. Sheet HSF. ETHYLENE. Trenton: New Jersey Department of Health and Senior Services; 2002. Contract No.: 0873.

332. Tabaran AF, O'Sullivan MG, Seabloom DE, Vevang KR, Smith WE, Wiedmann TS, et al. Inhaled Furan Selectively Damages Club Cells in Lungs of A/J Mice. Toxicol Pathol. 2019;47(7):842-50.

333. Terrill JvH, WE; Robinson, D; Thomas, DL Acute inhalation toxicity of furan, 2-methylfuran, furfuryl alcohol, and furfural in the rat American Industrial Hygiene Association Journal. 1989;50(5):A359-A61

334. Chain EPoCitF, Knutsen HK, Alexander J, Barregard L, Bignami M, Bruschweiler B, et al. Risks for public health related to the presence of furan and methylfurans in food. EFSA J. 2017;15(10):e05005.